University of Alberta

Numerical Modeling of the Turbulence and Gas Transfer Generated by Microscale Breaking Waves

by

Shaheli Masoom

A thesis submitted to the Faculty of Graduate Studies and Research
in partial fulfillment of the requirements for the degree of

Doctor of Philosophy

in

Water Resources Engineering

Department of Civil and Environmental Engineering

Edmonton, Alberta

Fall 2008

Library and Archives Canada

Published Heritage Branch

395 Wellington Street
Ottawa ON K1A 0N4
Canada

Bibliothèque et Archives Canada

Direction du Patrimoine de l'édition

395, rue Wellington
Ottawa ON K1A 0N4
Canada

Your file Votre référence
ISBN: 978-0-494-46381-9
Our file Notre référence
ISBN: 978-0-494-46381-9

NOTICE:
The author has granted a non-exclusive license allowing Library and Archives Canada to reproduce, publish, archive, preserve, conserve, communicate to the public by telecommunication or on the Internet, loan, distribute and sell theses worldwide, for commercial or non-commercial purposes, in microform, paper, electronic and/or any other formats.

The author retains copyright ownership and moral rights in this thesis. Neither the thesis nor substantial extracts from it may be printed or otherwise reproduced without the author's permission.

AVIS:
L'auteur a accordé une licence non exclusive permettant à la Bibliothèque et Archives Canada de reproduire, publier, archiver, sauvegarder, conserver, transmettre au public par télécommunication ou par l'Internet, prêter, distribuer et vendre des thèses partout dans le monde, à des fins commerciales ou autres, sur support microforme, papier, électronique et/ou autres formats.

L'auteur conserve la propriété du droit d'auteur et des droits moraux qui protège cette thèse. Ni la thèse ni des extraits substantiels de celle-ci ne doivent être imprimés ou autrement reproduits sans son autorisation.

In compliance with the Canadian Privacy Act some supporting forms may have been removed from this thesis.

While these forms may be included in the document page count, their removal does not represent any loss of content from the thesis.

Conformément à la loi canadienne sur la protection de la vie privée, quelques formulaires secondaires ont été enlevés de cette thèse.

Bien que ces formulaires aient inclus dans la pagination, il n'y aura aucun contenu manquant.

Canada

Dedicated

to

my mother

ABSTRACT

A turbulence model and a gas transfer parameterization suitable for microscale breaking waves is developed in this study. Laboratory experimental data obtained for a microscale breaking wave situation is used for the development and validation of the model and the gas transfer parameterization. As a part of the systematic approach followed in this study, a technique for estimating the required inputs for the turbulence model is presented at first. A one dimensional ocean model first proposed for large scale waves is adopted and then modified to model the turbulence produced by micro-breaking waves. The numerical model developed for microscale waves is modified to account for mass transport and to predict the gas transfer velocity across the air-water interface. Finally, an analytical approach for computing gas transfer velocity is developed. The principal motivation for this study is to improve our understanding of the role microscale wave breaking plays in air sea gas exchange.

A technique for the estimation of roughness height and friction velocity at the air-water interface is introduced. The roughness height representing the minimum scale of turbulence is an important input parameter for surface layer models and these models can not be regarded as a functional predictive tool without independently specifying the roughness height. Therefore, the technique introduced for the estimation of roughness height can be considered as a significant achievement. An expression for the turbulent length scale is derived using a 2.5 level turbulence closure scheme. An observation of the turbulent length scale profile indicates that beneath a wind driven water surface the

length scale remains zero up to the non-dimensional depth of approximately 10. The length scale equation used for the turbulence model is modified by introducing a viscous sub layer beneath the water surface. Small turbulence in the viscous sublayer zone is introduced to predict the gas transfer velocity accurately. The diffusion equation along with the simplified turbulent kinetic energy equation is used to derive an analytical parameterization of gas transfer velocity.

ACKNOWLEDGEMENT

The author expresses her profound gratitude and respect to Dr. Peter Steffler for his constant supervision, encouragement, and keen interest throughout the work. His constructive suggestions and expertise helped the author for pursuing the study. The author also sincerely acknowledges the guidance and supervision provided by Dr. M. R. Loewen. His guidance during the thesis writing was extremely valuable. His constructive remarks helped the author for better presentation of the research findings.

Special appreciation goes to Mr. Perry Fedun for his technical assistance during the study. Special thanks to Mohamed Elkamash for his valuable suggestions and remarks. Elkamash provided his experimental data for the present study. The author gratefully acknowledges the excellent work atmosphere in the water resources research group.

The author extends her gratitude to her parents and friends for their encouragement. The author profoundly acknowledges the support, confidence, love and encouragement provided by her husband. The author sincerely acknowledges his valuable technical suggestions.

The author is also grateful for the research funds provided by the Faculty of Graduate Studies and Research (FGSR) and Natural Sciences and Engineering Research Council of Canada (NSERC).

TABLE OF CONTENTS

Chapter	**1**	**Introduction**	1
	1.1	General	1
	1.2	Microscale breaking waves and air-water gas transfer	3
	1.3	Study of gas transfer prediction	5
	1.4	Ocean Turbulence modeling	6
	1.5	Objectives of the Study	9
	1.6	Organization of the Thesis	11
	1.7	References	17
Chapter	**2**	**Experimental Data and Analyses**	
	2.1	Data Preparation	23
		2.1.1 Instrumentation and Method	11
		2.1.2 Experimental Procedures	24
		2.1.3 Analysis of Experimental data	28
		2.1.3.1 Air-side friction velocity	28
		2.1.3.2 Water side friction velocity and roughness height	28
		2.1.3.3 Turbulent Kinetic Energy Dissipation Calculations	29
	2.2	Data Preparation for GOTM	31
		2.2.1 Roughness Length (z_{ot}) Calculations	32
		2.2.2 Results from the length scale method and discussion	36
	2.3	Data used for Model Validation	40
	2.4	References	57
Chapter	**3**	**Turbulence Model for Microscale Breaking Waves**	
	3.1	Introduction	60
	3.2	Literature Review	62

	3.3	Turbulence Model for Breaking Waves	69
	3.4	Differences between large-scale and microscale breaking waves	70
		3.4.1 Calibration of the GOTM Model	74
	3.5	Modification of GOTM model for microscale breaking wave	76
	3.6	Gas Transfer Model Development	82
	3.7	Modification of microscale breaking wave model for gas transfer velocity	86
	3.8	Discussion	90
	3.9	Conclusions	93
	3.10	References	122
Chapter	**4**	**Gas Transfer Parameterization for Microscale Breaking Waves**	
	4.1	Introduction	130
	4.2	Literature Review	132
	4.3	Analytical study of gas transfer velocity	135
	4.4	Discussion	140
	4.5	Conclusions	146
	4.9	References	152
Chapter	**5**	**Conclusions and Recommendations**	
	5.1	Summary	156
	5.2	Conclusions of the Study	156
	5.3	Recommendations for Future Study	160
	5.4	References	162

Appendix A

A.1 First order second moment uncertainty analysis 163

A.2 Turbulent length scale profile for microscale breaking wave 164

A.3 Velocity and Dissipation profile predicted by the turbulence model developed for microscale breaking wave 165

A.4 Selection of length scale equation for k_g optimization 165

A.4.1 Functional forms of length scale (for $z^+ < 10$) used for k_g optimization 165

A.4.2 Effect of viscous sublayer thickness (δ_v^+) on k_g 166

A.5 Analytical relationship between the eddy diffusivity (D_t) and depth (z) 166

A.6 Velocity and Dissipation profile predicted by the turbulence model developed for gas transfer parameterization 169

Appendix B

B.1 Modification of Turbulent Length Scale Equation 170

B.2 Modification of Turbulent Kinetic Energy Flux 182

B.2.1 Source File name: fk_craig.f90 182

B.2.2 Source File name: production.f90 183

B.3 Modification of boundary condition of Heat Transport Equation to account for mass transport 185

LIST OF TABLES

Table	Caption	Page
2.1	Values of shear stress in air (τ_a), roughness height in air (z_{oa}), shear stress in water (τ) and roughness height in water (z_o) determined from the velocity profile method. Values are determined for both clean and surfactant affected water surfaces at various wind speeds (U).	43
2.2	Values of the water side friction velocity (u_*), shear stress (τ_{ol}), roughness length (z_{ol}) determined using the length scale method and z_{ol} / λ, the ratio of the roughness length (z_{ol}) to the dominant surface wave length (λ). Values are listed for both clean and surfactant affected water surface at various wind speeds (U)	44
3.1	Values of $S_{u\tau}$, the sensitivity of velocity (u) to changes in τ; $S_{u\alpha}$, the sensitivity of u to changes in α; and $S_{u\,zol}$ the sensitivity of u to changes in z_{ol}. Values are determined for a clean water surface at a depth of 0.27cm for a wind speed range of 3.8 to 9.5m s^{-1}.	97
3.2	Values of $S_{\varepsilon\tau}$, the sensitivity of dissipation (ε) to changes in τ; $S_{\varepsilon\alpha}$, the sensitivity of ε to changes in α; and $S_{\varepsilon\,zol}$ the sensitivity of ε to changes in z_{ol}. Values are determined for a clean water surface at a depth of 0.27cm for a wind speed range of 3.8 to 9.5m s^{-1}.	97
3.3	Values of optimized wave energy factor (α) determined using the least square method. Values are determined for both clean and surfactant affected water surfaces at various wind speeds (U) and corresponding wave ages (C_p/u_{*a})	98
3.4(a)	Values of $k_{g\text{-}expt}$, the experimental measurement of gas transfer velocity, k_g; $k_{g\text{-}MSBW}$, transfer velocity predicted by the MSBW model; $k_{g\text{-}Prandtl}$, transfer velocity predicted by the Prandtl-type (1952) length scale model. Values are determined for SF_6 diffusing through both clean and surfactant affected water surfaces at various wind speeds (U)	99
3.4(b)	Values of $k_{g\text{-}expt}$, the experimental measurement of gas transfer velocity, k_g; $k_{g\text{-}MSBW}$, k_g predicted by the MSBW model; $k_{g\text{-}Prandtl}$, k_g predicted by the	100

Prandtl-type (1952) length scale model. Values are determined for He diffusing through both clean and surfactant affected water surfaces at various wind speeds (U)

3.5 Values of $S_{kg-\tau}$, the sensitivity of gas transfer velocity (k_g) to changes in τ; S_{kg-zot}, the sensitivity of k_g to changes in z_{ot}; $S_{kg-\alpha}$, the sensitivity of k_g to changes in α; $S_{kg-\delta v+}$, the sensitivity of k_g to changes in δ_v^+ and S_{kg-A+}, the sensitivity of k_g to changes in the van Driest damping coefficient (A^+). Values are determined for a clean water surface at a depth of 0.27 cm for wind speed range of 3.8 to 9.5 m s^{-1}. 100

3.6 Values of optimized length scale slope (κ_s) and corresponding gas transfer velocity (k_g) determined from the concentration profile predicted by the model. Values are determined for both SF_6 and He diffusing through clean and surfactant affected water surfaces at various wind speeds (U) 101

3.7 Values of ΔTKE, the percentage increase in the depth averaged turbulent kinetic energy due to microscale breaking waves; $R_{z+=15}$, ratio of turbulent kinetic energy with microscale breaking waves and without at a depth of $z^+ = 15$. Values are determined for both clean and surfactant affected water surfaces at various wind speeds (U). 102

3.8 Values of z_o^+, the non-dimensional roughness height ($z_o^+ = u_* z_o / \nu$); dominant surface wave length (λ) and z_{ot} / λ, ratio between roughness length (z_{ot}) and λ. Values are determined for clean and surfactant affected water surface at various wind speeds (U). 103

A.1 Functional forms of turbulent length scale used in the zone $z^+ < 10$ to find the best possible length scale equation. 190

A.2 Values of optimized length scale slope (κ_s) using different thickness of the viscous sublayer (δ_v^+) determined from the concentration profile predicted by the model. Values are determined for both SF_6 and He diffusing through clean and surfactant affected water surface at various wind speeds (U). 191

LIST OF FIGURES

Figure	Caption	Page
1.1	Surface ocean processes controlling the air-sea exchange of CO2 (Source: http://www.pmel.noaa.gov/co2/gasex2/)	13
1.2	Definition sketch of Microscale Breaking wave occurring in a laboratory flume, C_b = Crest speed, U=Wind speed. From Siddiqui (2002)	14
1.3	A wind driven water surface (4m x 3m). From (M. L. Banner) (1997)	15
1.4	Infrared image of microscale breaking wave. A_B = the areal coverage by micro scale breaking waves. Reproduced from Siddiqui, M. (2002)	16
2.1	Schematics of Experimental setup (not to scale) (From Elkamash 2005)	45
2.2	Plot of mean velocity (U) versus depth (z) (a) for clean water surface and (b) for surfactant contaminated surface. ◆, = 3.8 m·s^{-1}; ●, = 4.9 m·s^{-1}; ▲, = 6.2 m·s^{-1}; x, = 8.0 m·s^{-1}; ■, = 9.6 m·s^{-1}.	46
2.3	Plot of $\ln(c_m/c_o)$ versus time, (t) for SF_6 diffusing through clean water surface at a wind speed of 4.9 m sec^{-1}. ◆,= experimental data points and solid line is the linear regression line fitted through the data points.	47
2.4	Plot of gas transfer velocity (k_g) versus wind speed (U) (a) for SF_6 and (b) for He. ○, = clean surface experiments and ●, = surfactant affected surface experiments for SF_6 diffusing through water surface. Δ , = clean surface experiments and ▲, = surfactant affected surface experiments for He diffusing through water surface.	48
2.5	Plot of dissipation (ε) versus depth (z) (a) for clean water surface and (b) for surfactant contaminated surface. ◆, = 3.8 m·s^{-1}; ●, = 4.9 m·s^{-1}; ▲, = 6.2 m·s^{-1}; x, = 8.0 m·s^{-1}; ■, = 9.6 m·s^{-1}.	49
2.6	Plot of the non-dimensional turbulent length scale (l^+) versus non-	50

dimensional depth (z^+) at a wind speed of 7.9 m s^{-1} on a clean water surface. Δ = experimental data points. The solid line is a second order least square regression line fitted between $z^+ > 30$ and $z/H < 0.035$, the dashed line corresponds to the non-dimensional depth $z^+ = 30$, the dashed-dotted line corresponds to the non-dimensional depth $z/H = 0.035$

2.7 Plot of the shear stress (τ) versus the wind speed (U) (a) Clean water surface, ○ = τ_{ov} (the shear stress estimated using the velocity profile method) and Δ = τ_{ol} (the shear stress estimated using the length scale method). (b) Surfactant influenced water surface, ● = τ_{ov} and ▲ = τ_{ol}. 51

2.8 Plot of the roughness length (z_{ol}) versus the wind speed (U). ○ = clean water surfaces and × = surfactant influenced water surfaces. 52

2.9 Plot of the ratio of the roughness height to the dominant wave length (z_{ol} / λ) versus wind speed (U). ○ = clean water surfaces; × = surfactant influenced water surfaces and the solid line is the regression power law fitted to the data points. The regression equation is $z_{ol} / \lambda = 1.83U^{-2}$ with a correlation coefficient of 0.86 53

2.10 The profiles of measured (a) dissipation (ε) and (b) velocity (u) for wind speed of 6.8 m s^{-1} on clean water surface, ▲ are experimental data points 54

2.11 Plot of gas transfer velocity (k_{600}) for $S_c = 600$ versus water side friction velocity (u_*). Data points are measurements of experimental data at the NASA Air–Sea Interaction Research Facility, ○, = fetch 4.8, ●, = fetch 8.8 and Δ , = fetch 12.4 m. 55

2.12 Plot of gas transfer velocity (k_{660}) for $S_c = 660$ for CO_2 in sea water at 20°C versus water side friction velocity (u_*). +, = CoOP97 measurements of field data (courtesy of Nelson Frew). 56

3.1 Comparison of the profiles of predicted and measured (a) velocity (u) and (b) dissipation (ε) for a wind speed of 8.0 m s^{-1} on a clean water surface. Solid line is the GOTM model predictions of (a) u and (b) ε, for parameter values of $\tau = \tau_a = 0.444 Nm^{-2}$, $z_{ol} = 0.004$m and $\alpha = 100$, 104

▲are experimental data points.

3.2 Plot of shear stress (τ) versus wind speed (U) on clean water surface. ○, estimate of air side shear stress and Δ, = estimate of water side shear stress. 105

3.3 Plot of difference between measurements and predictions in dissipation estimate (δ) versus wave energy factor (α) for a wind speed of 9.5 m s^{-1} on clean surface. Plot shows a well defined minimum error at $\alpha = 5$. 106

3.4 Plot of optimum wave energy factor (α) versus wind speed (U). ○, = clean surface experiments and ●, = surfactant affected surface experiments 107

3.5 Plot of optimum wave energy factor (α) versus wave age (C_p/u_{*a}). ○, = clean surface experiments and ●, = surfactant affected surface experiments; dotted line is Terry et al. (1996) equation (Eq. 3.8). 108

3.6 Comparison of the profiles of predicted and measured (a) dissipation (ε) and (b) velocity (u) for wind speed of 8.0 m s^{-1} on a clean water surface. Solid line is the model predictions using CB94 of (a) ε and (b) u for model optimized parameter values of τ, z_{ot} and α_*, ▲is experimental data points 109

3.7 Plot of non dimensional length scale (l^+) versus non dimensional depth (z^+) for clean water surfaces for five wind speeds. ♦, = 3.8 m s^{-1}; ● 4.9m s^{-1}; Δ , =6.2 m s^{-1}; □, = 8.0 m s^{-1} and , ○ = 9.5 m s^{-1} 110

3.8 Plot of non dimensional length scale (l^+) versus non dimensional depth (z^+) for a wind speed of 4.9 m s^{-1} on a clean surface. ●, = experimental data points and solid line is the proposed length scale according to Eq. 3.12 111

3.9 Comparison of predicted and measured profiles of (a) velocity (u) and (b) dissipation (ε) for wind speed of 8.0 m s^{-1} on a clean water surface. Solid line is the modified model's predictions of (a) u and (b) ε, dashed-dotted lines are the CB94 predictions, ▲are experimental data points 112

3.10	Comparison of the profiles of predicted and measured (a) dissipation (ε) and (b) velocity (u) for wind speed of 6.8 m s^{-1} on clean water surface. Solid line is the model predictions of (a) ε and (b) u for parameter values of $\tau = 0.065$ Nm^{-2}, $z_{ot} = 0.004$m and $\alpha = 15.$, ▲are experimental data points	113
3.11	Plot of non dimensional length (l^+) versus non dimensional depth (z^+) at a wind speed of 6.2m s^{-1}on clean water surface. Dashed-dotted line corresponds to Eq. (3.16) for $z^+ < 10$, dotted line corresponds to Eq. (3.16) for $z^+ > 10$ and the solid line is the third order polynomial is fitted between $z^+ = 8$ to $z^+ = 13$.	114
3.13(a)	Plot of concentration profile versus non dimensional depth (z^+) at a wind speed of 6.2 m s^{-1}on clean water surface.	115
3.13(b)	Plot of log (c_m/c_o) versus time (t) at a wind speed of 6.2 m s^{-1}on clean water surface. •, = data points obtained for different concentration profile at different time from Figure 3.14(a), Solid line corresponds to the straight line fitted through the data points	117
3.14	Plot of length scale slope (κ_s) versus the wave breaking kinetic energy flux (αu_*^3) for both He and SF_6 diffusing through clean and surfactant influenced water surfaces. ○, = data for the clean water surface; Δ, = data for the surfactant influenced water surface and solid line is a linear regression line passing through origin. The regression line has a slope of 0.0524 and $R^2 = 0.7$.	118
3.15	Plot of length scale slope (κ_s) versus the the mean square wave slope $\langle S^2 \rangle$ for both He and SF_6 diffusing through clean and surfactant influenced water surfaces. ○, = data for the clean water surface; Δ, = data for the surfactant influenced surface and solid line is a linear regression line passing through origin. The regression line has a slope of 5.33 and $R^2 = 0.9$.	119
3.16	Comparison of the profiles of predicted and measured (a) velocity (u) and (b) dissipation (ε) for wind speed of 8.0 m s^{-1} on clean water	120

surface. Solid line is the modified model's predictions of (a) u and (b) ε, ○, = experimental data points.

3.17 Plot of turbulent kinetic energy versus non dimensional depth (z^+) at a wind speed of 8.0 m s^{-1} on a clean water surface. The solid line is the kinetic energy profile when microscale breaking waves are present and the dotted line is when there are no microscale breaking waves present. 121

4.1 Plot of concentration profile versus non dimensional depth (z^+) at a wind speed of 6.2 m s^{-1}on clean water surface at 6 hr. 149

4.2 Plot of gas transfer velocity (k_{600}) for S_c = 600 versus water side friction velocity (u_*). Data points are measurements of experimental data at the NASA Air–Sea Interaction Research Facility, ○, = fetch 4.8, •, = fetch 8.8 and Δ , = fetch 12.4 m, solid line is the model prediction of k_{600} for a wave energy factor α = 24 and dashed-dotted line is the model prediction of k_{600} for α = 5, dotted line is the empirical relationship suggested by Liss and Marlivat (1986) 150

4.3 Plot of gas transfer velocity (k_{660}) for S_c = 660 for CO_2 in sea water at 20°C versus water side friction velocity (u_*). +, = CoOP97 measurements of field data, solid line is the model prediction of k_{660} for a wave energy factor α = 5, dotted line is the model prediction of k_{660} for a wave energy factor α = 24 and dashed-dotted line is the model prediction of k_{660} for α = 100. 151

A.1 Plot of non dimensional length (l^+) versus non dimensional depth (z^+) at a wind speed of 3.5 m s^{-1}on clean surface. Δ, = experimental data points. Solid line corresponds to the second order least square regression line fitted in between $z^+ > 30$ and $z/H < 0.035$. The correlation coefficient R^2 = 0.956. 192

A.2 Plot of non dimensional length (l^+) versus non dimensional depth (z^+) at a wind speed of 4.8 m s^{-1}on clean surface. Δ, = experimental data points. Solid line corresponds to the second order least square 193

regression line fitted in between $z^+ > 30$ and $z/H < 0.035$. The correlation coefficient $R^2 = 0.998$.

A.3 Plot of non dimensional length (l^+) versus non dimensional depth (z^+) at a wind speed of 6.2 m s^{-1} on clean surface. Δ, = experimental data points. Solid line corresponds to the second order least square regression line fitted in between $z^+ > 30$ and $z/H < 0.035$. The correlation coefficient $R^2 = 0.989$. 194

A.4 Plot of non dimensional length (l^+) versus non dimensional depth (z^+) at a wind speed of 7.9 m s^{-1} on clean surface. Δ, = experimental data points. Solid line corresponds to the second order least square regression line fitted in between $z^+ > 30$ and $z/H < 0.035$. The correlation coefficient $R^2 = 0.993$. 195

A.5 Plot of non dimensional length (l^+) versus non dimensional depth (z^+) at a wind speed of 9.5 m s^{-1} on clean surface. Δ, = experimental data points. Solid line corresponds to the second order least square regression line fitted in between $z^+ > 30$ and $z/H < 0.035$. The correlation coefficient $R^2 = 0.997$. 196

A.6 Plot of non dimensional length (l^+) versus non dimensional depth (z^+) at a wind speed of 3.9m s^{-1} on surfactant contaminated surface. ▲, = experimental data points. Solid line corresponds to the second order least square regression line fitted in between $z^+ > 30$ and $z/H < 0.035$. The correlation coefficient $R^2 = 0.974$ 197

A.7 Plot of non dimensional length (l^+) versus non dimensional depth (z^+) at a wind speed of 4.9m s^{-1} on surfactant contaminated surface. ▲, = experimental data points. Solid line corresponds to the second order least square regression line fitted in between $z^+ > 30$ and $z/H < 0.035$. The correlation coefficient $R^2 = 0.983$. 198

A.8 Plot of non dimensional length (l^+) versus non dimensional depth (z^+) at a wind speed of 6.2 m s^{-1} on surfactant contaminated surface. ▲, = experimental data points. Solid line corresponds to the second order least square regression line fitted in between $z^+ > 30$ and $z/H < 0.035$. 199

The correlation coefficient $R^2 = 0.991$.

A.9 Plot of non dimensional length (l^+) versus non dimensional depth (z^+) at a wind speed of 8.2 m s^{-1}on surfactant contaminated surface. ▲, = experimental data points. Solid line corresponds to the second order least square regression line fitted in between $z^+ > 30$ and $z/H < 0.035$. The correlation coefficient $R^2 = 0.977$. 200

A.10 Plot of non dimensional length (l^+) versus non dimensional depth (z^+) at a wind speed of 7.9m s^{-1}on surfactant contaminated surface. ▲, = experimental data points. Solid line corresponds to the second order least square regression line fitted in between $z^+ > 30$ and $z/H < 0.035$. The correlation coefficient $R^2 = 0.997$. 201

A.11 Comparison of the profiles of predicted and measured (a) dissipation (ε) and (b) velocity (u) for wind speed of 3.9 m s^{-1} on clean water surface. Solid line is the model predictions of (a) ε and (b) u for parameter values of $\tau = 0.0202$ Nm^{-2}, $z_{ot} = 0.0069$m and $\alpha = 20$, Δ is experimental data points. 202

A.12 Comparison of the profiles of predicted and measured (a) dissipation (ε) and (b) velocity (u) for wind speed of 4.9 m s^{-1} on clean water surface. Solid line is the model predictions of (a) ε and (b) u for parameter values of $\tau = 0.028$ Nm^{-2}, $z_{ot} = 0.0032$m and $\alpha = 24$, Δ is experimental data points. 203

A.13 Comparison of the profiles of predicted and measured (a) dissipation (ε) and (b) velocity (u) for wind speed of 6.2 m s^{-1} on clean water surface. Solid line is the model predictions of (a) ε and (b) u for parameter values of $\tau = 0.039$ Nm^{-2}, $z_{ot} = 0.0031$m and $\alpha = 10$, Δ is experimental data points. 204

A.14 Comparison of the profiles of predicted and measured (a) dissipation (ε) and (b) velocity (u) for wind speed of 8.0 m s^{-1} on clean water surface. Solid line is the model predictions of (a) ε and (b) u for parameter values of $\tau = 0.065$ Nm^{-2}, $z_{ot} = 0.004$m and $\alpha = 10$, Δ is experimental data points. 205

A.15 Comparison of the profiles of predicted and measured (a) dissipation (ε) and (b) velocity (u) for wind speed of 9.5 m s^{-1} on clean water surface. Solid line is the model predictions of (a) ε and (b) u for parameter values of $\tau = 0.094$ Nm^{-2}, $z_{ot} = 0.0032$m and $\alpha = 5$, Δ is experimental data points. 206

A.16 Comparison of the profiles of predicted and measured (a) dissipation (ε) and (b) velocity (u) for wind speed of 3.9 m s^{-1} on surfactant contaminated water surface. Solid line is the model predictions of (a) ε and (b) u for parameter values of $\tau = 0.023$ Nm^{-2}, $z_{ot} = 0.0049$m and $\alpha = 10$, ▲is experimental data points. 207

A.17 Comparison of the profiles of predicted and measured (a) dissipation (ε) and (b) velocity (u) for wind speed of 4.9 m s^{-1} on surfactant contaminated water surface. Solid line is the model predictions of (a) ε and (b) u for parameter values of $\tau = 0.028$ Nm^{-2}, $z_{ot} = 0.004$m and $\alpha = 10$, ▲is experimental data points. 208

A.18 Comparison of the profiles of predicted and measured (a) dissipation (ε) and (b) velocity (u) for wind speed of 6.2 m s^{-1} on surfactant contaminated water surface. Solid line is the model predictions of (a) ε and (b) u for parameter values of $\tau = 0.035$ Nm^{-2}, $z_{ot} = 0.0031$m and $\alpha = 13$, ▲is experimental data points. 209

A.19 Comparison of the profiles of predicted and measured (a) dissipation (ε) and (b) velocity (u) for wind speed of 8.2 m s^{-1} on surfactant contaminated water surface. Solid line is the model predictions of (a) ε and (b) u for parameter values of $\tau = 0.055$ Nm^{-2}, $z_{ot} = 0.0026$m and $\alpha = 5$, ▲is experimental data points. 210

A.20 Comparison of the profiles of predicted and measured (a) dissipation (ε) and (b) velocity (u) for wind speed of 9.8 m s^{-1} on surfactant contaminated water surface. Solid line is the model predictions of (a) ε and (b) u for parameter values of $\tau = 0.069$ Nm^{-2}, $z_{ot} = 0.001$m and $\alpha = 6$, ▲is experimental data points. 211

A.21 Comparison of the profiles of predicted and measured (a) dissipation 212

(ε) and (b) velocity (u) for wind speed of 3.9 m s^{-1} on clean water surface. Solid line is the model predictions (using Eq. 3.16) of (a) ε and (b) u for parameter values of $\tau = 0.0202$ Nm^{-2}, $z_{ot} = 0.0069$m and $\alpha = 20$, Δ is experimental data points.

A.22 Comparison of the profiles of predicted and measured (a) dissipation (ε) and (b) velocity (u) for wind speed of 4.9 m s^{-1} on clean water surface. Solid line is the model predictions (using Eq. 3.16) of (a) ε and (b) u for parameter values of $\tau = 0.028$ Nm^{-2}, $z_{ot} = 0.0032$m and $\alpha = 24$, Δ is experimental data points. 213

A.23 Comparison of the profiles of predicted and measured (a) dissipation (ε) and (b) velocity (u) for wind speed of 6.2 m s^{-1} on clean water surface. Solid line is the model predictions (using Eq. 3.16) of (a) ε and (b) u for parameter values of $\tau = 0.039$ Nm^{-2}, $z_{ot} = 0.0031$m and $\alpha = 10$, Δ is experimental data points. 214

A.24 Comparison of the profiles of predicted and measured (a) dissipation (ε) and (b) velocity (u) for wind speed of 8.0 m s^{-1} on clean water surface. Solid line is the model predictions of (using Eq. 3.16) (a) ε and (b) u for parameter values of $\tau = 0.065$ Nm^{-2}, $z_{ot} = 0.004$m and $\alpha = 10$, Δ is experimental data points. 215

A.25 Comparison of the profiles of predicted and measured (a) dissipation (ε) and (b) velocity (u) for wind speed of 9.5 m s^{-1} on clean water surface. Solid line is the model predictions of (using Eq. 3.16) (a) ε and (b) u for parameter values of $\tau = 0.094$ Nm^{-2}, $z_{ot} = 0.0032$m and $\alpha = 5$, Δ is experimental data points. 216

A.26 Comparison of the profiles of predicted and measured (a) dissipation (ε) and (b) velocity (u) for wind speed of 3.9 m s^{-1} on surfactant contaminated water surface. Solid line is the model predictions (using Eq. 3.16) of (a) ε and (b) u for parameter values of $\tau = 0.023$ Nm^{-2}, $z_{ot} = 0.0049$m and $\alpha = 10$, ▲is experimental data points. 217

A.27 Comparison of the profiles of predicted and measured (a) dissipation (ε) and (b) velocity (u) for wind speed of 4.9 m s^{-1} on surfactant 218

contaminated water surface. Solid line is the model predictions (using Eq. 3.16) of (a) ε and (b) u for parameter values of $\tau = 0.028$ Nm^{-2}, z_{ot} = 0.004m and $\alpha = 10$, ▲is experimental data points.

A.28 Comparison of the profiles of predicted and measured (a) dissipation (ε) and (b) velocity (u) for wind speed of 6.2 m s^{-1} on surfactant contaminated water surface. Solid line is the model predictions (using Eq. 3.16) of (a) ε and (b) u for parameter values of $\tau = 0.035$ Nm^{-2}, z_{ot} = 0.0031m and $\alpha = 13$, ▲is experimental data points. 219

A.29 Comparison of the profiles of predicted and measured (a) dissipation (ε) and (b) velocity (u) for wind speed of 8.2 m s^{-1} on surfactant contaminated water surface. Solid line is the model predictions (using Eq. 3.16) of (a) ε and (b) u for parameter values of $\tau = 0.055$ Nm^{-2}, z_{ot} = 0.0026m and $\alpha = 5$, ▲is experimental data points. 220

A.30 Comparison of the profiles of predicted and measured (a) dissipation (ε) and (b) velocity (u) for wind speed of 9.8 m s^{-1} on surfactant contaminated water surface. Solid line is the model predictions (using Eq. 3.16) of (a) ε and (b) u for parameter values of $\tau = 0.069$ Nm^{-2}, z_{ot} = 0.001m and $\alpha = 6$, ▲is experimental data points. 221

LIST OF SYMBOLS

A	=	eddy viscosity;
A_B	=	fractional area coverage of microscale waves during the breaking process;
A^+	=	damping constant (10);
A'	=	cross-sectional area;
a	=	coefficient of the power function of turbulent eddy diffusivity with depth;
a_*	=	dimensionless coefficient of the power function of dimensionless turbulent eddy diffusivity with dimensionless depth;
B	=	turbulent model constant for 2.5 level closure (16.6);
b	=	turbulent kinetic energy density;
C	=	effective phase speed related to wind input
C_1	=	constant;
C_2	=	constant;
C_3	=	constant;
C_p	=	wave phase speed;
C_p'	=	specific heat of water;
c	=	gas concentration;
c_{air}	=	gas concentration in air;
c_m	=	average concentration;
c_o	=	initial gas concentration;
$c(z)$	=	gas concentration profile;
D	=	molecular diffusivity;
D_g	=	molecular diffusivity of gas;
D_t	=	turbulent eddy diffusivity;
D_t^+	=	dimensionless turbulent eddy diffusivity ($D_t^+ = D_t / \upsilon$);
dt	=	time step;
F	=	gas flux;
F_{KE}	=	kinetic energy flux;
g	=	gravitational acceleration;
H	=	total depth of water;

H_c = Hanry's law constant;

He = Helium;

h_g = grid thickness at $z^+ = 15$;

i = integer;

K_1 = constant of derivation;

K_2 = constant of derivation;

K_3 = constant of derivation;

k_g = gas transfer velocity;

$k_{g\text{-}expt}$ = experimental estimate of gas transfer velocity;

l = turbulent length scale;

l^+ = dimensionless turbulent length scale ($u_* l/\nu$);

N = total number of measurement points for each experiment;

m_i = constant where i=1,2,3….N;

n = exponent of Schmidt number for the surface renewal model;

P_{rt} = turbulent Prandtl number;

P_w = production due to wave breaking;

q = turbulent velocity scale;

R = pipe radius;

R' = function of variables;

$R_{z+=15}$ = ratio of b at a depth of $z^+ = 15$ when microscale breaking waves are present and when they are absent;

r = model constant (1.0);

R^2 = coefficient of correlation ;

S_{ab} = dimensionless measure of the sensitivity of a to changes in b;

S_c = molecular Schmidt number;

S_{ct} = turbulent Schmidt number;

S_M = turbulent model constant for 2.5 level closure (0.39);

S_q = turbulent model constant for 2.5 level closure (0.387);

$\langle S^2 \rangle$ = mean square wave slope;

SF_6 = Sulfur hexafluoride;

T_m = time period for numerical model;

T = characteristic time scale for surface renewal;

t = time period;

U = wind speed;

U_s = surface velocity;

U_{SL} = Lagrangian surface drift velocity;

U_{stokes} = Stokes drift velocity;

u = the mean stream wise velocity;

$u(z)$ = the mean stream wise velocity profile;

u' = turbulent velocity fluctuation in streamwise direction;

u_* = friction velocity in water;

u_{*a} = friction velocity in air;

u_{wt} = wave and turbulent component of velocity in the longitudinal direction;

V_i = independent variable where i=1,2,3….N;

v' = turbulent velocity fluctuation in lateral direction;

v = horizontal velocity component perpendicular to the direction of wind;

W_i = uncertainty of variable V_i where i=1,2,3….N;

W_R = uncertainty into the result R';

w = instantaneous vertical velocity;

w' = turbulent velocity fluctuation in vertical direction;

w_{wt} = wave and turbulent component of velocity in the vertical direction;

$-\rho\overline{u'w'}$ = Primary Reynolds shear stress on x-z plane;

z = perpendicular distance from the air-water interface, positive upwards and its origin is at the interface;

z^+ = dimensionless depth $(-u_* z/\upsilon)$;

z_o = roughness height representing the depth where the velocity defect in water side $(U_s - u(z))$ is zero;

z_{oa} = roughness height representing the depth where the velocity defect in air side $(U_s - u(z))$ is zero;

z_{oH} = roughness height representing the minimum scale of the turbulence for bottom boundary of ocean;

z_{ot} = roughness height representing the minimum scale of the turbulence at air

water interface;

z_t = depth of the transition from the wave enhanced layer to the shear layer;

α = wave energy factor;

β' = dimensionless transfer resistance;

β = exponent of the power function of turbulent velocity scale;

Δc = concentration difference across the boundary layer;

δ = least square difference;

δ_c = thickness of concentration boundary layer;

δ_v = thickness of the viscous sub-layer;

δ_v^+ = non-dimensional thickness of the viscous sub-layer;

ε = dissipation of turbulent kinetic energy;

ε_{expt} = experimental estimate of dissipation of turbulent kinetic energy;

ε_i = model estimate of dissipation of turbulent kinetic energy for measurement point i;

$\hat{\varepsilon}_i$ = experimental estimate of dissipation of turbulent kinetic energy for measurement point i;

φ = coefficient of the power function of turbulent velocity scale;

κ = von Karman's constant;

κ_s = slope of the length scale in the zone $z^+ < 10$;

λ = dominant surface wave length;

μ = molecular viscosity;

ν = kinematic viscosity of water;

ρ = density of fluid;

ρ_w = density of water;

ρ_a = density of air;

ψ = model constant $(\sqrt{3/S_q\kappa^2 B})$;

τ = shear stress;

τ_a = shear stress in air;

τ_{expt} = experimental estimate of shear stress;

τ_o = boundary shear stress;

τ_{ol} = estimates of the shear stress obtained using the length scale method;

τ_{ov} = estimates of the shear stress obtained using the velocity defect profile method;

τ_{lang} = viscous or tangential stress;

τ_w = form or wave drag;

ω = vorticity;

Chapter 1: Introduction

1.1 General

Global warming is one of the most debated topics at present time. Climate change caused by human activity is one of the most pervasive threats to our planet. The atmospheric concentration of CO_2, a green house gas, is increasing by about 0.5% yr^{-1} due to burning of fossil fuels since the industrial revolution (IPCC 2007). The atmospheric concentration of CO_2 was approximately 280 ppm in the early nineteenth century. Currently this concentration has increased by a factor of 1.3 and is projected to increase by a factor of 2 by the middle of this century (IPCC 2007, Donelan and Wanninnkhof 2002). This anticipated increase in green house gas concentration is likely to increase global temperature up to 5 degrees Celsius and affect the infra-red radiation balance (IPCC 2007). Without proper action global warming and climate change will cause the extinction of many species and shift the world's ecological balance (Sabine et al. 2004).

The ocean plays an important role as a sink in taking up a large fraction of fossil fuel produced CO_2. Therefore evaluation of the exchange of CO_2 between the ocean and atmosphere becomes an important factor for the study of global warming. The ocean-air interface presents the first barrier against the exchange of CO_2 from atmosphere to the ocean (Peng 1984). The mixing rate of the ocean determines the total amount of CO_2 exchange. Close to the ocean-air interface turbulence generated by waves and wind shear causes the CO_2 molecules to be mixed with the flow quickly and distributed evenly. Underneath the surface layer the vertical mixing rates causes the CO_2 molecules to be penetrated into deeper parts of the ocean (Peng 1984)

The flux of a gas across the air-sea interface is determined by the product of the gas transfer velocity, which characterizes the resistance to gas exchange across the boundary layers, and the air-sea concentration difference of the gas. Conventional estimates of the exchange rate rely on simple, empirical, wind-speed dependent parameterizations of the gas transfer velocity (Wanninkhof 1992, Duce et al. 2000). At present the prediction of gas transfer using these equations is in an unsatisfactory state. Estimates of the global CO_2 uptake can vary by up to a factor of 3 depending on the equation used (Donelan and Wanninnkhof 2002). This discrepancy in the estimation is primarily caused by neglecting other factors beside wind that affect gas transfer. A number of physical processes contribute to gas transfer across the interface. These include penetrative convection due to heat loss (Csanady 1997), shear due to wind forcing, microscale wave breaking at moderate wind speeds (Zappa et al. 2001) and bubbles at high wind speeds (Woolf 1993). The different surface ocean processes that control CO_2 transfer at the air water interface are shown in Figure 1.1.

The exchange of gases across air-water interface occurs by molecular and turbulent diffusion. Turbulence mixing in the zone away from the interface can be considered a governing parameter for the mass transport across the interface. As the surface is approached the turbulent process is suppressed and diffusion occurs by molecular diffusion (Jähne et al. 1987, Donelan and Wanninnkhof 2002). This process results in a diffusive or concentration boundary layer on both sides of the interface. Outside these sub layers, due to turbulent vertical mixing, the concentration profile of the gas becomes almost uniform at the bulk concentration. Inside the diffusive sublayer the

concentration gradient is the strongest and provides greatest resistance to transport and controls the transfer rate.

For relatively insoluble gases in water (e.g. CO_2) the molecular diffusivity of gases are much larger in the air compared to the water (Wanninnkhof 1992). As a result the transfer of the gas at the air-water interface is controlled by the diffusive aqueous boundary layer as it gives greater resistance to the transport. Therefore, prediction of the gas transfer rate should be based on water side process.

Laboratory experiments have shown that wave-related mechanisms regulate gas transfer rates at low to moderate wind speeds (i.e. 4 to 9 m sec^{-1}) (Jähne et al. 1987 and Bock et al. 1999). For this range of wind speeds microscale-breaking waves occur much more frequently than large-scale breaking waves which lead researchers to propose that microscale wave breaking are important in governing the flux of heat, gas and momentum across the interface (Banner and Peregrine 1993; Melville 1996).

Therefore, this study is focused on the role of microscale breaking waves on gas transfer at the air-water interface. The goal of this study is to develop a gas transfer parameterization which is based on realistic physics of the transfer process to give improved predictions of the CO_2 transfer rate and hence global warming.

1.2 Microscale breaking waves and air-water gas transfer

Microscale breaking waves have gained increasing attention over the last three decades due to their role in air-sea gas transfer. A definition sketch and image of a microscale breaking wave occurring in a laboratory flume is shown in Figure 1.2 (from Siddiqui 2002). The term 'micro-breaking' was first introduced by Banner and Phillips (1974) to describe the breaking of short wind waves that break without air entrainment or

whitecapping. These waves are about 10 cm to 1m in length and a few centimeters in height. Surface tension force plays a significant role in the breaking process of microscale breaking waves and prevents air entrainment (Jessup et al. 1997). An aerial view of microscale breaking waves appearing on the top of large scale waves is shown in Figure 1.3. Large scale waves produce bubbles by entraining air during breaking process so these are often referred to as "white caps" (see Figure 1.3). Recent studies suggest that microscale breaking waves occur much more frequently and cover a larger fraction of ocean surface compared to large scale breaking waves (Siddiqui et al. 2001; Zappa et al. 2001; Holthuijsen and Herbers 1986).

The scale of microscale breaking waves makes it difficult to detect them in the laboratory or field. Therefore, an infrared image (IR) is used to detect the waves. A typical IR image used to detect microscale waves in the laboratory is shown in Figure 1.4. When the wave breaks, it brings warm bulk water to the surface. This warm fluid at the water surface is identified by temperature signature in the IR image. It has been shown that the surface area occupied by microscale breaking waves (A_B) is correlated with the gas transfer velocity and that these waves make a significant contribution to air-sea gas transfer (Zappa et al. 2001). It has been estimated that up to 60 to 75% of the gas transfer across the air-water interface is due to microscale wave breaking (Siddiqui et al. 2004 and Zappa et al. 2004). On average the transfer velocity is enhanced by a factor of ~3 inside the wakes generated by microscale breaking waves compared to the value outside the wakes (Zappa et al. 2001, 2004 and Siddiqui et al. 2004).

1.3 Study of gas transfer prediction

The transfer of a gas across the air water interface depends on the resistance that it encounters to cross the concentration boundary layer. Therefore, the concept of the resistive boundary layer can be used as a basis for the models developed for gas transfer prediction (Donelan and Wanninnkhof 2002). If turbulence in the bulk water is strong enough it can cause eddies from bulk fluid to force into the concentration boundary layer by displacing fluids from the sub-layer. This will result in a reduction in the thickness of the sub layer and hence increase the gas flux (Jähne et al. 1987). The turbulence in the bulk fluid can be created by shear due to wind forcing or by microscale wave breaking at moderate wind speeds (Zappa et al. 2001) and bubbles at high wind speeds (Woolf 1993). The models developed for gas transfer prediction needs to be based on the dominant mechanism responsible for generating the turbulence. If the turbulence is generated by wind shear induced tangential stress then the well established mixing length model first introduced by Prandtl (1952) is the simplest choice of model (Donelan and Wanninnkhof 2002).

Among other types of gas transfer parameterizations surface renewal model first proposed by Higbie (1935) has been used widely. The model is based on the concept that the water surface is turned over and renewed by bulk water due to the action of turbulent eddies. This process is typically referred to as surface renewal. The rate of renewal of the eddies determines the gas transfer rate ((Jähne et al. 1987).

Apart from surface renewal model the gas transfer velocity (k_g) has been correlated with different turbulent characteristics of the flow in a number of previous studies. Lamont and Scott (1970) assumed that very small scales of turbulent motion

control the transfer rate. In their model they developed an analytical relationship between k_g and dissipation of turbulent kinetic energy (ε) considering the mass transfer by small eddies in the inertial sub-range. Kitaigorodskii (1984) proposed that k_g could be parameterized with ε in the turbulent wakes generated by wave breaking. Siddiqui et al. (2004) estimated the gas transfer velocity using the characteristics of the coherent structures that are produced beneath microscale breaking waves. In a recent study Zappa et al. (2004) and Frew et al. (2004) correlated k_g with the mean square slope for wave breaking situation. Siddiqui and Loewen (2007) found that the mean square wave slope was correlated with ε demonstrating that as the wind speed increased the waves became steeper and generated stronger near-surface turbulence via microscale wave breaking. It has been realized from the previous studies that if the turbulence created by microscale breaking waves can be modeled properly, the turbulent characteristics of the flow can be used to correlate it with the gas transfer velocity.

1.4 Ocean Turbulence modeling

The modeling of the ocean has been in two separate streams. Ocean modelers attempt to model the full three dimensional nature of the ocean and capture the nature of currents and deep circulations. Atmospheric modelers, on the other hand, have progressively constructed zero or one dimensional ocean models that can be used to act as a boundary condition to their atmospheric model but these ocean models do not have the physical detail or response of the real ocean (McGuffie and Sellers 2005). Thus, modeling of the ocean processes by the climate modelers has been a hierarchical

procedure and the coupling of the ocean-atmospheric models can be thought of in terms of a hierarchy of oceanic components.

For this study it has been chosen to focus on the physical aspects of the air-sea exchange, namely contribution of the turbulence created by microscale breaking waves to the transfer velocity. The long term goal of this research is to predict the average gas transfer rates for use in the global climate models. The parameterization developed for gas transfer prediction will be based on the averaged properties of the near surface turbulence. For simplicity, a 1-D vertical turbulence model will be developed that will be used to improve estimation of the CO_2 flux at the air-water interface.

Uptake of CO_2 at the ocean is usually calculated using one dimensional box diffusion type ocean models (Peng 1984). There are numerous examples of one dimensional ocean models designed to simulate the ocean-mixing processes for the purpose of estimating the uptake of fossil fuel CO_2 (Craig 1957, Oeschger et al. 1975, Lal and Suess 1983, Kheshgi and White 1996, Joos et al. 1997). Higher dimensional models may not necessarily prove to be a better choice to predict the CO_2 uptake when compared to a 1-D vertical mixing type ocean model (Peng 1984).

One dimensional modeling of turbulent flow in ocean has been introduced in various contexts (Kerstein 1999, Axell and Liungman 2001, Burchard and Bolding 2001, Jeffery et al. 2007). For ocean circulations modeling most models are one dimensional vertical model because in ocean the longitudinal and transverse dimensions are infinite. Therefore, variation of the flow along the vertical become dominant compared to the variation in the other directions. There are many available 1-D horizontally averaged turbulence models for use in public domain e.g. GOTM, OGCM, POM, OMLM etc.

Instead of developing a completely new numerical model, a public domain 1-D vertical ocean turbulence model, the General Ocean Turbulence Model (GOTM) (available at http://www.gotm.net) is used in this study. A comparative study on the model performance showed that GOTM gives a better representation of the mixed layer depth compared to other ocean circulation models (Acreman and Jeffery, 2007). There are many practical applications of GOTM for simulating oceanic mixed layer (e.g. Northern Pacific), turbulent dissipation rate (North sea) (Burchard and Bolding 2001). The model computes solutions for the one-dimensional version of the transport equations of momentum, salt and heat. The GOTM software consists of well described documentation. The software is developed in modular form, has a module for wave breaking simulation and it allows modifications. Therefore, for the present study the GOTM algorithm was used with necessary modifications to simulate the turbulence beneath microscale breaking waves.

Several laboratory studies have been conducted on microscale breaking waves that provide reliable estimates of velocity profiles, turbulent kinetic energy dissipation rates and gas transfer velocities. e.g. Elkamash (2005), Siddiqui (2002). It is a daunting task to obtain velocity profile measurements and rate of dissipation estimates in the ocean. The beauty of microscale breaking wave is that the scale of the waves is so small that it allows the field situation to be represented in the laboratory. Therefore, laboratory experiments can be used as a data base for a numerical model development for microscale breaking waves and validation of the model. The use of GOTM to study mean flow beneath an air-water interface in laboratory wind wave flume has been reported previously by Craig (1996) and Zhang and Chan (2003). In this study a 1-D turbulence

model suitable for microscale breaking waves will be developed by adopting the GOTM algorithm and using laboratory experiments by Elkamash (2005).

1.5 Objectives of the Study

The focus of the proposed study is to advance our understanding of the role microscale wave breaking plays in air sea gas exchange. The specific objectives of this research include:

i) Description and analysis of experimental data obtained for microscale breaking wave.

ii) Development of a numerical model to predict the near surface turbulence and concentration profile caused by microscale breaking waves and prediction of the turbulent flux of gas across the air-water interface using the turbulence model.

iii) Development of an improved parameterization of the air-sea gas exchange using the properties of the near-surface turbulence.

The experimental data set used for the development of the model is obtained from a wind wave tank experiment on microscale breaking wave by Elkamash and Loewen (2004) and Elkamash (2005). The focus of this experiment was to study the mean flow in the aqueous boundary layer. The velocity fields beneath the wind waves were measured by Digital Particle Image Velocimetry (DPIV). Measurement of mean velocity and dissipation of turbulent kinetic energy were spatially (over the DPIV image dimension) and temporally (over 10 minute period) averaged. Bulk gas transfer velocities measured by Atmane et al. (2004) are used for this research to aid in the development of an accurate gas transfer algorithm. Gas transfer data from a complementary experimental

study conducted at NASA Goddard Space Flight Center/Wallops Flight Facility, VA, in April–May 2004 and field data from Frew et al. (2004) are used for validation of the gas transfer algorithm. The velocity, dissipation and gas transfer data will be analyzed to obtain the necessary input parameters for GOTM.

'The General Ocean Turbulence Model' (GOTM) algorithm will be used with necessary modifications to develop a turbulence model that can predict the vertical structure of the turbulence beneath microscale breaking waves. A 2.5 level scheme from Mellor and Yamada (1974, 1982) will be used to obtain turbulence closure. To simulate the effect of wave breaking, the technique proposed by Craig and Banner (1994) will be used in this study. Craig and Banner (1994) proposed that the effect of wave breaking can be simulated by a flux of kinetic energy applied at the surface. The turbulence model will be calibrated to reproduce profiles of the mean velocity and dissipation of turbulent kinetic energy as observed in the experiments (Elkamash 2005). The difference in physics between large scale and microscale breaking waves will be addressed and feasible modifications will be applied in the model to make the turbulence model applicable for microscale breaking waves. The GOTM turbulent transport algorithm will be modified to predict the concentration profile of the dissolved gas in the water. According to a recent study (McGillis and Wanninkhof 2006) the concentration gradient in the aqueous boundary layer determines the magnitude and direction of the flux. The concentration gradient at the boundary predicted by the model will be used to estimate the gas transfer velocity. Necessary modifications will be applied in the turbulent length scale equation so that the model is capable to predict the gas transfer velocity accurately.

It is also required that the model predicts both momentum and dissipation profiles reasonably accurately after the modifications.

An analytical approach for computing gas transfer velocity will be derived in the next stage. The numerical model predictions will be used to apply simplifications to the derivation. In near surface region turbulent forces are negligible compared to viscous forces. However, these turbulent forces are not necessarily small compared to diffusive forces and might play a significant role in gas transfer. The role of this turbulent force in gas transfer will be investigated based on the properties of near surface turbulence and the concentration profile. If an analytical relationship between the turbulent eddy diffusivity and depth can be established for the model then the basic diffusion equation can be used to estimate the gas transfer velocity. The analytical parameterization will be validated by comparing the predicted gas transfer velocity with the measured values in laboratory (NASA 2004 experiments) and field (Frew et al. 2004).

1.6 Organization of the Thesis

This thesis presents the step wise development of a turbulence model and an improved gas transfer parameterization for microscale breaking wave. Following is a brief introduction to each chapter presented in this thesis. The study is performed in three major steps and results from each step are complementary to the next step.

A description about the experimental data used for model development, properties of the aqueous boundary layer, data analysis, data preparation for GOTM input, description of the data used for model validation are presented in Chapter 2.

In Chapter 3 GOTM algorithm is modified and the model is calibrated to develop a turbulence model for microscale breaking waves. The inputs of GOTM model are modified for application at a wind drift layer. The effect of wave age on the mean flow is studied and incorporated in the turbulence model. Near surface viscous effects are found to be dominant in the flow beneath wind drift layer and an improved turbulent length scale equation is proposed to incorporate this effect. The proposed turbulence model has been found to give satisfactory predictions when compared with the measurements of gas transfer velocity, mean velocity and dissipation profiles

In Chapter 4 an analytical gas transfer parameterization is developed to predict gas transport across the air-water interface accurately. The parameterization is developed based on the properties of near surface turbulence and the concentration profile as predicted by the turbulence model described in Chapter 3.

The conclusions of the entire study and recommendations for future studies are presented in Chapter 5.

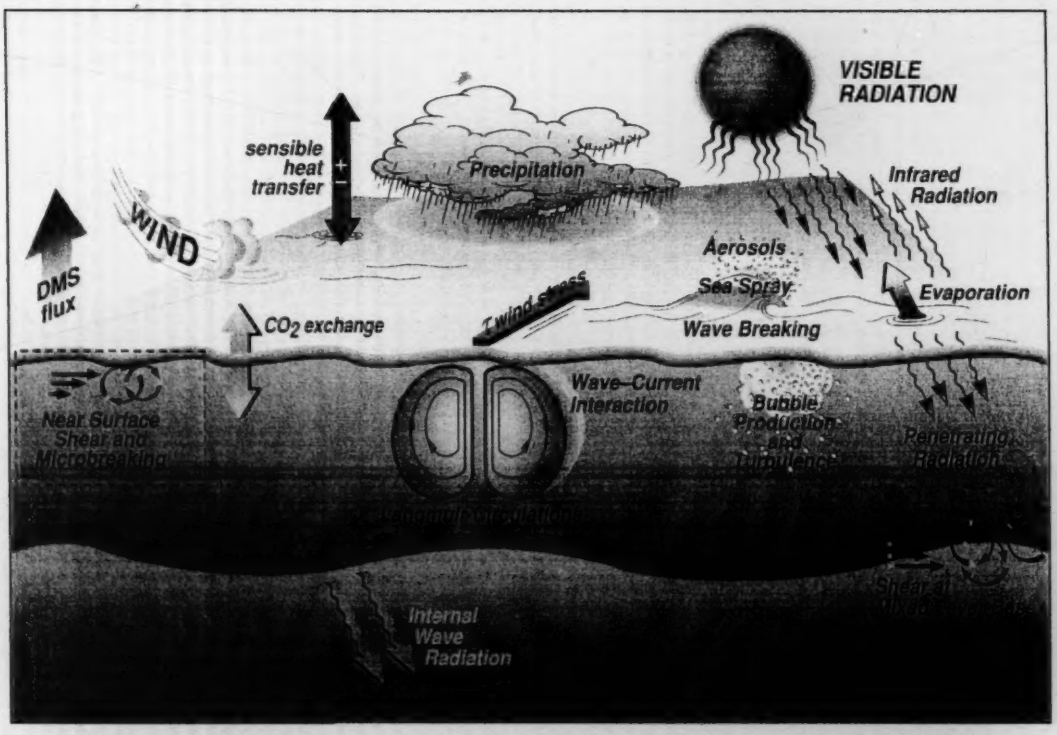

Figure 1.1: Surface ocean processes controlling the air-sea exchange of CO2

(Source: http://www.pmel.noaa.gov/co2/gasex2/)

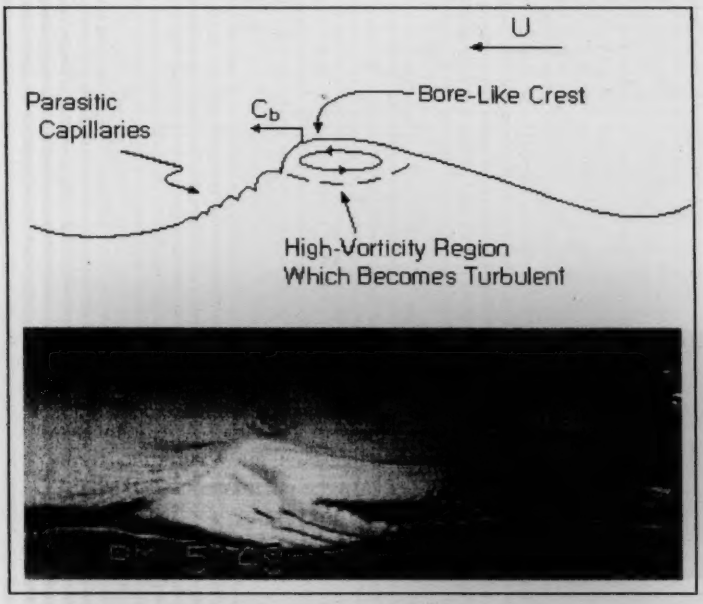

Figure 1.2: Definition sketch of Microscale Breaking wave occurring in a laboratory flume, C_b = Crest speed, U=Wind speed. From Siddiqui (2002).

Figure 1.3: A wind driven water surface (4m x 3m).

From M. L. Banner (1997)

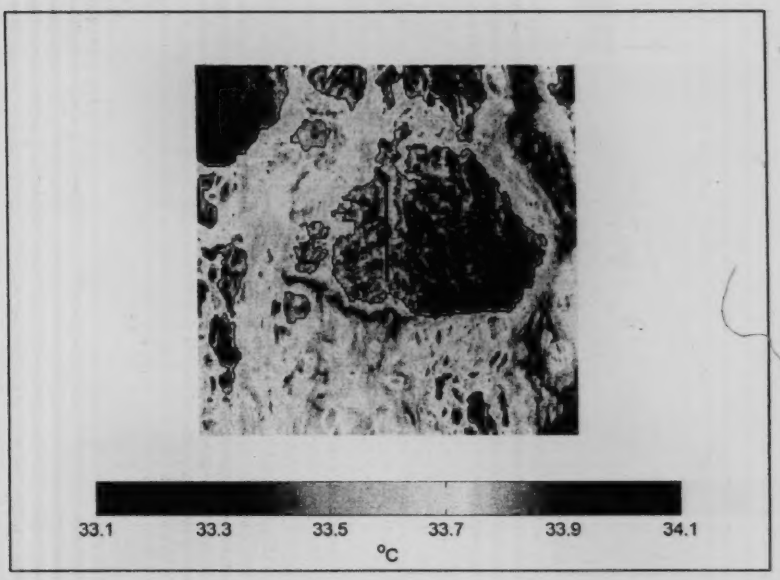

Figure 1.4: Infrared image of microscale breaking wave. A_B = the areal coverage by micro scale breaking waves. Reproduced from Siddiqui, M. (2002).

1.7 References

Acreman, D.M. and Jeffery, C.D. (2007). "The use of Argo for validation and tuning of mixed layer models." *Ocean Modeling*. 19 (1-2), 53-69.

Atmane, M. A., Asher, W. E. and Jessup, A. T. (2004). "On the Use of the Active Infrared Technique to Infer Heat and Gas Transfer Velocities at the Air-Water Free Surface." *Journal of Geophysical Research*, Vol. 109(C8), C08S14, pp.1-15.

Axell L.B. and Liungman O. (2001). "A One-Equation Turbulence Model for Geophysical Applications: Comparison with Data and the k-ε Model." *Environmental Fluid Mechanics*, 1(1), 71-1006(36).

Banner, M. L. and Peregrine, D. H. (1993). "Wave breaking in deep water." *Ann. Rev. Fluid Mech.* 25, 373-397.

Banner, M. L. and Phillips, O. M. (1974). "On the incipient breaking of small scale waves." *J. Fluid Mech.*, 65, 647-656.

Bock, E.J., Hara, T., Frew, N.M. and Mcgillis, W.R. (1999). "Relationship between air-sea gas transfer and short wind waves." *J. Geophys. Res.* 104, 25821-25831.

Burchard, H. and Bolding, K. (2001). "Comparative analysis of four second-moment turbulence closure for the oceanic mixed layer.," *Journal of Physical Oceanography*, 31(8), 1943-1968.

Csanady, G.T. (1997). "The 'Slip Law' of the free surface." *Journal of Oceanography* 53, 67-80.

Craig, H. (1957). "The natural distribution of radiocarbon and the exchange time of carbon dioxide between atmosphere and sea." *Tellus*, 9(1), 1-17.

Craig, P.D. and Banner, M.L. (1994). "Modeling wave-enhanced turbulence in the ocean surface layer." *Journal of Physical Oceanography*, 24, 2546-2559.

Craig, P.D. (1996). "Velocity Profiles and Surface Roughness Under Breaking Waves." *Journal of Geophysical Research*, 101, 1265-1277.

Donelan, M.A. and Wanninkhof R. (2002). "Gas transfer at water surfaces – concepts and issues." *Proceedings of the4th International Symposium on Gas Transfer at Water Surfaces*, Miami, Florida, USA.

Duce, R., Liss, P., Barber, R., Farmer, D., Huebert, B., Jenkins, W., Matrai, P., Platt, U., Taylor, P. and Wallace, D. (2001). Surface Ocean-Lower Atmosphere Study (SOLAS) Science Plan.

Elkamash, M. K. and Loewen, M. R. (2004). "Air-sea gas transfer and turbulence for clean and surfactant contaminated surfaces." *Proceedings of the 1st Water and environment Specialty Conference, 32nd Annual Conference*, Canadian Society for Civil Engineering, Saskatoon, Saskatchewan, Canada.

Elkamash, M. K. M. (2005). *The effect of surfactants on microscale wave breaking and the aqueous boundary layer*, Ph. D. thesis, University of Alberta, Edmonton, Alberta, Canada.

Frew, N. M., Bock, E. J., Schimpf, U., Hara, T., Haußecker, H., Edson, J. B., McGillis, W. R., Nelson, R. K., McKenna, S. P., Uz, B. M., and Jähne, B. (2004). "Air-sea gas transfer: Its dependence on wind stress, small-scale roughness, and surface films." *J. Geophys. Res.*, 109, C08S17.

Higbie, R., (1935). "The rate of absorption of a pure gas into a still liquid during short periods of exposure." *Trans. Am. Inst. Chem. Eng.*, 35, 365 - 389.

Holthuijsen, L.H. and Herbers, T.H.C. (1986). "Statistics of breaking waves observed as whitecaps in the open sea." *Journal of physical oceanography*, 16, 290-297.

IPCC, (2007). *Summary for Policymakers*. In: Climate Change 2007: The Physical Science Basis. Contribution of Working Group I to the Fourth Assessment Report of the Intergovernmental Panel on Climate Change. Cambridge University Press, Cambridge, United Kingdom and New York, NY, USA.

Jähne, B., Munnich, K. O., Bosinger, R., Dutzi, A., Huber, W. and Libner, P. (1987). "On the parameters influencing air-water gas exchange." *J. Geophys. Res.*, 92, 1937-1949.

Jeffery, C. D., Woolf, D. K., Robinson, I. S. and Donlon, C. J. (2007). "One-dimensional modeling of convective CO2 exchange in the Tropical Atlantic."*Ocean Modelling*, 19 (3-4), 161-182.

Jessup, A.T., Zappa, C.J. and Yeh, H. (1997). "Defining and quantifying microscale wave breaking with infrared imagery." *J. Geophys. Res.-Oceans*, 102, C-10, 23145-23153.

Joos, F., Orr. J.C. and Siegenthaler, U. (1997). "Ocean carbon transport in a box-diffusion versus a general circulation model." *Journal of geophysical research-oceans*, 120(C6),12367-12388.

Kerstein A. R. (1999). "One-dimensional turbulence: model formulation and application to homogeneous turbulence, sheer flows and buoyant stratified flows." *Journal of fluid mechanics*, 392, 277-334.

Kheshgi, H. S. and White, B. S. (1996). "Modelling ocean carbon cycle with a nonlinear convolution model." *Tellus Series B-Chemical and Physical Meteorology*, 48(1), 3-12.

Kitaigorodskii, S.A., (1984). "On the fluid dynamical theory of turbulent gas transfer across an air sea interface in the presence of breaking wind-waves." *Journal of physical oceanography*, 14 (5), 960-972.

Lal, D. and Suess, H.E. (1983). "Some comments on the exchange of CO_2 across the air-sea interface." *Journal of Geophysical Research-Oceans and Atmospheres,* 88(NC6), 3643-3646.

Lamont, J.C. and Scott, D.S. (1970). "An eddy cell model of mass transfer into surface of a turbulent liquid." *AICHE Journal,* 16 (4), 513-519.

McGillis, W.R. and Wanninkhof, R. (2006). "Aqueous CO2 gradients for air–sea flux estimates." *Marine Chemistry,* 98, 100-108.

McGuffie K. and Henderson-Sellers, A. (2005). *A Climate Modelling Prime,* John Willy and Sons.

Mellor, G. L. and Yamada, T. (1982). "Development of a turbulence closure-model for geophysical fluid problems." *Reviews of Geophysics*, 20 (4), 851-875.

Mellor, G. L. and Yamada, T. (1974). "Hierarchy of turbulence closure models for planetary boundary-layers." *Journal of the Atmospheric Sciences*, 31(7), 1791-1806.

Melville, W. K. (1996). "The role of surface-wave breaking in air-sea interaction." *Ann. Rev. Fluid Mech.* 28, 279-321.

Oeschger, H., Siegenthaler, U. and Schotterer U. (1975). "Box diffusion-model to study carbon-dioxide exchange in nature." *Tellus*, 27(2), 168-192.

Peng, T. H. (1984). "Invasion of fossil fuel CO_2 into the ocean." *Proceedings of the International Symposium on Gas Transfer at Water Surfaces held at Cornell University, NY, USA* from June 13 to 15, 1983. Edited By Wilfried Brutsaert, Gerhard H. Jirka.

Prandtl L. (1952). *Essentials of fluid mechanics*. Blackie and sons. 452.

Sabine, C.L., Feely R. A., Gruber, N., Key, R. M., Lee, K., Bullister, J. L., Wanninkhof, R., Wong, C.S., Wallace, D.W.R., Tilbrook, B., Millero, F.J., Peng, T.H., Kozyr, A.,

Ono, T. and Rios, A. (2004). "The oceanic sink for anthropogenic CO_2." *Science*, 305(5682), 367 – 371.

Siddiqui, M. H. K., Loewen, M. R., Richardson, C., Asher, W. E. and Jessup, A. T. (2001). "Simultaneous particle image velocimetry and infrared imagery of microscale breaking waves." *Physics of Fluids*, 13, 1891-1903.

Siddiqui, M. H. K. (2002). "Laboratory Measurements of the flow beneath microscale breaking waves." *Ph.D. Thesis*, Department of Mechanical and Industrial Engineering, University of Toronto.

Siddiqui, M. H. K., Loewen, M. R., Asher, W. E. and Jessup, A. T. (2004). "Coherent structures beneath wind waves and their influence on air-water gas transfer." *Journal of Geophysical Research*, 109, C03024.

Siddiqui, M. H. K. and Loewen, M. R. (2007). "Characteristics of the wind drift layer and microscale breaking waves." *J. Fluid Mech.*, 573, 417-456.

Wanninkhof, R. (1992). "Relationship between wind speed and gas exchange over the ocean." *Journal of Geophysical Research*, 97 (C5), 7373-7382.

Woolf, D.K. (1993). "Bubbles and air–sea transfer velocity of gases." *Atmosphere-Ocean* 31, 517–540.

Zappa, C. J., Asher, W. E. and Jessup, A. T. (2001). "Microscale wave breaking and air-water gas transfer." *Journal of Geophysical Research*, 106, 9385-9391.

Zappa, C. J., Asher, W. E., Jessup, A. T., Klinke, J. and Long, S. R. (2004). "Microbreaking and the enhancement of air-water gas transfer velocities." *J. Geophys. Res.*, 109, C8, C08S16.

Zhang, H., Chan, E.S. (2003). "Modeling of the turbulence in the water column under breaking wind waves." *Journal of Oceanography*. 53(3), 331-341

Chapter 2: Experimental Data and Analyses

2.1 Data Preparation

2.1.1 Instrumentation and Method

Elkamash (2005) conducted a series of experiments investigating microscale breaking waves in a wind-wave tank at the Harris Hydraulics Laboratory, University of Washington, Seattle, USA. The wave flume was 1.18m wide and 9.2m long. The water depth was held constant at 0.87m and experiments were conducted for clean and surfactant influenced water surfaces. The flume was equipped with a centrifugal fan at the upstream end of the tank at 16 cm above the water surface. The fan is installed to produce wind speeds up to 11 m s^{-1}. A wave absorbing "beach" made of rubberized horsehair was placed at the downstream end and a water heater and circulation pump were used to vary the water temperature. The air water temperature difference varied from -1.8 to +2.6 °C and had an average value of 0.4 °C. Essential features of the experimental set up are shown in Figure 2.1.

For the surfactant-influenced experiments, one part per million of the soluble surfactant Triton X-100 was added to the water. The water in the tank was filtered tap water, and the surface was vacuumed before each experiment to remove accumulated surface contaminants. The experiments were conducted at a fetch of 5.5 m and for a wind speed range from 3.5 to 10.0 m s^{-1} for both clean and surfactant contaminated experiments.

2.1.2 Experimental Procedures

In order to measure the wind velocity profile above the interface, a wind sensor (OMEGA FMA-905-V) with an output voltage range 0-5 Volts was used. The output voltage values were converted to wind speed values according to the sensor's calibration equation. Bulk air and water temperature, wind speed and relative humidity were measured during every run. These data were sampled at a rate of 100 Hz per channel using an eight-channel A/D board.

In order to estimate the Lagrangian surface drift velocity (U_{SL}), circular heated patches were created on the water surface using CO_2 laser. These heated patches were then tracked using an infrared (IR) imager with a resolution of 256 by 256 pixels^2. The IR imager was mounted on top of the tank with a field of view of approximately 64.3 cm × 64.3 cm. At each wind speed and surface condition, the surface velocity (U_s) was computed by subtracting the Stokes drift velocity (U_{stokes}) from U_{SL} (Bye 1967). The two dimensional velocity fields beneath the wind waves were measured using Digital Particle Image Velocimetry (DPIV). The flow field imaging camera captured 8-bit gray scale images with a resolution of 1008 by 1008 pixels^2. The field of view was set at 10.2 cm wide and 10.2 cm high in these experiments.

Elkamash (2005) used a technique based on the fact that the laser light sheet is visible only in the water in order to locate the interface in the DPIV images. He used the technique after Banner and Peirson (1998) that the waterside is brighter due to the reflection of the seed particles and therefore the difference in the gray-scale values on the airside and the waterside was used to detect the water surface in the profile images. To detect the location of the water surface in the wave profile images, Elkamash (2005) used

an algorithm based on a threshold gray scale value. This threshold was set based on the average gray scale below the water surface. The final threshold value was set by plotting the computed profiles on top of the original profile images and visually determining when the match was optimal. The uncertainty in computing the wave profile was estimated to be ±0.2 mm.

The instantaneous velocity fields in a fixed Eulerian coordinate system were obtained from the DPIV measurements. Elkamash (2005) estimated the velocity field by computing a cross correlation between an interrogation window (48×48 pixels^2) in the first image and a corresponding search window (96×96 pixels^2) in the second image. A 50% window overlap was used resulting in a nominal resolution of the velocity field of 2.6 mm. The cross-correlation algorithm computes a displacement vector within every interrogation region. Below the interface the algorithm uses the local median value of eight or fewer neighboring velocity vectors depending on the location of the given vector with reference to the water surface. Using an adaptive Gaussian window (AGW) interpolator, Elkamash (2005) interpolated the velocity vectors onto a rectangular grid. This velocity data was transformed to a wave-following Eulerian coordinate system, in which the air-water interface is the origin (Siddiqui and Loewen 2007). Velocity measurements in the wave-following coordinate system extended to depths of 5.9 cm below the interface at the highest wind speed (9.5 m s^{-1}) and 7.5 cm below the interface at the lowest wind speed (3.8 m s^{-1}) for the clean water surface runs. The measurements extended to depths 6.7 cm and 8.07 cm for the surfactant influenced runs for the highest and lowest wind speed respectively. The mean velocity components were obtained by time-averaging 10 minutes of instantaneous velocity measurements at a given grid point

in the wave-following coordinate system and then averaging in space across the width of the DPIV velocity field. The percentage error in the DPIV velocities was estimated to be 2.5%. Vertical profiles of the mean stream wise velocity are shown plotted at five wind speeds in Figure 2.2(a) for clean water surfaces and in Figure 2.2(b) for surfactant-influenced water surfaces. It is observed that the mean horizontal velocity increases with wind speed and decreases monotonically with depth. It can be also be observed that the magnitudes of the mean stream wise velocities beneath the surfactant-influenced water surface were typically smaller than beneath the clean water surface for a similar wind speed. It is evident from Figure 2.2 (a) and (b) that the near-surface velocity gradients are greater beneath the surfactant-influenced water surface at all the wind speeds.

Bulk gas transfer velocities were measured by Atmane et. al (2004) for Helium (He) and Sulfur hexafluoride (SF_6) by super saturating the water with the gases and measuring the decrease in their concentration over time (Asher et al. 1996). The water samples used for concentration measurements were collected at five different sampling locations. Samples were drawn from three evenly spaced depths at a fetch of 5m and at mid-depth at fetches of 1m and 8.5m. A tank averaged concentration (c_m) was calculated by averaging the individual concentrations at the five sampling locations.

The gas flux, F is conventionally expressed as the product of the gas transfer velocity (k_g) (Liss 1973), and the concentration difference of the gas across the boundary layer at the air-water interface (Δc),

$$F = -k_g \Delta c \qquad (2.1)$$

The concentration difference can be expressed as $\Delta c = c_m - H_c c_{air}$, where, c_m is the mean gas concentration in the turbulent water beneath the concentration boundary layer c_{air} is

the gas concentration in the air side boundary and H_c is the Hanry's law constant. For water-side limited gases such as He and SF_6 the gas concentration in the air (c_{air}) is negligible compared to that in water. Therefore, Eq. (2.1) can be rewritten as;

$$F = -k_g c_m \tag{2.2}$$

For a wind wave tank of height H and cross-sectional area A', the mass flow rate $\dot{m}$ is expressed as;

$$\frac{d(c_m HA')}{dt} = \dot{m} \tag{2.3}$$

Expressing $\dot{m} = F \cdot A'$ and substituting F from Eq. (2.2);

$$\frac{d(c_m)}{dt} = -\frac{k_g c_m}{H} \tag{2.4}$$

Integrating Eq. (2.4) with respect to time;

$$\ln\left(\frac{c_m}{c_o}\right) = -\frac{k_g t}{H} \tag{2.5}$$

where, c_o is the initial gas concentration in the water, c_m is the mean gas concentration at time t and H is the water depth. The gas transfer velocity (k_g) can be found from the slope of a plot of $\ln(c_m/c_o)$ versus t. A typical plot of the variation of $\ln(c_m/c_o)$ with respect to time, t is shown in Figure 2.3 for SF_6 diffusing from a clean water surface at a wind speed of 4.9 m s^{-1}. Atmane et. al (2004) computed the gas transfer velocity using Figure 2.3 and Eq. 2.5 to be 12.2 cm hr^{-1}.

Atmane et. al (2004) estimated the tank averaged gas transfer velocity (k_g) using the method described above for different wind speeds and for clean and surfactant contaminated water surface. The values of k_g, for SF_6 and He are plotted in Figure 2.4 as

a function of wind speed, U, for both clean water and surfactant influenced water surfaces.

2.1.3 Analysis of Experimental data

2.1.3.1 Air-side friction velocity

Vertical velocity profiles of the mean horizontal wind speed were used to compute the airside friction velocities (Elkamash 2005). The velocity profiles on the air side followed a semi-logarithmic velocity distribution expressed as,

$$\frac{u(z)}{u_{*a}} = \frac{1}{\kappa} \ln\left(\frac{z}{z_{oa}}\right) \tag{2.6}$$

where, $u(z)$ is the mean velocity, z, the is the height above the mean air-water interface, κ is the von Karman's constant ($\kappa \approx 0.4$), u_{*a} is the air side friction velocity and z_{oa} is the air side roughness height. Values of u_{*a} and z_{oa} were computed by performing a linear regression of the mean velocity data using Eq. 2.6. The estimated values of the shear stress in air ($\tau_a = \rho_a u_{*a}^2$, where, ρ_a is the air density) and roughness height in air (z_{oa}) are given in Table 2.1 for all wind speeds and for both clean and surfactant influenced water surfaces. The average value of the correlation coefficient between the measured velocity profiles and Eq. 2.6 was 0.98, confirming that the mean velocity profiles were logarithmic.

2.1.3.2 Water side friction velocity and roughness height

The mean streamwise velocity profile in the wind drift layer can be expressed as a velocity defect law in the form,

$$\frac{U_s - u(z)}{u_*} = \frac{1}{\kappa}\ln(-\frac{z}{z_o}) \tag{2.7}$$

where, U_s is the surface velocity, $u(z)$ is the mean stream wise velocity, u_* is the friction velocity on the waterside, z_o is the roughness height representing the depth where the velocity defect is zero. Performing a linear regression between the measured velocity data to Eq. 2.7, the average value of the correlation coefficient was found to be 0.99 which confirmed that the mean velocity profiles were logarithmic in the water. Elkamash (2005) obtained estimates of u^* directly from the slope of the regression equation for $100 < z^+ < 300$, where $z^+ = -u_* z/\upsilon$ is the dimensionless depth. In the next step he computed values of z_o from the intercept. The maximum error in u_* was estimated to be 10%. It should be noted that estimates of z_o were very sensitive to variations in U_s and u_*. For example, a 5% variation in the value of U_s may cause up to a 100% variation in z_o. The estimated values of the shear stress in water ($\tau = \rho_w u_*^2$ where, ρ_w is the water density) and roughness height (z_o) are given in Table 2.1 at all wind speeds for both clean and surfactant influenced water surfaces.

2.1.3.3 Turbulent Kinetic Energy Dissipation Calculations

The rate of dissipation of turbulent kinetic energy (ε) was estimated by Elkamash (2005) using the 'direct' method (Doron et al. 2001). Doron et al. (2001) stated that turbulent kinetic energy dissipation can be calculated using the velocity gradients computed from the DPIV data as follows,

$$\varepsilon = 3\nu\left\{\overline{\left(\frac{\partial u'}{\partial x}\right)^2} + \overline{\left(\frac{\partial w'}{\partial z}\right)^2} + \overline{\left(\frac{\partial u'}{\partial z}\right)^2} + \overline{\left(\frac{\partial w'}{\partial x}\right)^2} + 2\overline{\left(\frac{\partial u'}{\partial z}\frac{\partial w'}{\partial x}\right)} + \frac{2}{3}\overline{\left(\frac{\partial u'}{\partial x}\frac{\partial w'}{\partial z}\right)}\right\} \tag{2.8}$$

where, ε is the dissipation of turbulent kinetic energy, u' and w′ are the stream wise (x) and vertical turbulent velocities and v is the kinematic viscosity of water.

If microscale wave occurs, the instantaneous near surface velocities will be composed of mean, wave-induced and turbulent velocities (Benilov, Kouznetsov & Panin 1974). If the mean velocity component is subtracted from the instantaneous velocity, the resultant velocity (u_{wt}, w_{wt}) is comprised of the wave and turbulent velocity components. The wave component of velocity gradients are typically considerably smaller in magnitude than the corresponding turbulent velocity gradients. Elkamash (2005) found that the magnitudes of the wave velocity gradients were approximately 2.5 times smaller than the corresponding gradients in the turbulent velocities. Therefore, the wave velocity component can not be accurately separated from the turbulent component. However, Elkamash (2005) showed that it is possible to get a reliable estimate of ε using the gradients of u_{wt} and w_{wt} instead of the gradients of u' and w'. Therefore, the gradients of u_{wt} and w_{wt} were used to compute the dissipation of turbulent kinetic energy using Eq. 2.8. Elkamash (2005) also computed dissipation by two other methods, first by the inertial dissipation method and second by integrating the dissipation spectrum. He compared estimates of ε obtained using the direct method to the other two methods and found that on average the different methods agreed to within 10%. Therefore, the direct method was used by Elkamash (2005) in all subsequent analyses to estimate values of ε.

Vertical profiles of the ε are shown plotted at five wind speeds in Figure 2.5(a) for clean water surfaces and in Figure 2.5(b) for surfactant-influenced water surfaces. As the wind speed increased from 3.8 to 9.5 m s^{-1}, ε increased by a factor of 5 and 3.5 respectively for clean and surfactant-influenced water surfaces. The profiles in Figure 2.5

(a and b) show that ε decreased rapidly from the water surface down to a depth of approximately 3.0 cm. Underneath this layer ε decreased slowly with depth. Presence of surfactant did not significantly affect the values of ε at the lowest wind speed. However, at the highest wind speed presence of surfactant reduced both the values of ε and the rate of decay of ε with depth.

2.2 Data Preparation for GOTM

A public domain 1-D ocean turbulence model, the General Ocean Turbulence Model (GOTM) is used in this study. GOTM was developed in a modular form and it includes a module for simulating wave breaking. In GOTM the effect of breaking surface waves is parameterized by injecting turbulent kinetic energy at the ocean surface (Craig and Banner 1994). The flux of turbulent kinetic energy is parameterized as au^{*3}, where a is the wave energy factor and u_* is the water side friction velocity.

The inputs for the GOTM model are of three types; hydraulic, functional and geometric. The hydraulic inputs include surface shear stress, roughness length (z_{ot}) representing the minimum scale of turbulence at both the top and bottom boundaries, fluid density (ρ_w), molecular viscosity (μ), specific heat of water (C_p') and wave energy factor (a). The functional inputs are the grid spacing, time step (dt) and the time period to reach a steady state (T_m). Geometric inputs include water depth (H) and the water surface gradient or slope ($\delta h/\delta x$). When applying GOTM to the open ocean it is commonly assumed that $\delta h/\delta x = 0$. For a laboratory experiment in a wind wave tank a positive water surface gradient occurs i.e. depth increases in the direction of wind. The surface gradient ($\delta h/\delta x$) in a confined tank can be determined either by trial and error to

ensure that the net discharge, integrated over the vertical, is zero or by direct calculation from the surface shear. The direct calculation of $\delta h/\delta x$ is derived from a momentum balance considering the entire wind wave tank as a control volume. In this study $\delta h/\delta x$ is determined directly from surface shear (τ) as, $\delta h/\delta x = \tau\ (\rho_w Hg)^{-1}$, where τ is the water surface shear, ρ_w is the water density and H is the flow depth.

All of the required hydraulic (see Table 2.1) and geometric inputs (see section 2.1.1) for GOTM are available from Elkamash (2005) except for the roughness length z_{ot}.

2.2.1 Roughness Length (z_{ot}) Calculations

The one equation turbulence model used in GOTM is developed with the assumption of a linear variation of the turbulent length scale (l) with depth as originally suggested by Prandtl (1952) for the logarithmic velocity region. In a wind drift layer the equation for the turbulent length scale is,

$$l = \kappa(-z + z_{ot}) \tag{2.9}$$

where, z, the perpendicular distance from the air-water interface is positive upwards with its origin at the interface, κ is the von Karman's constant ($\kappa \approx 0.4$), z_{ot} is the roughness length representing the minimum scale of the turbulence at the boundary. Using the turbulent length scale distribution given by Eq. 2.9, the mean streamwise velocity profile can be expressed as a velocity defect law in the form,

$$\frac{U_s - u(z)}{u_*} = \frac{1}{\kappa}\ln\left(\frac{-z + z_{ot}}{z_{ot}}\right) \tag{2.10}$$

Performing a linear regression between the measured velocity data ($u(z)$) to ln ($-z$), the estimates of u^* can be obtained from the slope of the regression equation. Note that the

negative sign ($-z$) is needed since the depth is defined negative below the water surface. However, as the right hand side of Eq. (2.10) cannot be expanded to components of ln ($-z$) and a constant, it is not possible to compute values of z_{ot} from the intercept using the same technique as was used to compute z_o from Eq. 2.7 (see section 2.1.3.2). It should be noted that the roughness length z_{ot} and the roughness height z_o represent different parameters and therefore, should not be compared directly.

In this section a technique is described for estimating the friction velocity u_*, and roughness length z_{ot}, when profiles of the rate of dissipation of turbulent kinetic energy (ε) and the mean velocity (u) are available. The method is based on a one equation turbulence closure scheme developed by Mellor and Yamada (1974, 1982) with a turbulent length scale similar to the mixing length originally proposed by Prandtl (1952) (see Eq. 2.9). An expression for the turbulent length scale as a function of u_*, u and ε at the sea surface can now be derived. Using a dimensional argument the rate of dissipation (ε) is related to turbulent velocity scale (q) and length scale (l) as follows,

$$\varepsilon = \frac{q^3}{Bl} \tag{2.11}$$

where, $B = 16.6$ is a model constant (Mellor and Yamada 1974, 1982) and q is related to the turbulent kinetic energy density b, as $b = 0.5q^2$. The eddy viscosity (A) is proportional to the product of the turbulent length scale (l) and the turbulent velocity scale (q) and is expressed as,

$$A = lqS_M \tag{2.12}$$

where, $S_M = 0.39$ (Mellor and Yamada 1974, 1982). Outside the viscous sublayer but still sufficiently close to the wall, i.e. in the log layer the eddy viscosity A, can also be expressed as,

$$A = u_*^2 \left(\frac{\partial u}{\partial z} \right)^{-1} \tag{2.13}$$

where, u is the mean stream wise velocity. Substituting q and A from Eq. (2.12) and Eq. (2.13) respectively into Eq. (2.11) and rearranging gives,

$$l = \left[\frac{u_*^2}{(\partial u / \partial z)} \right]^{3/4} \varepsilon^{-1/4} \tag{2.14}$$

Equation (2.14) and Eq. (2.9) represent the same turbulent length scale (l) when applied in the logarithmic velocity region. Equating the right hand side of Eq. (2.14) to Eq. (2.9) gives,

$$\left[\frac{u_*^2}{(\partial u / \partial z)} \right]^{3/4} \varepsilon^{-1/4} = \kappa (-z + z_{ol}) \tag{2.15}$$

If the depth of flow (H) is sufficiently deep so that the lower boundary does not influence the flow, the zone $30 < z^+ < 300$ is a well defined logarithmic velocity region and Eq. (2.15) is applicable for the entire zone. However, for experiments conducted in a finite depth flume the law of the wall can not be applied below a certain depth as the effect of the lower boundary influences the flow. Therefore, the outer limit for the applicability of Eq. (2.15) should be scaled with respect to the flow depth (H). For pipe flow a reasonable assumption is that the linear distribution of length scale is valid for $z/R \leq 0.05$, where R is the pipe radius (Schlichting 1968).

The magnitudes of the velocity gradient at different depths are computed from the measured velocity profiles using a second order finite difference scheme. At a given depth measured values of the velocity gradient and ε are substituted into Eq. (2.15) and then the only unknowns in Eq. (2.15) are u_* and z_{ol}. Equation (2.15) can then be solved for an optimum set of values of u_* and z_{ol} which minimize the sum of the squares of the

differences between the left hand side and right hand side of Eq. (2.15) in the zone $z^+ > 30$ and $z/H < 0.05$. There are many available software tools to perform this function. In this study, the Excel solver tool is used to find the optimum u_* and z_{ol}. From an observation of the length scale profiles for all the wind speeds for both clean and surfactant affected water surface (see Figure A.1 to A.10 in Appendix A) it is found that for higher wind speeds the data points correspond to a slope of κ in the zone $z^+ > 30$ and $z/H < 0.05$. But for lower wind speeds for both clean and surfactant affected water surface the data points correspond to a slope of κ up to $z/H \sim 0.035$. Therefore, in the present study Eq. (2.15) is conservatively assumed to be valid in the region $z^+ > 30$ to $z/H < 0.035$ for all the wind speeds and the optimum set of values of u_* and z_{ol} are determined solving Equation (2.15) in this zone. The estimated values of the friction velocity u_*, shear stress ($\tau_{ol} = \rho u_*^2$), roughness length z_{ol} and the ratio between z_{ol} and the dominant surface wave length (λ) for clean and surfactant affected surfaces at all wind speeds are given in Table 2.2.

The uncertainty in these estimates of u_* and z_{ol} is determined using a second order sensitivity analysis method (Kennedy and Neville 1976). In this method the input variables of a system are described by probability density functions (PDF) and the extreme values are estimated by sampling from the PDF's for. Simulations are then performed using the extreme value input variables and a distribution of the output variable is created. The obtained distribution of the output variable is used to estimate the standard deviation and hence the statistical error in the output (Kennedy and Neville 1976).

The velocity gradient and dissipation of turbulent kinetic energy are the two input variables used in estimating u_* and z_{ol} by the length scale method. Elkamash (2005) estimated that the uncertainty in ε was ~ 30% because of the finite resolution of the PIV measurement (Tennekes and Lumley 1972). The uncertainty in the velocity gradient is estimated using a first order second moment uncertainty analysis method (Kline and McClintock 1953) (see Appendix A). This analysis predicted that the uncertainty in the computed velocity gradient is 3.5%.

Using the estimated uncertainties in the input variables ($\partial u/\partial z$ and ε), a uniform distribution of $\partial u/\partial z$ and ε are assumed. A profile wise 3.5% variation in the velocity gradient is assumed instead of a point wise variation. This is somewhat conservative since for a point wise variation, the error caused by $\partial u/\partial z$ at one grid point tends to cancel the error in the subsequent grid point. By sampling from the distribution of $\partial u/\partial z$ and ε for the extreme values, a distribution of the output variables (u_* and z_{ol}) are determined using Eq. 2.15 and the method described in the previous section. The distribution of u_* and z_{ol} are used to find the standard deviation for the individual variable. The maximum uncertainty in the estimates of u_* and z_{ol} are estimated to be 4.5% and 18%, respectively, considering all the wind speeds for clean and surfactant affected water surfaces.

2.2.2 Results from the length scale method and discussion

Equation 2.14 is used to compute the turbulent length scale profiles for different wind speeds using the measured profiles of dissipation and mean velocity. A typical plot of the variation of the dimensionless length scale, $l^+ = u_* l/\nu$ with respect to the

dimensionless depth, $z^+ = -u_* z/\nu$ is shown in Figure 2.6 for a wind speed of 7.9 m s^{-1} and a clean water surface. Length scale profiles for all the wind speeds for both clean and surfactant affected water surface are plotted in Figure A.1 to A.10 in Appendix A. Three distinct zones or layers can be identified in Figure 2.6. The first zone appears close to the surface where the length scale is found to be zero. The second zone starts at $z^+ \sim 30$ and is maintained up to approximately $z/H < 0.035$. In this zone there is a linear relationship between l and z and since the analysis presupposes a linear variation of l against z with slope κ, the slope of this relationship is 0.4. For the 10 sets of data including the clean surface and surfactant contaminated water surface experiments the l^+ values are found to be well correlated with z^+ with a mean correlation coefficient of 0.986. This indicates that the linear relationship between l and z agrees with a slope κ. The third zone occurs at $z/H > 0.035$ where the effect of the lower boundary starts to influence the flow and the relationship between l and z is no longer linear.

An interesting observation can be made in the zone close to the surface. The present study is based on measurements made at $z^+ \geq 10$. However, extrapolating the turbulent length scale data into the zone $z^+ < 10$, the turbulent length scale is found to be approximately zero in this zone (see Figure 2.6). This trend in turbulent length scale is observed for the 10 sets of data for both clean and surfactant contaminated water surfaces (see Figure A.1 to A.10, Appendix A). For the highest wind speeds the turbulent length scale is found to be zero for the zone $z^+ < 20$ (see Figure A.5 and A.10, Appendix A) but for the lowest wind speeds the turbulent length scale is zero for the zone $z^+ < 10$ (see Figure A.1 and A.6, Appendix A). Therefore, conservatively it can be assumed that for wind drift boundary layer the turbulent length scale is approximately zero into the zone z^+

< 10. This indicates that the thickness of the laminar sub-layer δ_v, beneath a wind driven water surface may be approximately twice as thick as the viscous sub-layer formed over a solid wall.

Estimates of the shear stress obtained using the length scale method (τ_{ol}) are compared with the estimates computed by Elkamash (2005) using the velocity defect profile method (τ_{ov}) in Figure (2.7a) and (2.7b) for clean and surfactant contaminated water surfaces respectively. On clean water surfaces at the two lower wind speeds ($U <$ 6.2 m s^{-1}) (Figure 2.7a) τ_{ol} is smaller than τ_{ov} by 3% to 13% while at the three higher wind speeds ($U \approx 6.2 - 9.5$ m s^{-1}) τ_{ol} is greater than τ_{ov} by 22% to 38%. Fig. 2.7(b) shows that on a contaminated water surface at the four lower wind speeds ($U <= 8$ m s^{-1}) τ_{ol} is smaller than τ_{ov} by 3.5% to 30% and at the highest wind speed ($U = 9.8$ m s^{-1}) τ_{ol} is greater than τ_{ov} by 7%. On average the shear stress obtained using the length scale method (τ_{ol}) agree with the stress using the velocity defect profile method (τ_{ov}) by 38% and by 30% for clean and surfactant influenced surface respectively.

The values of z_{ot} determined using the length scale method are plotted as a function of U in Figure 2.8. For clean water surface z_{ot} decreases initially as U increases but remains approximately constant at 0.3cm for $U > 5$ m s^{-1}. For surfactant contaminated water surfaces the roughness length follows a relatively monotonic trend with U and decreases from a value of 0.5 cm to 0.1 cm as U decreases from 4 to 10 m s^{-1}. For the similar wind speed the values of z_{ot} are generally smaller in the presence of a surfactant (see Figure 2.8). The ratio of the roughness length (z_{ot}) to the dominant wave length (λ) is plotted as a function of wind speed (U) in Figure 2.9. The ratio z_{ot} / λ decreases with U for both clean and surfactant contaminated surfaces following a similar trend. It decreases

from 0.12 to 0.02 as the wind speed increases from 4 to 10 m s^{-1}. A power law function was fitted to the data in Figure 2.9 and the resulting regression equation is given by,

$$z_{ot} / \lambda = 1.832 U^{-2} \tag{2.16}$$

where, the wind speed U is in m s^{-1} and the correlation coefficient is equal to 0.86. These z_{ot} / λ values are consistent with Sullivan et al. (2004) and Craig (1996). Sullivan et al. (2004) found that z_{ot} / λ varied from 0.04 to 0.06 and Craig (1996) found this ratio was 0.16.

The power law relation between z_{ot} / λ and U developed in Figure 2.9 is applicable for very young waves as the wave age of experimental data was less than 2. It may be possible to develop a similar relationship for older waves using profiles of $u(z)$ and $\varepsilon(z)$ measured in the field. Making simultaneous measurements of $u(z)$ and $\varepsilon(z)$ in the field would be very challenging but these measurements are currently feasible since Agrawal et al. (1992) describe measurements of this type that they carried out in Lake Ontario. A correlation relating z_{ot} / λ and U developed from field data could then be used to estimate z_{ot} from measurements of λ and U, which are both relatively easy to measure compared to $u(z)$ and $\varepsilon(z)$.

The value of von Karman's constant κ is assumed to be 0.40 in the length scale method. This assumption is partially based on the hypothesis that a neutral aqueous boundary layer is analogous to a neutral solid wall boundary layer where it has been established that $\kappa \approx 0.4$. Cheung and Street (1988) presented experimental evidence from the laboratory that in the wind drift layer the value of κ might depart from this standard value due to the influence of wave breaking. Sullivan et al. (2004) predicted that κ was constant and equal to 0.4 using a stochastic model of the effects of wave breaking on the

oceanic boundary layer. Siddiqui and Loewen (2007) concluded that Cheung and Street (1988) may have overestimated the value of κ. However, it is evident that there is still some uncertainty regarding the value of κ in the wind drift layer, this uncertainty will only be reduced by additional research.

The uncertainty analysis showed that errors in the estimates of u_* and z_{ot} are 4.5% and 18% respectively using the length scale method whereas Elkamash (2005) found that the error in u_* was 10% using the velocity defect method. The length scale method provides estimates of u_* that are twice as accurate compared to the velocity defect profile method. These estimates are more accurate because the method utilizes measured profiles of both the mean velocity and the rate of dissipation of turbulent kinetic energy. Therefore, u_* values estimated using the length scale method are used in this study for the turbulence model development.

2.3 Data used for Model Validation

The performance of the turbulence model will be evaluated using a comparison of the model predictions with experimental data obtained from a source different from the one used for calibration of the model. Experiments on microscale breaking waves were performed in the wind wave tank at the NASA Air–Sea Interaction Research Facility of the Observational Science Branch at NASA Goddard Space Flight Center/Wallops Flight Facility, VA, in April–May 2004. The test section of the wind wave tank was 18.29 m long, 1.22 m high and 0.91 m wide, the mean water depth was 0.76 m. Experiments were conducted on microscale breaking waves at five different wind speeds ranging from approximately 4.0 to 11.0 m s^{-1} and at fetches of 4.8, 8.8 and 12.4 m. The wind wave tank

had a circulating flow which caused the mean velocity to increase by 0.07 m s^{-1} over the depth. The average wave age (C_p/u_{*a}), ratio of the wave phase speed (C_p) to the friction velocity in air (u_{*a}) for fetches of 4.8, 8.8 and 12.4 m were 1.0, 1.1 and 1.76 respectively. Measured profiles of the rate of dissipation of turbulent kinetic energy and the mean velocity are plotted in Figure 2.10(a) and 2.10(b) at a typical wind speed of 6.8 m s^{-1}. Figure 2.10(b) shows that the mean velocity decreased rapidly from the water surface down to a depth of approximately 3.0 cm. Underneath this layer u decreased slowly with depth. It is observed that the dissipation of turbulent kinetic energy decreases monotonically with depth (Figure 2.10(a)).

The bulk gas transfer velocity for NASA 2004 experiments was determined for SF_6 and He diffusing through clean water using the conservative mass balance method described previously in section 2.1.2.2. In Figure 2.11, estimates of the gas transfer velocity k_{600} (transfer velocity for S_c = 600 for CO_2) are plotted as a function of water side friction velocity u_*. This gas transfer velocity data will be used to evaluate the prediction of the gas transfer parameterization.

The performance of the gas transfer parameterization for field situations will be investigated by comparing the model predictions with the field data obtained from Frew et al. (2004). As a part of the Coastal Ocean Processes (CoOP) program they made observations of wind stress and gas transfer velocity in coastal and offshore waters south of Cape Cod, New England, in July 1997. The gas transfer velocities were computed from aqueous heat transfer velocities derived from infrared imagery and bulk heat flux estimates (Frew et al. 2004). In Figure 2.12, the CoOP97 estimates of gas transfer velocity k_{660} (transfer velocity for S_c = 660 for CO_2 in sea water at 20°C) are plotted as a

function of water side friction velocity u_* (courtesy of Nelson Frew, 2007). Frew et al. (2004) wrote that the large scatter in this field data was a result of a wave field dependent transition between limiting transport regimes.

Table 2.1: Values of shear stress in air (τ_a), roughness height in air (z_{oa}), shear stress in water (τ) and roughness height in water (z_o) determined from the velocity profile method. Values are determined for both clean and surfactant affected water surfaces at various wind speeds (U).

Clean					Surfactant				
U	τ_a	z_{oa}	τ	z_o	U	τ_a	z_{oa}	τ	z_o
(m s^{-1})	(N m^{-2})	(cm)	(N m^{-2})	(cm)	(m s^{-1})	(N m^{-2})	(cm)	(N m^{-2})	(cm)
3.8	0.041	0.0053	0.023	0.0270	3.9	0.041	0.0042	0.033	0.0107
4.9	0.103	0.1040	0.029	0.0030	4.9	0.078	0.0067	0.036	0.0037
6.2	0.206	0.0490	0.032	0.0011	6.2	0.190	0.0400	0.041	0.0006
8.0	0.440	0.1000	0.047	0.0028	8.2	0.290	0.0270	0.057	0.00031
9.5	0.480	0.0470	0.074	0.0029	9.8	0.310	0.0091	0.064	0.00036

Table 2.2: Values of the water side friction velocity (u_*), shear stress (τ_{ol}), roughness length (z_{ol}) determined using the length scale method and z_{ol}/λ, the ratio of the roughness length (z_{ol}) to the dominant surface wave length (λ). Values are listed for both clean and surfactant affected water surface at various wind speeds (U).

	Clean					Surfactant			
U	u_*	τ_{ol}	z_{ol}	z_{ol}/λ	U	u_*	τ_{ol}	z_{ol}	z_{ol}/λ
(m s^{-1})	(m s^{-1})	(N m^{-2})	(cm)		(m s^{-1})	(m s^{-1})	(N m^{-2})	(cm)	
3.8	0.0045	0.0202	0.69	0.140	3.9	0.0047	0.023	0.49	0.096
4.9	0.0053	0.0280	0.32	0.048	4.9	0.0053	0.028	0.40	0.060
6.2	0.0063	0.0390	0.31	0.036	6.2	0.0059	0.035	0.31	0.035
7.9	0.0081	0.0650	0.40	0.035	8.2	0.0074	0.055	0.26	0.023
9.5	0.0097	0.09400	0.32	0.021	9.8	0.0084	0.069	0.10	0.0067

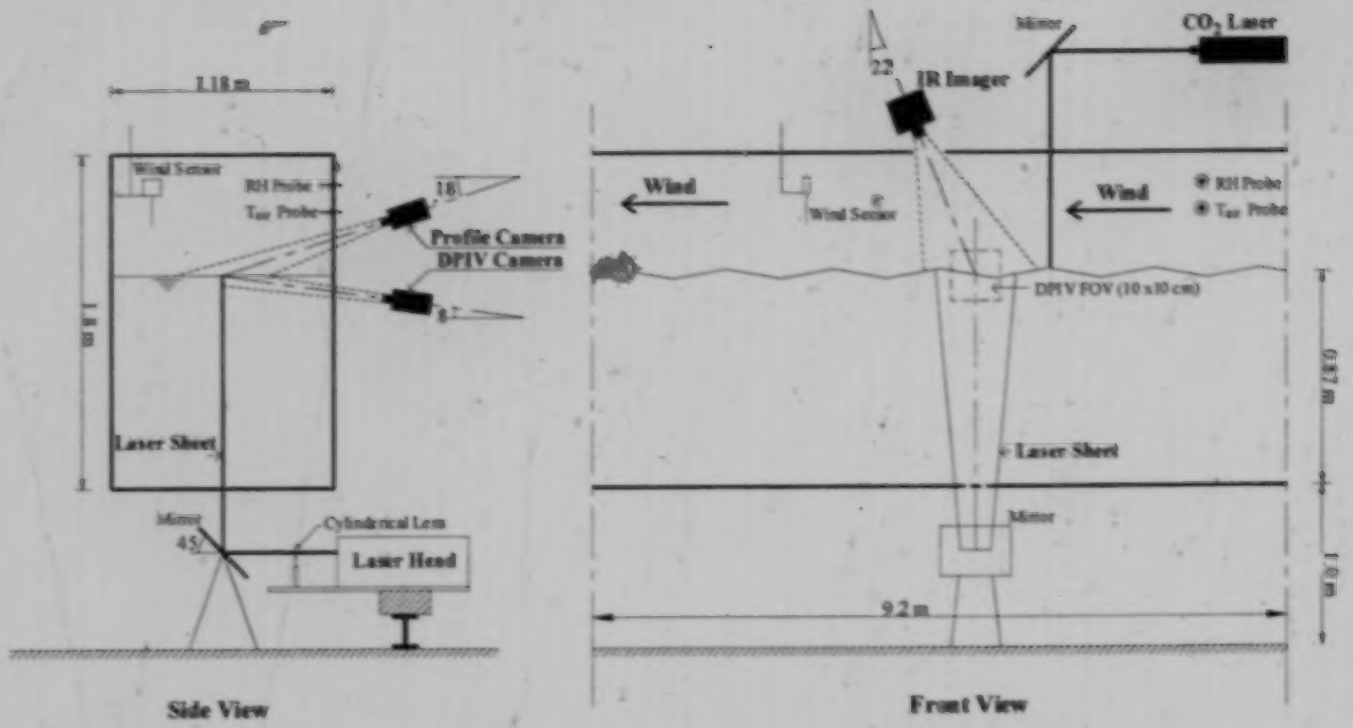

Figure 2.1 Schematics of Experimental setup (not to scale) (From Elkamash 2005)

(a)

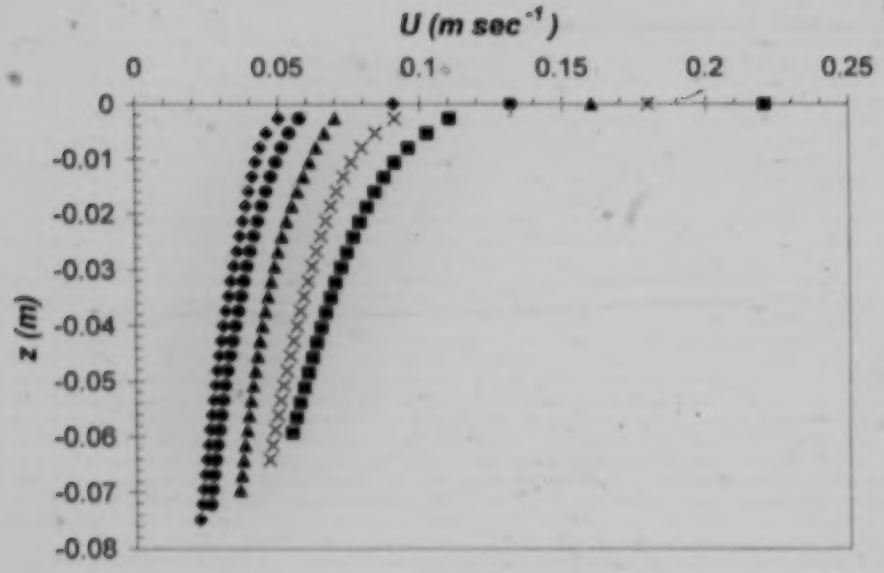

(b)

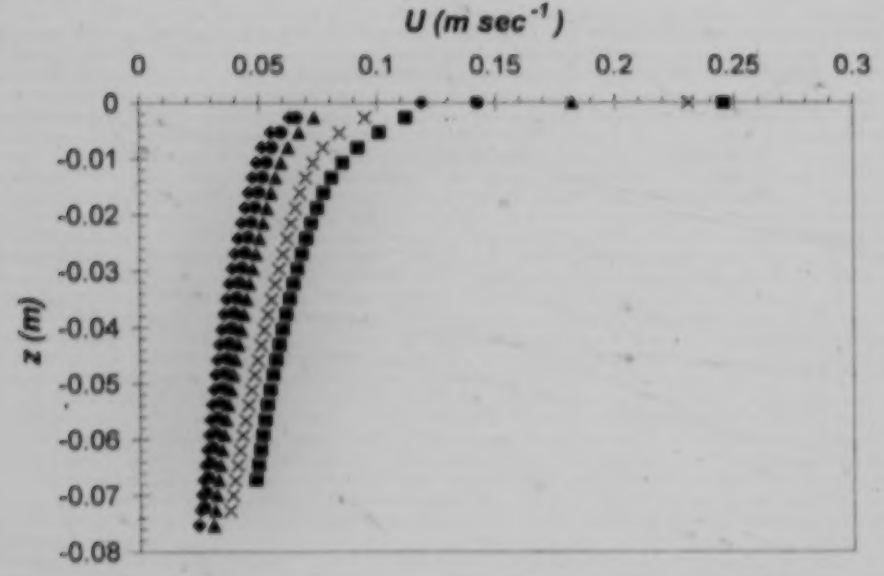

Figure 2.2: Plot of mean velocity (U) versus depth (z) (a) for clean water surface and (b) for surfactant contaminated surface. ◆, = 3.8 m·s^{-1}; ●, = 4.9 m·s^{-1}; ▲, = 6.2 m·s^{-1}; x, = 8.0 m·s^{-1}; ■, = 9.6 m·s^{-1}.

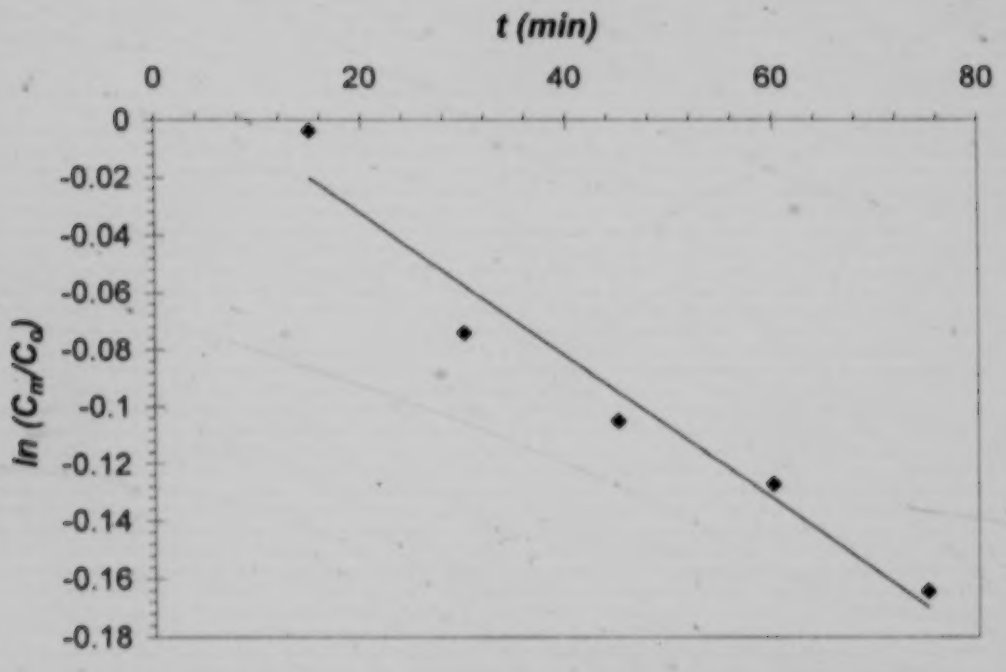

Figure 2.3: Plot of $\ln(c_m/c_o)$ versus time, (t) for SF_6 diffusing through clean water surface at a wind speed of 4.9 m sec^{-1}. ◆,= experimental data points and solid line is the linear regression line fitted through the data points.

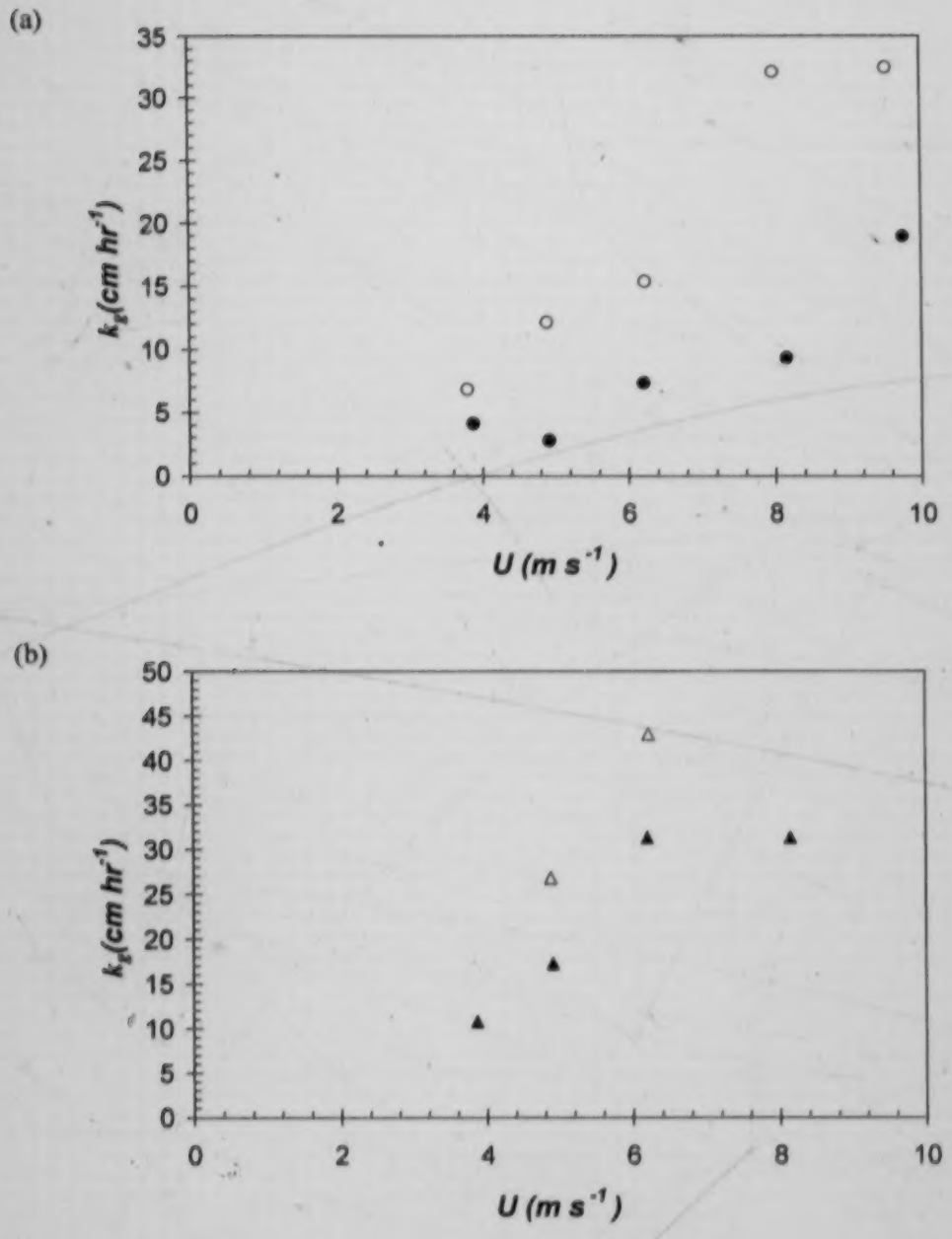

Figure 2.4: Plot of gas transfer velocity (k_g) versus wind speed (U) (a) for SF_6 and (b) for He. ○, = clean surface experiments and ●, = surfactant affected surface experiments for SF_6 diffusing through water surface. Δ , = clean surface experiments and ▲, = surfactant affected surface experiments for He diffusing through water surface.

(a)

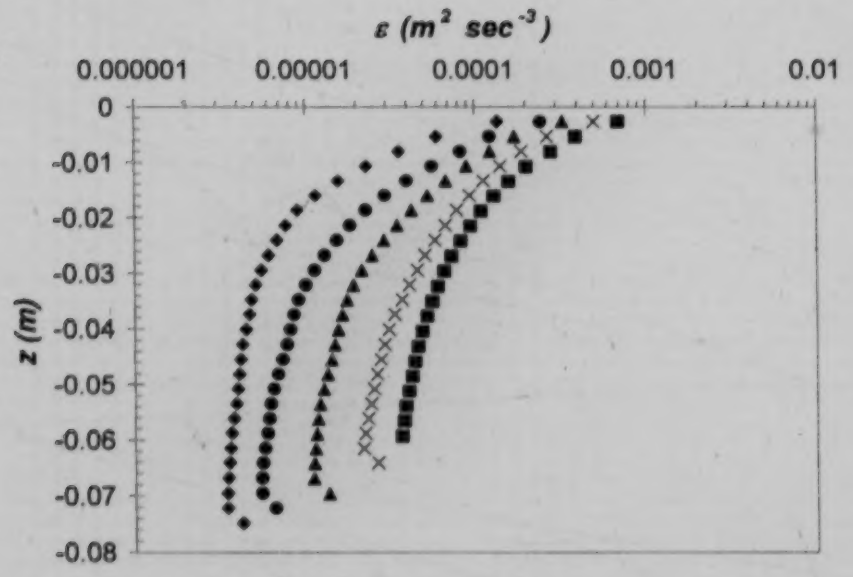

(b)

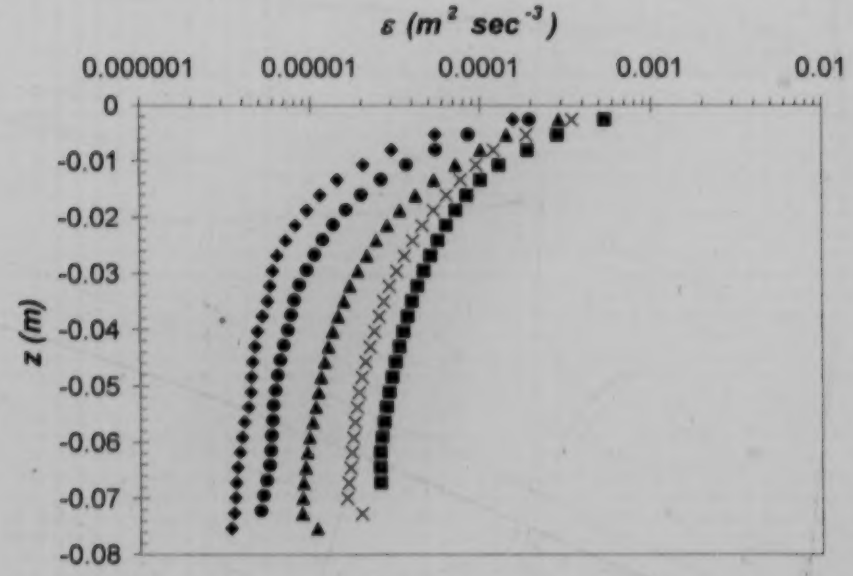

Figure 2.5: Plot of dissipation (ε) versus depth (z) (a) for clean water surface and (b) for surfactant contaminated surface. ◆, = 3.8 $m \cdot s^{-1}$; ●, = 4.9 $m \cdot s^{-1}$; ▲, = 6.2 $m \cdot s^{-1}$; x, = 8.0 $m \cdot s^{-1}$; ■, = 9.6 $m \cdot s^{-1}$.

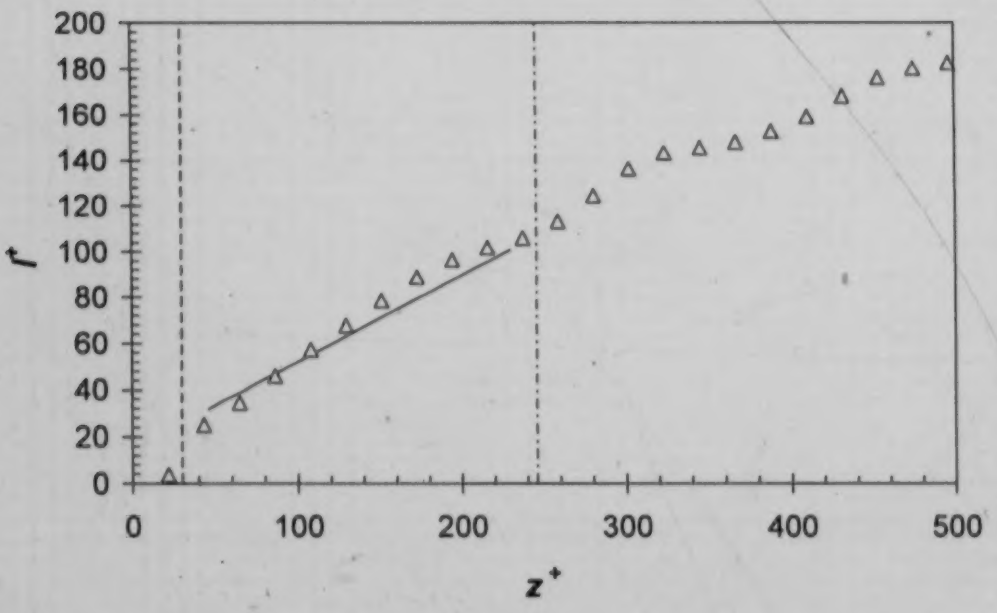

Figure 2.6: Plot of the non-dimensional turbulent length scale (l^+) versus non-dimensional depth (z^+) at a wind speed of 7.9 m s^{-1} on a clean water surface. Δ = experimental data points. The solid line is a second order least square regression line fitted between $z^+ > 30$ and $z/H < 0.035$, the dashed line corresponds to the non-dimensional depth $z^+ = 30$, the dashed-dotted line corresponds to the non-dimensional depth $z/H = 0.035$.

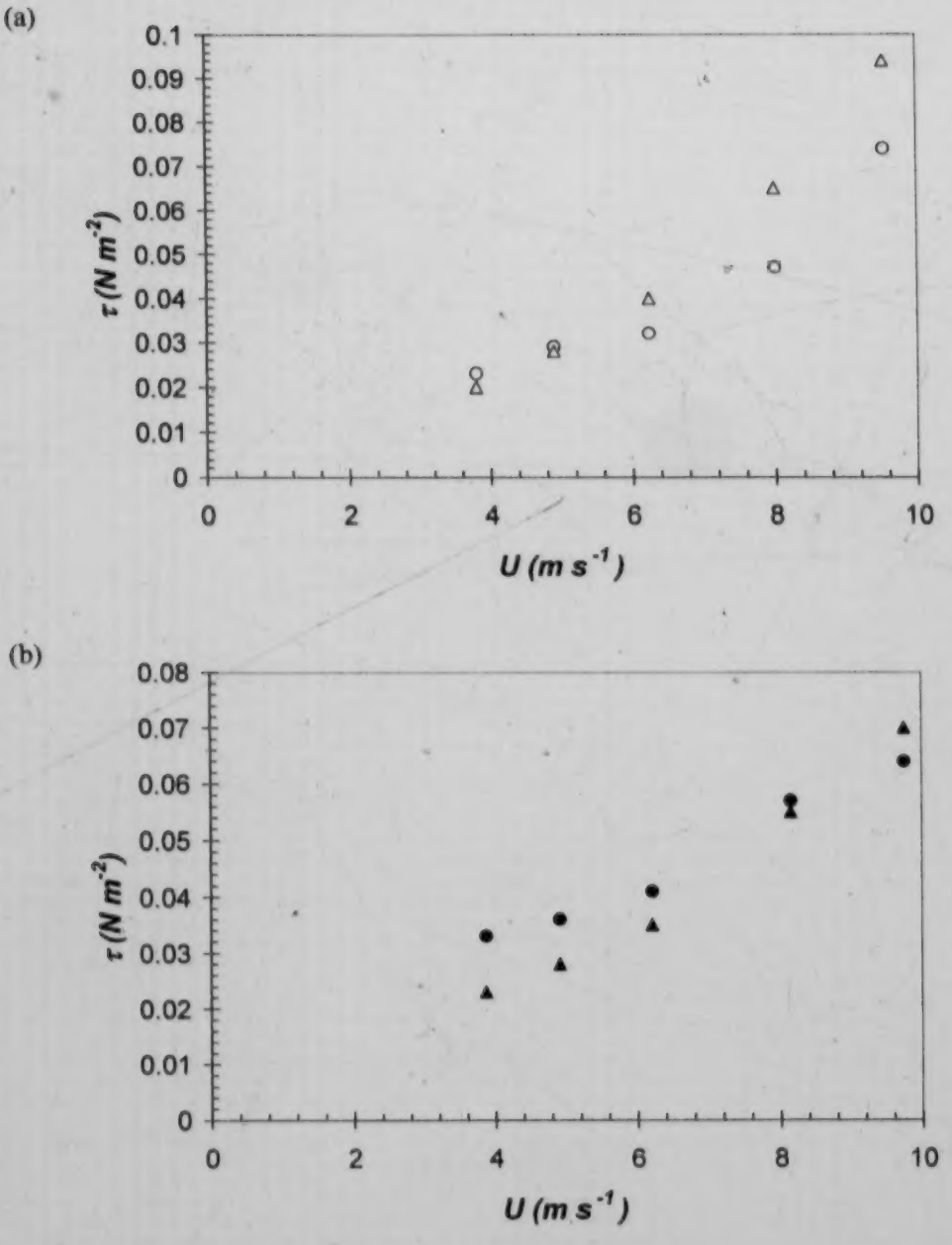

Figure 2.7: Plot of the shear stress (τ) versus the wind speed (U) (a) Clean water surface, ○ = τ_{ov} (the shear stress estimated using the velocity profile method) and Δ = τ_{ol} (the shear stress estimated using the length scale method). (b) Surfactant influenced water surface, ● = τ_{ov} and ▲ = τ_{ol}.

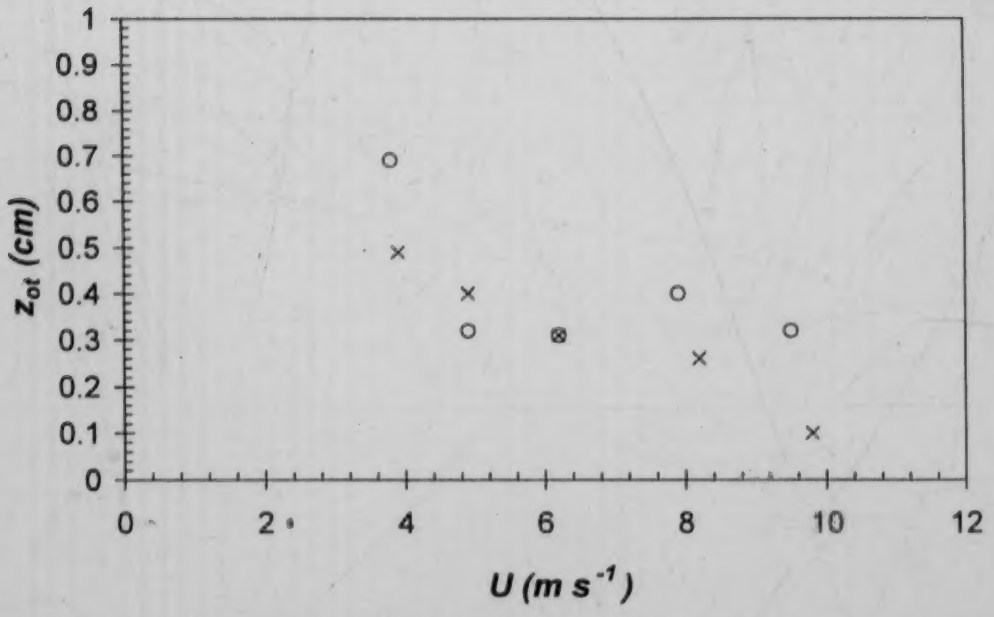

Figure 2.8: Plot of the roughness length (z_{ot}) versus the wind speed (U). ○ = clean water surfaces and × = surfactant influenced water surfaces.

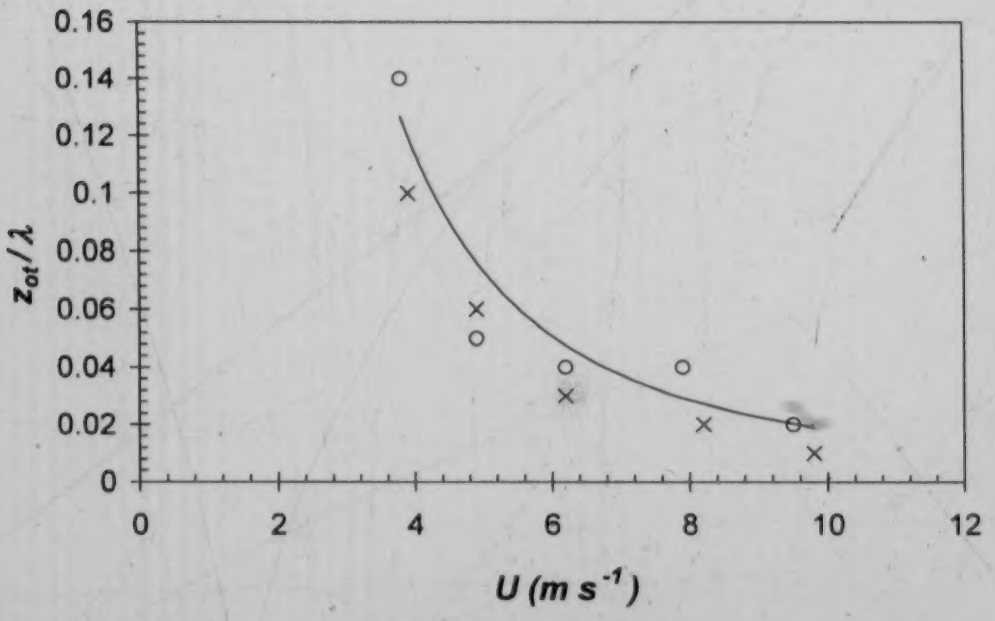

Figure 2.9: Plot of the ratio of the roughness height to the dominant wave length (z_{ot} / λ) versus wind speed (U). ○ = clean water surfaces; × = surfactant influenced water surfaces and the solid line is the regression power law fitted to the data points. The regression equation is $z_{ot} / \lambda = 1.83 U^{-2}$ with a correlation coefficient of 0.86.

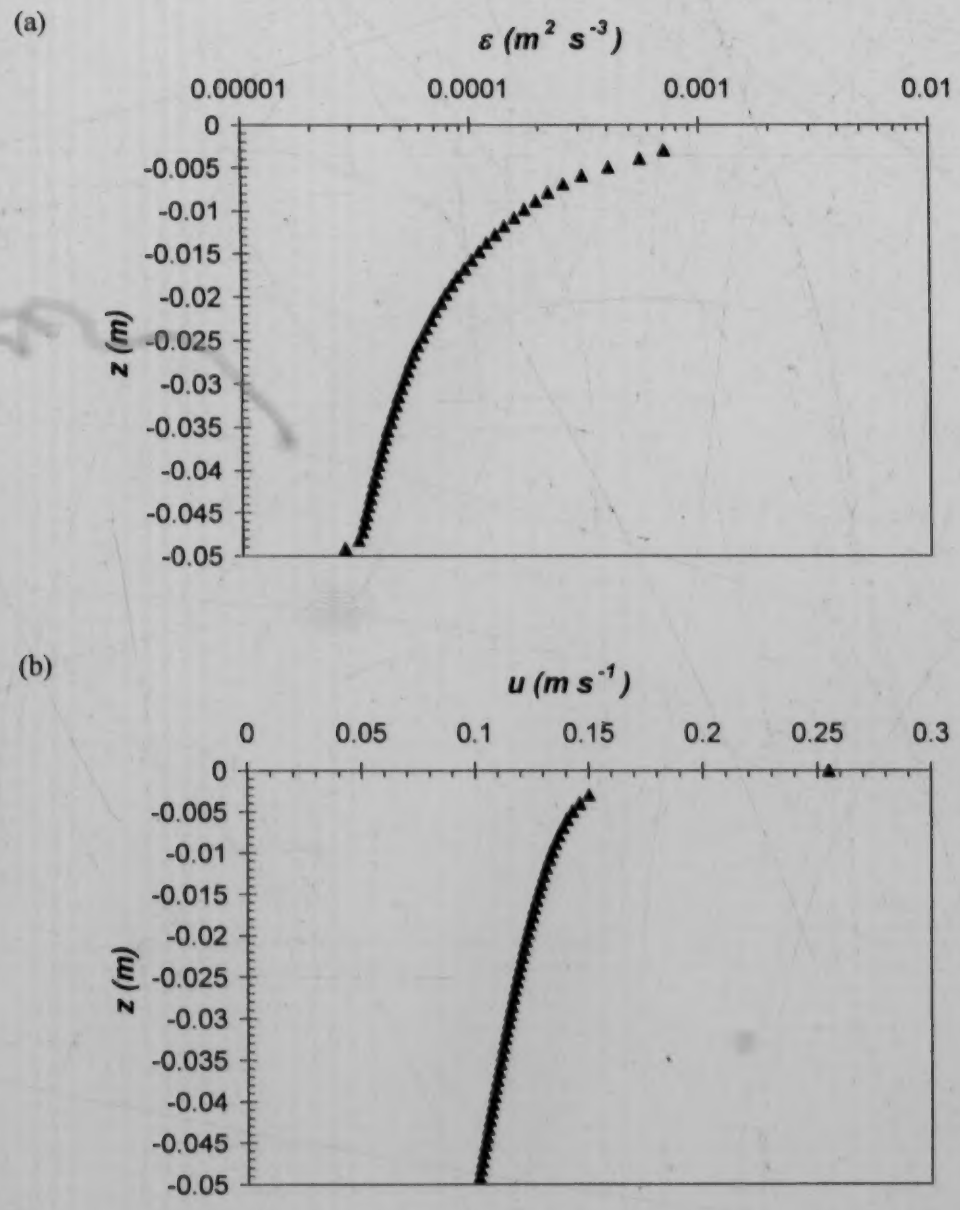

Figure 2.10: The profiles of measured (a) dissipation (ε) and (b) velocity (u) for wind speed of 6.8 m s^{-1} on clean water surface, ▲are experimental data points.

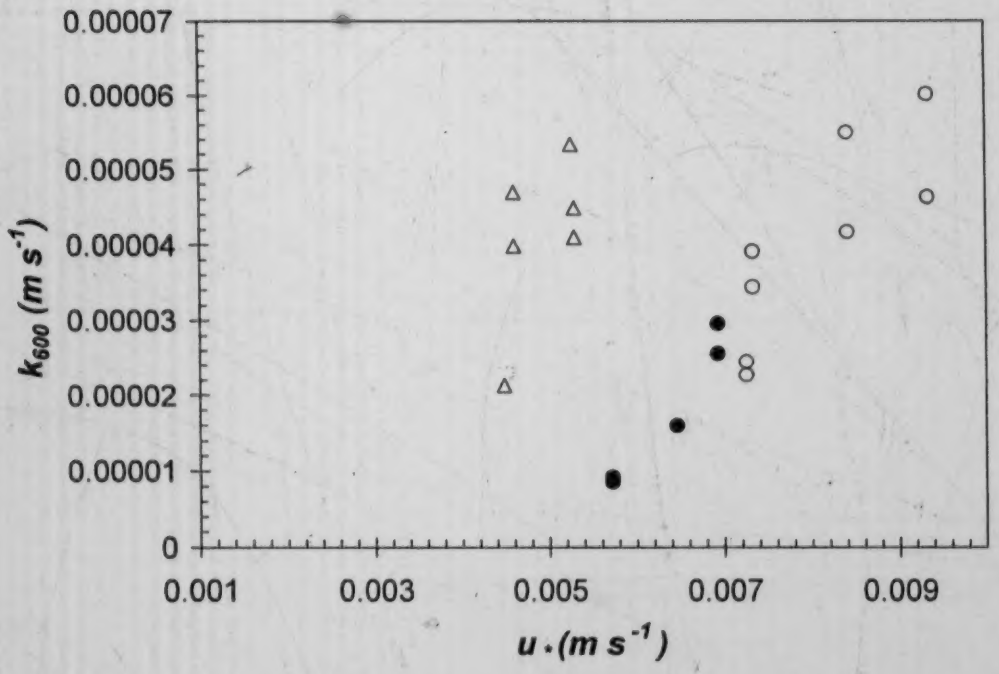

Figure 2.11: Plot of gas transfer velocity (k_{600}) for S_c = 600 versus water side friction velocity (u_*). Data points are measurements of experimental data at the NASA Air–Sea Interaction Research Facility, ○, = fetch 4.8, ●, = fetch 8.8 and Δ , = fetch 12.4 m.

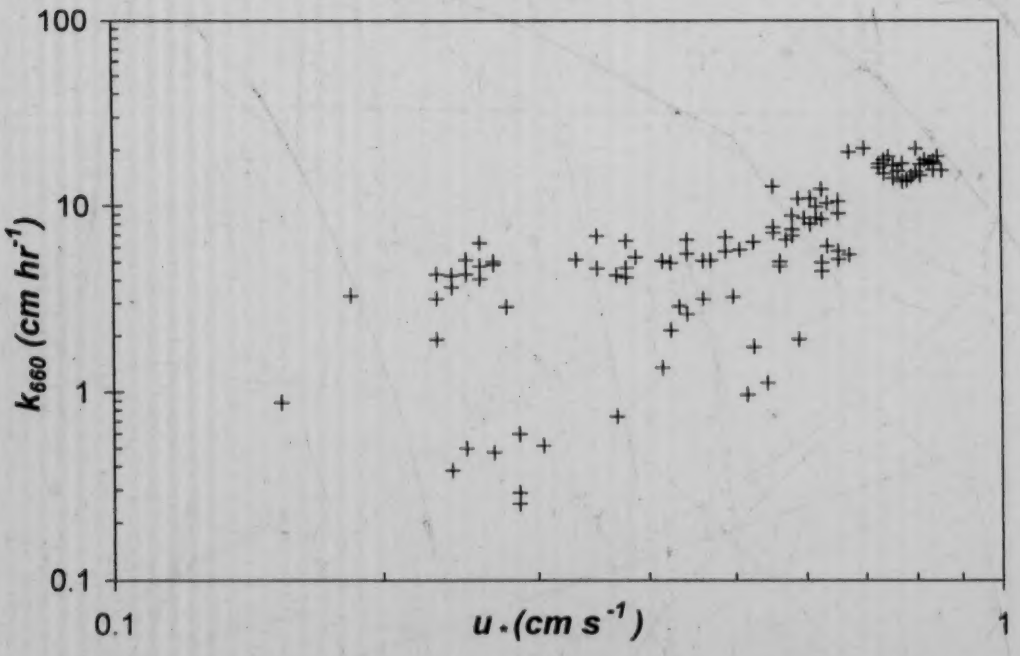

Figure 2.12: Plot of gas transfer velocity (k_{660}) for S_c = 660 for CO_2 in sea water at 20°C versus water side friction velocity (u_*). +, = CoOP97 measurements of field data (courtesy of Nelson Frew).

2.4 References

Agrawal, Y. C., Terray, E. A., Donelan, M. A., Hwang, P. A., Williams, A. J., Drennan, W. M., Kahma, K. K., Kitaigorodskii, S. A. (1992). "Enhanced dissipation of kinetic-energy beneath surface-waves." *Nature*, 359 (6392), 219-220.

Asher, W. E., Karle, L. M., Higgins, B. J., Farley, P. J., Monahan, E. C. and Leifer, I. S. (1996). "The influence of bubble plumes on air-seawater gas transfer velocities." *J. Geophys. Res.*, 101, 12,027 - 12,041.

Atmane, M. A., Asher, W. E. and Jessup, A. T. (2004). "On the Use of the Active Infrared Technique to Infer Heat and Gas Transfer Velocities at the Air-Water Free Surface." *Journal of Geophysical Research*, Vol. 109(C8), C08S14, pp.1-15.

Benilov, A. Y., Kouznetsov, O. A. and Panin, G. N. (1974). "On the analysis of wind-induced disturbances in the atmospheric turbulent surface layer." *Boundary-Layer Met*, 6, 269-285.

Bye, J. A. T. (1967). "The wave-drift current." *Journal of Marine Research*, 25, 95–102.

Cheung, T. K. and Street, R. L. (1988). "The turbulent layer in the water at an air-water interface." *Journal of Fluid Mechanics*, 194, 133-151.

Burchard, H. and Bolding, K. (2001). "Comparative analysis of four second-moment turbulence closure for the oceanic mixed layer.," *Journal of Physical Oceanography*, 31(8), 1943-1968.

Craig, P.D. and Banner, M.L. (1994). "Modeling wave-enhanced turbulence in the ocean surface layer." *Journal of Physical Oceanography*, 24, 2546-2559.

Craig, P.D. (1996). "Velocity Profiles and Surface Roughness Under Breaking Waves." *Journal of Geophysical Research*, 101, 1265-1277.

Doron, P., Bertuccioli, L., Katz, J. and Osborn T. R. (2001). "Turbulence characteristics and dissipation estimates in the coastal ocean bottom boundary layer from PIV data." *Journal of Physical Oceanography*, (31), 2108-2134.

Elkamash, M. K. M. (2005). *The effect of surfactants on microscale wave breaking and the aqueous boundary layer*, Ph. D. thesis, University of Alberta, Edmonton, Alberta, Canada.

Elkamash, M. K. and Loewen, M. R. (2004). "Air-sea gas transfer and turbulence for clean and surfactant contaminated surfaces." *Proceedings of the 1st Water and environment Specialty Conference, 32nd Annual Conference,* Canadian Society for Civil Engineering, Saskatoon, Saskatchewan, Canada.

Elkamash, M. K. and Loewen, M. R. (2007). "Laboratory studies of stress partitioning at wind-driven air-water interfaces." Unpublished manuscript.

Frew, N. M., Bock, E. J., Schimpf, U., Hara, T., Haußecker, H., Edson, J. B., McGillis, W. R., Nelson, R. K., McKenna, S. P., Uz, B. M., and Jähne, B. (2004). "Air-sea gas transfer: Its dependence on wind stress, small-scale roughness, and surface films." *J. Geophys. Res.*, 109, C08S17.

Kennedy, J. B. and Neville, A. M. (1976). *Basic statistical methods for engineers and scientists.* 2nd Edition, Harper and Row, NY, USA.

Kline, S.J. and McClintock, F. A. (1953). "Describing uncertainties in single-sample experiments." *Mech. Engrg., ASME*, (75), 3-8.

Liss, P.S. (1973). *Deep Sea Res., 20*, 221-238.

Mellor, G. L. and Yamada, T. (1982). "Development of a turbulence closure-model for geophysical fluid problems." *Reviews of Geophysics*, 20 (4), 851-875.

Mellor, G. L. and Yamada, T. (1974). "Hierarchy of turbulence closure models for planetary boundary-layers." *Journal of the Atmospheric Sciences*, 31(7), 1791-1806.

Nezu, I. and Nakagawa, H. (1993). *Turbulence in Open-Channel Flows*. Balkema, Rotterdam.

Prandtl L. (1952). *Essentials of fluid mechanics*. Blackie and sons. 452.

Schlichting, H. (1968). *Boundary-layer theory*, 6th Edition, McGraw-Hill Book Company, NY, USA.

Siddiqui, M. H. K. and Loewen, M. R. (2007). "Characteristics of the wind drift layer and microscale breaking waves." *Journal of Fluid Mechanics*, 573, 417-456.

Siddiqui, M. H. K., Loewen, M. R., Asher, W. E. and Jessup, A. T. (2004). "Coherent structures beneath wind waves and their influence on air-water gas transfer." *Journal of Geophysical Research*, 109(C3), C03024, 1-14.

Sullivan, P. P., Mcwilliams, J. C., And Melville, W. K. (2004). "The Oceanic Boundary Layer Driven by Wave Breaking with Stochastic Variability. Part1. Direct Numerical Simulations." *J. Fluid Mech.* 507, 143-174

Chapter 3: Turbulence model for microscale breaking waves

3.1 Introduction

Climate change is one of the most pervasive threats to our planet. Accurate forecasts of global warming are essential to policy makers as they plan mitigation strategies and negotiate agreements to limit fossil fuel generated carbon dioxide (CO_2).

Prediction of the rate of CO_2 transfer between the ocean and atmosphere is important for the study of global warming. In global climate models this transfer rate is typically estimated using empirical equations that relate the average wind speed to the gas transfer rate (Duce et al. 2001). Using these equations estimates of the CO_2 transfer rate between the ocean and the atmosphere can vary by up to 300% depending on the equation used. This discrepancy is caused by poor understanding of the physics regulating the gas transfer process. A model which is based on more realistic physics of the transfer process will give improved predictions of the CO_2 transfer rate and ultimately lead to better forecasts of global warming. Therefore, the objective of this study is to develop a turbulence model that can predict gas transfer rates accurately at air-water interfaces populated by young steep wind waves.

The scale of ocean waves can vary from millimeters to several hundreds of meters. Surface tension forces become important for small-scale waves and this may inhibit air entrainment when the wave breaks. Waves that break without entraining air are referred to as the microscale breaking waves. When larger scale waves break a whitecap typically forms because of the large number of air bubbles that are entrained. Most previous attempts at modeling ocean turbulence only account for the turbulence generated by large scale breaking waves (Craig and Banner 1994). However, recent

studies suggest microscale breaking waves occur much more frequently and cover a larger fraction of ocean surface compared to large scale breaking waves (Siddiqui et al. 2001; Zappa et al. 2001; Holthuijsen and Herbers 1986). Laboratory experiments have shown that more than 80% of the short wind waves were microscale breaking waves at wind speeds greater than 7.4 m s^{-1} (Loewen and Siddiqui 2006). Peirson and Banner (2003) found that for a wind speed range of 4.8 to 8.1 m s^{-1} approximately 40 to 70% waves were microscale breaking.

Siddiqui et al. (2001) found that the fraction of the surface area covered by microscale breaking waves is correlated with the turbulent properties of the flow such as near surface vorticity. They found that the wakes produced by microscale breaking waves are regions of high near surface vorticity that are responsible for enhancing the rate of air-water heat transfer. The depth averaged dissipation increases by 1.4 to 2.3 times and the near surface dissipation increases by 3-4 times beneath microscale breaking waves compared to beneath a non-breaking wave (Loewen and Siddiqui 2006, Siddiqui and Loewen 2007). This increased dissipation is the result of wakes comprised of intense turbulence that are generated by microscale breaking waves (Siddiqui et al. 2004). Zappa et al. (2001, 2004) measured the local transfer velocities inside and outside the wakes generated by microscale breaking waves and found that on average the transfer velocity was enhanced by a factor of 3.5 inside the wakes. Siddiqui et al. (2004) found this factor to be 2.8. Siddiqui et al. (2004) and Zappa et al. (2004) estimated that up to 60 to 75% of the gas transfer across the air–water interface was due to microscale wave breaking. Zappa et al. (2001) observed that the surface area occupied by microscale breaking waves was correlated with the gas transfer velocity and concluded that microscale breaking

waves make a significant contribution to air-sea gas transfer. Peirson and Banner (2003) concluded that microscale wave breaking is potentially a very effective process in the enhancement of constituent transfer at wind speeds greater than 3.8 m s^{-1}. Lamont and Scott (1970) suggested that the very small scales of turbulent motion control the gas transfer rate and that the gas transfer velocity is a function of the rate of dissipation of turbulent kinetic energy. Therefore, accurate predictions of the characteristics of the turbulence generated by microscale wave breaking should lead to more accurate predictions of air-sea gas transfer. This has motivated us to develop a turbulence model that can predict the vertical structure of the turbulence beneath microscale breaking waves. The turbulence model will be used to predict gas transfer across the air water interface. This is a challenging task because the model must accurately predict the turbulent transport of both momentum and mass in the water column and it must also provide accurate predictions of the transport across the thin concentration boundary layer formed at the water surface. This turbulence model developed for microscale breaking waves can be used by future studies as a basis for generating improved gas transfer parameterization.

3.2 Literature Review

Modeling the turbulent flow in the ocean surface boundary layer is complicated because of the presence of surface waves. Waves change the dynamics at the ocean surface in a number of different ways but their most significant influence is the result of wave breaking. Breaking waves dramatically increase the levels of near-surface turbulent kinetic energy which is responsible for mixing momentum in the water column and

determining the magnitude of the current close to the ocean surface (Drennan et al. 1992). Kitaigorodskii et al. (1983) found a region of enhanced turbulent kinetic energy in Lake Ontario which extended to depths of approximately ten times the wave amplitude below the surface. Thorpe (1984, 1992) and Osborn et al. (1992) also observed enhanced dissipation in this near surface layer as compared to a logarithmic boundary layer. The near surface layer is referred to as the wave enhanced zone. Dissipation and velocity measurements below the wave enhanced zone indicated that the traditional wall layer existed below the wave zone (Osborn et al. 1992).

Velocity measurements in the wave enhanced zone showed that the velocity decayed as z^{-1} (Drennan et al. 1992), where z is the depth below the water surface. Cheung and Street (1988) also found a linear variation of velocity with the inverse of depth in near surface sublayer zone for tank observations.

In the wave enhanced zone measurements showed that the dissipation rate decayed much faster with depth compared to a wall layer. In traditional wall layers the dissipation rate is known to decay as z^{-1}. Gargett (1989) and Drennan et al. (1992), during their field studies, observed that the dissipation rate decayed as z^{-4} in the wave enhanced zone. However, Anis and Moum (1992) found the near surface dissipation decay rate as z^{-3} in the equatorial Pacific.

Thompson and Turner (1975) developed a model based on the turbulent kinetic energy equation to assess the influence of breaking waves on near-surface oceanic turbulence. Their turbulence model was one of the very first models to use the turbulent kinetic energy equation to simulate the effect of wave breaking. Thompson and Turner's model supported the power law behavior of dissipation rate in the wave enhanced zone.

However, the value of the exponent of dissipation rate was derived empirically from data and was found to be -4. Other models which simulate wave breaking but are not based on the turbulent kinetic energy equation include: Jenkin (1986, 1987) developed models that used an explicit representation of Reynolds stresses to incorporate wave and current dynamics. Weber (1981) and Davies (1985, 1987) used eddy viscosity as a function of wind and wave conditions to account for the action of breaking waves. For one and two equation turbulence models, which include solution of the turbulent kinetic energy equation, the influence of breaking waves can be incorporated as a source of kinetic energy at the surface (Kundu 1980, Klein and Coantic 1981, Craig and Banner 1994). The kinetic energy input at the surface is typically taken to be proportional to the cube of the friction velocity on dimensional grounds.

The flow beneath a wind-driven air-water interface can be modeled as a shear flow with wave induced motions superimposed. For the simple shear flow case over a solid boundary the turbulent length scale is typically assumed to increase linearly with depth. This simple description of the turbulent length scale was first introduced by Prandtl (1952) as: $l=\kappa z$ where, κ is the von Karman constant. In the present study a one-equation turbulence model with a Prandtl-type (1952) mixing length specification is used instead of a more complicated two equation model. However, the performance of two equation models e.g. k - ε model and k - ω model is also examined and it is found that a linear length scale model performs much better than these two equation models beneath microscale breaking waves.

To simulate the effect of wave breaking, the technique proposed by Craig and Banner (1994) is used in this study. For a wave breaking situation the most complete

attempt to incorporate the idea of a well mixed surface layer into a model was made by Craig and Banner (1994) (Melville 1996). In their model Craig and Banner (1994) accounted for the effects of large-scale breaking waves by introducing a kinetic energy flux at the surface that was proportional to the cube of the friction velocity. The flux of kinetic energy (F_{KE}) is the product of the shearing force applied to the surface and an effective phase speed related to wind input C (i.e. $F_{KE} = \tau_w \frac{C}{\rho_w} \approx u_*^2 C$) (Terray et al. 1996). Therefore, Craig and Banner (1994) assumed that the kinetic energy flux due to wave breaking is proportional to the cube of friction velocity based on this dimensional argument. Simulation of the vertical structure of the turbulence beneath large scale breaking waves was the objective of Craig and Banner's (1994) study. Their model predicted that during wave breaking the near surface dissipation decayed as $z^{-3.4}$ and that the mean horizontal velocity varied inversely with depth in the wave affected zone. There have been many successful applications of Craig and Banner (1994) model for simulation of realistic upper ocean processes. Stacey and Pond (1997) found that the model produces reasonable estimates of near surface velocities. Craig (1996) used the Craig and Banner's (1994) model to predict the velocities beneath wind generated waves in a wind wave tank. Other applications of the Craig and Banner's (1994) model for large scale breaking wave include Stacey (1999), Noh and Kim (1999) and Noh et al. (2002).

The General Ocean Turbulence Model (GOTM) uses Craig and Banner's (1994) concept to simulate the turbulence generated by large-scale wave breaking (Burchard and Bolding 2001). For the wave breaking module GOTM adopted the 2.5 level turbulence closure scheme of Mellor and Yamada (1974, 1982). At level 2.5 the turbulence closure is specified in terms of an eddy viscosity, which is determined from a simplified set of

Reynolds-stress equations requiring five constants and a mixing length (Craig et. al 1993). In the presence of breaking waves the surface layer becomes well mixed and the five empirical constants required in Mellor-Yamada's 2.5 level scheme reduce to three empirical constants. It was found that this scheme provides reasonable results in the wave affected surface layer of the ocean even though the empirical constants for the model have been determined for situations where shear production of turbulence balances dissipation (Craig and Banner 1994). However, during wave breaking the shear production of turbulence does not balance dissipation.

The original GOTM model has been modified in the present study so that it can simulate near surface turbulence produced by microscale breaking waves. A summary of the essential elements of GOTM wave breaking module is presented below. The model used a Prandtl-type (1952) mixing length as given below:

$$l = \kappa(z_{ot} - z), \quad -(H - z_{ot} + z_{oH})/2 \le z \le 0$$

$$l = \kappa(H + z_{oH} + z), \quad -H \le z \le -(H - z_{ot} + z_{oH})/2 \qquad (3.1)$$

where, z the vertical coordinate is positive upwards and its origin is at the ocean surface, l is the mixing length, κ is the von Karman constant ($\kappa \approx 0.4$), z_{ot} and z_{oH} are the roughness lengths for the upper and bottom boundaries of the ocean respectively representing the minimum scale of turbulence and H is the flow depth. The eddy viscosity (A) is proportional to the product of turbulent length scale (l) and the turbulent velocity scale (q) and expressed as: $A = lqS_M$, where, S_M is a model constant (according to Mellor and Yamada (1982) $S_M = 0.39$). The model uses an equation for the turbulent kinetic energy that represents a balance between parameterized versions of diffusion, dissipation and shear generation. The equation for the turbulent kinetic energy is given by,

$$\underbrace{\frac{\partial b}{\partial t}}_{(A)} \underbrace{-\frac{\partial}{\partial z}\left(lqS_q \frac{\partial b}{\partial z}\right)}_{(B)} = \underbrace{lqS_M\left(\left(\frac{\partial u}{\partial z}\right)^2 + \left(\frac{\partial v}{\partial z}\right)^2\right)}_{(C)} \underbrace{-\frac{2qb}{Bl}}_{(D)} \qquad (3.2)$$

where, b is the turbulent kinetic energy density ($b \equiv 0.5q^2$), S_q and B are model constants (according to Mellor and Yamada (1982) $S_q = 0.387$, $B = 16.6$), u and v are the horizontal velocity components in the direction of wind and perpendicular to the direction of wind respectively. Term (A) in Eq. (3.2) represents the time rate of change of turbulent kinetic energy; term (B) parameterizes a convective transport i.e. the mean rate of vertical transport of kinetic energy or the vertical diffusion of turbulent kinetic energy, term (C) on right hand side is the shear production and term (D) is the dissipation of turbulent kinetic energy. Equation 3.2 is a highly approximated form of the turbulent kinetic energy balance where the energy is assumed to diffuse according to an eddy diffusion relationship. The term for production is obtained using the gradient transport theorem while the expression for dissipation is obtained from dimensional argument.

At the ocean surface GOTM set the stress equal to the wind stress. The boundary conditions for the velocity components are,

$$A\frac{\partial u}{\partial z} = u_*^2 \quad \text{at } z = 0 \qquad (3.3)$$

$$A\frac{\partial v}{\partial z} = 0 \quad \text{at } z = 0 \qquad (3.4)$$

where, A is the eddy viscosity and u_* is the friction velocity in the water obtained from the approximation that the shear stress on the air side and water side are equal (i.e.

$\rho_w u_*^2 = \rho_a u_{*a}^2$). At the sea bed the no-slip boundary condition requires: $u = v = 0$, at $z = -H$.

The wave breaking kinetic energy flux at the surface is expressed as αu_*^3 where, the constant of proportionality (α) is defined as the wave energy factor (Craig and Banner 1994). Craig and Banner (1994) state that for well developed ocean waves, the constant of proportionality is $O(100)$ and that it is relatively insensitive to wind and wave conditions in the open ocean. The boundary condition for turbulent kinetic energy at the ocean surface is given by,

$$lqS_q \frac{\partial b}{\partial z} = \alpha u_*^3 \quad \text{, at } z = 0 \tag{3.5}$$

where, $\alpha = 100$ for well developed waves. At the sea bed, at a $z = -H$, a zero flux of turbulent energy requires that the boundary condition be given by,

$$\frac{\partial b}{\partial z} = 0 \tag{3.6}$$

The wave affected zone close to the surface is referred to as the wave enhanced layer. It is assumed that dissipation and diffusion are in a balance in the wave-enhanced layer. Below the wave enhanced layer a layer referred to as the shear layer exists where the conventional equality between production and dissipation is valid. The depth of the transition (z_t) from the wave enhanced layer to the shear layer is,

$$z_t = z_{\alpha l}\left(1 - r^{-3/n}\alpha^{1/\psi}\right) \tag{3.7}$$

where, r is a model constant ($r \approx 1$), α is the wave energy factor and $\psi = \sqrt{3/S_q \kappa^2 B}$.

3.3 Turbulence Model for Breaking Waves

The GOTM model computes solutions for the one-dimensional version of the transport equations of momentum, salt and heat. Instead of developing a completely new numerical model, it has been decided to use the GOTM algorithm with necessary modifications to simulate the turbulence beneath microscale breaking waves. A discussion about the required inputs for GOTM is presented in Chapter 2 (see Section 2.2).

In the present study the hydraulic (see Table 2.1 and 2.2) and geometric inputs for GOTM are set according to the experimental conditions of Elkamash (2005). Note that the model assumes that the air side and water side shear stresses are equal, therefore, the surface shear stress is specified as $\tau_a = \rho_a u_{*a}^2$ where, ρ_a is the air density (see Table 2.1) and the values of z_{ot} listed in Table 2.2 is used for roughness length. The wave energy factor (α) was assumed to be 100 as per Craig and Banner (1994). The model predictions are then compared with the measured vertical profiles of the rate of dissipation of turbulent kinetic energy, ε, and the mean velocity, u, to assess the ability of GOTM to simulate the turbulence generated by microscale breaking waves. The mean velocity and dissipation profiles as predicted by the GOTM model are shown in Figure 3.1(a) and 3.1(b) along with the experimental observations for a wind speed of 8.0 m s^{-1} and a clean water surface. It can be observed from Figure 3.1(a) that the model overestimates the velocity by a factor of two to three compared to the experimental values. In addition, the model predicts a near surface velocity gradient that is significantly smaller compared to the experimental velocity profile. In Figure 3.1(b) it is evident that the model overestimates the rate of dissipation by an order of magnitude compared to that of the

measurements; however the predicted gradients of the dissipation profiles are not significantly different from the observed.

3.4 Differences between large-scale and microscale breaking waves

It can be observed from Figure 3.1(a,b) that GOTM does not accurately predict the turbulence beneath microscale breaking waves. The large discrepancies between the model predictions and the experimental data are likely caused by the differences between the dynamics of large-scale and microscale breaking waves. Several hypotheses are introduced in this study to account for the differences between large and small-scale breaking waves.

Large-scale breaking waves are usually older (i.e., more developed) compared to microscale breaking waves which are typically very young waves. Therefore, the wave energy factor (α), which was assumed to be ~ 100 for fully developed waves, needs to be re-examined for very young waves. Craig (1996) recognized that the assumption that α =100 might not be valid for very young laboratory tank waves. Terray et. al. (1996) used data from a number of field investigations (e.g. Donelan et al. 1985, Kahma 1981, Hasselmann et al. 1973, Birch and Ewing 1986) including their own to derive an expression for the wave energy factor, α as a function of 'wave age', where wave age is defined as the ratio of the wave phase speed (C_p) to the friction velocity on the air side (u_{*a}). They classified waves on the basis of wave age as well developed (wave age, C_p/u_{*a} >10.4) and young waves (C_p/u_{*a} < 10.4). Their analysis of these field measurements resulted in the following equation for young waves,

$$\alpha \sim 14.43\, C_p/u_{*a} \tag{3.8}$$

For well developed waves Terray et. al. (1996) proposed that α was equal to a constant value of 150. The wave age (C_p/u_{*a}) of the young wind waves observed by Elkamash and Loewen (2004) was found to be ~1.3. According to Terray et al. (1996) these experimental waves fall under the category of young waves (wave age < 10.4) and α is estimated to be ~20 according to Eq. (3.8). However, it should be noted that Terray et al. (1996) derived Eq. (3.8) using field data collected from Lake Ontario, where the wave age of the youngest wave was about 3.0 and the amplitude of the smallest wave was an order of magnitude larger than the waves in Elkamash and Loewen's (2004) experiment. Therefore, Terray et al.'s (1996) parameterization basically indicates that α should be much less than the value of 100 used by GOTM but the parameterization needs to be examined to see if it can be accurately extrapolated to very young waves.

One basic input in GOTM turbulence model is the surface shear stress (τ) and the model is based on the assumption that the air side and water side shear stresses are equal (i.e. $\tau \equiv \rho_a u_{*a}^2 \approx \rho_w u_*^2$, where, ρ_w is the water density). At the air-water interface the total stress, τ_a, or momentum flux is partitioned into two components, the form or wave drag (τ_w) and the viscous or tangential stress (τ_{tang}) (Uz et al. 2002). The tangential stress is the frictional drag acting on the water surface and the wave drag is the horizontal component of average pressure force acting on the waves. Stress partitioning has been investigated experimentally by a number of researchers. Snyder et al. (1981) found that the ratio τ_{tang}/τ_a to be approximately 0.43 using field measurements at wind speeds from 5 to 10 m s^{-1}. Bourassa (2000) found this ratio to be approximately 0.2 for a wind speed range of 6 to 10 m s^{-1}. Banner and Pierson (1998) performed experiments in a laboratory wind-wave flume using Particle Image Velocimetry (PIV) technique. They stated that before the

onset of wind waves, the water side tangential stress (τ_{tang}) balances the entire wind stress (τ_a). As the wave field is established, the wave drag (τ_w) increases and combines with the tangential stress (τ_{tang}) to augment the total wind stress. The ratio τ_{tang}/τ_a decreased as the wind speed increased at a given fetch. For the longest fetch the ratio τ_{tang}/τ_a decreased from a value of 0.6 at a wind speed of 4.1 m s^{-1} to 0.3 at 8.1 m s^{-1}. Banner and Pierson (1998) concluded that the relative contribution of τ_{tang} to the total wind stress depends on the wave age. As the wave age increases, the wave form drag (τ_w) becomes more important and soon provides the dominant contribution.

Stress partitioning has also been studied analytically (Hara and Kukulka 2005) and numerically (Makin et al 1995, Kudryavtsev et al. 1999, Makin and Kudryavtsev 1999 and 2002). Analytical and numerical models have been developed to estimate the stress ratio τ_{tang}/τ_a as a function of wind speed and sea state development. Makin and Kudryavtsev (1999) showed that the ratio τ_{tang}/τ_a decreased from 0.8 to 0.15 as the wind speed increased from 1 m s^{-1} to 25 m s^{-1}. Kukulka and Hara's (2005) analytical model was based on the experimental data of Banner and Pierson (1998) and the results were compatible with the numerical model of Meirink and Makin (2000). Their research leads to the conclusion that the only situations where the tangential shear stress ($\tau_{tang} = \rho_w u_*^2$) is equal to the total stress on the air side (τ_a) will be in the absence of waves or when the waves are fully-developed. In particular, in wind wave tank experiments where the waves are invariably young and steep, the ratio τ_{tang}/τ_a will be significantly smaller than one. Therefore, the fact that microscale breaking waves are very young will have an impact on the validity of the assumption of GOTM model that the water side and air side shear stresses are equal.

Ocean turbulence models created to simulate the effects of large scale breaking waves need to provide accurate estimates of the turbulence (e.g. dissipation rate) and mean velocity over depths of O(10 m). These models, including the GOTM (2002 version), do not allow for the possibility that a thin laminar sublayer may exist at the air-water interface. However, the flow beneath very small-scale breaking waves might include a laminar sub layer (see Chapter 2) therefore; the model should be capable of simulating a viscous sublayer. The turbulent length scale equation (Eq. 3.1) is applicable to a fully turbulent flow and will not apply to the viscous sublayer or the adjacent buffer layer. Therefore, the length scale equation may need to be modified to make it applicable for the entire flow region.

Prior to making any modifications to the GOTM model a sensitivity analysis is carried out to determine how sensitive the predictions of mean velocity (u) and dissipation rate (ε) are to the variations in the input surface shear stress (τ), roughness length (z_{ot}) and the wave energy factor (α). Each of the three input variables is varied over a range while the remaining variables are held constant in order to isolate its effect on model predictions. Predicted profiles of ε and u for each experimental condition are compared with the corresponding measured profiles to quantify the sensitivity of a particular variable. For example a dimensionless measure of the sensitivity of ε to changes in τ ($S_{\varepsilon\tau}$) is given by:

$$S_{\varepsilon\tau} = \frac{\left(d\varepsilon/\varepsilon_{\exp}\right)}{\left(d\tau/\tau_{\exp}\right)} \tag{3.9}$$

where, the numerator is the fractional change in ε and the denominator the fractional change in τ at a certain depth, $\varepsilon_{\exp}$ and $\tau_{\exp}$ are the experimental estimate of ε and τ

respectively. Each of the input variables (τ for example) is tested for sensitivity for a range of values centered at the experimental value of that variable (τ_{exp}). Finally, the changes in ε and τ (i.e. $d\varepsilon$ and $d\tau$) are normalized by the experimental values to express the significance of the variation without any dimensional ambiguity. The sensitivity of u and ε for the clean surface experiments are listed in Tables 3.1 and 3.2. The sensitivity analysis revealed that both u and ε are most sensitive to variations in shear stress (τ). Prediction of ε is also quite sensitive to variations in α but is insensitive to variations in z_{ot}. Prediction of u is relatively insensitive to variations in both α and z_{ot}. Similar results are obtained for the surfactant experiments.

3.4.1 Calibration of the GOTM Model

The values of water side stress (τ) obtained using the length scale method is found to be significantly smaller than the values of the air side shear stress (τ_a) estimated using Eq. 2.6. The values of τ are a factor of two to seven times smaller than τ_a for both clean and surfactant influenced surfaces. A plot comparing τ and τ_a as a function of wind speed and for clean water surfaces is shown in Figure 3.2. Similar results are obtained for surfactant affected water surfaces. Clearly, the tangential stress applied to the water surface is responsible for driving the currents, and therefore it can be concluded that for these young waves the correct model input for the surface shear stress is the tangential stress not the total stress.

The sensitivity analysis shows that, ε is quite sensitive to the wave energy factor α. In addition, it is shown in Fig. 3.1b that the GOTM model overestimated ε by an order of magnitude. A least square method is used to adjust the value of α so that predicted

values of ε more closely match the observed values. Different trial values of α are used as input to the GOTM model and the optimum value of α is defined as the value that minimized the least square difference between the measured and modeled ε. The least square difference is defined as,

$$\delta = \frac{\sum_{i=1}^{N}(\varepsilon_i - \hat{\varepsilon}_i)^2}{\sum_{i=1}^{N}\hat{\varepsilon}_i^{\,2}} \tag{3.10}$$

where, ε_i and $\hat{\varepsilon}_i$ are the modeled and measured ε, respectively, for measurement point i, N represents the total number of measurement points for each experiment.

The least square difference, δ, computed for a range of values of α is plotted in Figure 3.3 for a wind speed of 9.5 m s^{-1} and a clean water surface. The plot shows a well defined minimum error at $\alpha = 5$ which is chosen to be the optimum wave energy factor at a wind speed of 9.5 m s^{-1}. The same procedure is repeated for all experimental runs (i.e., five wind speeds for clean and surfactant influenced water surfaces). For clean and surfactant influenced water surfaces the optimum value of α varies from approximately 24 to 5 and from 13 to 5, respectively, as the wind speed increases from 3.8 to 9.8 m·s^{-1}. These values are listed in Table 3.3 and plotted in Figure 3.4 as a function of wind speed. The wave energy factor has a decreasing trend with increasing wind speed for both clean and surfactant influenced water surfaces.

The wave energy factor is plotted as a function of wave age (C_p/u_{*a}) in Figure 3.5. The data for both clean surface and surfactant affected surface experiments is rather scattered. Terry et al.'s (1996) suggested equation for young waves (see Eq. 3.8) is also plotted on Figure 3.5 for comparison. The data for the clean surface experiments agree relatively better with the Terry et al. (1996) equation than those of the surfactant affected

experiments. For surfactant influenced water surfaces a linear trend in α is evident in Figure 3.5 if the data point corresponding to wind speed 6.2 $m \cdot s^{-1}$ is ignored. A linear trend line may be drawn for the surfactant surface experiments but the slope of the trend line is significantly different from that suggested by Terry et al. (1996). Moreover, the data points cover only a small range of C_p/u_{*a}. Therefore, the trend line obtained from microscale breaking wave data cannot be used for higher values of C_p/u_{*a}. However, at a given wave age the optimum α for a surfactant influenced water surface is found to be on average 60% smaller than for a clean water surface except for the one case at a wind speed of 6.2 $m \cdot s^{-1}$. What is clear from this analysis is that when modeling the turbulence beneath microscale breaking waves α should be much smaller than the value of 100 recommended by Craig and Banner (1994) and that α increases with C_p/u_{*a} for both clean surface and surfactant affected surface.

From the above analyses and discussion it is evident that for modeling the turbulence generated by microscale breaking waves the input shear stress (τ) has to be equal to the water side or the tangential stress (τ_{tang}) and the wave energy factor (α) has to be an order of magnitude smaller than the value recommended by Craig and Banner (1994). In addition it was found that the predictions of both u and ε are most insensitive to the variations in roughness length, z_{ot}.

3.5 Modification of GOTM model for microscale breaking wave

Experimental measurements of the turbulent kinetic energy dissipation and mean velocity profiles are compared with GOTM model predictions at a wind speed of 8.0 $m\ s^{-1}$ in Figure 3.6 (a and b). Model inputs (τ, z_{ot} and α) are optimized, as described in section

3.4 and given in Table 2.2 and 3.3, and it is observed that the model predictions of mean velocity and dissipation are significantly improved compared to those plotted in Figure 3.1. However, it can be observed from Figure 3.6 (a) that the model still underestimates the surface velocity by a factor of ~2 and that the predicted near-surface velocity gradients are still significantly smaller than the observed gradients. This suggests that near the surface the turbulence is over estimated in the model.

The experimental data is used to determine how the turbulent length scale should be modified to correctly predict the turbulence beneath microscale breaking waves. The turbulent length scale (l) for different wind speed is estimated using the technique described in Chapter 2. The form of the length scale is given in Eq. (3.11),

$$l = \left[\frac{u_*^2}{(\partial \overline{u}/\partial z)} \right]^{3/4} \varepsilon^{-1/4} \tag{3.11}$$

where, u_* is the value of water side friction velocity. The non-dimensional length scale $l^+ = u_* l/\upsilon$ is plotted as a function of z^+ in Figure 3.7 for clean water surfaces for five wind speeds.

The data in Figure 3.7 indicate that for all wind speeds the near surface turbulent length scale is zero for z^+ smaller than 20. Similar results are obtained for the surfactant affected water surface data. For both clean water surface and surfactant contaminated surface the turbulent length scale is zero for z^+ smaller than ~10 for the lowest wind speed and for the highest wind speed l is zero for z^+ smaller than ~ 24 (See Appendix A, Figure A1, A5, A6, A10). Therefore, conservatively it can be assumed that l is zero for z^+ smaller than ~10. Three distinct zones or layers can be identified in Figure 3.7. A laminar or viscous sub-layer for, $z^+ < 10$, where l is zero, a buffer layer for, $10 < z^+ < 40$, where l

increases rapidly and a third layer, for $40 < z^+ < 300$, where l increases linearly with z^+ similar to the function in Eq. (3.1). Based on these findings we have modified the turbulent length scale equation so that it follows the near surface trends of the data in Figure (3.7). The modified length scale equation sets l equal to zero for $z^+ < 10$ and far from the interface it still varies linearly with distance as in the original equation. There are only a few data points within the buffer layer ($10 < z^+ < 40$) and therefore, it is difficult to justify the use of a particular function (e.g., polynomial or exponential) based on the trend of the data in Figure 3.7. However, we tested linear, polynomial and exponential functions in the buffer layer and found that a damping exponential function similar to the one suggested by van Driest (1956) for the viscous sublayer produces length scale profiles that fit the measured profiles best close to the interface. The value of the van Driest damping constant A^+ is changed from 26 to 10, because this value produces a better fit to the trend of the length scale data for $10 < z^+ < 40$. The new length scale equation has the following form,

$$l = 0,\ z^+ \le 10.0,\ z^+ = -\frac{u^* z}{\upsilon}$$

$$l = \kappa(z_{ot} - z)^*\left(1 - \exp\left(-\frac{z^+ - 10}{A^+}\right)\right),\quad 10.0 \le z^+ \le \left(\frac{u_*(H - z_{ot} + z_{oH})/2}{\upsilon}\right)$$

$$l = \kappa(H + z_{oH} + z),\ \left(\frac{u_*(H - z_{ot} + z_{oH})/2}{\upsilon}\right) \le z^+ \le \frac{u_* H}{\upsilon} \qquad (3.12)$$

where, $A^+ = 10$. Eq. (3.12) replaces the original length scale equation (Eq. 3.1) used in CB94 model. This new length scale equation is plotted as a function of depth in dimensionless form (i.e., l^+ versus z^+) and is compared to the clean water surface data at a

wind speed of 4.9 m s^{-1} in Figure 3.8. Note that for $z^+ > 40$ Eq. 3.12 provides a length scale that varies linearly with depth as suggested by Prandtl (1952).

The modified length scale equation sets l equal to zero for $z^+ < 10$ and if the wave breaking kinetic energy flux (αu_*^3) is applied at the surface (i.e., at $z = 0$) then it has no effect. This is because in the region where l is set to zero the turbulence model rapidly dissipates any turbulent kinetic energy and this ensures that the flow is laminar in this region. Therefore, all of the wave induced kinetic energy introduced at the surface is immediately dissipated and as a result the model predicts that wave breaking has practically no effect on the modeled profiles of velocity and dissipation. To rectify this problem the boundary condition for the wave breaking turbulent kinetic energy flux (αu_*^3) is modified so that the effect of wave breaking appears below the region where l = 0 at $z^+ = 15$. The effect of wave breaking is incorporated as an additional production term, P_w in the turbulent kinetic energy equation. Equation (3.2) is modified and is now given by,

$$\frac{\partial b}{\partial t} - \frac{\partial}{\partial z}\left(lqS_q \frac{\partial b}{\partial z}\right) = \left(lqS_M\left(\left(\frac{\partial u}{\partial z}\right)^2 + \left(\frac{\partial v}{\partial z}\right)^2\right) + P_w\right) - \frac{2qb}{Bl}, \text{ at } z^+ = 15 \quad (3.13)$$

$$\text{where, } P_w = \frac{\alpha u_*^3}{h_g} \text{ and } h_g \text{ is the grid thickness at } z^+ = 15$$

In summary, the GOTM model has been modified in the following ways to provide accurate predictions of the turbulent flow beneath microscale breaking waves:

- The tangential stress (τ_{tang}) has been specified as the input shear stress instead of the total stress on the air side (τ_a).
- The wave energy factor (α) is no longer a constant and is reduced by an order of magnitude compared to the value (α = 100) recommended by Craig and Banner

(1994). For clean and surfactant affected water surfaces the optimized values of α (see Table 3.3) are used.

- The turbulent length scale (l) equation has been modified (see Eq. 3.12) to account for the viscous sub-layer at the interface.
- The effect of wave breaking is incorporated as an additional production term, P_w at $z^+ = 15$ in the turbulent kinetic energy equation (see Eq. 3.13).

Measured profiles of the mean velocity and the rate of dissipation of turbulent kinetic energy are compared with profiles predicted using the modified model in Figure 3.9(a) and (b) at a wind speed of 8.0 m s^{-1} for a clean water surface. Predictions using GOTM original model are also plotted for comparison. Consideration of the effect of viscosity in the length scale equation influences the velocity profile close to the surface. It is impossible to get a reasonable value of surface velocity (U_s) and a constant velocity gradient at the surface without the modification of the turbulent length scale as given in Eq. 3.12. For $z^+ < 10$ there is no turbulence and therefore, no dissipation of turbulent kinetic energy. The only dissipation that takes place in the sub-layer will be the viscous dissipation. Therefore, the profile of the rate of dissipation of turbulent kinetic energy is only plotted for $z^+ > 10$ for the modified model (see Figure 3.9 (b)).

The performance of the proposed model is evaluated using a comparison of the model predictions with experimental data obtained from a source different from the one used for calibration and validation of the model. Experiments on microscale breaking waves were performed in the wind wave tank at the NASA Air–Sea Interaction Research Facility of the Observational Science Branch at NASA Goddard Space Flight Center/Wallops Flight Facility, VA, in April–May 2004. The test section of the wind

wave tank was 18.29 m long, 1.22 m high and 0.91 m wide, the mean water depth was 0.76 m. Experiments were conducted on microscale breaking waves at five different wind speeds ranging from approximately 4.0 to 11.0 m s^{-1} and at fetches of 4.8, 8.8 and 12.4 m. The wind wave tank had a circulating flow which caused the mean velocity to increase by 0.07 m s^{-1} over the depth. Considering a typical wind speed of 6.8 m s^{-1} at fetch 4.8m the wave age (C_p/u_{*a}) was observed to be 1.1. This wave age corresponds to a wave energy factor α, of 15 according to the Terry et al. (1996) proposed parameterization between α and wave age. For this typical experimental condition the water side shear stress τ, was estimated to be 0.065N m^{-2}. The model prediction of mean velocity and turbulent kinetic energy dissipation is obtained by setting the model input of shear stress equal to 0.065N m^{-2} and α = 15. The roughness length z_{ot} is assumed to be 0.004m for clean surface condition. The effect of circulating flow inside the flume is adjusted by setting the water surface slope equal to -0.000003 m m^{-1}. Measured profiles of the mean velocity and the rate of dissipation of turbulent kinetic energy are compared with profiles predicted using the turbulence model for microscale breaking waves in Figure 3.10(a) and (b) at the typical wind speed of 6.8 m s^{-1}. It can be observed that both the mean velocity and turbulent kinetic energy dissipation are reasonably well predicted by the model. At a depth of 3 cm there is a 17% deviation between the measured and the model predicted profiles of turbulent kinetic energy dissipation. The mean velocity is well predicted by the model at depths greater than 1 cm but close to the surface, at depth 0.5 cm the model under predicts the velocity by 4.5%. However, considering the uncertainty involved in the experimental measurements both the predictions of mean velocity and dissipation are

within the allowable limits. This comparison validates the applicability of the model for microscale breaking waves.

3.6 Gas Transfer Model Development

In the next stage the turbulence model developed for microscale breaking waves is extended to predict gas transfer across the air water interface. The transfer of relatively insoluble gases such as CO_2 across the air-water interface is controlled by processes occurring on the water side (Jähne and Haussecker 1998). The water side boundary layer adjacent to the air-water interface can be divided into two regions. The upper most region immediately underneath the water surface is a concentration boundary layer whose thickness is in an order of 0.1 mm and the lower region contains turbulent water Schwarzenbach et al. (1993). According to Fick's law the gas flux, F across the boundary layer is defined as,

$$F = -D\frac{\partial c}{\partial z} \tag{3.14}$$

where, D is the molecular diffusivity of the gas in water and $\partial c/\partial z$ is the concentration gradient. Equation (3.14) represents local and instantaneous diffusive flux. A model capable of predicting the concentration profile can be used to estimate the instantaneous gas transfer velocity across the boundary layer using Eq. (2.5).

The 2002 version of GOTM does not include solutions for mass transport. Therefore, the GOTM algorithm is modified so that it predicts a vertical concentration profile instead of a temperature profile. The boundary condition for heat transport is different from that of mass transport. In the turbulent transport algorithm the Neuman (flux) type boundary condition is changed to a Dirichlet (fixed value) type boundary

condition. The boundary value of gas concentration (c_{air}) is specified to be zero at the air-water interface as the concentration of water side limited gas (such as He and SF_6) is negligible in air compared to water.

The GOTM uses a turbulent Prandtl number $P_{rt} = 0.74$, for heat transport and this is changed to a turbulent Schmidt number (S_{ct}) to model mass transport. Experiments have shown that the typical value of S_{ct} ranges from 0.5 to 0.7 (Flesch et al. 2002). A turbulent Schmidt number of 0.6 is used based on the average values of S_{ct} reported in the literature (Dianat et al. 2006, Flesch et al. 2002, Panchapakesan and Lumley 1993).

The gas diffusivities in water (D_g) for SF_6 and He are set according to the experimental temperature of 23°C. A gas diffusivity value of 7.052×10^{-9} m^2 s^{-1} and 1.139×10^{-9} m^2 s^{-1} are used for He and SF_6 respectively (King and Saltzman 1995; Lide 2008). The initial gas concentration c_o, in water is assumed to be comparable with the initial gas concentration during the experiments. The value of c_o is assumed to be 21 moles $liter^{-1}$ and 250 moles $liter^{-1}$ for He and SF_6 respectively. The hydraulic and geometric inputs for the model are set according to the experimental conditions of Elkamash (2005) (see Table 2.2 and 3.3). The concentration profile predicted by the model is used to compute the mean gas concentration over the depth c_m, at different times, t. The gas transfer velocity k_g, is then calculated using Eq. (2.5).

Experimental measurements of k_g for SF_6 and He are compared with these predictions in Table 3.4(a) and 3.4(b) respectively for both clean water and surfactant contaminated water surfaces. It can be observed from Table 3.4 that the microscale breaking wave model underestimates k_g by an order of magnitude compared to the experimental values. Also listed in Table 3.4 are the values of k_g predicted by a Prandtl-

type (1952) turbulent length scale model using the same model inputs as used for microscale breaking wave model. The Prandtl-type (1952) length scale model was used by original version of GOTM where the turbulent length scale close to surface is specified as $l = \kappa(z_{ot} - z)$. It is observed from Table 3.4 that the Prandtl-type (1952) length scale model overestimates k_g by a factor of 2 to 14 compared to the experimental values. This suggests that the near surface turbulence is under-estimated in the microscale breaking wave model and over-estimated in the Prandtl-type length scale model.

Prior to making any modification to the microscale breaking wave model a sensitivity analysis is carried out to determine how sensitive the predictions of k_g are to variations in the input surface shear stress (τ), roughness length (z_{ot}), the wave energy factor (α), the value of the van Driest damping coefficient (A^+) used in the length scale equation and the thickness of the non-dimensional viscous sublayer (δ_v^+) (in the microscale breaking wave model $\delta_v^+ = 10$). Each of the five input variables is varied over a range while the remaining variables are held constant in order to isolate its effect on model predictions. Predicted values of k_g for each experimental condition are compared with the corresponding measured k_g to quantify the sensitivity of a particular variable. For example a dimensionless measure of the sensitivity of k_g to changes in τ, ($S_{kg-\tau}$) is given by;

$$S_{kg-\tau} = \frac{dk_g / k_{g-exp}}{d\tau / \tau_{exp}} \tag{3.15}$$

where, the numerator is the fractional change in k_g and the denominator is the fractional change in τ at a certain depth, $k_{g\text{-}exp}$ and τ_{exp} are the experimental values of k_g and τ respectively. Each of the input variables (τ for example) is tested for sensitivity for a

range of values centered at the experimental value of that variable (τ_{exp}). For example if the shear stress is varied by ± 20% from the experimental value τ_{exp}, the denominator in Eq. (3.15) would be ± 0.2. Finally, the changes in k_g and τ (i.e. dk_g and $d\tau$) are normalized by the experimental values to express the significance of the variation without any dimensional ambiguity. The sensitivity of k_g for SF_6 diffusing through clean water surface is listed in Tables 3.5. The sensitivity analysis reveals that k_g is most sensitive to variations in δ_v^+. Predictions of k_g are also sensitive to variations in τ but are insensitive to variations in z_{ot}, α and A^+. Similar results are obtained for a surfactant influenced water surface.

From the sensitivity analysis (see Table 3.5) it is apparent that a reduction of the viscous sub-layer thickness δ_v^+ increases k_g. This analysis indicates that the microscale breaking wave model will give better predictions of the gas transfer velocity if there is additional turbulence closer to the water surface. This analysis also implies that the microscale breaking wave model might be calibrated to predict more accurate values of k_g by reducing the thickness of the zero length scale region (δ_v^+) in Eq. (3.12). However, the predicted profiles of ε and u, which were optimized using the original form of Eq. (3.12), will also change. Therefore, it is obvious that if the turbulent length scale is to be modified to improve predictions of k_g, the resulting changes to ε and u should also be examined.

The microscale breaking wave model is based on the assumption that a viscous sub-layer exists at the air-water interface for z^+ less than 10. Within this layer the flow is laminar and the velocity profile is linear with a constant velocity gradient. However, in solid wall boundary layers the turbulent motion does not disappear sharply at any

particular distance from solid wall (Davies 1972). The turbulent eddies are damped progressively as they approach the wall and right at the wall the eddy motion becomes zero. Several investigators have experimentally measured eddies within the viscous sub-layer (Angus et al. 1969 and Nedderman 1961). Angus et al. (1969) have shown that while viscous forces are dominant within the sub-layer, there are small random movements superposed on the otherwise laminar flow. In addition, their measurements, from stereoscopic photographs of air bubbles in water, have confirmed that the velocity profile is linear within this sub-layer. Therefore, the assumption that the turbulent length scale remains zero close to the surface ($z^+ < 10$) might be an oversimplification. This discussion suggests that the turbulent length scale should be modified to allow a very small amount of turbulence close to the boundary. The turbulence should be small enough so that the flow still remains predominantly laminar with an almost linear mean velocity profile at $z^+ < 10$. However, at the same time the near surface turbulence should be strong enough to change the concentration gradient at the surface to produce the appropriate k_g.

3.7 Modification of microscale breaking wave model for gas transfer velocity

The experimental data of Atmane et. al (2004) (see Figure 2.4) is used to determine how the turbulent length scale should be modified in the region $z^+ < 10$, to correctly predict k_g. Different functional forms for l are tested e.g. constant, linear (using different length scale slope, κ_s), parabolic and hyperbolic functions in the buffer layer so that the model predicted k_g, ε and u, fit the measured gas transfer velocities, dissipation and velocity profiles accurately. The data set for SF_6 gas diffusing through water surface

is used for this analysis as this particular data set had the most extensive gas transfer rate measurements. The predicted concentration profile is used to compute the mean concentration over the depth c_m and then k_g is estimated using Eq. (2.5). The results are found to be most consistent when using the linear length scale type model (i.e. $l = \kappa_s(-z)$). The slope of the length scale κ_s, is found to increase with increasing wind speed using the linear length scale function. No such consistent behavior is observed using the other functional forms for l.

At a temperature of 23°C the molecular Schmidt number (S_c) for SF_6 and He is 830 and 132 respectively (Wanninkhof 1992). The gas transfer velocity for a given gas diffusing through water surface is inversely proportional to the square root of S_c of that gas in water (Jähne et al. 1979). As a result the experimental measurement of k_g for He is greater by a factor of about 2.5 times than for SF_6. Even though SF_6 and He represent different values of k_g it should be noted that for a given experimental condition the turbulence in the water remains the same for the two gases. A consistent behavior is observed in the value of the turbulent length scale slope (κ_s) required to predict the appropriate k_g for both SF_6 and He. It is found that for a given experimental condition the same value of κ_s is required for both SF_6 and He. This validates the selection technique of κ_s for different set of experiments.

The length scale slope κ_s, is chosen to be optimum when the difference between the experimental and model predicted values of k_g is less than 8%. The optimum values of κ_s obtained in this manner for SF_6 and He diffusing through clean and surfactant affected surfaces at all wind speeds are presented in Table 3.6. These values correspond to a turbulent Schmidt Number (S_{ct}) of 0.6. Also listed in Table 3.6 are the values of k_g,

predicted by the microscale breaking wave model using the modified length scale for the zone $z^+ < 10$. This modified microscale breaking wave model is also combined with different thickness of the viscous sublayer δ_v^+ (8 and 12, instead of 10). But the velocity profile, specially the velocity gradient at the surface moves away from the desired profile for such a case. Hence the second part of Eq. (3.12) is kept unchanged. The new length scale equation proposed for the microscale breaking wave model has the following form,

$$l = \kappa_s(-z) \text{ for } z^+ < 10$$

$$l = \kappa(z_{ot} - z)\left(1 - \exp\left(-\frac{z^+ - 10}{10}\right)\right) \text{ for } 10.0 \le z^+ \le \left(\frac{u_*(H - z_{ot} + z_{oH})/2}{\upsilon}\right) \qquad (3.16)$$

where, the value of κ_s is given in Table 3.6 for the gas diffusing across either a clean or surfactant contaminated water surface at a given wind speed. A third order polynomial is fitted between the two different parts of the length scale equation (i.e. from $z^+ = 8$ to $z^+ = 13$) to ensure a smooth transition in the length scale. A typical plot of the variation of the dimensionless length scale, $l^+ = u_* l/\nu$ with respect to the dimensionless depth, $z^+ = u_* z/\nu$ is shown in Figure 3.11 (wind speed of 6.2m s^{-1}on clean surface). The turbulent length scale by Prandtl (1952) $l = \kappa(z_{ot} - z)$ and the new length scale equation proposed in Eq. (3.16) are compared in Figure 3.12 for a wind speed of 6.2m s^{-1}on a clean water surface.

Typical profiles of concentration, c predicted using the turbulence model are shown in Figure 3.13(a) for He at a wind speed of 6.2m s^{-1}on a clean water surface for different time. The concentration profile predicted by the model is used to compute the mean concentration c_m over the depth at different time. The gas transfer velocity k_g is computed from the slope of the plot $\ln(c_m/c_o)$ versus t as shown in Figure 3.13(b).

The optimum values of κ_s are found to increase with increasing wind speed (see Table 3.6) except for the one case at the wind speed of 9.5 m s^{-1}on a clean water surface. Since the turbulent length scale is a measure of turbulence, the effect of wave breaking is most likely to be correlated with κ_s. The values of κ_s are plotted as a function of wave breaking kinetic energy flux (αu_*^3) in Figure 3.14. The data for both He and SF_6 diffusing across clean and surfactant affected water surface follow a similar trend in Figure 3.14. In Figure 3.14 a linear regression line passing through origin is also plotted for all the data points. The regression line has a slope of 0.0524 and a R^2 value of 0.7.

Laboratory results have shown that the percentage of microscale breaking waves (i.e. the probability of breaking) is highly correlated with the mean square wave slope (Siddiqui et al. 2001, Siddiqui and Loewen 2007). The values of the length scale slope κ_s are plotted as a function of the mean square wave slope $\langle S^2 \rangle$ in Figure 3.15. The data for both He and SF_6 diffusing across a clean and surfactant affected water surface follow a similar trend in Figure 3.15. In Figure 3.15 a linear regression line passing through origin is also plotted for all the data points. The regression line has a slope of 5.33 and a R^2 value of 0.9 indicating that the κ_s values are well correlated with $\langle S^2 \rangle$.

Measured profiles of u and ε are compared with profiles predicted using the modified microscale breaking wave model in Figure 3.16 (a) and (b) at a typical wind speed of 7.9 m s^{-1} for a clean water surface. It is possible to get a reasonable value of surface velocity (U_s) with the modification of the turbulent length scale as given in Eq. 3.16. There is a 17% difference between the measured and model predicted values of surface velocity. At a depth of 4cm there is a 2% and 15% difference between measured and model predicted values of u and ε respectively. The velocity gradient is found to be

almost constant with less than 5% variation in the zone $z^+ < 10$. The viscous shear stress is found to be much higher than the turbulent shear in this zone. This indicates that the flow and also the rate of dissipation of turbulent kinetic energy are dominated by viscosity in this region. Therefore, the profile of the rate of dissipation of turbulent kinetic energy is plotted for $z^+ > 10$ for the modified model (see Figure 3.16(b)).

3.8 Discussion

The increase in turbulent kinetic energy due to microscale breaking wave has been evaluated using the modified turbulence model i.e. using Eq. 3.16 and Eq. 3.13. Vertical profiles of the turbulent kinetic energy (b) with depth when microscale breaking waves are present and when they are absent are compared in Figure 3.17 at a wind speed of 8.0 m s^{-1} for a clean water surface. For the case when microscale breaking waves are present the wave energy factor α is 10 at a wind speed of 8.0 m s^{-1}. The turbulent kinetic energy flux is set to zero (i.e. $\alpha = 0$) for the case with no microscale breaking wave. In the absence of any microscale breaking wave b increases from zero at $z^+ = 0$ to a value of 0.00019 m^2 s^{-2} at $z^+ \sim 20$ and then is approximately constant at 0.0002 m^2 s^{-2} for $z^+ > 50$. When microscale breaking waves are present b has a maximum value of ~ 0.0005 m^2 s^{-2} at $z^+ = 15$. For $z^+ > 15$ b decreases to 0.00032 m^2 s^{-2} at $z^+ \sim 50$. Similar observations are found for all five wind speeds.

The effect of microscale breaking waves on the near-surface turbulence is assessed by comparing depth averaged values of b for the two cases. The depth averaged values of b are computed by integrating the profiles of b from the surface down to a depth where the difference between the two profiles is 5%. The percentage increases in the

depth averaged value of b produced by microscale wave breaking are listed in Table 3.7 at five wind speeds and for clean and surfactant affected water surfaces. For each wind speed the optimized values of α (see Table 3.3) are used for the case when microscale breaking waves are present. Also listed in Table 3.7 are values of $R_{z+=15}$, the value of the ratio of b at a depth of $z^+ = 15$ when microscale breaking waves are present and when they are absent. The results in Table 3.7 show that the model predicts that microscale wave breaking increases the depth averaged turbulent kinetic energy by 22% to 40% and 22% to 33% for clean and surfactant affected water surfaces, respectively. The model also predicts that at a depth of $z^+ = 15$ the value of b increases by a factor of 2.1 to 5.1 and 2.0 to 3.3 due to microscale wave breaking for clean and surfactant affected surfaces, respectively. However, the increases in the depth averaged b and the value of b at a depth of $z^+ = 15$ depends upon the wave energy factor used for the respective wind speed.

It is to be noted that there is no clear trend in the model optimized values of z_{ot} with u_* for clean surface (see Table 2.2). The roughness length z_{ot} data are too sparse to allow a definite relationship between the variables. Similar observation has been reported by Craig (1996) for wind tunnel experiments. However, the variation of z_{ot} with u_* is confined over a narrow range. For clean water surface experiments z_{ot} value ranges from 0.31cm to 0.69cm and for surfactant contaminated surface the value ranges from 0.10cm to 0.49cm over the respective range of friction velocities. Since the model predictions of both u and ε are insensitive to the variation in roughness length, an average value of z_{ot} might be recommended. For clean surface a z_{ot} value of 0.004m and for surfactant contaminated surface z_{ot} value of 0.003m is recommended for young steep wind waves.

The ratios of z_{ot} to the dominant wave length (λ) for different wind speeds are listed in Table 3.8 for both clean and surfactant influenced water surface. The ratio of z_{ot} / λ shows a decreasing trend with wind speed for clean and surfactant contaminated surfaces. The ratio of z_{ot} / λ decreases from 0.14 to 0.02 as the wind speed increases from 3.8 to 9.5 m s^{-1} on clean water surfaces and on surfactant contaminated surfaces z_{ot} / λ decreases from 0.10 to 0.01 as the wind speed increases from 3.9 to 9.8 m s^{-1}. Craig (1996) found this factor to be 0.16 and Sullivan et al. (2004) found that z_{ot} / λ ranged from 0.04 to 0.06. At a similar wind speed the values of z_{ot} and the ratio z_{ot} / λ for a surfactant influenced water surface are found to be smaller than for a clean water surface except for one case at wind speed 4.9 m s^{-1}. The presence of surfactant inhibits turbulence and it may be expected that the presence of surfactant would reduce the thickness of the wave affected zone, z_t. Since the thickness of wave affected zone, z_t and z_{ot} are directly proportional to each other (see Eq. 3.7), a smaller value of z_{ot} for surfactant influenced surface is not unexpected.

Also listed in Table 3.8 are the values of the non-dimensional roughness height z_o^+ ($z_o^+ = u_* z_o / \nu$, where z_o is the roughness height representing the depth where the velocity defect is zero). Boundary layer flow is classified as hydrodynamically smooth if the non-dimensional roughness height z_o^+ is less than 0.11 and as hydrodynamically rough if z_o^+ is greater than 2.3 (Donelan 1990). The non-dimensional roughness height z_o^+ varies from 0.03 to 1.44 for the clean water and surfactant contaminated surfaces (see Table 3.5). The z_o^+ values indicate that the flow in the aqueous boundary layer is either smooth or in the transitional regime and never hydrodynamically rough. This observation supports the hypothesis that a viscous sublayer might exist at the air-water interface.

The effect of surfactants on gas transfer is incorporated in the present model by using a different length scale slope than for clean water in the zone z^+ <10. The optimum κ_s for a surfactant influenced water surface is found to be about 40% smaller than for a clean water surface for both SF_6 and He diffusing through water (see Table 3.6). The presence of the surfactant inhibits the turbulence and therefore, a reduction in the length scale slope is justified. The values of κ_s for both clean and surfactant influenced experiments are well correlated (correlation coefficient, $R^2 = 0.9$) with the mean square wave slope $\langle S^2 \rangle$ (see Figure 3.15). The values of κ_s for both clean and surfactant influenced experiments are also correlated with the kinetic energy flux due to wave breaking, au_*^3 (correlation coefficient, $R^2 = 0.7$) (see Figure 3.14). Therefore, κ_s not only incorporates the effect of surface cleanliness but also the effect of wave breaking.

3.9 Conclusions

The results of the present study support the conclusion that the air side total stress (τ_a) and tangential stress (τ_{tang}) become significantly different with increasing wind speed for young waves. The tangential stress (τ_{tang}) is the mechanism that is responsible for generating the near surface current. Therefore, it has been concluded that τ_{tang} is the appropriate hydraulic input for turbulence models involving young waves. In recent years analytical (Kukulka and Hara 2005) and numerical models have been developed (Meirink and Makin 2000, Makin and Kudryavtsev 1999 and 2002) to estimate the tangential stress from wind speed for both fully developed and developing seas. Future research leading to the development of relationship between τ_{tang} and other easily measurable quantities

would help for further advancement in predicting turbulence characteristics beneath small scale waves in ocean.

The wave energy factor (α) is found to be dependant on the wave age (C_p/u_{*a}) of microscale breaking waves and also on the cleanliness of the water surface (i.e. clean or surfactant influenced). The value of α for both clean or surfactant influenced water surface is found to be an order of magnitude smaller (on average) than the value suggested by Craig and Banner (1994). For microscale breaking wave propagation on both clean and surfactant influenced water surface α has been found to vary with C_p/u_{*a}. However, the narrow range of wave ages observed in the experiments (C_p/u_{*a} ~0.52-1.39) does not allow us to determine how α varies with wave age with any certainty. For clean water surface experiments α values are found to be in close accordance with Terray et. al.'s (1996) equation and therefore, this equation can be used to estimate α. For surfactant affected water surfaces for most of the cases α values are found to be around 60% less than that found for the clean water surface at the same wave age. Future experiments conducted on surfactant contaminated surface with a wider range of wave age (C_p/u_{*a}) would allow a definite relationship to be established between the wave age and wave energy factor.

It was a major challenge to define the physics underlying the roughness length z_{ot} because without it the GOTM model can not be regarded as a functional predictive tool (Craig 1996). The length scale method for estimating roughness length (see Chapter 2) is an achievement as it is a new technique used to independently specify z_{ot}. The model predictions of z_{ot} values are in close accordance with Sullivan et al. (2004) and Craig (1996). The ratio of z_{ot} / λ is found to vary from a factor of 0.02 to 0.14 whereas Sullivan

et al. (2004) found this ratio to vary from 0.04 to 0.06 and Craig (1996) found this ratio to be 0.16. For both clean and surfactant contaminated water surfaces the variation of z_{ot} with u_* is confined over a narrow range. For clean surface z_{ot} value of 0.004m and for surfactant contaminated surface z_{ot} value of 0.003m is recommended for young steep wind waves for which micro scale wave breaking is a significant source of turbulence.

The most significant modification of GOTM that is implemented in this study to make it applicable for microscale breaking waves is the modification in the turbulent length scale. The turbulent length scale equation used in the modified model is determined from experimental data at five wind speeds with two different surface conditions (clean and surfactant affected). Near surface viscous effects are found to be dominant and a consistent trend of the length scale is observed close to the surface for the 10 sets of experiments. Accounting for the effect of viscosity near the surfaces by modifying the turbulent length scale equation produces much better estimates of surface velocity, velocity gradient and gas transfer rates across the air-water interface. A linear length scale with a very mild slope is introduced in the viscous sublayer. The small amount of turbulence that is introduced by this length scale does not create any significant variation in the desired momentum profile. The velocity profile predominantly remains laminar but the turbulence created by this new length scale is strong enough to result in the appropriate concentration profile. This enables the turbulence model to accurately predict the gas transfer rate.

Three characteristics of the flow beneath microscale breaking wave have been identified from the study. First, the viscous sublayer that exists at the air-water interface for $z^+ < 10$ contains a very small amount of turbulence. The turbulence is small enough

so that the flow is still predominantly laminar with an almost constant mean velocity gradient in that zone. Second: observations of z_o^+ values ($z_o^+ < 2.3$) indicate that the flow is either hydrodynamically smooth or in transitional regime. This characteristic supports the possibility of existence of a viscous sublayer at the aqueous boundary. Finally, the turbulent kinetic energy equation which is designed to apply in the fully turbulent flow zone, can also be applied in the viscous sublayer and it provides accurate predictions of velocity, dissipation and gas transfer velocity.

Table 3.1: Values of $S_{u\tau}$, the sensitivity of velocity (u) to changes in τ; $S_{u\alpha}$, the sensitivity of u to changes in α; and $S_{u\,zot}$ the sensitivity of u to changes in z_{ot}. Values are determined for a clean water surface at a depth of 0.27cm for a wind speed range of 3.8 to 9.5m s^{-1}.

$S_{u\tau}$	$S_{u\alpha}$	$S_{u\,zot}$
0.5 to 0.6	-0.03 to 0.04	-0.09 to -0.10

Table 3.2: Values of $S_{\varepsilon\tau}$, the sensitivity of dissipation (ε) to changes in τ; $S_{\varepsilon\alpha}$, the sensitivity of ε to changes in α; and $S_{\varepsilon\,zot}$ the sensitivity of ε to changes in z_{ot}. Values are determined for a clean water surface at a depth of 0.27cm for a wind speed range of 3.8 to 9.5m s^{-1}.

$S_{\varepsilon\tau}$	$S_{\varepsilon\alpha}$	$S_{\varepsilon\,zot}$
1.7 to 1.8	0.68 to 0.82	-0.01 to -0.18

Table 3.3: Values of optimized wave energy factor (α) determined using the least square method. Values are determined for both clean and surfactant affected water surfaces at various wind speeds (U) and corresponding wave ages (C_p/u_{*a}).

Clean			Surfactant		
U (m s^{-1})	(C_p/u_{*a})	α	U (m s^{-1})	(C_p/u_{*a})	α
3.8	1.20	20	3.9	1.39	10
4.9	0.88	24	4.9	1.04	10
6.2	0.68	10	6.2	0.73	13
8.0	0.52	10	8.2	0.65	5
9.5	0.60	5	9.8	0.77	6

Table 3.4 (a): Values of $k_{g\text{-}expt}$, the experimental measurement of gas transfer velocity, k_g; $k_{g\text{-}MSBW}$, transfer velocity predicted by the MSBW model; $k_{g\text{-}Prandtl}$, transfer velocity predicted by the Prandtl-type (1952) length scale model. Values are determined for SF_6 diffusing through both clean and surfactant affected water surfaces at various wind speeds (U).

Clean				Surfactant			
U	$k_{g\text{-}expt}$	$k_{g\text{-}MSBW}$	$k_{g\text{-}Prandtl}$	U	$k_{g\text{-}expt}$	$k_{g\text{-}MSBW}$	$k_{g\text{-}Prandtl}$
($m\ s^{-1}$)	($cm\ hr^{-1}$)	($cm\ hr^{-1}$)	($cm\ hr^{-1}$)	($m\ s^{-1}$)	($cm\ hr^{-1}$)	($cm\ hr^{-1}$)	($cm\ hr^{-1}$)
3.8	6.84	0.25	33.34	3.9	4.13	0.27	36.60
4.9	12.16	0.31	41.99	4.9	2.78	0.31	39.89
6.2	15.38	0.36	46.54	6.2	7.34	0.33	44.05
7.9	32.08	0.45	62.62	8.1	9.34	0.42	54.45
9.5	32.45	0.56	72.94	9.7	18.97	0.48	60.79

Table 3.4 (b): Values of $k_{g\text{-}expt}$, the experimental measurement of gas transfer velocity, k_g, $k_{g\text{-}MSBW}$, k_g predicted by the MSBW model; $k_{g\text{-}Prandtl}$, k_g predicted by the Prandtl-type (1952) length scale model. Values are determined for He diffusing through both clean and surfactant affected water surfaces at various wind speeds (U).

Clean				Surfactant			
U	$k_{g\text{-}expt}$	$k_{g\text{-}MSBW}$	$k_{g\text{-}Prandtl}$	U	$k_{g\text{-}expt}$	$k_{g\text{-}MSBW}$	$k_{g\text{-}Prandtl}$
(m s^{-1})	(cm hr^{-1})	(cm hr^{-1})	(cm hr^{-1})	(m s^{-1})	(cm hr^{-1})	(cm hr^{-1})	(cm hr^{-1})
3.8				3.9	10.74	1.64	61.81
4.9	26.82	1.86	71.02	4.9	17.26	1.86	67.05
6.2	42.98	1.07	77.48	6.2	31.29	1.99	73.47
7.9				8.1	31.29	2.53	90.88

Table 3.5: Values of $S_{kg\text{-}\tau}$, the sensitivity of gas transfer velocity (k_g) to changes in τ; $S_{kg\text{-}zot}$, the sensitivity of k_g to changes in z_{ot}; $S_{kg\text{-}\alpha}$, the sensitivity of k_g to changes in α; $S_{kg\text{-}\delta v+}$, the sensitivity of k_g to changes in δ_v^+ and S_{kg-A+}, the sensitivity of k_g to changes in the van Driest damping coefficient (A^+). Values are determined for a clean water surface at a depth of 0.27 cm for wind speed range of 3.8 to 9.5 m s^{-1}.

$S_{kg\text{-}\tau}$	$S_{kg\text{-}zot}$	$S_{kg\text{-}\alpha}$	$S_{kg-\delta v+}$	S_{kg-A+}
0.28 to 0.67	0.0025 to 0.006	0.001 to 0.0052	-1.6 to -2.3	-0.0016 to -0.0073

Table 3.6: Values of optimized length scale slope (κ_s) and corresponding gas transfer velocity (k_g) determined from the concentration profile predicted by the model. Values are determined for both SF_6 and He diffusing through clean and surfactant affected water surfaces at various wind speeds (U).

Clean				Surfactant			
U ($m\ s^{-1}$)	κ_s	k_g (SF_6) ($cm\ hr^{-1}$)	k_g (He) ($cm\ hr^{-1}$)	U ($m\ s^{-1}$)	κ_s	k_g (SF_6) ($cm\ hr^{-1}$)	k_g (He) ($cm\ hr^{-1}$)
3.8	0.13	7.03		3.9	0.08	4.47	10.40
4.9	0.17	11.61	28.63	4.9	0.11		16.22
6.2	0.185	14.74	39.73	6.2	0.11	7.62	
7.9	0.25	31.61		8.2	0.14	9.54	30.39
9.5	0.23	33.32		9.8	0.175	18.15	

Table 3.7: Values of ΔTKE, the percentage increase in the depth averaged turbulent kinetic energy due to microscale breaking waves; $R_{z+=15}$, ratio of turbulent kinetic energy with microscale breaking waves and without at a depth of $z^+ = 15$. Values are determined for both clean and surfactant affected water surfaces at various wind speeds (U).

Clean			Surfactant		
U (m s^{-1})	ΔTKE (%)	$R_{z+=15}$	U (m s^{-1})	ΔTKE (%)	$R_{z+=15}$
3.8	36	4.5	3.9	30	2.9
4.9	40	5.1	4.9	28	3.1
6.2	28	3.0	6.2	33	3.3
8.0	29	2.9	8.2	22	2.0
9.5	22	2.1	9.8	25	2.4

Table 3.8: Values of z_o^+, the non-dimensional roughness height ($z_o^+ = u_* z_o / \nu$); dominant surface wave length (λ) and z_{ot} / λ, ratio between roughness length (z_{ot}) and λ. Values are determined for clean and surfactant affected water surface at various wind speeds (U).

Clean				Surfactant			
U	$z_o^+ =$	λ	z_{ot} / λ	U	$z_o^+ =$	λ	z_{ot} / λ
m s^{-1}	$u_* z_o / \nu$	m		m s^{-1}	$u_* z_o / \nu$	m	
3.8	1.44	0.05	0.140	3.9	0.68	0.05	0.096
4.9	0.18	0.07	0.048	4.9	0.25	0.07	0.060
6.2	0.07	0.09	0.036	6.2	0.04	0.09	0.035
8.0	0.21	0.11	0.035	8.2	0.03	0.11	0.023
9.5	0.27	0.16	0.021	9.8	0.03	0.16	0.0067

(a)

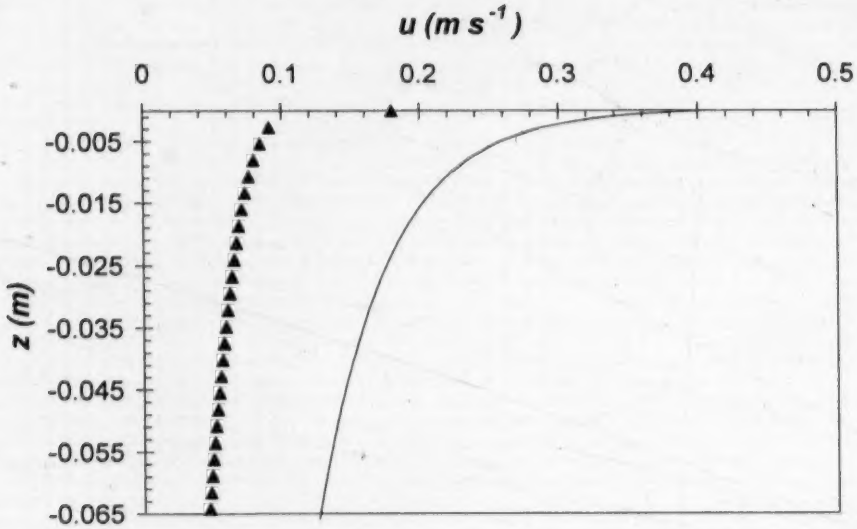

(b)

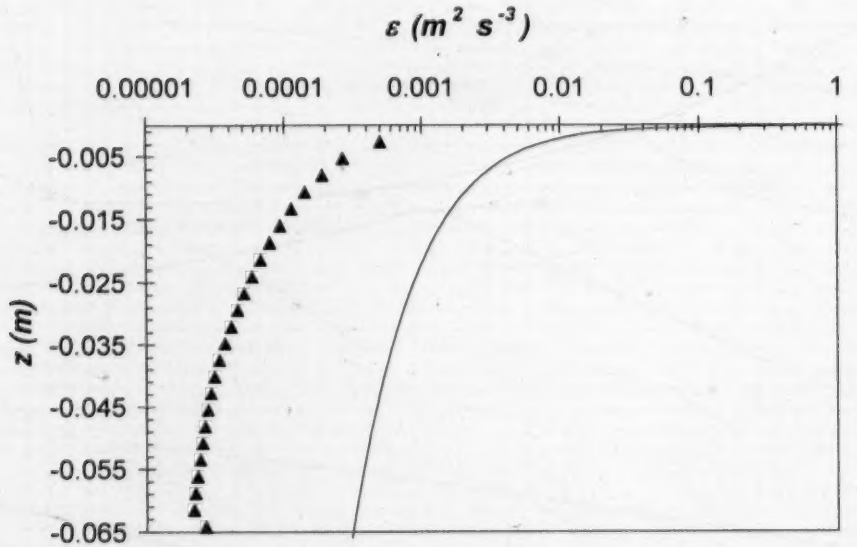

Figure 3.1: Comparison of the profiles of predicted and measured (a) velocity (u) and (b) dissipation (ε) for a wind speed of 8.0 m s^{-1} on a clean water surface. Solid line is the GOTM model predictions of (a) u and (b) ε, for parameter values of $\tau = \tau_a = 0.444 Nm^{-2}$, $z_{ol} = 0.004$m and $\alpha = 100$, ▲are experimental data points.

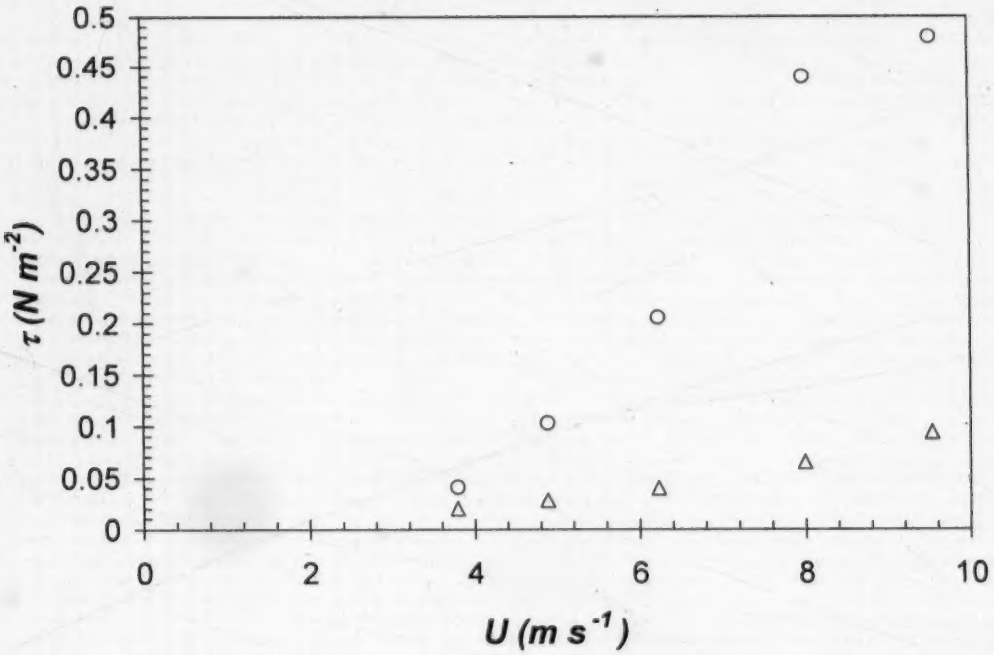

Figure 3.2: Plot of shear stress (τ) versus wind speed (U) on clean water surface. ○, estimate of air side shear stress and Δ, = estimate of water side shear stress.

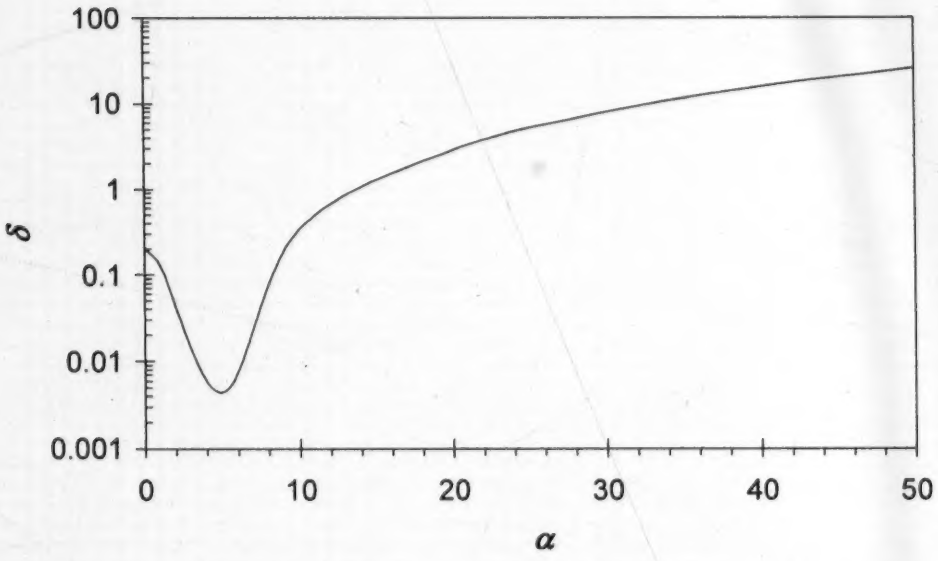

Figure 3.3: Plot of difference between measurements and predictions in dissipation estimate (δ) versus wave energy factor (α) for a wind speed of 9.5 m s^{-1} on clean surface. Plot shows a well defined minimum error at $\alpha = 5$.

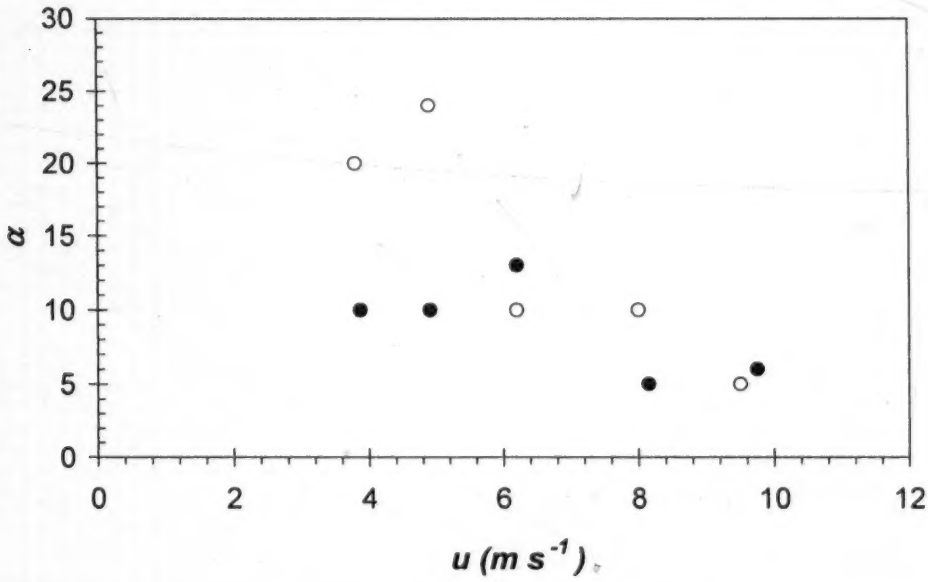

Figure 3.4: Plot of optimum wave energy factor (α) versus wind speed (U). ○, = clean surface experiments and ●, = surfactant affected surface experiments.

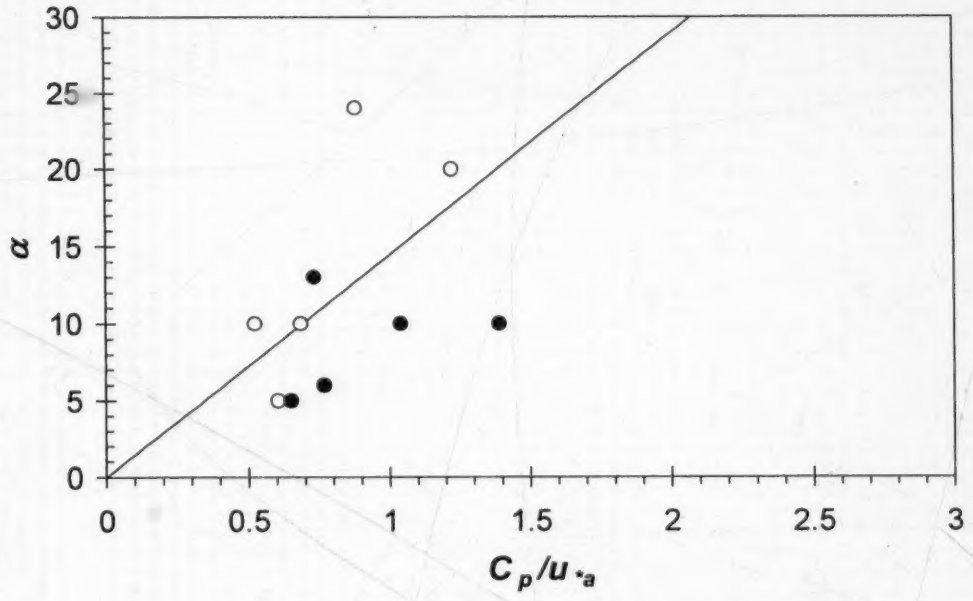

Figure 3.5: Plot of optimum wave energy factor (α) versus wave age (C_p/u_{*a}). ○, = clean surface experiments and ●, = surfactant affected surface experiments; dotted line is Terry et al. (1996) equation (Eq. 3.8).

(a)

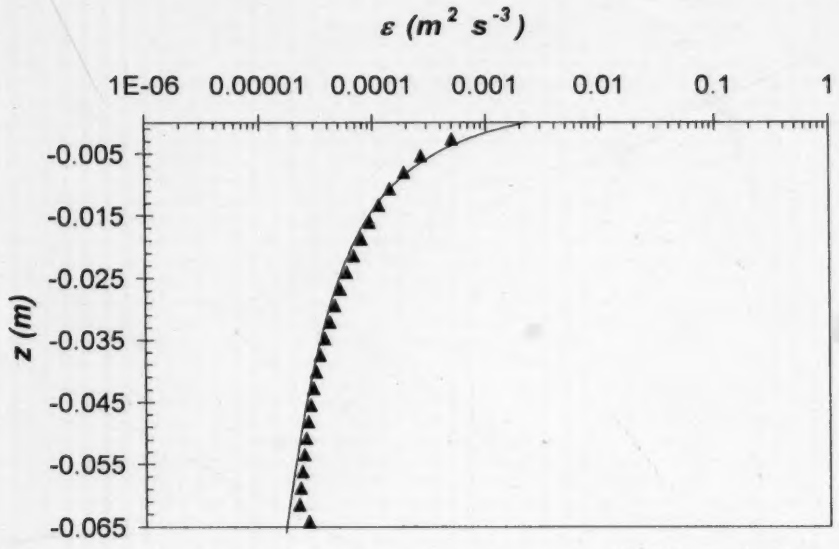

(b)

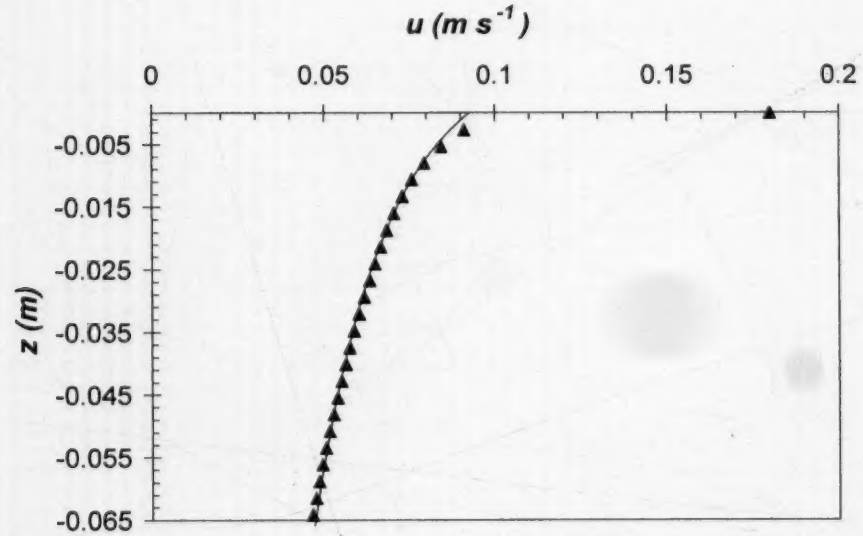

Figure 3.6: Comparison of the profiles of predicted and measured (a) dissipation (ε) and (b) velocity (u) for wind speed of 8.0 m s^{-1} on a clean water surface. Solid line is the model predictions using CB94 of (a) ε and (b) u for model optimized parameter values of τ, z_{ol} and $\alpha_.$, ▲is experimental data points.

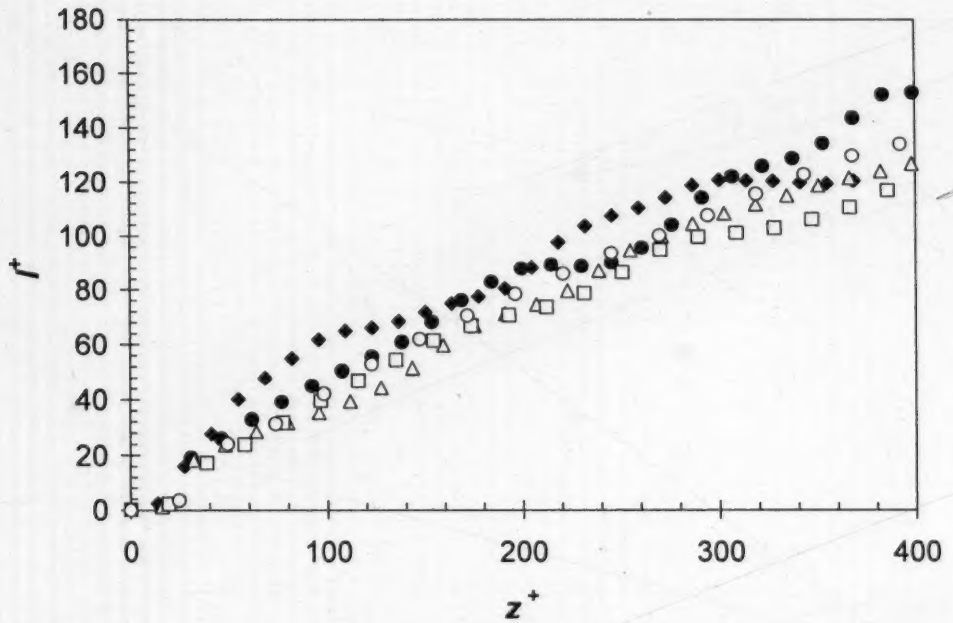

Figure 3.7: Plot of non dimensional length scale (l^+) versus non dimensional depth (z^+) for clean water surfaces for five wind speeds. ♦, = 3.8 m s^{-1}; ● 4.9m s^{-1}; Δ , =6.2 m s^{-1}; □, = 8.0 m s^{-1} and , ○ = 9.5 m s^{-1}.

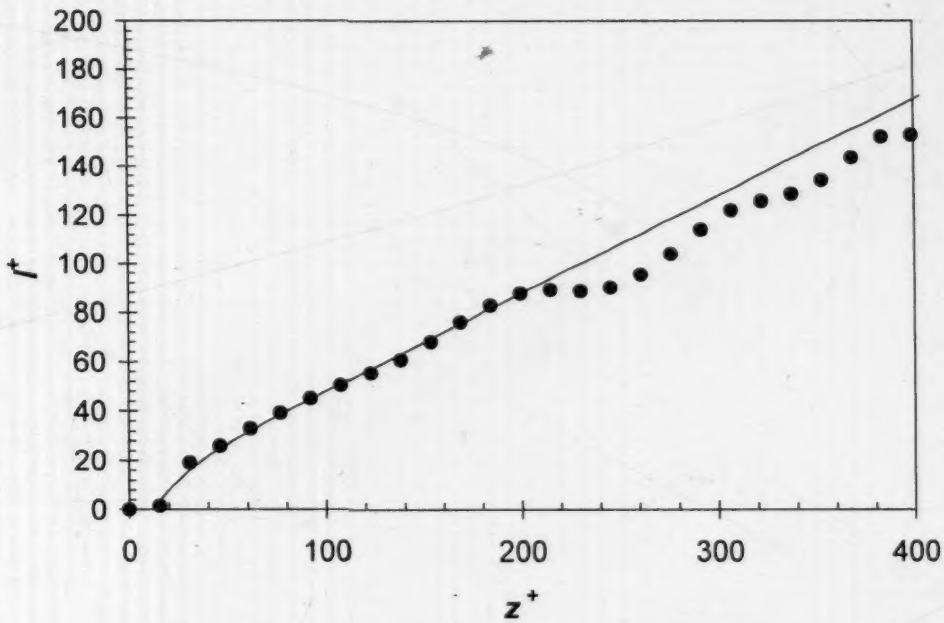

Figure 3.8: Plot of non dimensional length scale (l^+) versus non dimensional depth (z^+) for a wind speed of 4.9 m s^{-1} on a clean surface. •, = experimental data points and solid line is the proposed length scale according to Eq. 3.12.

(a)

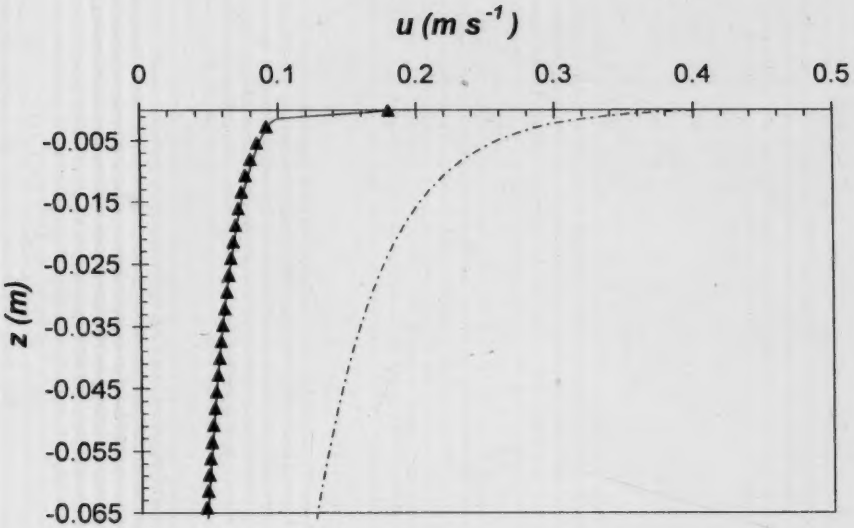

(b)

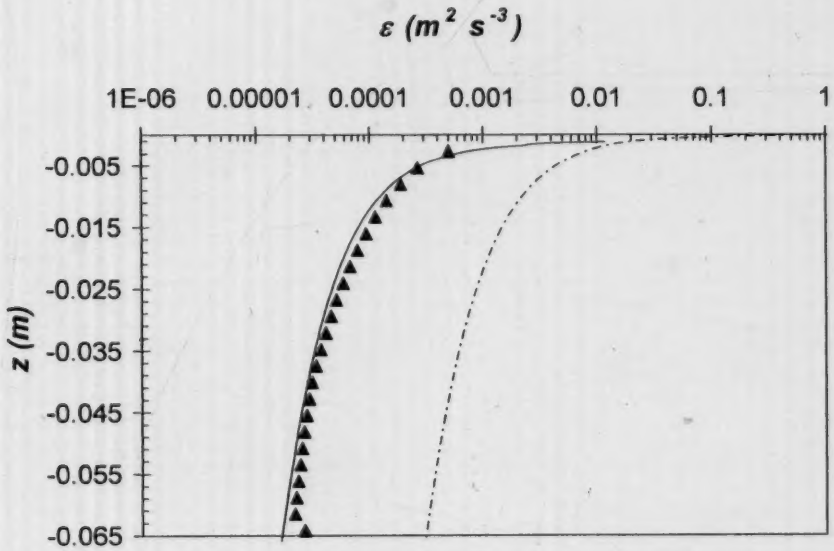

Figure 3.9: Comparison of predicted and measured profiles of (a) velocity (u) and (b) dissipation (ε) for wind speed of 8.0 m s^{-1} on a clean water surface. Solid line is the modified model's predictions of (a) u and (b) ε, dashed-dotted lines are the CB94 predictions, ▲are experimental data points.

(a)

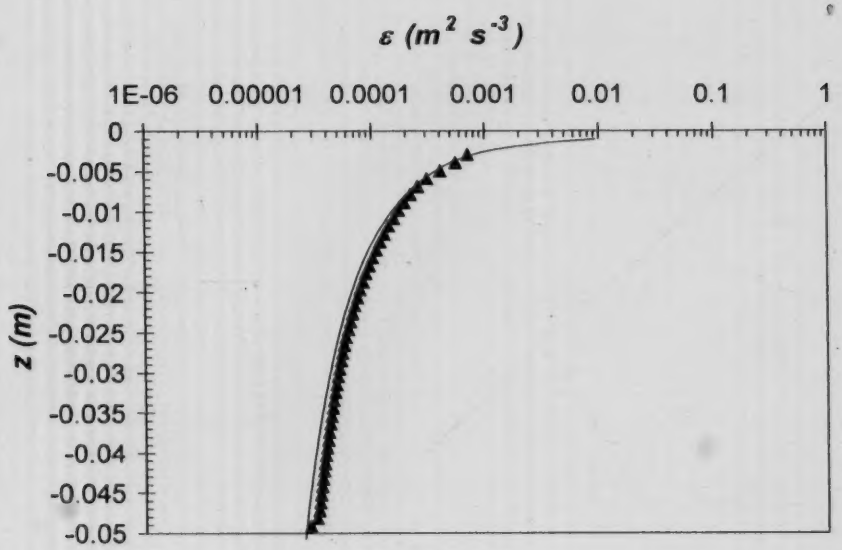

(b)

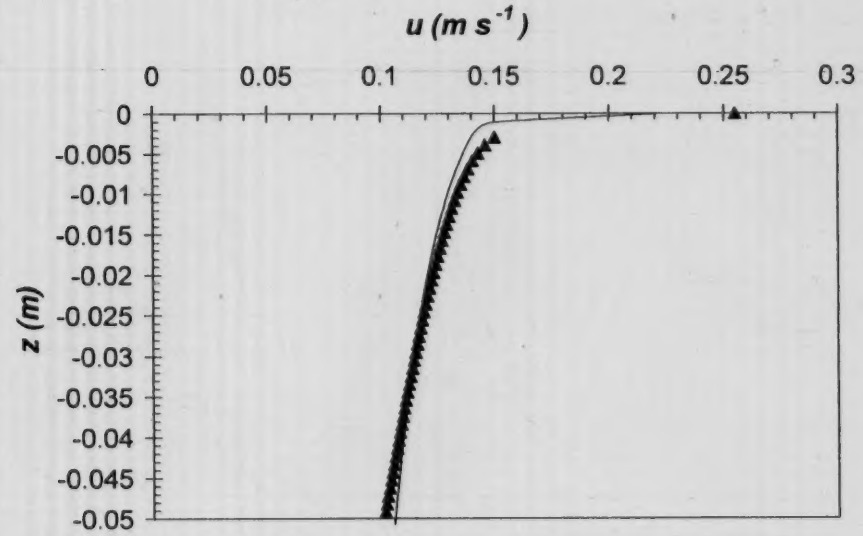

Figure 3.10: Comparison of the profiles of predicted and measured (a) dissipation (ε) and (b) velocity (u) for wind speed of 6.8 m s^{-1} on clean water surface. Solid line is the model predictions of (a) ε and (b) u for parameter values of $\tau = 0.065$ Nm^{-2}, $z_{ot} = 0.004$m and $\alpha = 15.$, ▲are experimental data points.

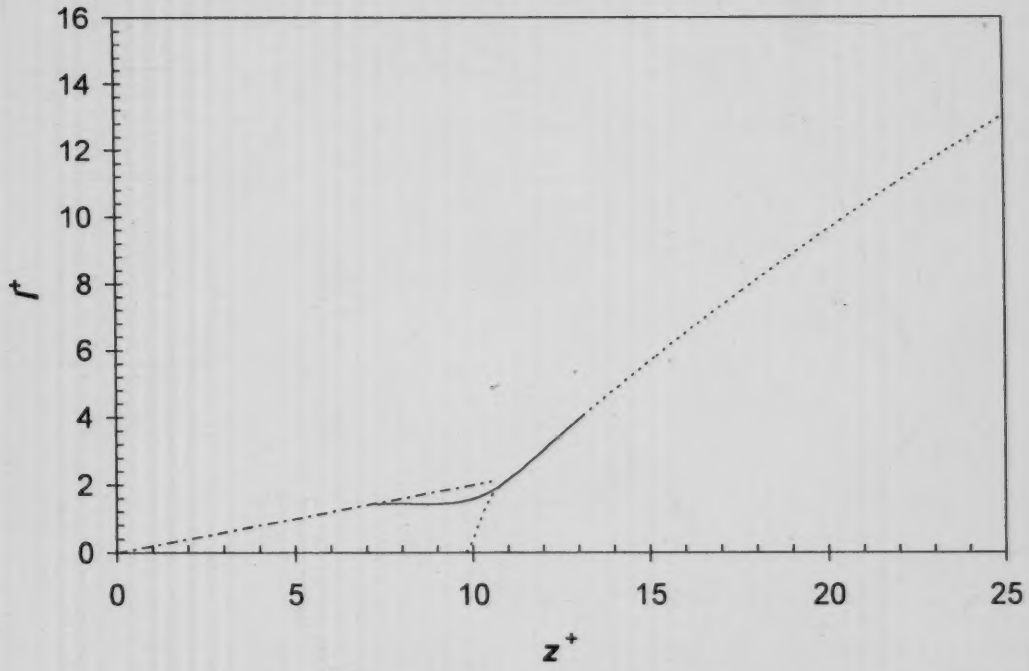

Figure 3.11: Plot of non dimensional length (l^+) versus non dimensional depth (z^+) at a wind speed of 6.2m s^{-1}on clean water surface. Dashed-dotted line corresponds to Eq. (3.16) for $z^+ < 10$, dotted line corresponds to Eq. (3.16) for $z^+ > 10$ and the solid line is the third order polynomial is fitted between $z^+ = 8$ to $z^+ = 13$.

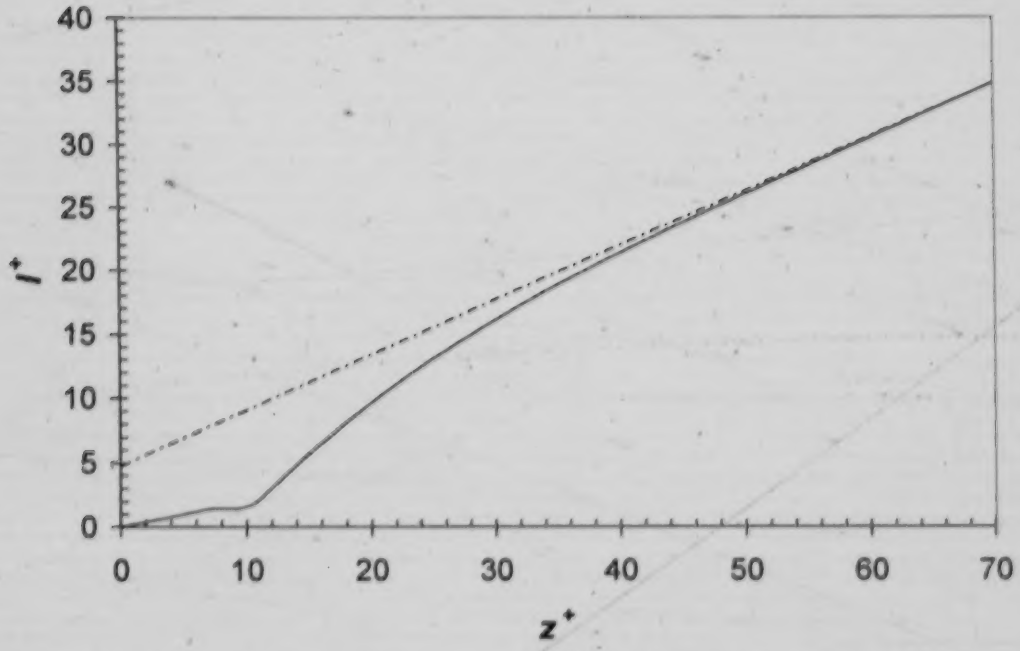

Figure 3.12: Plot of non dimensional length (l^+) versus non dimensional depth (z^+) at a wind speed of 6.2m s^{-1}on clean water surface. Dashed-dotted line corresponds to Prandtl-type (1952) length scale equation ($l = \kappa(z_{ol} - z)$) and the solid line corresponds to Eq. (3.16).

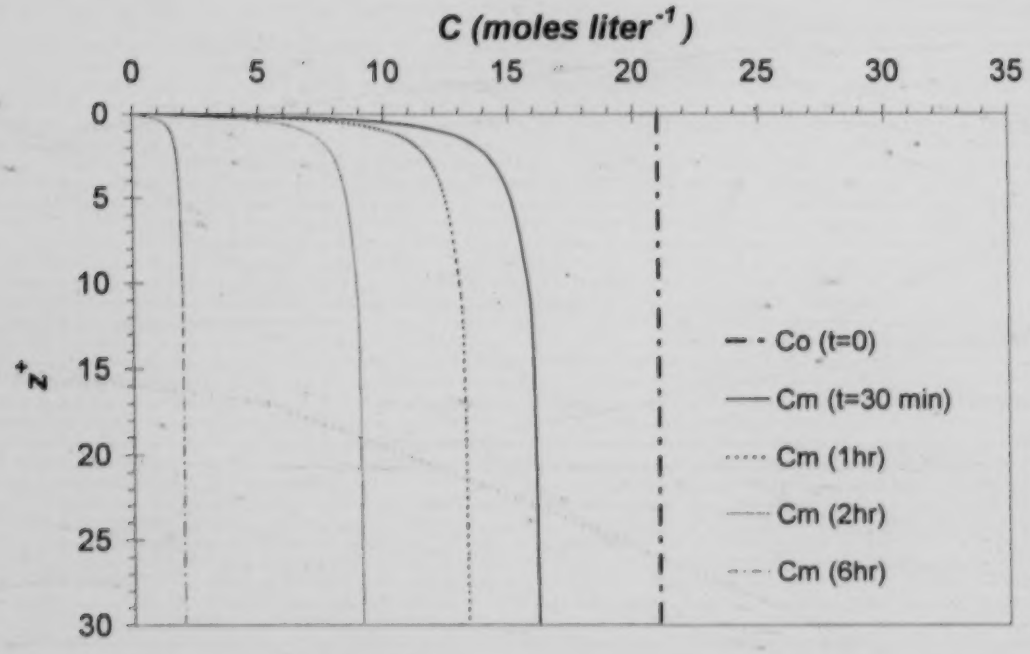

Figure 3.13(a): Plot of concentration profile versus non dimensional depth (z^+) at a wind speed of 6.2 m s^{-1} on clean water surface.

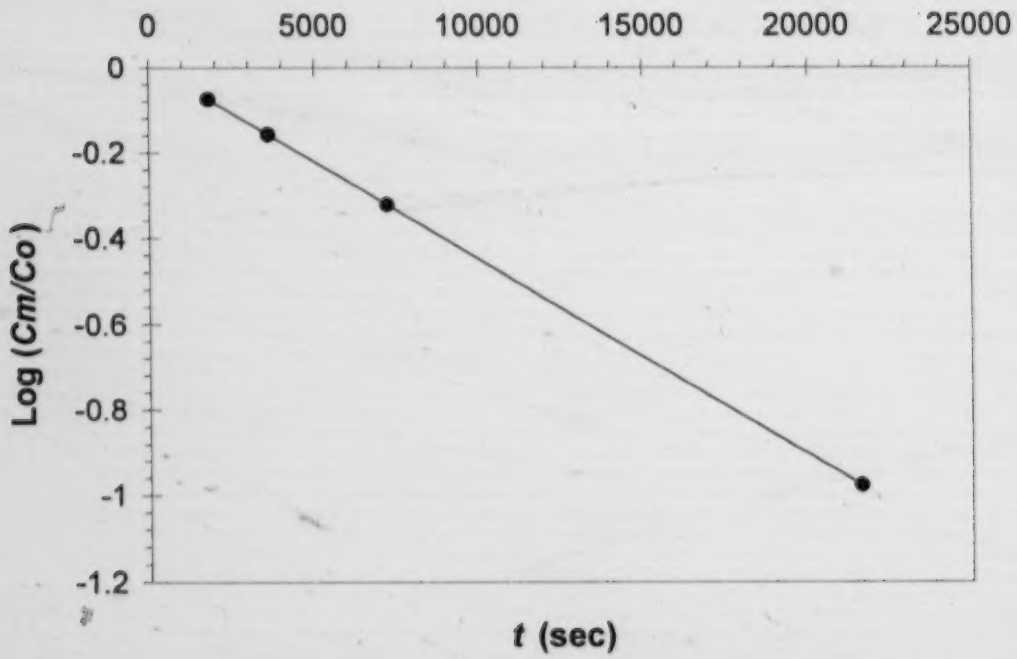

Figure 3.13(b): Plot of log (c_m/c_o) versus time (t) at a wind speed of 6.2 m s^{-1} on clean water surface, •, = data points obtained for different concentration profile at different time from Figure 3.14(a), Solid line corresponds to the straight line fitted through the data points

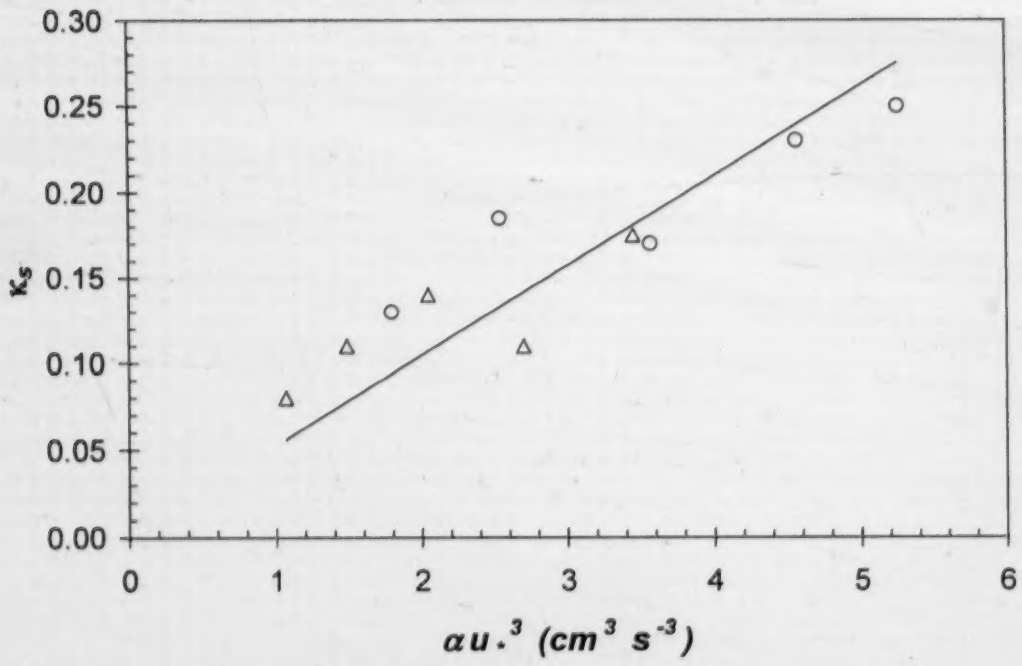

Figure 3.14: Plot of length scale slope (κ_s) versus the wave breaking kinetic energy flux (αu_*^3) for both He and SF_6 diffusing through clean and surfactant influenced water surfaces. ○, = data for the clean water surface; Δ, = data for the surfactant influenced water surface and solid line is a linear regression line passing through origin. The regression line has a slope of 0.0524 and $R^2 = 0.7$.

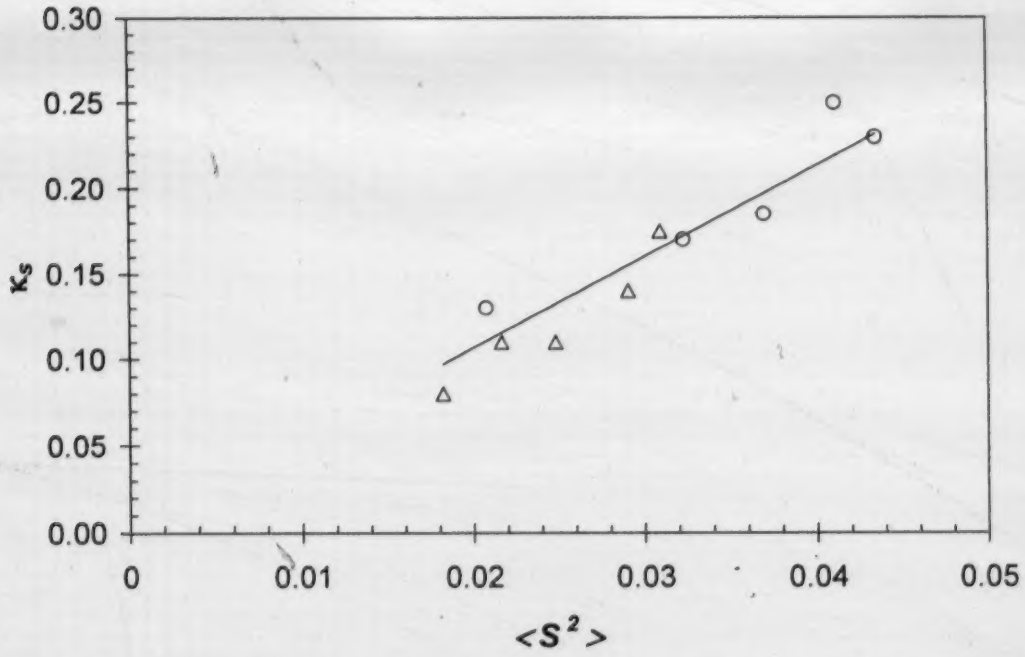

Figure 3.15: Plot of length scale slope (κ_s) versus the the mean square wave slope $\langle S^2 \rangle$ for both He and SF_6 diffusing through clean and surfactant influenced water surfaces. ○, = data for the clean water surface; Δ, = data for the surfactant influenced surface and solid line is a linear regression line passing through origin. The regression line has a slope of 5.33 and $R^2 = 0.9$.

(a)

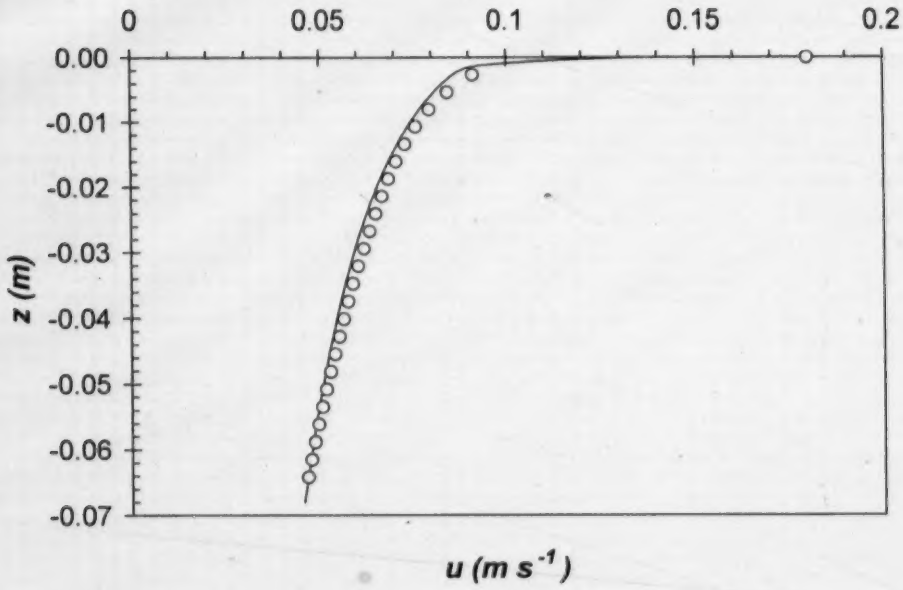

(b)

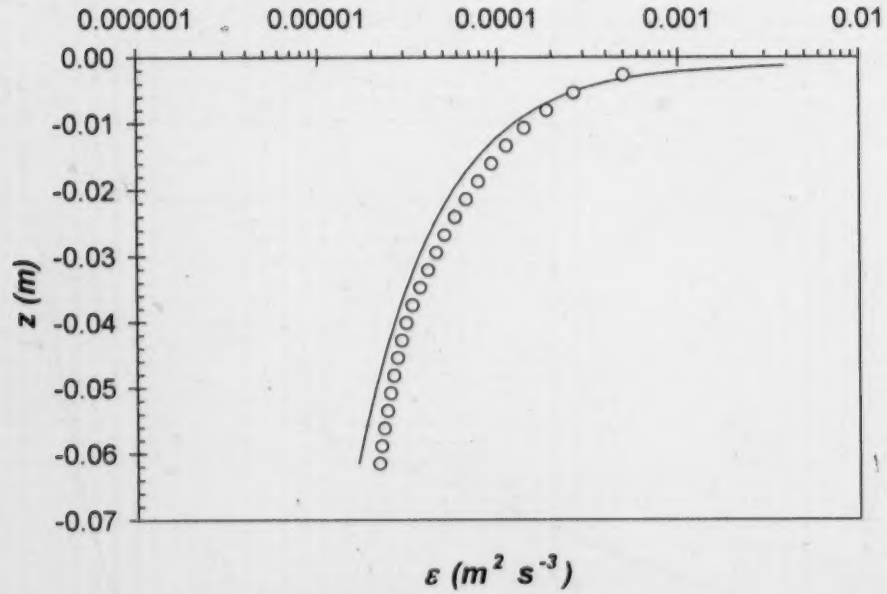

Figure 3.16: Comparison of the profiles of predicted and measured (a) velocity (u) and (b) dissipation (ε) for wind speed of 8.0 m s^{-1} on clean water surface. Solid line is the modified model's predictions of (a) u and (b) ε, ○, = experimental data points.

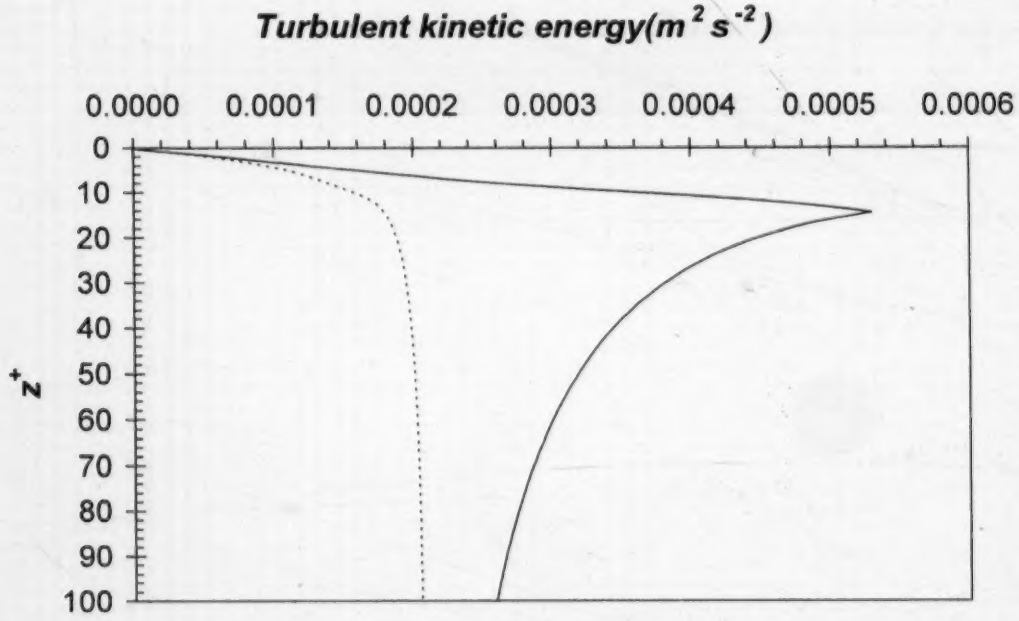

Figure 3.17: Plot of turbulent kinetic energy versus non dimensional depth (z^+) at a wind speed of 8.0 m s^{-1} on a clean water surface. The solid line is the kinetic energy profile when microscale breaking waves are present and the dotted line is when there are no microscale breaking waves present.

3.10 References

Angus, J. C., Morrow, D. L., Dunning, J. W. and French, M. J. (1969). "Motion measurement by laser doppler techniques." *Industrial and Engineering Chemistry*, 61(2), 8.

Anis, A. and Moum, J. N. (1992). "The superadiabatic surface-layer of the ocean during convection." *Journal of Physical Oceanography*, 22(10), 1221-1227.

Atmane, M. A., Asher, W. E. and Jessup, A. T. (2004). "On the use of the active infrared technique to infer heat and gas transfer velocities at the air-water free surface ." *Journal of Geophysical Research-Oceans*, 109 (C8): Art. No. C08S14.

Banner, M. L. and Peirson W. L. (1998). "Tangential stresses beneath wind-driven air-water interface." *Journal of Fluid Mechanics*, 364, 115-145.

Birch, K. G. and Ewing, J. A. (1986). "Observations of wind waves on a reservoir." Rep. 234, Institute of Oceanographic Sciences, Wormley, Surrey, England, pp. 34.

Bourassa, M.A. (2000). "Shear stress model for the aqueous boundary layer near the air-sea interface." *Journal of Geophysical Research*, 105(C1), 1167-1176.

Burchard, H. and Bolding, K. (2001). "Comparative analysis of four second-moment turbulence closure for the oceanic mixed layer.," *Journal of Physical Oceanography*, 31(8), 1943-1968.

Bye, J. A. T. (1967). "The wave-drift current." *Journal of Marine Research*, 25, 95–102.

Charnock, H. (1955). "Wind stress on a water surface." *Quarterly Journal of the Royal Meteorological Society*, 81, 639–640.

Cheung, T. K. and Street, R. L. (1988). "The turbulent layer in the water at an air-water interface." *Journal of Fluid Mechanics*, 194, 133-151.

Craig, P.D., Hunter, J.R. and Johnston, B.L. (1993). "The implications of linearly varying eddy viscosity for wind-driven current profiles." *Continental Shelf Research*, 13(1), 1-24.

Craig, P.D. and Banner, M.L. (1994). "Modeling wave-enhanced turbulence in the ocean surface layer." *Journal of Physical Oceanography*, 24, 2546-2559.

Craig, P.D. (1996). "Velocity profiles and surface roughness under breaking waves." *Journal of Geophysical Research*, 101, 1265-1277.

Davies, A. M. (1985). "A three dimensional model of wind induced flow in a sea region." *Progress in Oceanography*, 15, 71-128.

Davies, A. M. (1987). "On extracting current profiles from vertically integrated numerical models." *Coastal Engineering*, 11, 445-477.

Davies J. T. (1972). *Turbulence phenomena; an introduction to the eddy transfer of momentum, mass, and heat, particularly at interfaces,* New York, Academic Press, 1972.

Dianat, M., Yang, Z., Jiang, D. and McGuirk, J. J., (2006). "Large eddy simulation of scalar mixing in a coaxial confined jet." *Turbulence and Combustion,* 77 (1-4), 205-227.

Donelan, M. A., Hamilton, J. and Hui, W. H. (1985). "Directional spectra of wind-generated waves." *Philosophical Transactions of the Royal Society of London Series A-Mathematical Physical and Engineering Sciences*, 315 (1534), 509-562.

Drennan, W. M., Kahma, K. K., Terray, E. A., Donelan, M. A. and Kitaigorodskii, S. A. (1992). "Observations of the enhancement of kinetic energy dissipation beneath breaking wind waves." *Breaking Waves*, Banner, M.L. and Grimshaw, R.H.J., Eds., Springer, 95-101.

Duce, R., Liss, P., Barber, R., Farmer, D., Huebert, B., Jenkins, W., Matrai, P., Platt, U., Taylor, P. and Wallace, D. (2001). Surface Ocean-Lower Atmosphere Study (SOLAS) Science Plan.

Elkamash, M. K. and Loewen, M. R. (2004). "Air-sea gas transfer and turbulence for clean and surfactant contaminated surfaces." *Proceedings of the 1st Water and environment Specialty Conference, 32nd Annual Conference*, Canadian Society for Civil Engineering, Saskatoon, Saskatchewan, Canada.

Elkamash, M. K. M. (2005). *The effect of surfactants on microscale wave breaking and the aqueous boundary layer*, Ph. D. thesis, University of Alberta, Edmonton, Alberta, Canada.

Flesch, T. K., Prueger, J. H. and Hatfield, J. L. (2002). "Turbulent Schmidt number from a tracer experiment." *Agricultural and Forest Meteorology*, 111 (4), 299-307

Gargett, A. E. (1989). "Ocean Turbulence." *Annual Review of Fluid Mechanics*, 21, 419-451.

Hasselmann, K., Barnett, T. P., Bouws, E., Carlson, H., Cartwright, D. E., Enke, K., Ewing, J. A., Gienapp, H., Hasselmann, D. E., Kruseman, P., Meerburg, A., Muller, P., Olbers, D. J., Richter, K., Sell, W. and Walden, H. (1973). "Measurements of wind-wave growth and swell decay during the joint North Sea Wave Project (JONSWAP)." *Dtsch. Hydrogr. Z.*, 12, pp. 95.

Holthuijsen, L. H. and Herbers, T. H. C. (1986). "Statistics of breaking waves observed as whitecaps and the open sea." *Journal of Physical Oceanography*, 16, 290-297.

Jähne, B., Munnich, K. O. and Siegenthaler U. (1979). "Measurements of gas-exchange and momentum-transfer in a circular wind-water tunnel." *Tellus* 31 (4), 321-329

Jähne, B and Haussecker, H. (1998). "Air-water gas exchange." *Ann. Rev. Fluid Mech.* 30, 443-468.

Jenkins, A. D., (1986). "A theory for steady and variable wind and wave induced currents." *Journal of Physical Oceanography*, 16, 1370-1377.

Jenkins, A. D., (1987). "Wind and wave induced currents in a rotating sea with depth varying eddy viscosity." *Journal of Physical Oceanography*, 17, 938-951.

Kahma, K. K. (1981). "A study of the growth of the wave spectrum with fetch." *Journal of Physical Oceanography*, 11(11), 1503-1515.

King, D.B., and Saltzman, E. S. (1995). "Measurement f the diffusion-coefficient of sulfur-hexafluoride in water." *Journal of Geophysical Research-Oceans*, 100 (C4), 7083-7088.

Kitaigorodskii, S. A., Donelan, M. A., Lumley, J. L. and Terry, E. A. (1983). "Wave turbulence interactions in the upper ocean. Part II: Statistical characteristics of wave and turbulent components of the random velocity-field in the marine surface-layer." *Journal of Physical Oceanography,* 13(11), 1988-1999.

Klein, P. and Coantic, M. (1981). "A numerical study of turbulent processes in the marine upper layers." *Journal of Physical Oceanography*, 11, 849-863.

Kudryavtsev, V. N., Makin, V. K. and Chapron, B. (1999). "Coupled sea surface-atmosphere model - 2. Spectrum of short wind waves." *Journal of Geophysical Research-Oceans*, 104 (C4), 7625-7639.

Kukulka, T. and Hara, T. (2005). "Momentum flux budget analysis of wind-driven air-water interfaces." *Journal of Geophysical Research-Oceans*, 110(C12), C12020.

Kundu, K. P. (1980). "A numerical investigation of mixed layer dynamics." *Journal of Physical Oceanography*, 10, 220-236.

Lamont, J. C. and Scott, D. S. (1970). "An eddy cell model of mass transfer into the surface of a turbulent liquid." *AICHE Journal*, 16, 512-519.

Lide, D. R. 2008, ed., *CRC Handbook of Chemistry and Physics, 88th Edition (Internet Version 2008),* CRC Press/Taylor and Francis, Boca Raton, FL.

Loewen, M. R. and Siddiqui, M. H. (2006). "Detecting microscale breaking waves." *Journal of Measurement Science and Technology*, 17(4), 771-780.

Makin, V. K. (1995). "Drag of the sea-surface." *Boundary-Layer Meteorology*, 73 (1-2), 159-182.

Makin, V. K. and Kudryavtsev, V. N. (1999). "Coupled sea surface-atmosphere model - 1. Wind over waves coupling." *Journal of Geophysical Research-Oceans*, 104 (C4), 7613-7623.

Makin, V. K. and Kudryavtsev, V. N. (2002). "Impact of dominant waves on sea drag." *Boundary-Layer Meteorology*, 103(1), 83-99.

Meirink, J. F. and Makin, V. K. (2000). "Modeling low-Reynolds-number effects in the turbulent air flow over water waves." *Journal of Fluid Mechanics*, 415, 155-174.

Mellor, G. L. and Yamada, T. (1974). "Hierarchy of turbulence closure models for planetary boundary-layers." *Journal of the Atmospheric Sciences*, 31(7), 1791-1806.

Mellor, G. L. and Yamada, T. (1982). "Development of a turbulence closure-model for geophysical fluid problems." *Reviews of Geophysics*, 20 (4), 851-875.

Melville, W. K. (1996). "The role of surface-wave breaking in air-sea interaction." *Annual Review of Fluid Mechanics*, 28, 279-321.

Nedderman, R. M. (1961). "The measurement of velocities in the wall region of turbulent liquid pipe flow." *Chemical Engineering Science* 16 (1-2), 120-126.

Noh, Y. and Kim, H. J. (1999). "Simulations of temperature and turbulence structure of the oceanic boundary layer with the improved near-surface process." *Journal of Geophysical Research*, 104 (C7), 15621-15634.

Noh, Y., Jang, C. J., Yamagata, T., Chu, P. C. and Kim, C. H. (2002). "Simulation of more realistic upper-ocean processes from an OGCM with a new ocean mixed layer model." *Journal of Physical Oceanography*, 32(5), 1284-1307.

Osborn, T., Farmer, D. M., Vagle, S., Thorpe, S. A. and Cure, M. (1992). "Measurements of bubble plumes and turbulence from a submarine." *Atmosphere-ocean*, 30(3), 419-440.

Panchapakesan, N. R. and Lumley J. L. (1993). "Turbulence measurements in axisymmetrical jets of air and helium .Part 2. Helium-jet." *Journal of Fluid Mechanics*, 246, 225-247.

Peirson, W. L. and Banner, M. L. (2003). "Aqueous surface layer flows induced by microscale breaking wind waves." *Journal of Fluid Mechanics*, 479, 1-38.

Prandtl L. (1952). *Essentials of fluid mechanics*. Blackie and sons. 452.

Schlichting, H. (1968). *Boundary-layer theory*, 6th Edition, McGraw-Hill Book Company, NY, USA.

Schwarzenbach, R.P., Gschwend, P.M., Imboden, D.M. 1993. *Environmental Organic Chemistry. New* York, NY, John Wiley and Sons, Inc., p. 632.

Siddiqui, M. H. K., Loewen, M. R., Richardson, C., Asher, W. E. and Jessup, A. T. (2001). "Simultaneous particle image velocimetry and infrared imagery of microscale breaking waves." *Physics of Fluids*, 13, 1891-1903.

Siddiqui, M. H. K. (2002). "Laboratory Measurements of the flow beneath microscale breaking waves." *Ph.D. Thesis*, Department of Mechanical and Industrial Engineering, University of Toronto.

Siddiqui, M. H. K., Loewen, M. R., Asher, W. E. and Jessup, A. T. (2004). "Coherent structures beneath wind waves and their influence on air-water gas transfer." *Journal of Geophysical Research*, 109, C03024.

Siddiqui, M. H. K. and Loewen, M. R. (2007). "Characteristics of the wind drift layer and microscale breaking waves." *J. Fluid Mech.*, 573, 417-456.

Snyder, R. L., Dobson, F. W., Elliot, J. A. and Long, R. B. (1981). "Array measurements of atmospheric pressure fluctuations above gravity waves." *Journal of Fluid Mechanics*, 102, 1-59.

Stacey, M. W. and Pond, S. (1997). "On the Mellor-Yamada turbulence closure scheme: the surface boundary condition for q^2." *Journal of Physical Oceanography*, 27(10), 2081-2086.

Stacey, M. W. (1999). "Simulation of the wind-forced near-surface circulation in Knight Inlet: A parameterization of the roughness length." *Journal of Physical Oceanography*, 29(6), 1363-1367.

Sullivan, P. P., McWilliams, J. C. and Melville, W. K. (2004). "The oceanic boundary layer driven by wave breaking with stochastic variability. Part 1.Direct numerical simulations." *Journal of Fluid Mechanics*, 507, 143-174.

Terray, E. A., Donelan, M. A., Agrawal, Y. C., Drennan, W. M., Kahama, K. K., Williams III, A. J., Hwang, P. A. and Kitaigorodskii, S. A. (1996). "Estimates of kinetic

energy dissipation under breaking waves." *Journal of Physical Oceanography*, 26, 792-807.

Thompson S. M. and Turner, J. S. (1975). "Mixing across an interface due to turbulence generated by an oscillating grid." *Journal of Fluid Mechanics*, 67, 349-368.

Thorpe, S. A. (1984). "On the determination of K_v in the near-surface ocean from acoustic measurements of bubbles." *Journal of Physical Oceanography*, 14(5), 855-863.

Thorpe, S. A. (1992). "Bubble clouds and the dynamics of the upper ocean." *Quarterly Journal of the Royal Meteorological Society*, 118(503), 1-22 part A.

Uz, B. M., Donelan, M. A., Hara, T. and Bock, E. J. (2002). "Laboratory studies of the effect of short wind waves on wind stress." *Boundary Layer Meteorology*, 102, 301-331.

van Driest, E. R. (1956). "On turbulent flow near a wall." *Journal of Aeronaut. Sci.*, 23(11), 1007-1011.

Wanninkhof, R. (1992). "Relationship between wind-speed and gas-exchange over the ocean." *Journal of geophysical research-oceans*, 97 (c5), 7373-7382.

Weber, J. E. (1981). "Ekman currents and mixing due to surface gravity waves." *Journal of Physical Oceanography*, 11, 1431-1435.

Zappa, C. J., Asher, W. E. and Jessup, A. T. (2001). "Microscale wave breaking and air-water gas transfer." *Journal of Geophysical Research*, 106, 9385-9391.

Chapter 4: Gas transfer parameterization for microscale breaking waves

4.1 Introduction

Bulk parameterization is a simple and hence often an attractive way to estimate gas flux at the air water interface. Bulk parameterization of gas transfer velocity relates the transfer rate with measured variables. The feasible meteorological measurements at the ocean surface include average wind speed, temperature, humidity etc.

Based on laboratory and field measurements many parameterizations for gas transfer velocity have been developed that relates the transfer rate with the wind speed (Wanninkhof 1992, Liss and Marlivat 1986). However, these parameterizations involve a lot of uncertainties in the prediction as there are many other factors besides wind that influence the transfer rate (see Figure 1.1) (Donelan and Wanninnkhof 2002).

The thin diffusive sublayer on the water side controls the transfer rate of CO_2 at the air water interface. The turbulence is suppressed as the interface is approached and diffusion occurs mainly by molecular diffusion. However, the turbulence in the bulk water facilitates the transfer rate. It may reduce the thickness of the diffusive sublayer and increase the transport rate by displacing fluid from the sublayer. Therefore, role of turbulence needs to be accounted for to develop an accurate gas transfer parameterization.

It has been observed from previous research (Davies 1972) that the turbulent motion does not disappear sharply at any particular distance from solid wall boundary. Several investigators have experimentally measured eddies within the viscous sub-layer (Angus et al. 1969 and Nedderman 1961). The turbulent eddies are progressively damped

as the wall is approached and right at the wall the eddy motion becomes zero. Using experimental investigation Angus et al. (1969) have shown that while viscous forces are dominant and the velocity profile is linear within this sub-layer, there are small random movements superposed on the otherwise laminar flow. Therefore, a gas transfer parameterization should account for the role of small scale turbulence with in the diffusive sub layer.

In the previous chapter a turbulence model, originally developed for large scale breaking waves, was adapted to simulate the turbulence produced by microscale breaking waves. The model is made capable of predicting the gas transfer velocity at the air water interface accurately. The equation of the turbulent length scale adjacent to the water surface was modified to include the effect of viscous sub layer and the small scale turbulence with in the sublayer. The turbulence produced by microscale wave breaking was simulated as a flux of kinetic energy close to the surface. Model predictions were compared to the wind wave tank measurements of Elkamash and Loewen (2004), Elkamash (2005) and Atmane et al. (2004) in order to calibrate and verify the model. The modified turbulence model was shown to be capable of accurately predicting the near surface turbulence and gas transfer velocity generated by microscale breaking waves. The microscale breaking wave model requires several inputs in order to predict the gas transfer velocity for a given condition including the tangential shear stress (τ), surface roughness length (z_{ot}), gas diffusivity (D), wave energy factor (α) and water depth (H). Some of the model inputs are difficult to specify without measurements (e.g. z_{ot} requires measurements of both u and ε) and in the ocean it is daunting to make these measurements. Therefore, even though the turbulence model may be capable of

predicting accurate gas transfer velocities, the difficulty in obtaining accurate input for the model might discourage its use. A simplified parameterization of the gas transfer velocity with flow turbulence would be a more appealing technique to estimate k_g. Successful completion of this study will increase our understanding of the role that microscale breaking waves play in air-sea gas transfer.

4.2 Literature Review

The transfer of relatively insoluble gases such as CO_2 across the air-water interface is controlled by processes occurring on the water side (Jähne and Haussecker 1998). The water side boundary layer adjacent to the air-water interface can be divided into two regions. The upper most region immediately underneath the water surface is a concentration boundary layer whose thickness is in an order of 0.1 mm and the lower region contains turbulent water Schwarzenbach et al. (1993). According to Fick's law the gas flux, F across the boundary layer is defined as,

$$F = -D\frac{\partial c}{\partial z} \tag{4.1a}$$

where, D is the molecular diffusivity of the gas in water and $\partial c/\partial z$ is the concentration gradient. Equation (4.1a) represents local and instantaneous diffusive flux. Under steady state condition the flux becomes constant in space and can be expressed as,

$$F \approx -D\frac{\Delta c}{\delta_c} \tag{4.1b}$$

where, Δc is the concentration difference across the boundary layer and δ_c is the thickness of concentration boundary layer. This thin concentration boundary layer controls the rate

of flux of CO_2 across the air water interface. The gas flux, F is conventionally expressed as,

$$F = -k_g \Delta c \tag{4.2}$$

where, k_g is the gas transfer velocity (Liss 1973). Under unstirred or stagnant conditions the gas transfer velocity, k_g is estimated using a stagnant two film model (Schwarzenbach et al. 1993). According to this model k_g is given by,

$$k_g = \frac{D}{\delta_c} \tag{4.3}$$

However, if the water surface is renewed by turbulent motion, then the two film model does not provide accurate estimates of k_g.

Near surface turbulence in the water decreases the thickness of the concentration boundary layer (Chu and Jirka 1995) and enhances the gas transfer rate. Wave breaking is a process in which the water surface is turned over and renewed by bulk water due to the action of turbulent eddies; and as a result δ_c changes over time. This process is typically referred to as surface renewal. The surface renewal model was first proposed by Higbie (1935). According to the surface renewal model the transfer velocity (k_g) is given by,

$$k_g \approx \sqrt{\frac{D}{T}} \tag{4.4}$$

where, T is the characteristic time scale for surface renewal or the average lifetime of a parcel of water at the surface. Higbie (1935) assumed that all the fluid elements have the same exposure time at the interface. However, there remains a debate about how to estimate the time scale T as there is no universally accepted formula to calculate eddy life time. Danckwerts (1951) stated that T has to be determined from the distribution of surface element life times. According to Fortescue and Pearson (1967), surface renewal is

dominated by the largest-scale energy containing eddies and T can be estimated from the integral turbulent length scale and the root-mean-square turbulent velocity. Komori et al. (1993) used the frequency of occurrence of eddies to estimate T. The eddy life time, T is a turbulent characteristic of the flow. Jähne et al. (1979) stated that the driving force for near surface turbulence is wind shear and they related k_g to the friction velocity in water (u_*) as follows,

$$k_g = \beta'^{-1} S_c^{-n} u_* \tag{4.5}$$

where, β' is a constant termed as the dimensionless transfer resistance for momentum transfer, S_c is the molecular Schmidt number of the gas and the exponent n is a function of the boundary condition for water side turbulence. Eq. (4.5) is a form of the surface renewal model. The Schmidt number (S_c) dependence of k_g in this equation is likely to vary as a function of the hydrodynamic boundary condition at the air-water interface (Frew et al. 2004 and Jähne et al. 1987). The hydrodynamic boundary condition can vary from a free surface to a rigid surface condition. A free surface is typically clean and a rigid surface is one contaminated by surfactants. The presence of a surfactant causes a film on the water surface. The resulting film pressure causes a restoring force and if the concentration of surfactant is so strong that the surface stress fluctuations are too weak to overcome the restoring force, the free surface behaves like a rigid surface (Jähne et al. 1987).

A Taylor expansion can be applied to the concentration profile in the mass boundary layer and the Schmidt number (S_c) dependence of k_g can be calculated for the existing hydrodynamic boundary condition (Ledwell 1984). The exponent of S_c, n (see Eq. 4.5) is found to be $-2/3$ for rigid surface and $-1/2$ for free surface (Ledwell 1984,

Coantic 1986). Based on experimental data Jähne et al. (1987) suggested that there is a critical friction velocity, $u_* = 0.4$ cm s $^{-1}$. They stated that for a surfactant influenced water surface if $u_* < 0.4$ cm s $^{-1}$, the surface behaves like a rigid surface with $n = -2/3$ and if $u_* > 0.4$ cm s $^{-1}$, it behaves like a free surface and $n = -1/2$. Jähne et al. (1987) and Jähne and Haussecker (1998) found evidence that n varies gradually with increasing mean square wave slope $\langle S^2 \rangle$. Frew et al. (2004) suggested that for $\langle S^2 \rangle \leq 0.002$, $n = -2/3$ and for $\langle S^2 \rangle > 0.002$, $n = -1/2$.

Apart from the surface renewal model the gas transfer velocity (k_g) has been correlated with different turbulent characteristics of the flow in a number of previous studies (Lamont and Scott 1970, Kitaigorodskii 1984, Siddiqui et al. 2004, Zappa et al. 2004, Frew et al. 2004 and Siddiqui and Loewen 2007). These previous studies indicate that if the turbulence created by microscale breaking waves can be modeled properly, the predicted characteristics of the turbulent flow may be used to estimate the gas transfer velocity.

4.3 Analytical study of gas transfer velocity

In chapter 3 a turbulence model, is developed to accurately predict the gas transfer velocity, the mean velocity and dissipation of turbulent kinetic energy profile produced by microscale breaking waves. Near surface viscous effect was found to be dominant for flow beneath microscale breaking waves. Small scale turbulent motion with in the interfacial sub layer was found to be important for controlling the gas transfer rate. The value of the turbulent length scale adjacent to the water surface was modified to include the effect of micro breakers and the small scale turbulence. The turbulence model is

verified to accurately predict the gas transfer velocity generated by microscale breaking waves.

It is found from the model that the viscous forces are dominating in the zone $z^+ < 10$ i.e. the eddy viscosity (A) is small compared to kinematic viscosity of water (υ). However, for gases with high molecular Schmidt number ($S_c = \upsilon/D$), the eddy diffusivity (D_t) might not be small when compared with the molecular diffusivity of the gas in water (D).This is because the ratio of A to D_t is the turbulent Schmidt number (S_{ct}), which is a small value of 0.6. On the other hand the ratio of kinematic viscosity of water, υ to the D of the gas in water is the molecular Schmidt number (S_c) which for CO_2 diffusing from water is 518 at 23°C.

The gas transfer rate depends upon both the diffusivity of the gas in water (D) and also on D_t in the sub layer. The turbulent kinetic energy equation for the zone $z^+ < 10$ can be used to derive a relationship between the turbulent eddy diffusivity D_t and z. The eddy viscosity (A) is proportional to the product of the turbulent length scale (l) and the turbulent velocity scale (q) and is expressed as; $A = lqS_M$, where, $S_M = 0.39$ (Mellor and Yamada 1982). The turbulent kinetic energy is given by,

$$\frac{\partial b}{\partial t} - \frac{\partial}{\partial z}\left(lqS_q \frac{\partial b}{\partial z}\right) = lqS_M\left(\left(\frac{\partial u}{\partial z}\right)^2 + \left(\frac{\partial v}{\partial z}\right)^2\right) - \frac{2qb}{Bl} \tag{4.6}$$

where, b is the turbulent kinetic energy density ($b \equiv 0.5q^2$), $S_q = 0.387$, $B = 16.6$ (Mellor and Yamada 1982, 1974), u and v are the horizontal velocity components in the direction of the wind and perpendicular to the direction of wind, respectively. Considering a steady one dimensional flow and substituting $b = 0.5q^2$, Eq. (4.7) is rewritten as,

$$-\frac{\partial}{\partial z}\left(lqS_q \frac{\partial\left(q^2/2\right)}{\partial z}\right) = lqS_M\left(\frac{\partial u}{\partial z}\right)^2 - \frac{2q\left(q^2/2\right)}{Bl} \tag{4.7}$$

In the zone $z^+ < 10$ the velocity gradient is found to be constant and equal to the surface velocity gradient (u_*^2/υ). Substituting $l = \kappa_s(-z)$ and u_*^2/υ for the velocity gradient, Eq. (4.7) is rewritten as,

$$\left(-\frac{S_q\kappa_s}{2}\right)\left(\frac{\partial}{\partial z}\left(zq\frac{\partial}{\partial z}\left(q^2\right)\right)\right) = \left(\kappa_s S_M\right)zq\left(\frac{u_*^2}{\upsilon}\right)^2 - \left(\frac{1}{B\kappa_s}\right)\frac{q^3}{z} \tag{4.8}$$

Assuming q to be a power function of z, i.e. $q = \varphi z^\beta$, Eq. (4.8) can be reduced to,

$$\left(-\frac{S_q\kappa_s}{2}\right)\left(6\beta^2\varphi^3 z^{(3\beta-1)}\right) = \left(\kappa_s S_M\right)\left(\frac{u_*^2}{\upsilon}\right)^2 \varphi\ z^{\beta+1} - \left(\frac{1}{B\kappa_s}\right)\varphi^3 z^{(3\beta-1)} \tag{4.9}$$

A detailed description of the above simplification can be found in Appendix A. Equating the powers of z on the left and right hand sides in Eq. (4.9), β is found to be equal to one and,

$$\varphi = \frac{0.6245u_*^2\kappa_s}{\upsilon\sqrt{\left(0.06024 - 1.161\kappa_s^2\right)}} \tag{4.10}$$

Therefore, the turbulent velocity scale q, is given by, $q = \varphi z$. Substituting $l = \kappa_s(-z)$ and $q = \varphi z$ the eddy viscosity ($A = lqS_M$) can be expressed as,

$$A = \left(\kappa_s\varphi\ S_M\right)z^2 \tag{4.11}$$

The turbulent eddy diffusivity (D_t) and the eddy viscosity A are related by the turbulent Schmidt number (S_{ct}) as follows,

$$D_t = A/S_{ct} = \left(\frac{\kappa_s\varphi\ S_M}{S_{ct}}\right)z^2 \tag{4.12}$$

Let, $a = \dfrac{\kappa_s\varphi\ S_M}{S_{ct}}$ so that,

$$D_t = az^2 \tag{4.13}$$

To express the relationship between D_t and z in a non-dimensional form, let us assume that,

$$D_t^+ = a_* z^{+2} \tag{4.14}$$

where, $D_t^+ = D_t / \upsilon$, $z^+ = -\frac{u_* z}{\upsilon}$ and $a_* = \frac{a\upsilon}{u_*^2}$; substituting $a = \frac{\kappa_s \varphi\ S_M}{S_{ct}}$, a_* can be expressed as $a_* = \frac{\upsilon \kappa_s \varphi\ S_M}{S_{ct} u_*^2}$ and substituting φ from Eq. (4.10) gives,

$$a_* = \frac{0.24356 \kappa_s^2}{S_{ct}\sqrt{\left(0.06024 - 1.161\kappa_s^2\right)}} \tag{4.15}$$

Eq. (4.15) is a general expression for a_* where, the length scale slope κ_s, depends upon either the wave breaking kinetic energy flux (au_*^3) and or the mean square wave slope $\langle S^2 \rangle$ (see Figure 3.14 and 3.15). The relationship between D_t and z predicted by the microscale breaking wave model has been established by Eq. (4.13) with the assumption of a constant velocity gradient close to surface and this relationship is valid within the zone $z^+ < 10$. This relationship can now be used along with the basic diffusion equation to estimate k_g. The diffusion equation is expressed as following;

$$\frac{\partial}{\partial z}\left((D_t + D)\frac{\partial c}{\partial z}\right) = \frac{\partial c}{\partial t} \tag{4.16}$$

where, D is the molecular diffusivity. The boundary conditions are c =0 at z = 0, and $c \cong c_m$ at z^+ =10, because it is observed from the model predicted concentration profiles that at z^+ =10, the concentration profile almost reaches the mean concentration. A typical plot of the variation of concentration, c with respect to the dimensionless depth, $z^+ = u_* z/\nu$ is shown in Figure 4.1 for He at a wind speed of 6.2m s^{-1}on a clean water surface. At t = 6hr

the concentration profile corresponds to c_m = 2.0 moles liter^{-1} and the concentration at z^+ =10 is c = 1.99 moles liter^{-1}.Considering a steady process Eq. (4.16) can be rewritten as,

$$\frac{d}{dz}\left((D_t + D)\frac{dc}{dz}\right) = 0 \tag{4.17}$$

Substituting Eq. (4.13) in Eq. (4.17) gives,

$$\frac{d}{dz}\left((az^2 + D)\frac{dc}{dz}\right) = 0 \tag{4.18}$$

Integrating Eq. (4.18) with respect to z,

$$(az^2 + D)\frac{dc}{dz} = -F \tag{4.19}$$

where, F is the flux. Rearranging Eq.(4.19) and integrating with respect to z gives,

$$c(z) = \frac{-F}{\sqrt{aD}}\tan^{-1}\frac{z\sqrt{a}}{\sqrt{D}} + C_1 \tag{4.20}$$

where, C_1 is a constant of integration. Applying the boundary condition c =0 at z = 0 in Eq.(4.20), gives, C_1 =0. Substituting C_1 =0 and applying the boundary condition $c \cong c_m$ at z^+ =10 in Eq. 4.20 gives,

$$F = \frac{c_m\sqrt{aD}}{\tan^{-1}\left(10\upsilon\sqrt{a}/(u_*\sqrt{D})\right)} \tag{4.21}$$

Recalling that $F = -k_g c_m$, from Eq. (2.2) (Chapter 2) and that $a = \frac{a_* u_*^2}{\upsilon}$, Eq. (4.21) can be rewritten as,

$$k_g = \frac{\sqrt{a_* u_*^2 D/\upsilon}}{\tan^{-1}\left(10\sqrt{a_*}\left(\sqrt{\upsilon/D}\right)\right)} \tag{4.22}$$

Eq. (4.22) represents the rate of gas transfer from the water. Substituting for the molecular Schmidt number of the gas, $S_c = \upsilon/D$, gives,

$$k_g = \frac{\sqrt{a_* u_*^2 / S_c}}{\tan^{-1}\left(10\sqrt{a_* S_c}\right)} \tag{4.23}$$

For water side limited gases (e.g. SF_6, He, CO_2) the Schmidt number is usually high enough, so that the denominator of Eq. (4.23) approximately equals $\pi/2$ and hence Eq. (4.23) can be rewritten as,

$$k_g = C_3 u_* S_c^{-1/2} \tag{4.24}$$

where, $C_3 = \frac{\sqrt{a_*}}{(\pi/2)}$, u_* is the friction velocity in water and for a given wind speed and surface condition (clean or surfactant influenced) a_* is a fixed value given by Eq. (4.15). Equation (4.24) is the analytical form of the gas transfer model for microscale breaking waves. This equation can be used to predict the gas transfer velocity instead of using the turbulence model as long as the assumption of a constant velocity gradient in the zone z^+ <10 is valid. However, Equation (4.24) can not be used if the length scale slope with in viscous sublayer (κ_s) is greater or equal to 0.23 as the coefficient C_3 approaches infinity. It is observed from the turbulence model predicted concentration profiles that if $\kappa_s \geq 0.23$, the velocity gradient in the zone z^+ <10 is not constant and for such a case the turbulence model must be used to predict the transfer rate.

4.4 Discussion

For young steep wind waves appearing on water surface the turbulence on water side are comprised of the shear generated turbulence and of the turbulence caused by the wave breaking. The analytical form of the gas transfer model (Eq. 4.24) can be used to predict the transfer rate of water side limited gases for situations when microscale

breaking waves appear on water surface. If the turbulence created by breaking wave is so small that a concentration gradient is formed at the surface with thickness δ_c then δ_c can be expressed as, $\delta_c = D/u_*$. Substituting δ_c in Eq. (4.24); the gas transfer rate can be expressed as; $k_g = -C_3 S_c^{-1/2}\left(\frac{D}{\delta_c}\right)$. This expression represents 'the thin film model' for the extreme situation of very low turbulence ($\kappa_s \sim 0$).

At the other extreme of strong turbulence the surface fluid is fully renewed by energetic eddies generated by breaking waves. The eddy can be characterized by a frequency $1/T$ where, T is the characteristic time scale for surface renewal or the average lifetime of a parcel of water at the surface. On dimensional grounds the frequency can be expressed as $\frac{1}{T} = \frac{u_*^2}{\upsilon}$. Thus Eq. (4.24) can then be expressed as, $k_g = -C_3\sqrt{\frac{D}{T}}$. This expression represents the 'surface renewal' form of the gas transfer velocity.

The present model is developed to predict the gas transfer velocity due to microscale wave breaking on both clean and surfactant influenced water surfaces. In the analytical study (see Eq. 4.24) the exponent of Schmidt Number (S_c), is found to be $-1/2$ for both clean and surfactant contaminated water surface which agrees with the suggestion by Jähne et al. (1987) and Frew et al. (2004) for free surfaces. For the surfactant influenced water surface the lowest wind speed corresponded to a friction velocity of u_* = 0.5 cm s $^{-1}$ and a mean square slope of $\langle S^2 \rangle = 0.018$. Both of these values are higher than the limits proposed for a rigid surface by Jähne et al. (1987) ($u_* \geq$ 0.4 cm s $^{-1}$) and Frew et al. (2004) ($\langle S^2 \rangle \geq 0.002$). Therefore, all of the experimental data used in this study should be modeled using a free surface boundary condition.

The effect of surfactants on gas transfer is incorporated in the parameterization by using a different length scale slope than for clean water in the zone z^+ <10 (see Table 3.6). The values of κ_s for both clean and surfactant influenced experiments are well correlated with the mean square wave slope $\langle S^2 \rangle$ and with the kinetic energy flux due to wave breaking, αu_*^3 (see Figure 3.15 and 3.14). In Chapter 3 the wave energy factor (α) was found to be dependant on the wave age (C_p/u_{*a}). It was found that for microscale breaking waves propagating on clean water surface α ranges from 5 to 24 for a wave age range of 0.5 to 1.2. It was suggested that for clean water surface α could be computed using the parameterization between α and wave age proposed by Terry et al. (1996), though their parameterization was derived using field data where the wave age of the youngest wave was about 3.0 and the amplitude of the smallest wave was an order of magnitude larger than microscale breaking wave. If the waves are very young (C_p/u_{*a} < 2) α should be used in range of 5 to 24 for microscale breaking wave consideration (see Chapter 3). For surfactant contaminated surfaces a 60% reduction in the value of wave energy factor can be assumed compared to a clean water surface.

The performance of the analytical model (Eq. 4.24) is evaluated by comparing of the model predictions with experimental data obtained from a source different from the one used for calibration and validation of the model. Air-water gas transfer measurements were made in the wind wave tank at the NASA Air–Sea Interaction Research Facility of the Observational Science Branch at NASA Goddard Space Flight Center/Wallops Flight Facility, VA, in April–May 2004. The main test section of the wind wave tank was 18.29 m long, 1.22 m high and 0.91 m wide, the mean water depth was 0.76 m. Experiments were conducted on microscale breaking waves at five different wind speeds ranging from

approximately 4.0 to 11.0 m s^{-1} and at fetches of 4.8, 8.8 and 12.4 m. The bulk gas transfer velocity was determined for SF_6 and He diffusing through clean water using the conservative mass balance method. The average wave age (C_p/u_{*a}) for fetches of 4.8, 8.8 and 12.4 m were 1.0, 1.1 and 1.76 respectively.

In Figure 4.2, the experimental estimates of gas transfer velocity for $S_c = 600$, k_{600} are plotted as a function of water side friction velocity u_* at three different fetches. The waves were too young ($C_p/u_{*a} < 2$), to use the Terry et al. (1996) proposed parameterization between α and wave age. However, the C_p/u_{*a} values of these experiments were similar to the experiments conducted by Elkamash and Loewen (2004). It was found in Chapter 3 that α ranges from 5 to 24 for the experimental data obtained from Elkamash and Loewen (2004). Therefore, the model (Eq. 4.24) predicted k_{600} are computed using α value equal to 5 and 24 for very young microscale waves and plotted in Figure 4.2. The correlation between the wave breaking kinetic energy flux, αu_*^3 and κ_s (see Figure 3.14) is used to find appropriate κ_s for a given u_*. Finally k_{600} is computed from the analytical equation for gas transfer velocity (Eq. 4.24). It can be observed that the experimental data at a fetch 12.4 m are particularly well predicted by the model using $\alpha = 24$. It is interesting to note that k_{600} for fetch 4.8, 8.8 are reasonably well predicted by the model using $\alpha = 5$. The experimental data at fetches of 4.8 and 8.8m have approximately the same wave age ($C_p/u_{*a} \sim 1.0$) therefore, it is reasonable that the same value of α applies to both.

Predictions of gas transfer velocity using bulk parameterization suggested by Liss and Marlivat (1986) are also plotted in Figure 4.2 for comparison. This parameterization

is a well used one that correlates the k_{600} with wind speed. According to Liss and Marlivat (1986) the relationship between wind speed and k_{600} can be expressed as:

$$k_{600} = 0.17U_{10} \ (U_{10} < 3.6 \text{ m s}^{-1})$$

$$k_{600} = 2.85U_{10} - 9.65 \ (3.6 \text{ m s}^{-1} < U_{10} < 13 \text{ m s}^{-1})$$

$$K_{600} = 5.9U_{10} - 49.3 \ (U_{10} > 13 \text{ m s}^{-1}) \qquad (4.26)$$

where, U_{10} is the wind speed measured at 10m height and k_{600} is computed in cm hr $^{-1}$. It can be observed from Figure 4.2 that Liss and Marlivat's (1986) parameterization highly under predicts gas transfer velocity at high u^*. At lower friction velocity the parameterization gives reasonable prediction only for fetch 4.8, 8.8m i.e. for very young waves. However, the parameterization is also unable to give reasonable prediction of k_{600} at any range of friction velocity for fetch 12.4m. This indicates the effect of wave age on the gas transfer velocity can not be reflected in the simple empirical wind speed based parameterizations.

The performance of the model for field situations was investigated by comparing of the model predictions with the field data obtained from Frew et al. (2004). As a part of the Coastal Ocean Processes (CoOP) program they made observations of wind stress, transfer velocity in coastal and offshore waters south of Cape Cod, New England, in July 1997. The gas transfer velocities were computed from aqueous heat transfer velocities derived from infrared imagery and bulk heat flux estimates (Frew et al. 2004). In Figure 4.3, the CoOP97 estimates of gas transfer velocity k_{660} (transfer velocity for S_c = 660 for CO_2 in sea water at 20°C) are plotted as a function of water side friction velocity u_*. Frew et al. (2004) wrote that the large scatter in field data was a result of a wave field dependent transition between limiting transport regimes.

If it is assumed that microscale wave breaking is the dominant physical mechanism then the wave energy factor should be set to a value in the range of 5 to 24. However, Craig and Banner (1994) suggested $\alpha = 100$ for well developed large scale waves. Although the present model is not intended to model large scale breaking waves, model predictions of k_{660} with $\alpha = 100$ are nonetheless computed. Model predictions (using Eq. 4.24) of k_{660} for $\alpha = 5$, 24 and 100 are plotted in Figure 4.3. It is observed that majority of the field data fall within the band $5 < \alpha < 24$. However, some of the field data also agree well with the model prediction using $\alpha = 100$. The trend of the field data is reasonably well predicted by the model. Therefore, it is possible to get sensible predictions of gas transfer velocities in field condition using the present model.

There have been numerous studies of gas transfer velocity which led to an expression for k_g comparable to Eq. (4.24). For example, Ledwell (1984) derived an expression for D_t as a function of z for free and rigid surfaces using a Taylor expansion of the fluctuating velocity normal to the interface. He used this expression along with the 1-D diffusion equation to derive an equation for estimating k_g. The constants in Ledwell's equation were derived empirically from experimental measurements. Ledwell found that k_g was a linear function of u_* but this equation did not account for the variation of k_g due to wave breaking or the presence of a surfactant. Similar to the study of Ledwell (1984), the surface renewal model proposed by Jähne et al. (1979) and Frew et al. (2004) also included a constant, the dimensionless transfer resistance (β), which is independent of the flow turbulence (see Eq. 4.5). However, in the present study the coefficient C_3 in Eq. (4.24) is a function of κ_s that incorporates the effect of wave breaking and surface cleanliness, and k_g varies with u_* in a nonlinear pattern. This nonlinear variation of k_g

with u_* is observed for both and field measurement of transfer rates (see Figure 4.2 and 4.3). The present model is unique in the sense that it is the first surface renewal type of gas transfer model that accounts for both the effect of wave breaking and the presence of a surfactant.

4.5 Conclusions

An analytical approach for computing the gas transfer velocity is presented in present study. The simplified turbulent kinetic energy equation along with the assumption of a constant velocity gradient at $z^+ < 10$ are used to derive a relationship between the turbulent diffusivity and the depth ($D_t \sim z^2$). Then using Fick's law an expression for the gas transfer velocity (k_g) is derived (see Eq. 4.24). The constant (C_3) in the equation is dependent on the slope of the length scale equation (κ_s) in the viscous sublayer. The value of κ_s is obtained from the model as two different set of constants for clean water surfaces and surfactant contaminated water surfaces (see Table 3.6). The values of κ_s are found to be correlated with the wave breaking kinetic energy flux, au_*^3 (see Figure 3.14) and the relationship between them can be used to find κ_s for a given condition (i.e. given values of u_* and a). Using Eq. (4.24) it is possible to predict the gas transfer velocity without determining the value of the concentration gradient at the surface. It is thus, an alternate and simple approach to compute gas transfer velocity analytically, avoiding the difficult task of measuring the microscale breaking wave model inputs (e.g. z_{ot}).

The analytical equation (Eq. 4.24) is a parameterization of the gas transfer velocity with the flow turbulence (u_* and κ_s). This equation is unique as it provides a transition from the extreme case of zero turbulence to the extreme case of strong

turbulence. Neither the 'thin film model' nor the 'surface renewal' model is perfect because in reality the turbulence exists in between these two extreme situations. A model capable of a transition between these two models is therefore, expected to be a more logical solution to the problem. Moreover this parameterization is the first of its kind as the friction velocity does not represent the total shear stress for young waves. In Eq. (4.24) u_* represents the tangential stress and can be obtained by partitioning the total stress. In order to predict k_g, the equation requires the value of u_* and α. In recent years analytical (Kukulka and Hara 2005) and numerical models have been developed (Meirink and Makin 2000, Makin and Kudryavtsev 1999 and 2002) to estimate the tangential stress from wind speed and wave age and these models can be used to estimate the value of u_*. The wave energy factor α can be estimated using Terry et al.'s (1996) proposed parameterization between α and wave age for clean water surfaces. For very young waves ($C_p/u_{*a} < 2$) it is suggested that the value of α be set in the range of 5 to 24 for microscale breaking waves (see Chapter 3).

The scale of microscale breaking waves is essentially the same in the laboratory and in the field. Although the proposed parameterization is developed using the laboratory data acquired by Elkamash and Loewen (2004), the parameterization can be applied to the field in cases where microscale wave breaking is thought to be the dominant physical mechanism controlling the transfer rate. The proposed parameterization has been found to give satisfactory predictions when compared with laboratory and field measurements of gas transfer velocity. The parameterization captures the physics controlling the transfer process by correctly modeling the turbulence very close to surface. Therefore, the parameterization is capable of predicting gas transfer rate

at the air-water interface with significant accuracy and the predictions will lead to improved long-term forecasts of climate change.

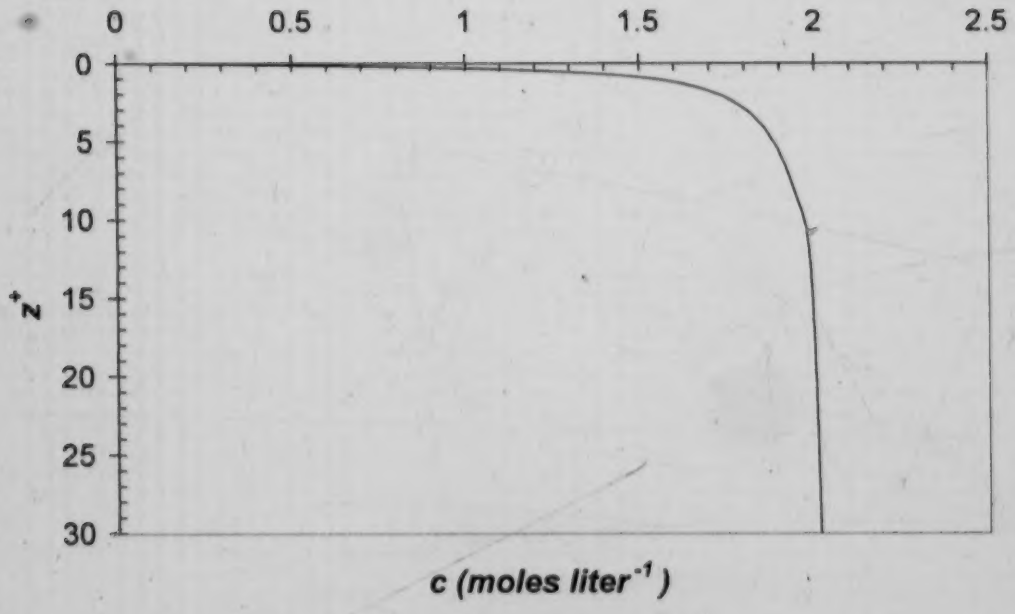

Figure 4.1: Plot of concentration profile versus non dimensional depth (z^+) at a wind speed of 6.2 m s^{-1} on clean water surface at 6 hr.

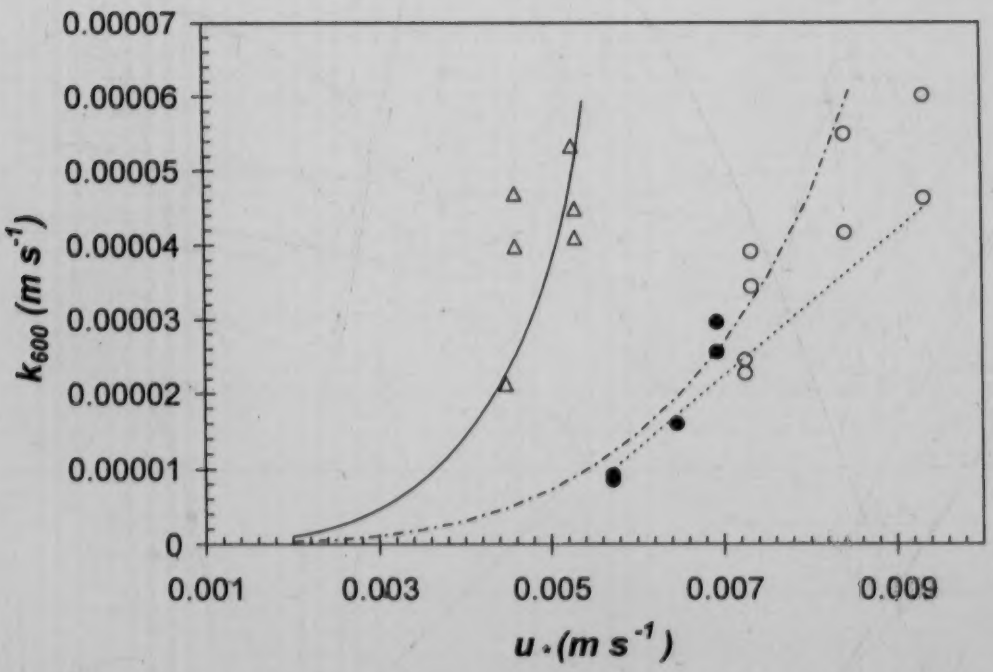

Figure 4.2: Plot of gas transfer velocity (k_{600}) for S_c = 600 versus water side friction velocity (u_*). Data points are measurements of experimental data at the NASA Air–Sea Interaction Research Facility, ○, = fetch 4.8, ●, = fetch 8.8 and Δ , = fetch 12.4 m, solid line is the model prediction of k_{600} for a wave energy factor α = 24 and dashed-dotted line is the model prediction of k_{600} for α = 5, dotted line is the empirical relationship suggested by Liss and Marlivat (1986).

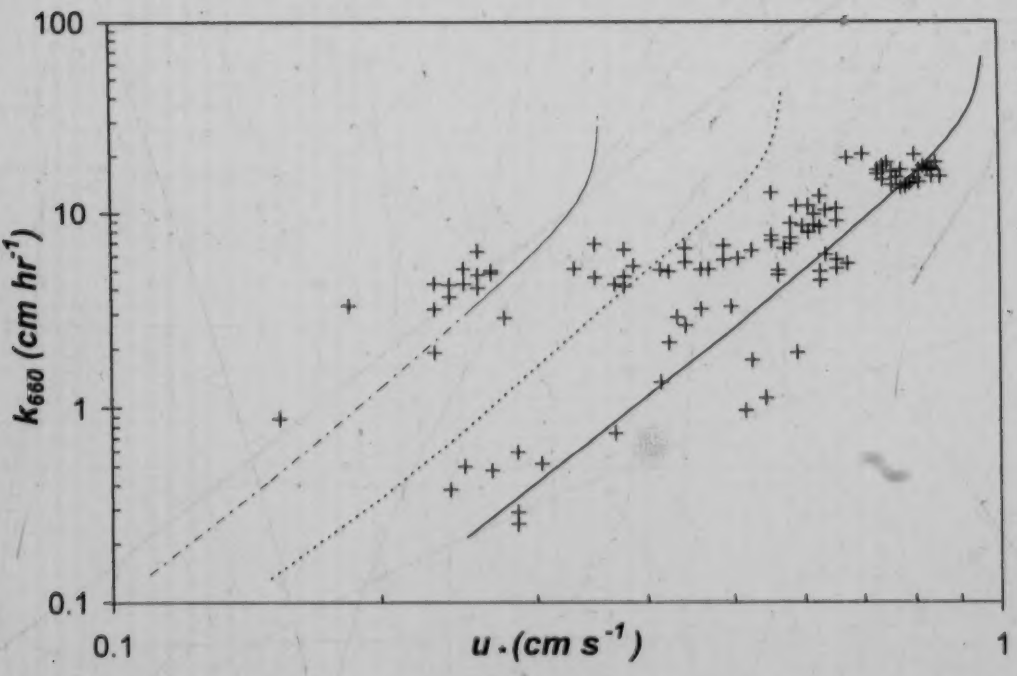

Figure 4.3: Plot of gas transfer velocity (k_{660}) for S_c = 660 for CO_2 in sea water at 20°C versus water side friction velocity (u_*). +, = CoOP97 measurements of field data, solid line is the model prediction of k_{660} for a wave energy factor α = 5, dotted line is the model prediction of k_{660} for a wave energy factor α = 24 and dashed-dotted line is the model prediction of k_{660} for α = 100.

4.6 References

Angus, J. C., Morrow, D. L., Dunning, J. W. and French, M. J. (1969). "Motion measurement by laser doppler techniques." *Industrial and Engineering Chemistry*, 61(2), 8.

Atmane, M. A., Asher, W. E. and Jessup, A. T. (2004). "On the use of the active infrared technique to infer heat and gas transfer velocities at the air-water free surface ." *Journal of Geophysical Research-Oceans*, 109 (C8): Art. No. C08S14.

Chu, C.R. and Jirka, G.H., (1995). "Reaeration in combined wind/stream driven flows." In *Air-water Gas Transfer, Selected papers from the third international symposium on air-water gas transfer*, edited by Jähne, B. and Monahan, E.C., AEON Verlag and studio, Hanau, Germany, pp. 79 - 88.

Craig, P.D. and Banner, M.L. (1994). "Modeling wave-enhanced turbulence in the ocean surface layer." *Journal of Physical Oceanography*, 24, 2546-2559.

Danckwerts, P.V. (1951). "Significance of liquid-film coefficients in gas absorption." *Industrial and Engineering Chemistry*, 43 (6), 1460-1467.

Davies J. T. 1972, *Turbulence phenomena; an introduction to the eddy transfer of momentum, mass, and heat, particularly at interfaces,* New York, Academic Press, 1972.

Donelan, M.A. and Wanninkhof R. (2002). "Gas transfer at water surfaces – concepts and issues." *Proceedings of the4th International Symposium on Gas Transfer at Water Surfaces,* Miami, Florida, USA.

Elkamash, M. K. and Loewen, M. R. (2004). "Air-sea gas transfer and turbulence for clean and surfactant contaminated surfaces." *Proceedings of the 1st Water and*

environment Specialty Conference, 32nd Annual Conference, Canadian Society for Civil Engineering, Saskatoon, Saskatchewan, Canada.

Elkamash, M. K. M. (2005). *The effect of surfactants on microscale wave breaking and the aqueous boundary layer*, Ph. D. thesis, University of Alberta, Edmonton, Alberta, Canada.

Fortescue, G. F., and Pearson J. R. A., (1967). "On gas absorption into a turbulent liquid." *Chem. Eng. Sci.*, 22, 1163 -1180.

Frew, N. M., Bock, E. J., Schimpf, U., Hara, T., Haußecker, H., Edson, J. B., McGillis, W. R., Nelson, R. K., McKenna, S. P., Uz, B. M., and Jähne, B. (2004). "Air-sea gas transfer: Its dependence on wind stress, small-scale roughness, and surface films." *J. Geophys. Res.*, 109, C08S17.

Higbie, R., (1935). "The rate of absorption of a pure gas into a still liquid during short periods of exposure." *Trans. Am. Inst. Chem. Eng.*, 35, 365 - 389.

Jähne, B., Munnich, K. O. and Siegenthaler U. (1979). "Measurements of gas-exchange and momentum-transfer in a circular wind-water tunnel." *Tellus* 31 (4), 321-329

Jähne, B and Haussecker, H. (1998). "Air-water gas exchange." *Ann. Rev. Fluid Mech.* 30, 443-468.

Jähne, B., Munnich, K. O., Bosinger, R., Dutzi, A., Huber, W. and Libner, P. (1987). "On the parameters influencing air-water gas exchange." *J. Geophys. Res.*, 92, 1937-1949.

Kitaigorodskii, S.A., (1984). "On the fluid dynamical theory of turbulent gas transfer across an air sea interface in the presence of breaking wind-waves." *Journal of physical oceanography*, 14 (5), 960-972.

Komori, S., Nagaosa, R. and Murakami, Y., (1993). "Turbulence structure and mass transfer across a sheared air-water interface in wind driven turbulence." *J. Fluid Mech.* 249, 161-183.

Kukulka, T. and Hara, T. (2005). "Momentum flux budget analysis of wind-driven air-water interfaces." *Journal of Geophysical Research-Oceans*, 110(C12), C12020.

Lamont, J.C. and Scott, D.S. (1970). "An eddy cell model of mass transfer into surface of a turbulent liquid." *AICHE Journal*, 16 (4), 513-519.

Ledwell, J. J. (1984). "The variation of the gas transfer coefficient with molecular diffusivity." in *Gas Transfer at Water Surfaces*, edited by W. Brutsaert and G. H. Jirka, 293-302, D. Reidel, Norwell, Mass.

Liss, P. S. and Merlivart, L. (1986). "Air-sea gas exchange rates: Introduction and synthesis". In *The role of Air-sea exchange in geo-chemical cycling*, edited by P. Burt Menard, 113-129, Boston, 1986.

Makin, V. K. and Kudryavtsev, V. N. (1999). "Coupled sea surface-atmosphere model - 1. Wind over waves coupling." *Journal of Geophysical Research-Oceans*, 104 (C4), 7613-7623.

Makin, V. K. and Kudryavtsev, V. N. (2002). "Impact of dominant waves on sea drag." *Boundary-Layer Meteorology*, 103(1), 83-99.

Meirink, J. F. and Makin, V. K. (2000). "Modeling low-Reynolds-number effects in the turbulent air flow over water waves." *Journal of Fluid Mechanics*, 415, 155-174.

Mellor, G. L. and Yamada, T. (1974). "Hierarchy of turbulence closure models for planetary boundary-layers." *Journal of the Atmospheric Sciences*, 31(7), 1791-1806.

Mellor, G. L. and Yamada, T. (1982). "Development of a turbulence closure-model for geophysical fluid problems." *Reviews of Geophysics*, 20 (4), 851-875.

Nedderman, R. M. (1961). "The measurement of velocities in the wall region of turbulent liquid pipe flow." *Chemical Engineering Science* 16 (1-2), 120-126.

Schwarzenbach, R.P., Gschwend, P.M., Imboden, D.M. 1993, *Environmental Organic Chemistry. New* York, NY, John Wiley and Sons, Inc., p. 632.

Siddiqui, M. H. K., Loewen, M. R., Asher, W. E. and Jessup, A. T. (2004). "Coherent structures beneath wind waves and their influence on air-water gas transfer." *Journal of Geophysical Research*, 109, C03024.

Siddiqui, M. H. K. and Loewen, M. R. (2007). "Characteristics of the wind drift layer and microscale breaking waves." *J. Fluid Mech.*, 573, 417-456.

Terray, E. A., Donelan, M. A., Agrawal, Y. C., Drennan, W. M., Kahama, K. K., Williams III, A. J., Hwang, P. A. and Kitaigorodskii, S. A. (1996). "Estimates of kinetic energy dissipation under breaking waves." *Journal of Physical Oceanography*, 26, 792-807.

Wanninkhof, R. (1992). "Relationship between wind-speed and gas-exchange over the ocean." *Journal of geophysical research-oceans,* 97 (c5), 7373-7382.

Zappa, C. J., Asher, W. E., Jessup, A. T., Klinke, J. and Long, S. R. (2004). "Microbreaking and the enhancement of air-water gas transfer velocities." *J. Geophys. Res.*, 109, C8, C08S16.

Chapter 5: Conclusions and Recommendations

5.1 Summary

The stepwise procedures for the development of a turbulence model and an improved gas transfer parameterization for microscale breaking wave are presented in this thesis. At the beginning of the study, the data obtained for microscale breaking wave is described and analyzed and a technique for estimating the boundary shear stress and roughness length is presented. The technique is used to estimate the required inputs for the turbulence model for microscale breaking waves. A one dimensional model that was developed to predict the turbulence generated by large scale waves is modified to predict the turbulence beneath microscale breaking waves. The turbulence model developed for microscale waves is then modified to account for gas transport across the air-water interface. Modifications to the turbulent length scale equation are made to ensure that the predicted gas transfer velocities are realistic. An analytical approach for computing gas transfer velocities is also developed. The parameterization is validated using laboratory and field measurements of gas transfer velocities.

5.2 Conclusions of the Study

Conclusions are described in detail in previous chapters. The general conclusions of the entire study are summarized in the following paragraphs.

A technique for estimating the boundary shear stress and roughness length is proposed in this study. The roughness length z_{ot} is an important input parameter for surface layer models. These models can not be regarded as functional predictive tools without a technique to independently specify z_{ot} (Craig 1996). Therefore, a significant

achievement is made in this study by introducing a technique for the estimation of z_{ot} at the air-water interface. The method is referred to as the length scale method and will be applicable when accurate measurements of $u(z)$ and $\varepsilon(z)$ are available. An expression for the turbulent length scale (l) as a function of u_*, $u(z)$ and $\varepsilon(z)$ has been derived. The turbulent length scale profiles indicate that the thickness of laminar sub-layer δ_v, beneath a wind driven water surface extends up to $10\upsilon/u_*$.

The length scale method provides more accurate estimates of u_* compared to the velocity defect profile method since it utilizes measured profile of both the mean velocity and the rate of dissipation of turbulent kinetic energy. A comparative analysis shows that the new length scale method provides twice as accurate estimates of u_* compared to the velocity defect profile method. The estimated z_{ot} generally decrease with increasing U. The ratio z_{ot} / λ decreases with increasing U from 0.14 to 0.02 and from 0.10 to 0.01 for clean surfaces and surfactant contaminated surfaces respectively. For most cases the z_{ot} and z_{ot} / λ values for a surfactant influenced water surface are found to be smaller than for a clean water surface. A power law relation between z_{ot} / λ and U applicable for very young waves (wave age < 2) is developed.

A one dimensional ocean model with 2.5 level closure scheme is used to develop a turbulence model that can predict the vertical structure of the turbulence beneath microscale breaking waves. The public domain General Ocean Turbulence Model (GOTM) is adopted to develop a turbulent transport algorithm for microscale breaking waves. The effect of wave breaking is simulated using a technique proposed by Craig and Banner (1994). The most significant modification of GOTM that is implemented in this study is the modification in the turbulent length scale. The turbulent length scale is

modified by introducing a zero length scale in the zone $z^+ < 10$ using the observation of turbulent length scale profiles close to the interface. In order to be consistent with the zero length scale region for $z^+ < 10$, the additional production term representing the effect of wave breaking, $\alpha u_*^3/h_g$ is applied at a z^+ value of 15.

The value of the wave energy factor (α) for both clean or surfactant influenced water surface is found to be an order of magnitude smaller than the value suggested by Craig and Banner (1994) for large scale breaking waves. The wave energy factor α, is found to be dependant on the wave age (C_p/u_{*a}) of microscale breaking waves and also on the cleanliness of the water surface (i.e. clean or surfactant influenced). For surfactant affected water surfaces on average α values are found to be 60% less than that found for the clean water surfaces. For clean water surface experiments α values are found to be in close accordance with the parameterization suggested by Terray et. al. (1996) between α and wave age and their equation can be used to find α for $C_p/u_{*a} > 2$. For the very young waves ($C_p/u_{*a} < 2$) studied here the value of α is found to be in the range of 5 to 24.

The results of the present study demonstrate that τ_{kang} is the appropriate hydraulic input for turbulence models involving young waves. It is observed that for both clean and surfactant contaminated surface the variation of z_{ot} with u_* is insignificant and confined over a narrow range. It is recommended that z_{ot} values of 0.004m and 0.003m be used for clean and surfactant contaminated surfaces respectively, for modeling the turbulence beneath very young wind waves when microscale wave breaking is prevalent.

It is found that the small scale turbulence that exists within the interfacial viscous dominating sublayer plays an important role in gas transfer. The turbulence is small enough so that the flow remains predominantly laminar within the sublayer. The

turbulent length scale equation is modified close to the interface to account for this small scale turbulence. A linear length scale with a very mild slope (length scale slope κ_s) is introduced in the viscous sublayer ($z^+ < 10$) to predict the appropriate gas transfer velocity.

The characteristics of the flow beneath microscale breaking waves that are identified in this study are; the viscous sublayer that exists at the air-water interface for $z^+ < 10$ contains a very small amount of turbulence which plays an important role in the mass transport across interface and the non-dimensional roughness height, z_o^+ is found to be less than 2.3 which indicates that the flow is either hydrodynamically smooth or in the transition regime.

In Chapter 4 an analytical gas transfer parameterization is presented for microscale breaking waves. The simplified turbulent kinetic energy equation along with the assumption of a constant velocity gradient in the zone $z^+ < 10$ are used to derive a relationship between the turbulent diffusivity and the depth. Then using Fick's law an expression for the gas transfer velocity (k_g) is derived. The analytical equation is an alternate and direct approach to compute gas transfer velocity, avoiding the need for challenging measurements of microscale breaking wave model inputs (e.g. z_{ot} requires measurement of ε profile).

The analytical equation is a parameterization of the gas transfer velocity in terms of u_* and the length scale slope κ_s for $z^+ < 10$. This equation is unique as it provides a transition from the extreme case of the 'thin film model' to the other extreme case of the 'surface renewal' model. The thin film model assumes that there is no turbulence in the boundary layer of an air-water interface. Previous laboratory studies (Angus et al. 1969

and Nedderman 1961) experimentally measured eddies within the viscous sub-layer. Therefore, the assumption that the turbulent length scale remains zero in the viscous sublayer might be an oversimplification and in reality the turbulence exists in between the two extreme situations represented by the above mentioned models. A model capable of a transition between these two cases is therefore, expected to be a more logical solution to the problem. The friction velocity represents the tangential stress and can be obtained by partitioning the total stress. The values of κ_s are found to be correlated with the wave breaking kinetic energy flux, au_*^3 and the relationship between them can be used to find κ_s for a given condition (i.e. given values of u_* and a).

The most important conclusion from the gas transfer parameterization study can be summarized as: the turbulent kinetic energy equation designed to work in the fully turbulent flow zone, can also be applied in the zone $z^+ < 10$ where viscous effects dominate to give a good predictions of momentum and mass transfer.

5.3 Recommendations for Future Study

In order to enhance our understanding of the role microscale wave breaking plays in air sea gas exchange the following studies are recommended.

1) The experimental data that is used to develop the turbulence model had the first measurement at a depth of $z^+ \sim 10$. Future experiments conducted with significantly higher resolution of DPIV and profile measurements will allow the viscous sublayer thickness to be studied more precisely.

2) The experimental data used for the turbulence model development and validation were conducted at short fetches of 5.5m and 4.8m respectively. Future studies

should include measurements at longer fetches to validate the applicability of the model.

3) The study focused on very young waves and a narrow range of wave age. Future experiments conducted with a wider range of wave age (C_p/u_{*a}) would allow a definite relationship to be established between the wave age and wave energy factor (α).

4) Estimation of the roughness length z_{ot}, requires measurement of the dissipation profile. However, dissipation measurements in the ocean or in lakes are often a daunting a task and the resulting measurement may not be precise enough to enable accurate estimation of z_{ot}. Therefore, establishing a relationship between z_{ot} and other more easily measurable quantities such as the dominant wave length would be valuable. Extensive experimental study will be required to determine a relationship between z_{ot} and λ.

5) This study is based on a 1-D ocean model. Future study might be carried out using higher dimensional models to capture different features of the wave generated turbulence. The higher dimensional models could be important for studies of coherent structures developed under breaking waves or for the prediction of mean square wave slopes.

5.4 References

Angus, J. C., Morrow, D. L., Dunning, J. W. and French, M. J. (1969). "Motion measurement by laser doppler techniques." *Industrial and Engineering Chemistry*, 61(2), 8.

Craig, P.D. and Banner, M.L. (1994). "Modeling wave-enhanced turbulence in the ocean surface layer." *Journal of Physical Oceanography*, 24, 2546-2559.

Craig, P.D. (1996). "Velocity Profiles and Surface Roughness Under Breaking Waves." *Journal of Geophysical Research*, 101, 1265-1277.

Nedderman, R. M. (1961). "The measurement of velocities in the wall region of turbulent liquid pipe flow." *Chemical Engineering Science* 16 (1-2), 120-126.

Terray, E. A., Donelan, M. A., Agrawal, Y. C., Drennan, W. M., Kahama, K. K., Williams III, A. J., Hwang, P. A. and Kitaigorodskii, S. A. (1996). "Estimates of kinetic energy dissipation under breaking waves." *Journal of Physical Oceanography*, 26, 792-807.

Appendix A

A.1 First order second moment uncertainty analysis

Experiments fall under two categories from the point of view of reliability estimate: multiple sample and single sample. An experiment is called multiple sample, if sufficiently large number of measurements are performed using different methods and instruments so that a statistical analysis can be done for the reliability of the results. On the other hand for single sample experiments no such reliability estimate can be done from repeated measurements. Most engineering experiments, including the one performed by Elkamash and Loewen (2007), are single sample experiments. For single sample experiments the most useful method of defining uncertainty was first introduced by Kline and McClintock (1953). This uncertainty analysis is also known as the first order second moment uncertainty analysis. The analysis is based on the uncertainty of the basic variable and the propagation of uncertainty on other dependent variables. The first order second moment uncertainty estimate into a result R' is described briefly in this section. Let R' be a function of N independent variable $V_1, V_2, \ldots V_N$ i.e.

$$R' = R'\langle V_1, V_2, \ldots V_N \rangle \tag{A.1}$$

If the uncertainty of variable $V_1, V_2, \ldots V_N$ are $W_1, W_2, \ldots W_N$ respectively, then the uncertainty into the result R' is given by W_R as follows:

$$W_R = \left[\left(\frac{\partial R'}{\partial V_1} W_1 \right)^2 + \left(\frac{\partial R'}{\partial V_2} W_2 \right)^2 + \ldots + \left(\frac{\partial R'}{\partial V_N} W_N \right)^2 \right]^{1/2} \tag{A.2}$$

Expressing R' as a power function of the variables as follows:

$$R' = R'\langle V_1^{m_1}, V_2^{m_2}, \ldots V_N^{m_N} \rangle \tag{A.3}$$

Substituting Eq. (A.3) into Eq. (A.2) and rearranging gives:

$$\frac{W_R}{R'} = \left[\left(m_1 \frac{W_1}{V_1} \right)^2 + \left(m_2 \frac{W_2}{V_2} \right)^2 + \ldots\ldots\ldots + \left(m_N \frac{W_N}{V_N} \right)^2 \right]^{1/2} \tag{A.4}$$

where, $\frac{W_R}{R'}$ is the percentage uncertainty in result R'.

Using the uncertainty in u measurements (2.5%), the uncertainty in velocity gradient can be estimated. The velocity gradient $\partial u/\partial z$, can be expressed as:

$$\frac{\partial u}{\partial z} = \left(\frac{u_1 - u_2}{z_1 - z_2} \right) = f(\Delta u) \tag{A.5}$$

The uncertainty in $\partial u/\partial z$ is estimate is computed using Equation (A.4) as;

$$\frac{W_{\partial u/\partial z}}{\partial u/\partial z} = \left[\left(\frac{1.W_{u_1}}{u_1} \right)^2 + \left(\frac{1.W_{u_2}}{u_2} \right)^2 \right]^{1/2} = \left[0.025^2 + 0.025^2 \right]^{1/2} = 0.0354 = 3.5\%$$

A.2 Turbulent length scale profile for microscale breaking wave

Plots of the variation of the dimensionless turbulent length scale, $l^+ = u_* l/\nu$ with respect to the dimensionless depth, $z^+ = -u_* z/\nu$ are shown in Figure A.1 to Figure A.10 (for both clean surface and surfactant contaminated surface experiments). The length scale values are computed using Eq. 2.6. Also plotted in these figures are the second order least square regression line fitted in between $z^+ > 30$ and $z/H < 0.035$. This line corresponds to Eq. 2.1. From the observation of these figures it is found that the turbulent length scale is approximately zero in the zone $z^+ < 10$.

A.3 Velocity and Dissipation profile predicted by the turbulence model developed for microscale breaking wave

Measured profiles of the mean velocity and the rate of dissipation of turbulent kinetic energy are compared with profiles predicted using the turbulence model developed for microscale breaking waves in Figure A.11 to A.20 (for both clean surface and surfactant contaminated surface experiments). The modified length scale equation for microscale breaking waves (Eq. 3.12) is used for turbulent length scale and the wave breaking production term, P_w ($\alpha u_*^3/h_g$) is injected at $z^+ = 15$. The inputs for the turbulence model for different wind speeds are given in the corresponding figure caption.

A.4 Selection of length scale equation for k_g optimization

A.4.1 Functional forms of length scale (for $z^+ < 10$) used for k_g optimization

Different functional forms for the length scale equation in the buffer layer are tested e.g. constant, linear (using different length scale slope, κ_s), and exponential functions so that the model predicted k_g, ε and u, fit the measured gas transfer velocities, dissipation and velocity profiles the best. The different forms of length scale equation that are used in the zone $z^+ < 10$ to find the best possible length scale equation are given in Table A.1.

The results are found to be most consistent using the linear length scale type equation. The slope of the length scale κ_s, is found to increase with increasing wind speed using the linear length scale function. No such consistent correlation is observed using the other functional form of l. It is observed that for a given experimental condition the optimum value of coefficient K or exponent m (see Table A.1) is different to predict the

appropriate k_g for SF_6 and He using the constant, power law or the exponential form of length scale respectively. But for the same experimental condition the same value of the turbulent length scale slope (κ_s) is required for the zone $z^+ < 10$ for both SF_6 and He. This validates the selection of the linear length scale function for k_g optimization.

A.4.2 Effect of viscous sublayer thickness (δ_v^+) on k_g

The length scale slope κ_s, is chosen to be optimum when the difference between the experimental and model predicted value of gas transfer velocity k_g is less than 8%. The linear length scale equation used for the zone $z^+ < \delta_v^+$ (viscous sublayer thickness) is also combined with different thickness of the viscous sublayer δ_v^+, but no improvement in the desired momentum profile is observed for such a case. The optimum values of κ_s obtained using different thickness of the viscous sublayer δ_v^+, for SF_6 and He diffusing through clean and surfactant affected surfaces at all wind speeds are presented in Table A.2.

A.5 Analytical relationship between the eddy diffusivity (D_t) and depth (z)

Using the assumption that the energy diffuses according to an eddy diffusion relationship and that dissipation is based on dimensional arguments, the simplified form of turbulent kinetic energy equation is given by,

$$\frac{\partial b}{\partial t} - \frac{\partial}{\partial z}\left(lqS_q \frac{\partial b}{\partial z} \right) = lqS_M \left(\left(\frac{\partial u}{\partial z} \right)^2 + \left(\frac{\partial v}{\partial z} \right)^2 \right) - \frac{2qb}{Bl} \qquad \text{(A.6)}$$

where, z is the vertical coordinate, b is the turbulent kinetic energy density ($b = 0.5q^2$), q is the turbulent velocity scale, l is the turbulent length scale, $S_q = 0.387$, $S_M = 0.39$, $B =$

16.6 (Mellor and Yamada (1982), u and v are the horizontal velocity components in the direction of wind and perpendicular to the direction of wind respectively. Considering a steady one dimensional flow and substituting $b = 0.5q^2$, Eq. (A.6) is rewritten as;

$$-\frac{\partial}{\partial z}\left(lqS_q\frac{\partial(q^2/2)}{\partial z}\right) = lqS_M\left(\frac{\partial u}{\partial z}\right)^2 - \frac{2q(q^2/2)}{Bl} \qquad \text{(A.7)}$$

From the model predicted velocity profiles the velocity gradient is found to be constant in the zone $z^+ < 10$ which is equal to the surface velocity gradient (u_*^2/υ). Considering the zone $z^+ < 10$, substituting $l = \kappa_s(-z)$ and u_*^2/υ for the velocity gradient, Eq. (A.7) is rewritten as;

$$\left(-\frac{S_q\kappa_s}{2}\right)\left(\frac{\partial}{\partial z}\left(zq\frac{\partial}{\partial z}(q^2)\right)\right) = (\kappa_s S_M)zq\left(\frac{u_*^2}{\upsilon}\right)^2 - \left(\frac{1}{B\kappa_s}\right)\frac{q^3}{z} \qquad \text{(A.8)}$$

Assuming, $K_1 = \left(-\frac{S_q\kappa_s}{2}\right)$, $K_2 = (\kappa_s S_M)\left(\frac{u_*^2}{\upsilon}\right)^2$ and $K_3 = \left(\frac{1}{B\kappa_s}\right)$; Eq. (A.8) can be simplified as,

$$K_1\left(\frac{\partial}{\partial z}\left(zq\frac{\partial}{\partial z}(q^2)\right)\right) = K_2 zq - K_3\frac{q^3}{z} \qquad \text{(A.9)}$$

Assuming q to be a power function of z, i.e. $q = \varphi z^{\beta}$, Eq. (A.9) can be rewritten as;

$$K_1\left(\frac{\partial}{\partial z}\left(\varphi\ z^{\beta+1}\frac{\partial}{\partial z}\left(\varphi^2 z^{2\beta}\right)\right)\right) = K_2\varphi\ z^{\beta+1} - K_3\varphi^3 z^{3\beta-1} \qquad \text{(A.10)}$$

Simplifying the left hand side and rearranging Eq. (A.10) can be rewritten as;

$$K_1\left(6\beta^2\varphi^3 z^{(3\beta-1)}\right) + K_3\varphi^3 z^{3\beta-1} = K_2\varphi\ z^{\beta+1} \qquad \text{(A.11)}$$

Dividing the left hand side and right hand side of Eq. (A.11) by φ and simplifying gives;

$$z^{3\beta-1}\varphi^2\left(K_1 6\beta^2 + K_3\right) = K_2 z^{\beta+1} \qquad \text{(A.12)}$$

Equating the powers of z between left hand side and right hand side in Eq. (A.12),

$$3\beta - 1 = \beta + 1 \tag{A.13}$$

Eq. (A.13) can be solved for $\beta = 1$. Substituting $\beta = 1$ in Eq. (A.12) φ is solved as,

$$\varphi = \sqrt{\frac{K_2}{(6K_1 + K_3)}} \tag{A.14}$$

Substituting $K_1 = \left(-\frac{S_q \kappa_s}{2}\right)$, $K_2 = (\kappa_s S_M)\left(\frac{u_*^2}{\upsilon}\right)^2$, $K_3 = \left(\frac{1}{B\kappa_s}\right)$, $S_q = 0.387$, $S_M = 0.39$ and $B = 16.6$; Eq. (A.14) is simplified as;

$$\varphi = \frac{0.6245 u_*^2 \kappa_s}{\upsilon\sqrt{(0.06024 - 1.161\kappa_s^2)}} \tag{A.15}$$

Therefore, the turbulent velocity scale is expressed as a linear function of z as, $q = \varphi z$, where φ is expressed by Eq. (A.15).

The eddy viscosity (A) is proportional to the product of turbulent length scale (l) and the turbulent velocity scale (q) and expressed as; $A = lqS_M$. Substituting $l = \kappa_s(-z)$ and $q = \varphi z$ the eddy viscosity ($A = lqS_M$) can be expressed as,

$$A = (\kappa_s \varphi\ S_M) z^2 \tag{A.16}$$

The turbulent eddy diffusivity (D_t) and the eddy viscosity A are related by the turbulent Schmidt number (S_{ct}) as;

$$D_t = A / S_{ct} = \left(\frac{\kappa_s \varphi\ S_M}{S_{ct}}\right) z^2 \tag{A.18}$$

Assuming, the constants in Eq. (A.18) $\frac{\kappa_s \varphi\ S_M}{S_{ct}} = a$, the turbulent eddy diffusivity (D_t) is expressed as,

$$D_t = az^2 \qquad \text{(A.19)}$$

A.6 Velocity and Dissipation profile predicted by the turbulence model developed for gas transfer prediction

Measured profiles of the mean velocity and the rate of dissipation of turbulent kinetic energy are compared with profiles predicted using the turbulence model developed for microscale breaking waves in Figure A.21 to A.30 (for both clean surface and surfactant contaminated surface experiments). The modified length scale equation for gas transfer parameterization (Eq. 3.16) is used for turbulent length scale and the wave breaking production term, P_w (au_*^3/h_g) is injected at $z^+ = 15$. The inputs for the turbulence model for different wind speeds are given in the corresponding figure caption.

Appendix B

This appendix contains the General Ocean Turbulence Model (GOTM) source files that were modified for the purpose of the study. A DIGITAL visual Fortran (Version 5.0A) platform is required to run GOTM. LaTex software is required to read the description of the source files. The portion of the source file where modification is applied for the present study is marked by bold-italic font.

B.1 Modification of Turbulent Length Scale Equation

Source File name: algebraiclength.f90

```
!BOP
! !ROUTINE: The algebraic length--scale equations \label{sec:algebraiclength}

! !INTERFACE:
  subroutine algebraiclength(method,nlev,z0b,z0s,depth,h,NN,u_taus,u_taub)

! !DESCRIPTION:
! This subroutine computes the vertical profile of the turbulent
! scale $l$ from different types of analytical expressions. These
! range from simple geometrical forms to more complicated expressions
! taking into account the effects of stratification and shear. The
! users can select their method in the input file {\tt gotmturb.inp}.
! For convenience, we define here $d_b$ and $d_s$ as the distance
! from the bottom and the surface, respectively. The water
! depth is then given by $H=d_b+d_s$, and $z_0^b$ and
! $z_0^s$ are the repective roughness lengths. With these
! abbreviations, the expressions implemented in GOTM are as follows.
! \begin{enumerate}
```

```
! \item The parabolic profile is defined according to
!  \begin{equation}
!   l=\kappa \frac{(d_s+z_0^s) (d_b+z_0^b)}
!                 {d_s+d_b+z_0^b+z_0^s}
!  \comma
!  \end{equation}
!  where it should be noted that only for large water depth
!  this equation converges to $\kappa(z+z_0)$ near the bottom
! or near the surface.
! \item The triangular profile is defined according to
!  \begin{equation}
!   l = \kappa \, \min(d_s+z_0^s,d_b+z_0^b)
!  \comma
!  \end{equation}
!  which converges always to $\kappa(z+z_0)$ near the bottom
! or near the surface.
! \item A distorted parabola can be constructed by
!  using a slightly modified form of the equation
!  used by \cite{XingDavies95},
!  \begin{equation}
!   l = \kappa \frac{(d_s+z_0^s)(d_b^\text{Xing}+z_0^b)}
!                 {d_s+d_b^\text{Xing}+z_0^s+z_0^b}
!   \comma
!   d_b^\text{Xing} =
!   d_b \exp{\left(-\beta \frac{d_b}{H} \right)}
!  \comma
!  \end{equation}
!  where it should be noted that only for large water depth
!  this equation converges to $\kappa(z+z_0)$ near the bottom
! or near the surface. The constant $\beta$ is a form parameter
! determining the distortion of the profile. Currently we use
```

```
!  $\beta = 2$ in GOTM.
! \item A distorted parabola can be constructed by
!   using a slightly modified form of the equation
!   used by \cite{RobertOuellet87},
!  \begin{equation}
!    l = \kappa (d_b+z_0^b)
!        \sqrt{1-\frac{d_b-z_0^s}{H}}
!  \comma
!  \end{equation}
!   where it should be noted that only for large water depth
!   this equation converges to $\kappa(z+z_0)$ near the bottom.
!   Near the surface, the slope of $l$ is always different from
!   the law of the wall, a fact that becomes important when model
!   solutions for the case of breaking waves are computed, see
!   \sect{sec:analyse}.
! \item Also the famous formula of \cite{Blackadar62} is based on
!    a parabolic shape, extended by an extra length--scale $l_a$.
!   Using the form of \cite{Luytenetal96}, the algebraic relation
!   is expressed by
!    \begin{equation}
!      l = \left( \frac{1}{\kappa (d_s+z_0^s)}
!            +\frac{1}{\kappa (d_b+z_0^b)}
!            +\dfrac{1}{l_a} \right)
!   \comma
!    \end{equation}
!   where
!  \begin{equation}
!      l_a = \gamma_0 \frac{\int_{-H}^\eta k^\frac{1}{2} z dz}
!                          {\int_{-H}^\eta k^\frac{1}{2} dz}
! \end{equation}
!   is the natural kinetic energy scale resulting from the
```

```
!   first moment of the rms turbulent velocity. The constant
!   $\gamma_0$ usually takes the value $\gamma_0 = 0.2$.
!   It should be noted that this expression for $l$
!   converges to $\kappa(z+z_0)$ at the surface and the bottom
!   only for large water depth, and when $l_a$ plays only a
!   minor role.
! \item The so--called ISPRAMIX method to compute the length--scale
!   is described in detail in \sect{sec:ispramix}.
! \end{enumerate}
! After the length--scale has been computed, it is optionally
! limited by the method suggested by \cite{Galperinetal88}. This
! option can be activated in {\tt gotmturb.inp} by setting
! {\tt length\_lim = .true.} The rate of dissipation is computed
! according to \eq{epsilon}.

! !USES:
  use turbulence, only: L,eps,tkeo,tke,k_min,eps_min,   &
                        cde,galp,kappa,length_lim
  IMPLICIT NONE

! !INPUT PARAMETERS:
  integer, intent(in)             :: method,nlev
  double precision, intent(in)          :: z0b,z0s
  double precision, intent(in)          :: depth,h(0:nlev),NN(0:nlev)
  double precision, intent(in)                        :: u_taus,u_taub
!
! !DEFINED PARAMETERS:
  integer, parameter              :: Parabola=1
  integer, parameter              :: Triangle=2
  integer, parameter              :: Xing=3
  integer, parameter              :: RobertOuellet=4
```

```
  integer, parameter              :: Blackadar=5
  integer, parameter              :: ispra_length=7

!EOP
! !LOCAL VARIABLES:
  integer             :: i,m,j
  double precision              :: ds,db,dbxing,b
  double precision              :: beta,gamma,La,int_qz,int_q
  double precision              ::Lcrit,L_min,Lnum,Lm(0:nlev),Lt,epsv,epst,Lip,geps(0:nlev)
  double precision              :: dsp,z0sp,d,Lmin,L1,H1,H2,SL,A,C,E,F,dsp1,dsp2
  double precision              :: dspl,dspu,m1,m2,z1,z2,lm1,lm2
  double precision  ::
a11,a12,a13,a14,a21,a22,a23,a24,a31,a32,a33,a34,a41,a42,a43,a44
  double precision              :: u11,u12,u13,u14,u22,u23,u24,u33,u34,u44
  double precision              :: l21,l31,l32,l41,l42,l43
  double precision              :: f1,f2,f3,f4
  double precision              :: y1,y2,y3,y4
  double precision              :: p1,p2,p3,p4,ks
!BOC
! distance from bottom and surface initialised
  db=0.
  ds=0.
!
! parabolic shape
  select case (method)

    case(parabola)
      do i=1,nlev-1
        db=db+h(i)
        ds=depth-db
        L(i)=kappa*(ds+z0s)*(db+z0b)/(ds+db+z0b+z0s)
```

```
      end do
      L(0)   = kappa*z0b
      L(nlev) = kappa*z0s

! triangular shape
! Modified by Shaheli (2004)
!! triangular shape length scale first modified for zero length scale for z+<10
!! For z+ >10 a van driest damping equation is applied to make sure a rapid transition
to the law of wall
 case(triangle)
! distance from bottom and surface initialised
      ds=0.
!     dsp is the non dimensional depth = u*z/v
      dsp=0.
      db=0.
      do i=nlev-1,1,-1
                  ds=ds+h(i)
                  db=depth-ds
                  dsp=(u_taus*ds)/0.000000947

! Making length scale L(i)= kappa*z
                  L(i)=kappa*min(ds+z0s,db+z0b)
! then apply a van driest damping equation to make sure
! a rapid transition to the law of wall for z+ or dsp> 10
                  if (ds.lt.db) then
                  L(i)=L(i)*(1-exp(-(dsp-10)/10))

! Applying near zero length scale for z+ less than 10
                        if (dsp.le.10) then
                        L(i)=0.00000000000000000000000001
! Then apply a linear variation of the length scale with a
```

```
!very mild slope (ks) for z+ less than 10 to satisfy
!the gas transfer velocity for the corresponding wind speed.
!The value of ks in the following equation has to be changed
!for each run according to the applicable length scale slope in the zone z+ < 10.
                    L(i)=L(i)+ks*ds
                    endif
! Getting info about fitting a 3rd order polynomial function
! between the two segments of length scale
!(i.e. first segment a linear scale for z+<10 and
! second segment an exponential van Driest transion after z+>10).
! lower limit of z+ at which transition will start = dspl
! upper limit of z+ at which transition will stop = dspu
! the 4x4 matrix is solved by LU decomposition.
                    dspl=8
                    dspu=13
                    if (dsp.le.dspl) then
                    z1=dsp
                    lm1=(u_taus*L(i))/0.000000947
                    if (i .lt. (nlev-1)) then
                    m1=(L(i)-L(i+1))/h(i+1)
                    endif
                    endif

                    if (dsp.le.dspu) then
                    z2=dsp
                    lm2=(u_taus*L(i))/0.000000947
                    if (i .lt. (nlev-1)) then
                    m2=(L(i)-L(i+1))/h(i+1)
                    endif
                    endif
```

```
            endif
end do

            ! Define the force matrix
            f1=lm1
            f2=lm2
            f3=m1
            f4=m2

            !define the known 4X4 matrix
            a11=z1**3
            a12=z1**2
            a13=z1
            a14=1
            a21=z2**3
            a22=z2**2
            a23=z2
            a24=1
            a31=3*z1**2
            a32=2*z1
            a33=1
            a34=0
            a41=3*z2**2
            a42=2*z2
            a43=1
            a44=0

            !Define L and U matrix
            u11=a11
            u12=a12
            u13=a13
```

```
u14=a14

l21=a21/u11
l31=a31/u11
l41=a41/u11

u22=a22-l21*u12
u23=a23-l21*u13
u24=a24-l21*u14

l32=(a32-l31*u12)/u22
l42=(a42-l41*u12)/u22

u33=a33-l31*u13-l32*u23
u34=a34-l31*u14-l32*u24

l43=(a43-l41*u13-l42*u23)/u33

u44=a44-l41*u14-l42*u24-l43*u34

      !Solve for Y matrix

      y1=f1
      y2=f2-l21*y1
      y3=f3-y1*l31-y2*l32
      y4=f4-y1*l41-y2*l42-y3*l43

      !Solve for unknown matrix

      p4=y4/u44
      p3=(y3-p4*u34)/u33
```

```
                    p2=(y2-p3*u23-p4*u24)/u22
                    p1=(y1-p2*u12-p3*u13-p4*u14)/u11

! Addition of the 3-D polynomial curve between
! two parts (z+ 8 to z+ 13)of the length scale equation
                    ds=0.
                    dsp=0.

                    do i=nlev-1,1,-1
                    ds=ds+h(i)
                    dsp=(u_taus*ds)/0.000000947
                    if ((dsp.ge.dspl) .and. (dsp.le.dspu)) then

    L(i)=(p1*dsp**3+p2*dsp**2+p3*dsp+p4)*(0.000000947/u_taus)
                    endif
                    end do

   L(0)   = kappa*z0b
   L(nlev) = kappa*z0s*0

! modified Xing and Davies (1995)
! modification of parabolic mixing length
     case(Xing)
       beta = 2. ! a tuning parameter
       do i=1,nlev-1
        db=db+h(i)
        ds=depth-db
! lu changed a bug in here
        dbxing=db*exp(-beta*db/depth)
        L(i)=kappa*(ds+z0s)*(dbxing+z0b)/(ds+dbxing+z0s+z0b)
       end do
```

```
      L(0)   = kappa*z0b
      L(nlev) = kappa*z0s
! modified Robert and Ouellet(1987)
! modification of parabolic mixing length
    case(RobertOuellet)
      do i=1,nlev-1
       db=db+h(i)
       ds=depth-db
! lu changed a bug in here
        L(i)= kappa*(db+z0b)*sqrt(1-(db-z0s)/depth)
      end do
      L(0)   = kappa*z0b
      L(nlev) = kappa*(depth+z0b)*sqrt(z0s/depth) ! no log-law (!)

! Blackadar (1962).
! In the form suggested by Luyten et al. (1996) for two boundary layers.
    case(Blackadar)
      int_qz  = 0.
      int_q   = 0.
      do i=1,nlev-1
        db=db+h(i)
! compute the first moment turbulent velocity
        int_qz = int_qz + sqrt(tkeo(i))*(db+z0b)*h(i)
! compute vertically averaged turbulent velocity
        int_q  = int_q  + sqrt(tkeo(i))*h(i)
      end do
      gamma=0.2            ! an empirical factor
      La=gamma*int_qz/int_q  ! free turbulence length-scale
      db=0.0
      do i=1,nlev-1
```

```
        db=db+h(i)
        ds=depth-db
        L(i)=1/(1/(kappa*(ds+z0s))+1/(kappa*(db+z0b))+1/La)
      end do
      L(0)   = kappa*z0b
      L(nlev) = kappa*z0s

! Ispramix
    case(ispra_length)
      call ispralength(nlev,NN,h,depth)
      L(0)   = kappa*z0b
      L(nlev) = kappa*z0s
    case default
  end select
  do i=0,nlev
!   clip the length-scale at the Galperin et al. (1988) value
!   under stable stratifcitation
    if ((NN(i).gt.0).and.(length_lim)) then
      Lcrit=sqrt(2*galp*galp*tke(i)/NN(i))
      if (L(i).gt.Lcrit) L(i)=Lcrit
    end if
!   compute the dissipation rate
    eps(i)=cde*sqrt(tke(i)*tke(i)*tke(i))/L(i)
! substitute minimum value
    if (eps(i).lt.eps_min) then
      eps(i) = eps_min
      L(i) = cde*sqrt(tke(i)*tke(i)*tke(i))/eps_min
    endif
  end do

  return
```

```
  end subroutine algebraiclength
!EOC
```

B.2 Modification of Turbulent Kinetic Energy Flux

B.2.1 Source File name: fk_craig.f90

```
!This source file is modified to apply zero kinetic energy flux at the surface.
!BOP
! !ROUTINE: TKE flux from wave--breaking \label{sec:fkCraig}
! !INTERFACE:
  double precision  function fk_craig(u_tau)

! !DESCRIPTION:
! This functions returns the flux of $k$ caused by breaking surface waves
! according to
! \begin{equation}
!  \label{craig}
!   F_k = \eta u_*^3
!  \point
! \end{equation}
! This form has also been used by \cite{CraigBanner94}, who suggested
! $\eta \approx 100$.
! !USES:
  IMPLICIT NONE
!
! !INPUT PARAMETERS:
  double precision, intent(in)            :: u_tau
!
! !DEFINED PARAMETERS:
! eta value has been defined = 0 instead of Craig and Banner defined value of 100
! to apply zero flux at surface
  double precision, parameter             :: eta=0.0
```

```
!EOP
!-----------------------------------------------------------------------
!BOC
  fk_craig = eta*u_tau**3.
  end function fk_craig
!EOC
```

B.2.2 Source File name: production.f90

```
! This source file is modified to apply the kinetic energy flux (αu*^3)
! at a depth of z+ = 15 as a source of wave breaking turbulence
!BOP
! !ROUTINE: Turbulence production  \label{sec:production}
! !INTERFACE:
  subroutine production(nlev,alpha,u_taus,z0s,num,nuh,h)
! !DESCRIPTION:
! This subroutine calculates the production terms of TKE as defined
! in \eq{PandG}. The shear--production follows from
! \begin{equation}
!   \label{computeP}
!    P=\nu_t (M^2 + \alpha_w N^2) + X_P
!   \comma
! \end{equation}
! with the turbulent diffusivity of momentum, $\nu_t$, defined in
! \eq{nu}. The shear--frequency, $M$, is discretised as described
! in \sect{sec:uequation}. The term with $\alpha_w$ traces back to
! a prameterisation of breaking internal waves suggested by
! \cite{Mellor89}. $X_P$ is an extra production term, connected for
! example with turbulence production caused by sea--grass, see
! \eq{sgProduction} in  \sect{sec:seagrass}.
! Similarly, the buoyancy production is computed from the expression
! \begin{equation}
```

```
! \label{computeB}
!  B=-\nu_t'N^2
!  \comma
! \end{equation}
! with the turbulent diffusivity of heat, $\nu'_t$, defined in
! \eq{nu}. The buoyancy--frequency, $N$, is discretised as described
! in \sect{sec:stratification}.

! !USES:
  use meanflow, only: NN,SS,xP,P,B,no_shear
  IMPLICIT NONE

! !INPUT PARAMETERS:
  integer, intent(in)             :: nlev
  double precision, intent(in)          :: alpha
  double precision, intent(in)          :: u_taus,z0s
  double precision, intent(in)          :: num(0:nlev),nuh(0:nlev)
  double precision, intent(in)          :: h(0:nlev)

!LOCAL VARIABLES:
  double precision          :: ds,Pw,Hrms,u_a,dsp,CI
  integer             :: i,a
!EOP
!BOC
  if (no_shear) then
    P= xP
  else
    P=num*(SS+alpha*NN) + xP
  end if
  B=-nuh*NN
!! Modified by Shaheli (2005)
```

```
! Apply K.E (eta.u*^3)at z+ ~ 15 and distribute it over one grid space
! distance from surface initialized
  ds=0.
! the non dimensional depth,  u*z/υ = dsp
  dsp=0.
! identify the depth where the depth z+ or dsp is ~15
                    do i=nlev-1,1,-1
                                  if (dsp.lt.15) then
                                      ds=ds+h(i)
                                      dsp=(u_taus*ds)/0.000000947
                                  end if
                                      if (dsp.ge.15) goto 112
                    end do
!Production term due to wave breaking added to the production (P) at z+=15
! and distribute it over one grid space
! define the value of the wave energy factor (α) as alpha in the following equation
! for example alpha is set = 10 for the given case
Alpha=10.0
112                 P(i)=P(i)+(alpha*u_taus**3)/h(i)

  return
  end subroutine production
!EOC
```

B.3 Modification of boundary condition of Heat Transport Equation to account for mass transport

Source File name: temperature.f90

```
!BOP
! !ROUTINE: The temperature equation \label{sec:temperature}
! !INTERFACE:
  subroutine temperature(nlev,dt,cnpar,I_0,heat,nuh,rad)
```

```
! !DESCRIPTION:
! This subroutine computes the balance of heat in the form
! \begin{equation}
!  \label{TEq}
!   \dot{\theta}
!   = {\cal D}_\theta
!   - \frac{1}{\tau_R(\theta)}(\theta-\theta_{obs})
!   + \frac{1}{C_p \rho_0} \partder{I}{z}
!   \comma
! \end{equation}
! where $\dot{\theta}$ denotes the material derivative of the potential
! temperature $\theta$, and
! ${\cal D}_\theta$ is the sum of the turbulent and viscous transport
! terms modelled according to
! \begin{equation}
!  \label{DT}
!   {\cal D}_\theta
!   = \frstder{z}
!    \left(
!      \left( \nu'_t + \nu^\theta \right) \partder{\theta}{z}
!    \right)
!   \point
! \end{equation}
! In this equation, $\nu'_t$ and $\nu^\theta$ are the turbulent and
! molecular diffusivities of heat, respectively. The computation
! of $\nu'_t$ is discussed in \sect{sec:turbulenceIntro}.
!
! Horizontal advection is optionally
! included  (see {\tt obs.inp}) by means of prescribed
! horizontal gradients $\partial_x\theta$ and $\partial_y\theta$ and
! calculated horizontal velocities $u$ and $v$.
```

```
! Relaxation with the time scale $\tau_R (\theta)$
! towards a precribed (changing in time)
! profile $\theta_{obs}$ is possible.
! The sum of latent, sensible, and longwave radiation is treated
! as a boundary condition. Solar radiation is treated as an inner
! source, $I(z)$. It is computed according the
! exponential law (see \cite{PaulsonSimpson77})
! \begin{equation}
!   \label{Iz}
!   I(z) = I_0 \bigg(Ae^{-\eta_1z}+(1-A)e^{-\eta_2z}\bigg).
! \end{equation}
! The absorbtion coefficients $\eta_1$ and $\eta_2$ depend on the water type
! and have to be prescribed either by means of choosing a \cite{Jerlov68} class
! (see \cite{PaulsonSimpson77}) or by reading in a file through the namelist
! {\tt extinct} in {\tt obs.inp}.

! Diffusion is numerically treated implicitly, see equations (\ref{sigmafirst})-
! (\ref{sigmalast}).
! The tri--diagonal matrix is solved then by a simplified Gauss elimination.
! Vertical advection is included for accounting for adaptive grids,
! see {\tt adaptivegrid.F90}.

! !USES:
  use meanflow, only: avmolt,rho_0,cp
  use meanflow, only: h,ho,u,v,T,avh,w,grid_method,w_grid
  use observations, only: dtdx,dtdy,t_adv,w_adv,w_adv_discr,w_adv_method
  use observations, only: tprof,TRelaxTau
  use observations, only: A,g1,g2
  IMPLICIT NONE

! !INPUT PARAMETERS:
```

```
   integer, intent(in)             :: nlev
   double precision, intent(in)            :: dt,cnpar
   double precision, intent(in)            :: I_0,heat
   double precision, intent(in)            :: nuh(0:nlev)

! !OUTPUT PARAMETERS:
   double precision                  :: rad(0:nlev)
!EOP

! !LOCAL VARIABLES:
   integer             :: i,Bcup,Bcdw,flag
   double precision            :: Qsour(0:nlev)
   double precision            :: Tup,Tdw,z
   logical             :: surf_flux,bott_flux
!-----------------------------------------------------------------------
!BOC
! hard coding of parameters, to be included into namelist for gotm2.0
!  Bcup=1!BC Neumann
!  Tup=-heat/(rho_0*cp)!Heat flux (positive upward)
! The upper two lines are modified by Shaheli to change Bcup = Dirichlet type B.C
! and to specify upper boundary value of mass (Tup) = 0
   Bcup=2!BC Dirichlet
   Tup=0!Surface concentration (always zero)

   Bcdw=1!BC Neumann
   Tdw=0.!No flux
   surf_flux=.false.
   bott_flux=.false.

   rad(nlev)=I_0/(rho_0*cp)
   z=0.
```

```
do i=nlev-1,0,-1
  z=z+h(i+1)
  rad(i)=I_0/(rho_0*cp)*(A*exp(-z/g1)+(1-A)*exp(-z/g2))
  avh(i)=nuh(i)+avmolT
end do

do i=1,nlev
  Qsour(i)=(rad(i)-rad(i-1))/h(i)
  if (t_adv) Qsour(i)=Qsour(i)-u(i)*dtdx(i)-v(i)*dtdy(i)
end do

flag=1  ! divergence correction for vertical advection

call Yevol(nlev,Bcup,Bcdw,dt,cnpar,Tup,Tdw,TRelaxTau,h,ho,avh,w,      &
       Qsour,tprof,w_adv_method,w_adv_discr,T,surf_flux,bott_flux,  &
       grid_method,w_grid,flag)
return
end subroutine temperature
!EOC
```

Table A.1: Functional forms of turbulent length scale used in the zone $z^+ < 10$ to find the best possible length scale equation.

Function Type	Length scale equation used in the zone $z^+ < 10$
Linear	$l = -\kappa_s z$
Constant	$l = K\left(\frac{\upsilon}{u_*}\right)$
Power function (Type 1)	$l = -z\left(\frac{u_* z}{\upsilon}\right)^m$
Power function (Type 2)	$l = -Kz\left(\frac{u_* z}{\upsilon}\right)^{-0.5}$

Table A.2: Values of optimized length scale slope (κ_s) using different thickness of the viscous sublayer (δ_v^+) determined from the concentration profile predicted by the model. Values are determined for both SF_6 and He diffusing through clean and surfactant affected water surface at various wind speeds (U).

Clean				Surfactant			
U (m s^{-1})	κ_s (δ_v^+=10)	κ_s (δ_v^+=8)	κ_s (δ_v^+=12)	U (m s^{-1})	κ_s (δ_v^+=10)	κ_s (δ_v^+=8)	κ_s (δ_v^+=12)
3.8	0.13	0.13	0.15	3.9	0.08	0.08	0.085
4.9	0.17	0.17	0.18	4.9	0.11	0.095	0.12
6.2	0.19	0.18	0.19	6.2	0.11	0.11	0.11
7.9	0.25	0.25	0.26	8.2	0.14	0.14	0.14
9.5	0.23	0.23	0.23	9.8	0.175	0.175	0.19

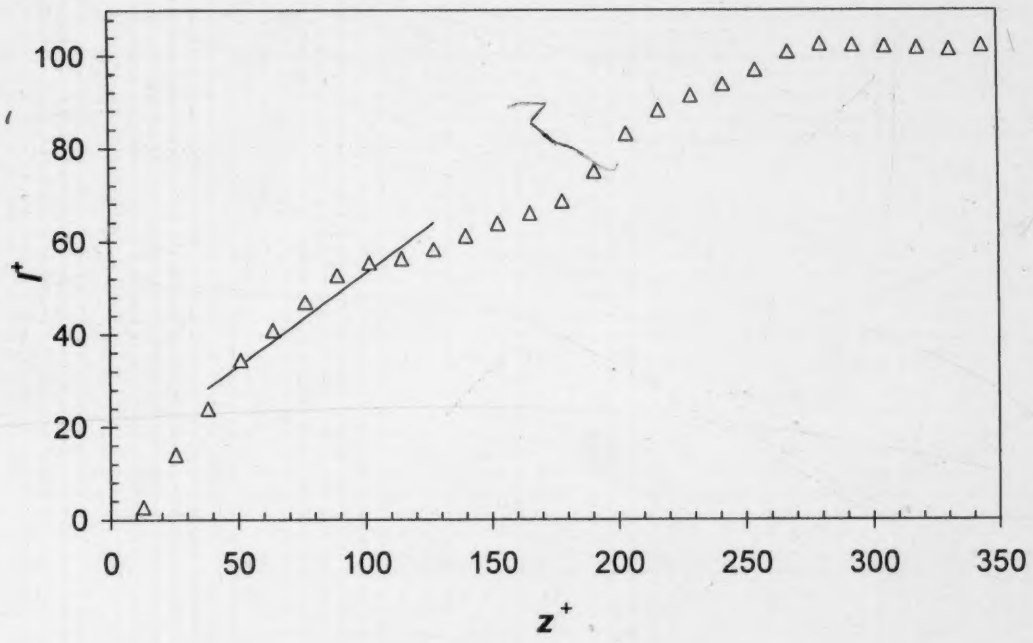

Figure A.1: Plot of non dimensional length (l^+) versus non dimensional depth (z^+) at a wind speed of 3.5 m s^{-1} on clean surface. Δ, = experimental data points. Solid line corresponds to the second order least square regression line fitted in between $z^+ > 30$ and $z/H < 0.035$. The correlation coefficient $R^2 = 0.956$.

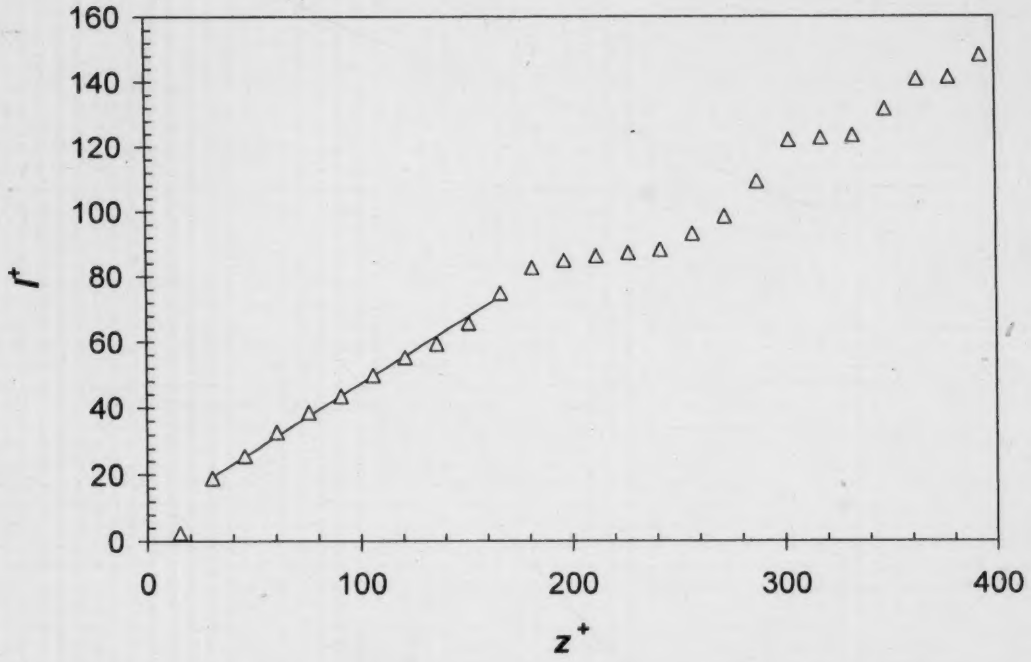

Figure A.2: Plot of non dimensional length (l^+) versus non dimensional depth (z^+) at a wind speed of 4.8 m s^{-1} on clean surface. Δ, = experimental data points. Solid line corresponds to the second order least square regression line fitted in between $z^+ > 30$ and $z/H < 0.035$. The correlation coefficient $R^2 = 0.998$.

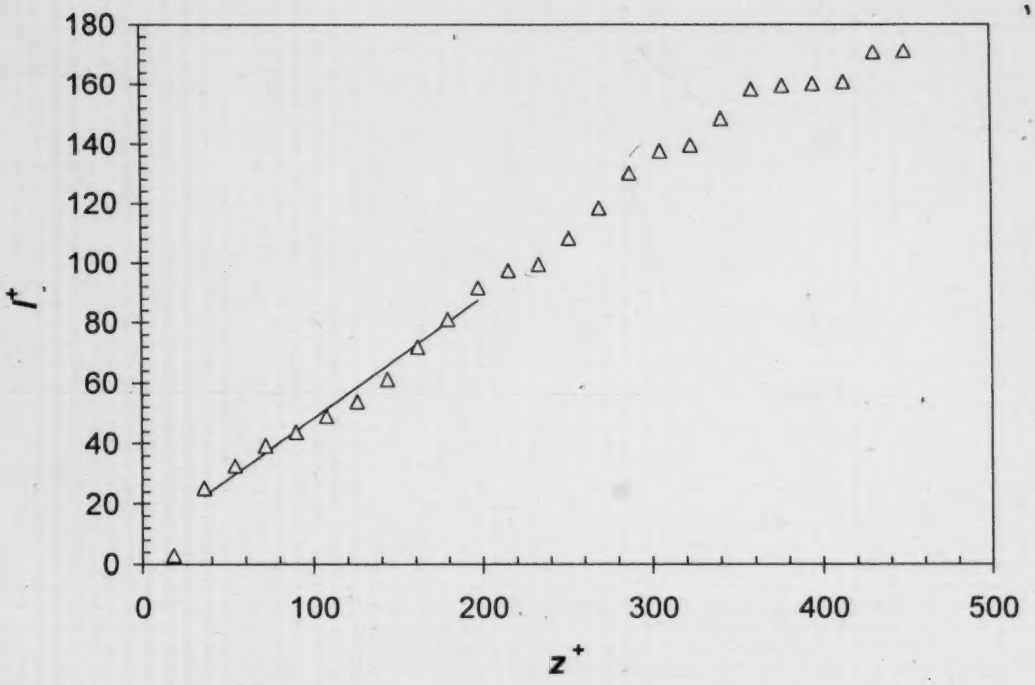

Figure A.3: Plot of non dimensional length (l^+) versus non dimensional depth (z^+) at a wind speed of 6.2 m s^{-1}on clean surface. Δ, = experimental data points. Solid line corresponds to the second order least square regression line fitted in between $z^+ > 30$ and $z/H < 0.035$. The correlation coefficient $R^2 = 0.989$.

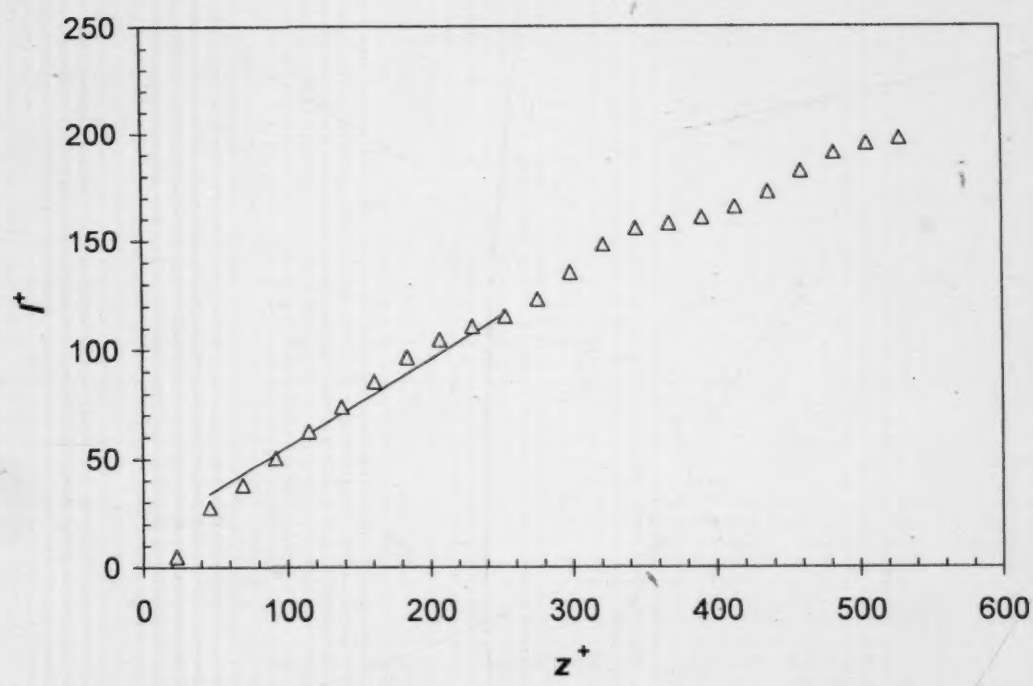

Figure A.4: Plot of non dimensional length (l^+) versus non dimensional depth (z^+) at a wind speed of 7.9 m s^{-1} on clean surface. Δ, = experimental data points. Solid line corresponds to the second order least square regression line fitted in between $z^+ > 30$ and $z/H < 0.035$. The correlation coefficient $R^2 = 0.993$.

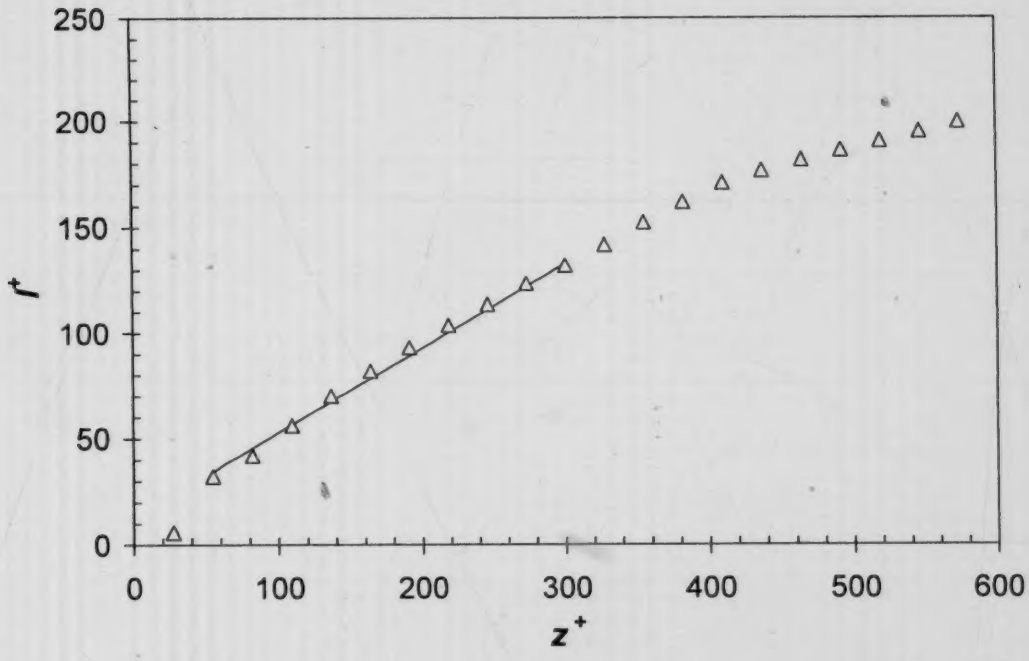

Figure A.5: Plot of non dimensional length (l^+) versus non dimensional depth (z^+) at a wind speed of 9.5 m s^{-1} on clean surface. Δ, = experimental data points. Solid line corresponds to the second order least square regression line fitted in between $z^+ > 30$ and $z/H < 0.035$. The correlation coefficient $R^2 = 0.997$.

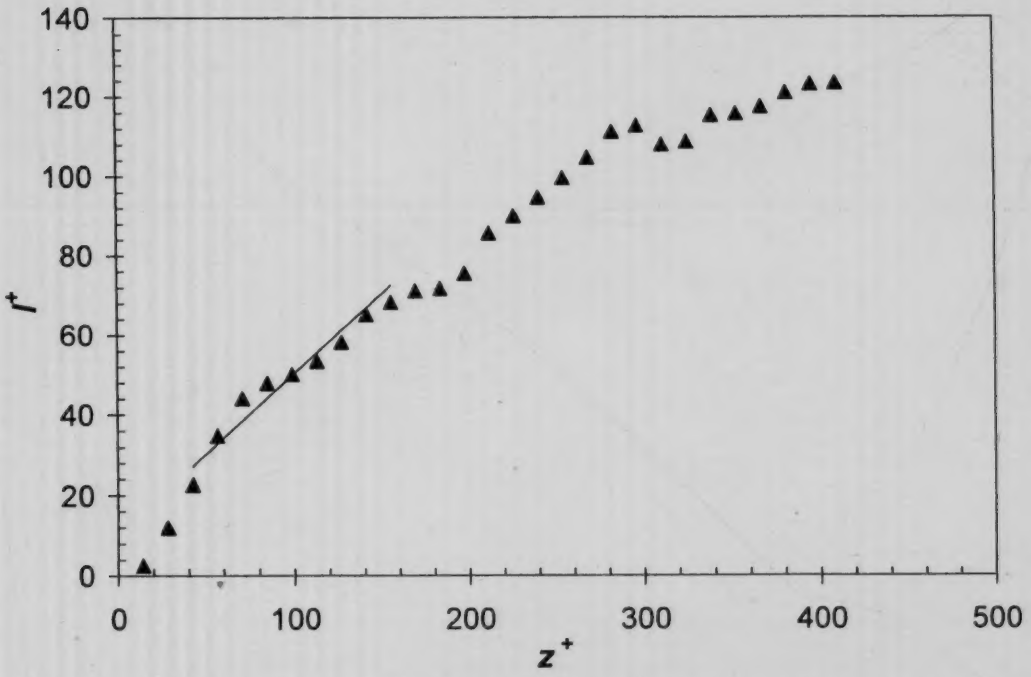

Figure A.6: Plot of non dimensional length (l^+) versus non dimensional depth (z^+) at a wind speed of 3.9m s^{-1} on surfactant contaminated surface. ▲, = experimental data points. Solid line corresponds to the second order least square regression line fitted in between $z^+ > 30$ and $z/H < 0.035$. The correlation coefficient $R^2 = 0.974$

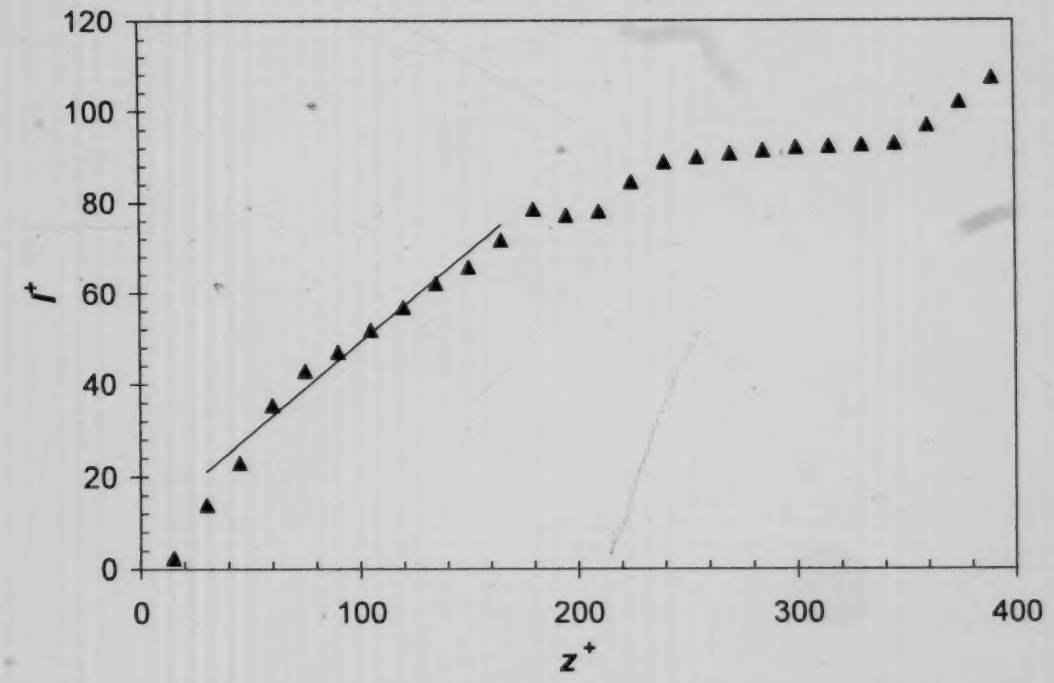

Figure A.7: Plot of non dimensional length (l^+) versus non dimensional depth (z^+) at a wind speed of 4.9m s^{-1}on surfactant contaminated surface. ▲, = experimental data points. Solid line corresponds to the second order least square regression line fitted in between $z^+ > 30$ and $z/H < 0.035$. The correlation coefficient $R^2 = 0.983$.

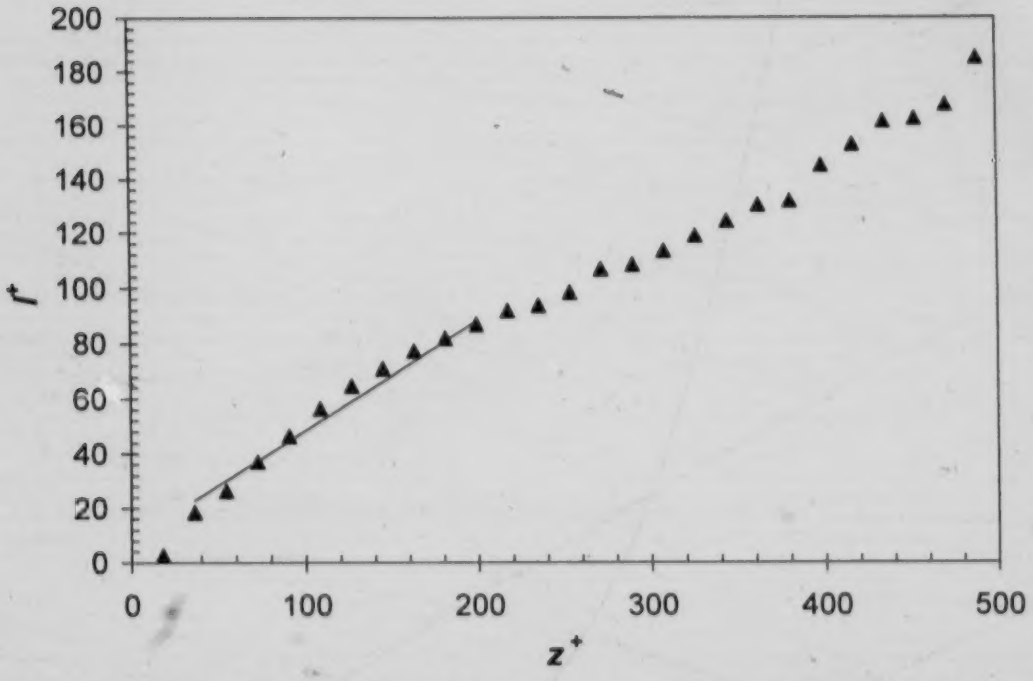

Figure A.8: Plot of non dimensional length (l^+) versus non dimensional depth (z^+) at a wind speed of 6.2 m s^{-1}on surfactant contaminated surface. ▲, = experimental data points. Solid line corresponds to the second order least square regression line fitted in between $z^+ > 30$ and $z/H < 0.035$. The correlation coefficient $R^2 = 0.991$.

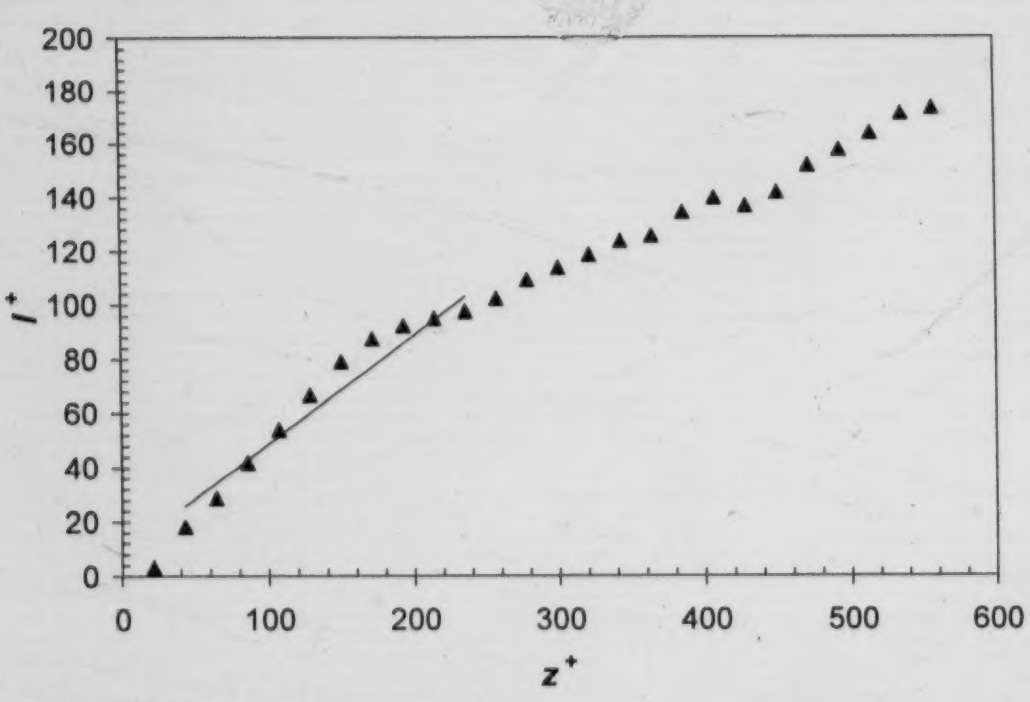

Figure A.9: Plot of non dimensional length (l^+) versus non dimensional depth (z^+) at a wind speed of 8.2 m s^{-1} on surfactant contaminated surface. ▲, = experimental data points. Solid line corresponds to the second order least square regression line fitted in between $z^+ > 30$ and $z/H < 0.035$. The correlation coefficient $R^2 = 0.977$.

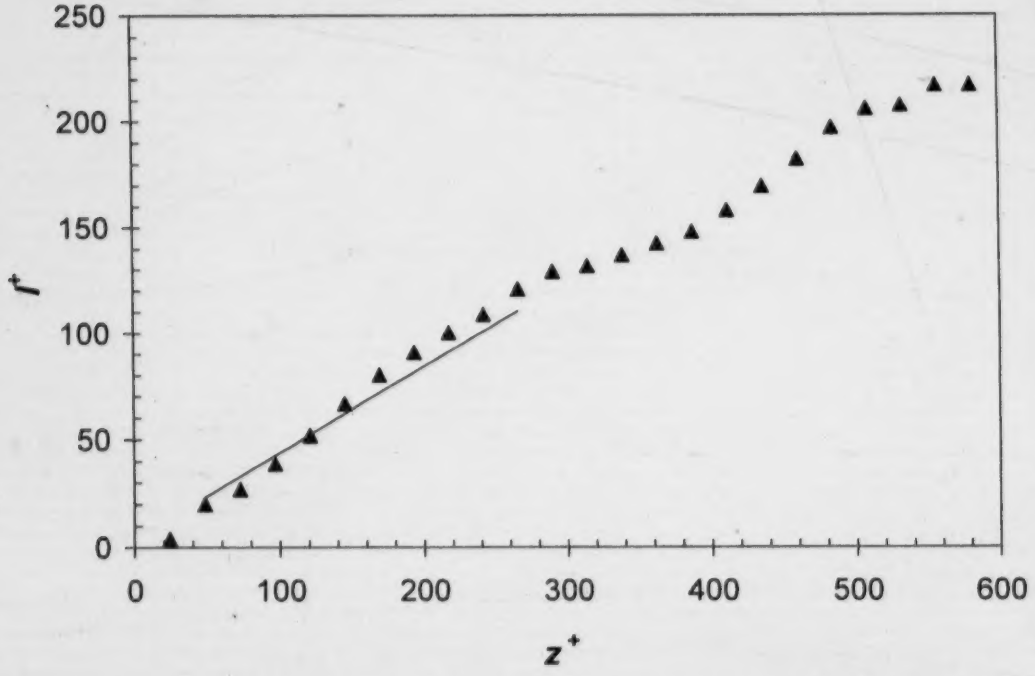

Figure A.10: Plot of non dimensional length (l^+) versus non dimensional depth (z^+) at a wind speed of 7.9m s^{-1}on surfactant contaminated surface. ▲, = experimental data points. Solid line corresponds to the second order least square regression line fitted in between $z^+ > 30$ and $z/H < 0.035$. The correlation coefficient $R^2 = 0.997$.

(a)

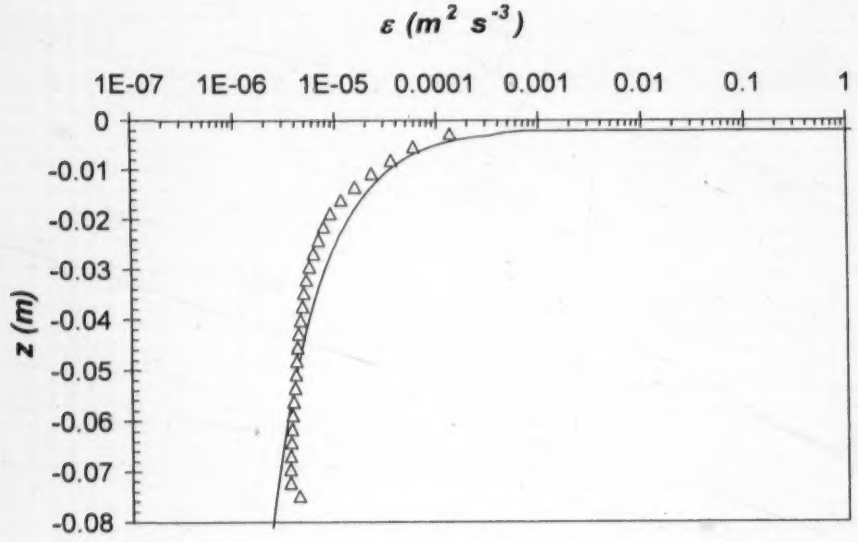

(b)

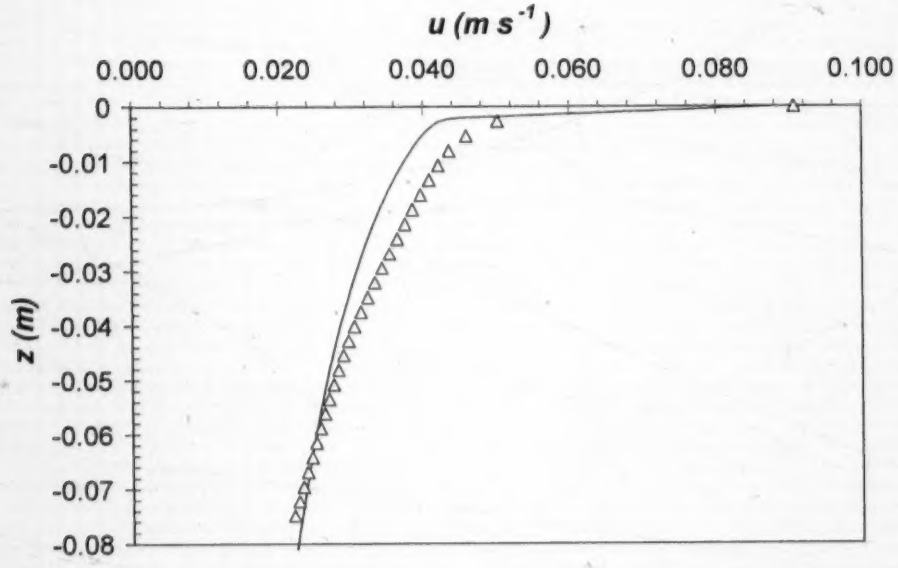

Figure A.11: Comparison of the profiles of predicted and measured (a) dissipation (ε) and (b) velocity (u) for wind speed of 3.9 m s^{-1} on clean water surface. Solid line is the model predictions of (a) ε and (b) u for parameter values of $\tau = 0.0202$ Nm^{-2}, $z_{ol} = 0.0069$m and $\alpha = 20$, Δ is experimental data points.

(a)

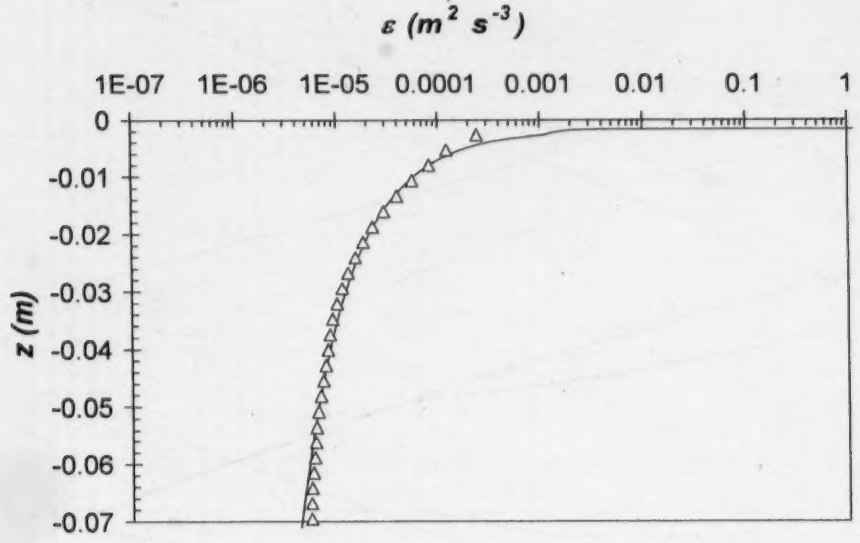

(b)

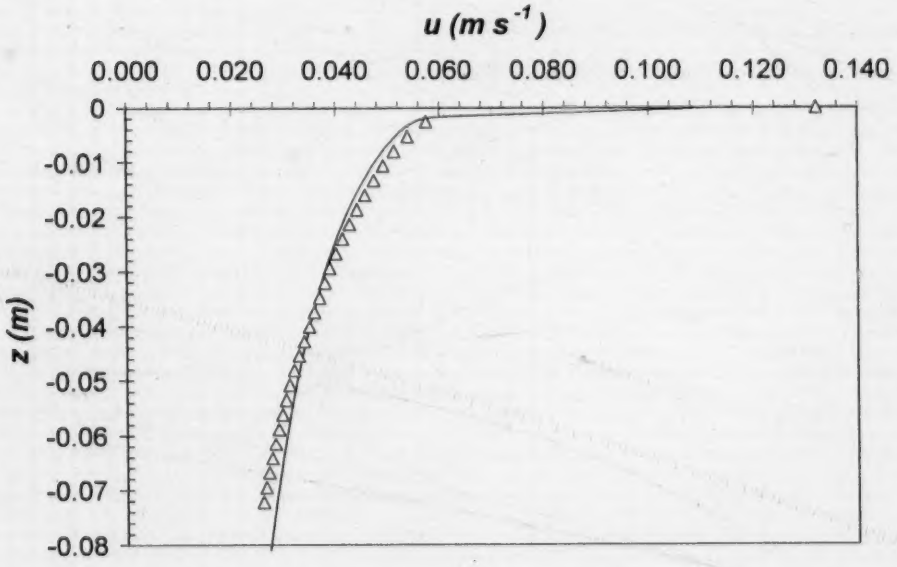

Figure A.12: Comparison of the profiles of predicted and measured (a) dissipation (ε) and (b) velocity (u) for wind speed of 4.9 m s^{-1} on clean water surface. Solid line is the model predictions of (a) ε and (b) u for parameter values of $\tau = 0.028$ Nm^{-2}, $z_{ot} = 0.0032$m and $\alpha = 24$, Δ is experimental data points.

(a)

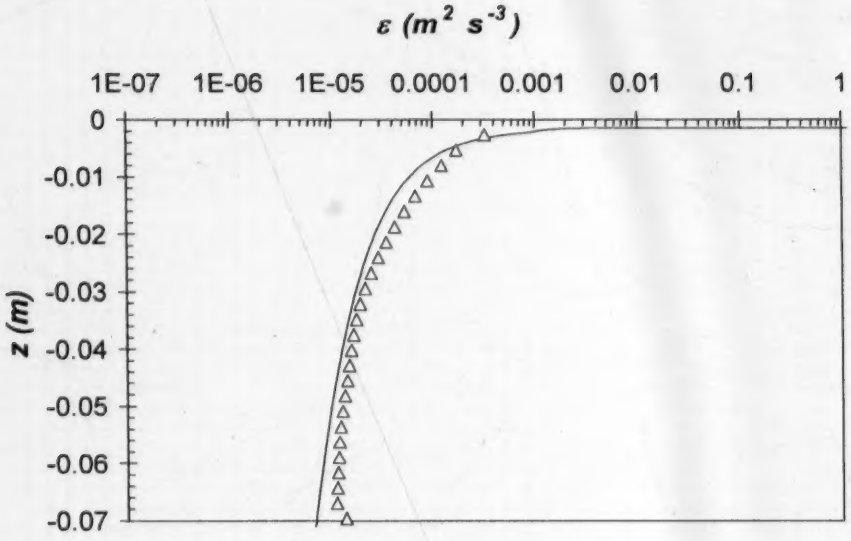

(b)

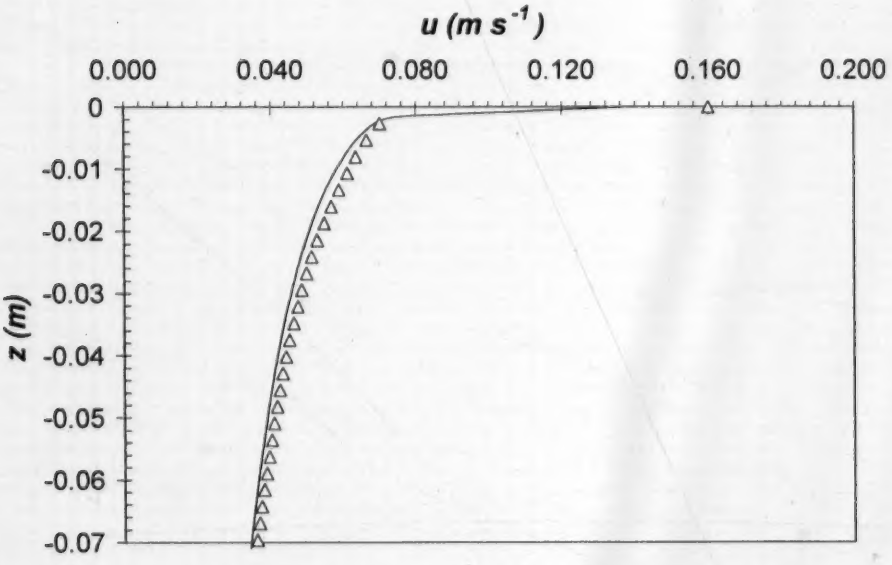

Figure A.13: Comparison of the profiles of predicted and measured (a) dissipation (ε) and (b) velocity (u) for wind speed of 6.2 m s^{-1} on clean water surface. Solid line is the model predictions of (a) ε and (b) u for parameter values of $\tau = 0.039$ Nm^{-2}, $z_{ol} = 0.0031$m and $\alpha = 10$, Δ is experimental data points.

(a)

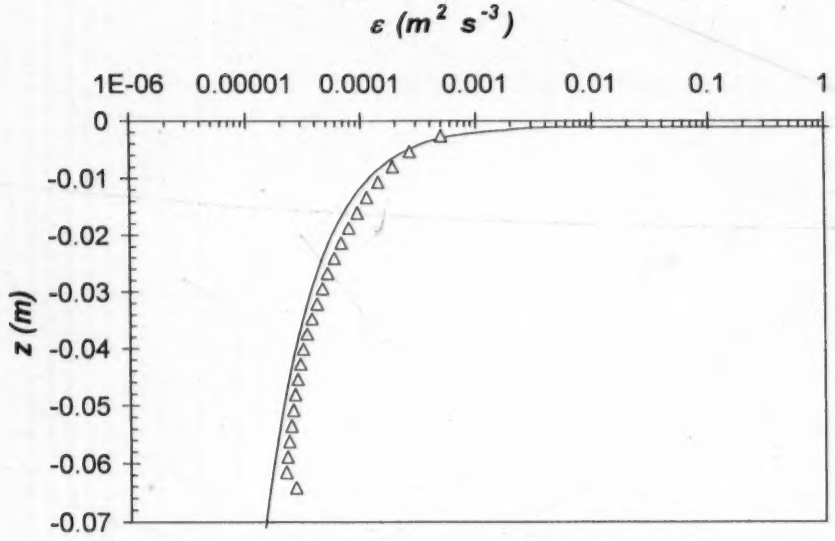

(b)

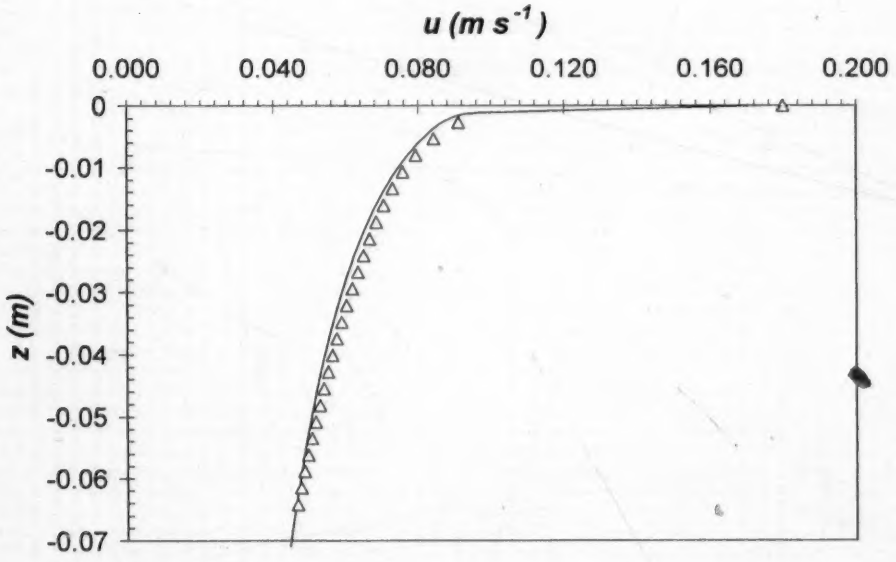

Figure A.14: Comparison of the profiles of predicted and measured (a) dissipation (ε) and (b) velocity (u) for wind speed of 8.0 m s^{-1} on clean water surface. Solid line is the model predictions of (a) ε and (b) u for parameter values of $\tau = 0.065$ Nm^{-2}, $z_{ot} = 0.004$m and $\alpha = 10$, Δ is experimental data points.

(a)

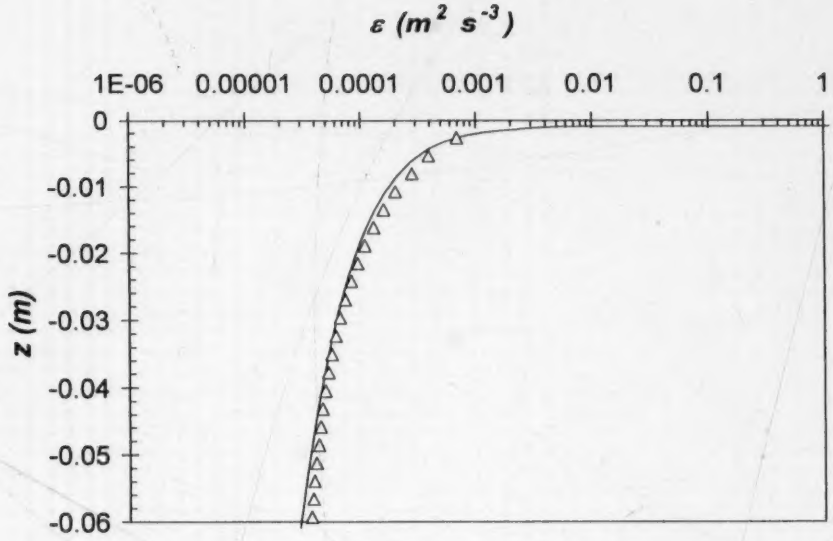

(b)

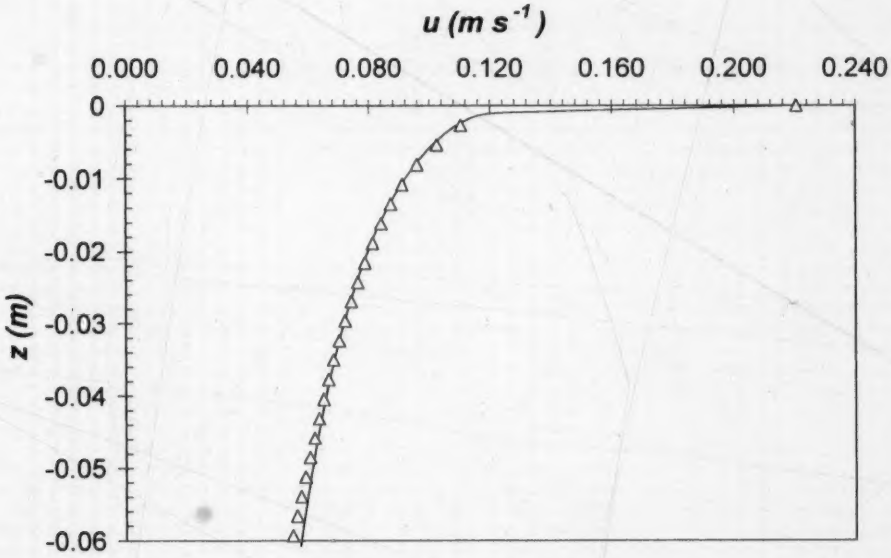

Figure A.15: Comparison of the profiles of predicted and measured (a) dissipation (ε) and (b) velocity (u) for wind speed of 9.5 m s^{-1} on clean water surface. Solid line is the model predictions of (a) ε and (b) u for parameter values of $\tau = 0.094$ Nm^{-2}, $z_{ot} = 0.0032$m and $\alpha = 5$, Δ is experimental data points.

(a)

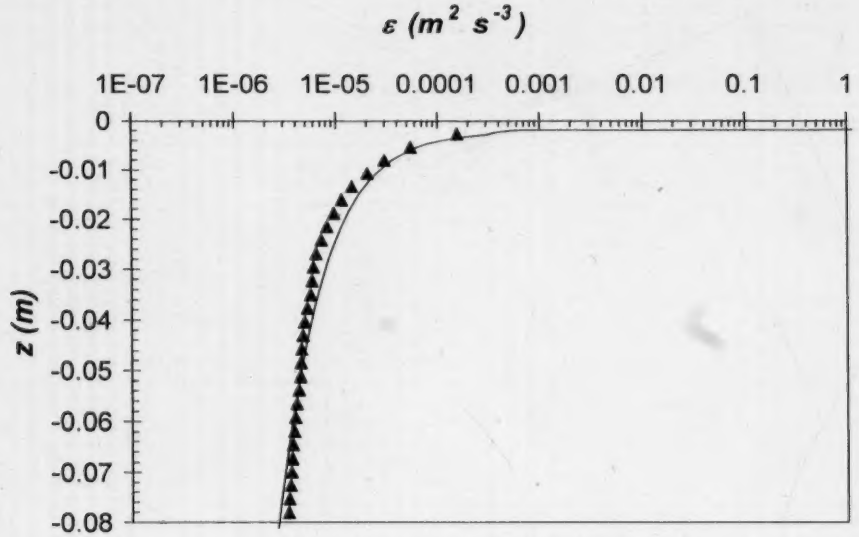

(b)

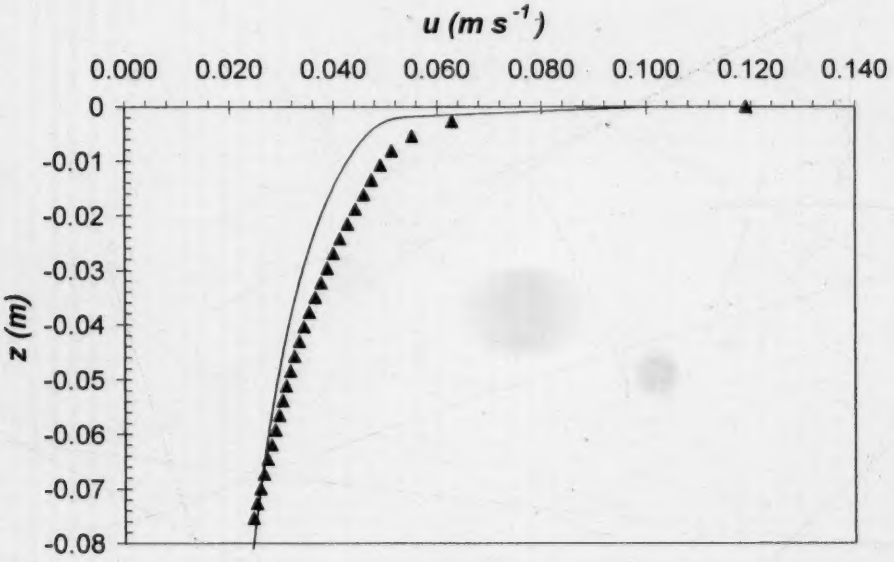

Figure A.16: Comparison of the profiles of predicted and measured (a) dissipation (ε) and (b) velocity (u) for wind speed of 3.9 m s^{-1} on surfactant contaminated water surface. Solid line is the model predictions of (a) ε and (b) u for parameter values of $\tau = 0.023$ Nm^{-2}, $z_{ot} = 0.0049$m and $\alpha = 10$, ▲is experimental data points.

(a)

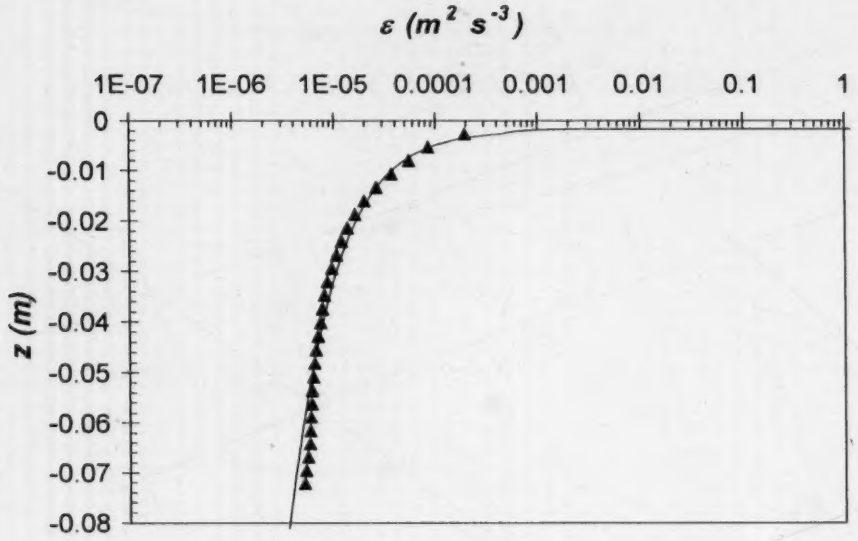

(b)

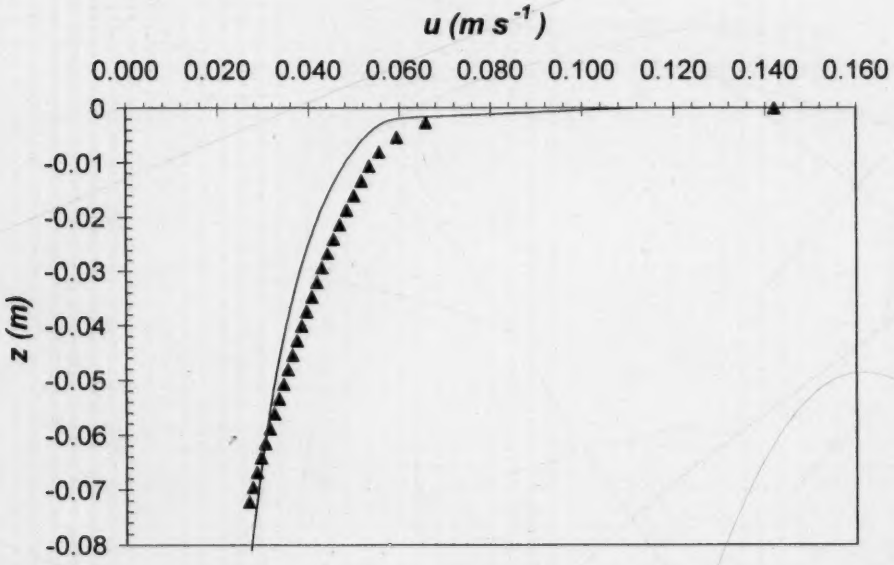

Figure A.17: Comparison of the profiles of predicted and measured (a) dissipation (ε) and (b) velocity (u) for wind speed of 4.9 m s^{-1} on surfactant contaminated water surface. Solid line is the model predictions of (a) ε and (b) u for parameter values of $\tau = 0.028$ Nm^{-2}, $z_{ot} = 0.004$m and $\alpha = 10$, ▲is experimental data points.

(a)

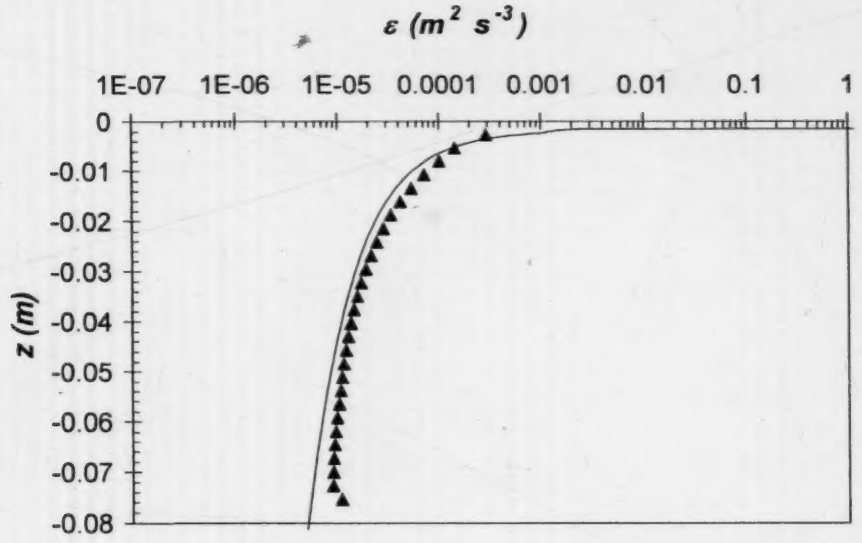

(b)

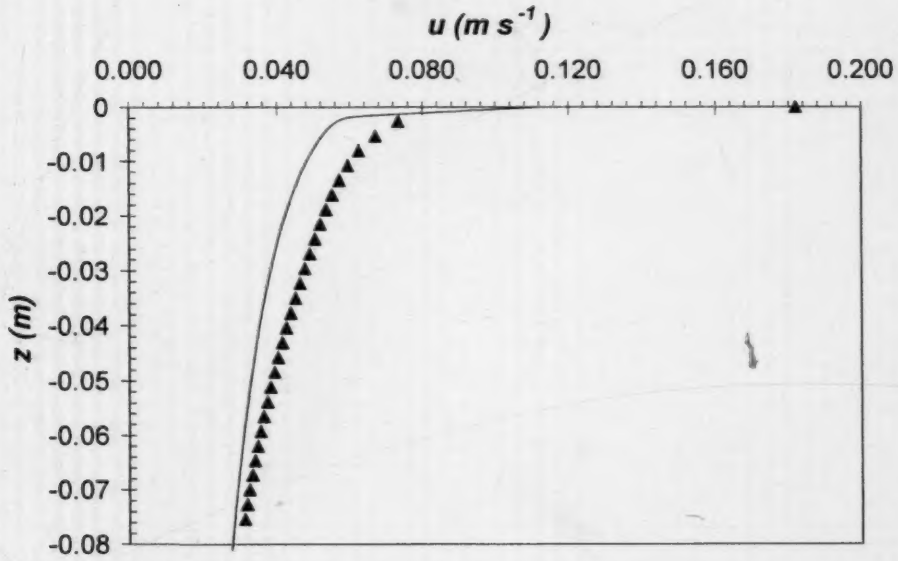

Figure A.18: Comparison of the profiles of predicted and measured (a) dissipation (ε) and (b) velocity (u) for wind speed of 6.2 m s^{-1} on surfactant contaminated water surface. Solid line is the model predictions of (a) ε and (b) u for parameter values of $\tau = 0.035$ Nm^{-2}, $z_{ot} = 0.0031$m and $\alpha = 13$, ▲is experimental data points.

(a)

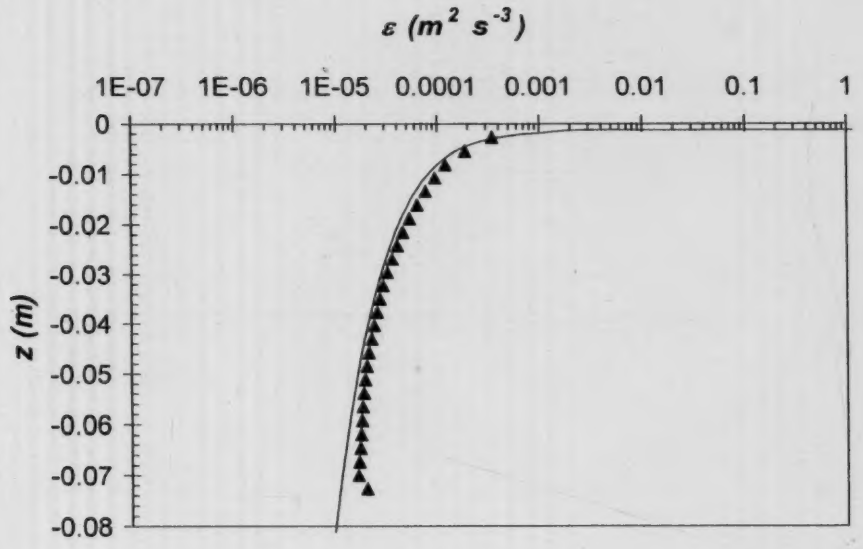

(b)

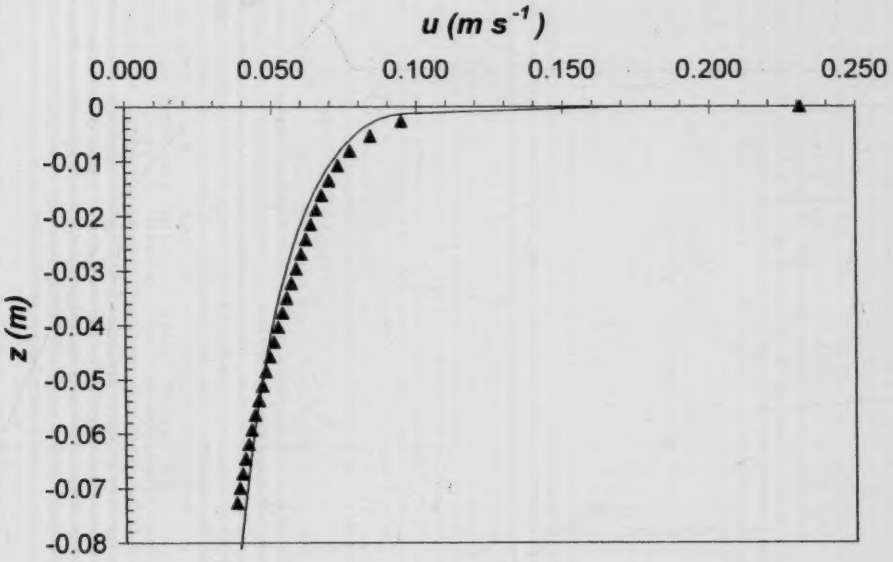

Figure A.19: Comparison of the profiles of predicted and measured (a) dissipation (ε) and (b) velocity (u) for wind speed of 8.2 m s^{-1} on surfactant contaminated water surface. Solid line is the model predictions of (a) ε and (b) u for parameter values of $\tau = 0.055$ Nm^{-2}, $z_{of} = 0.0026$m and $\alpha = 5$, ▲is experimental data points.

(a)

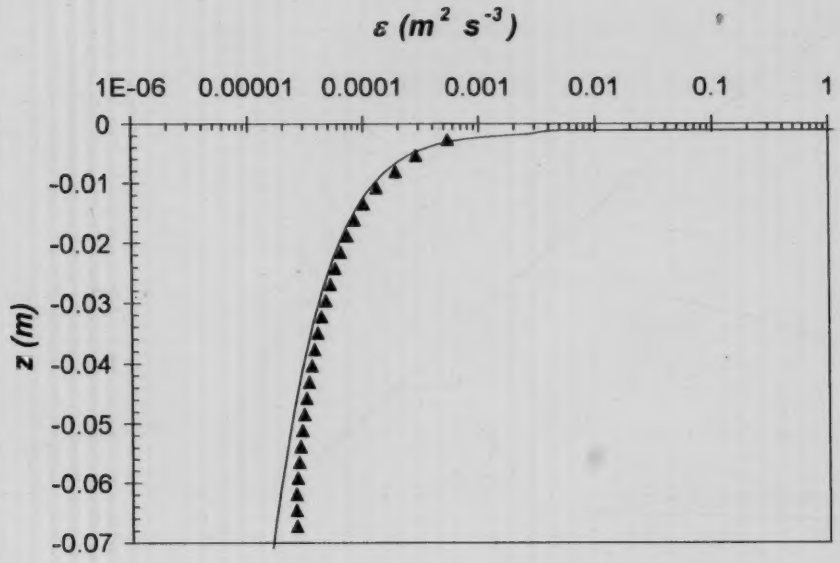

(b)

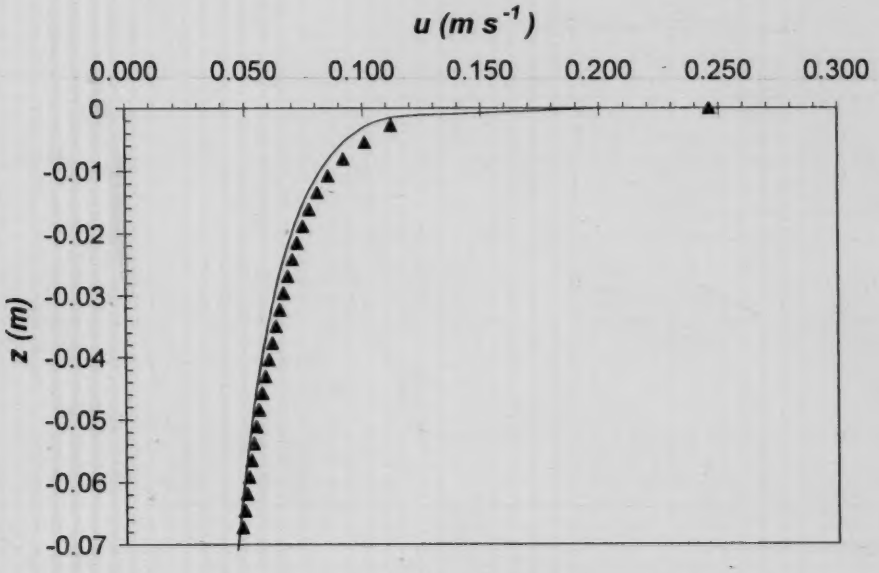

Figure A.20: Comparison of the profiles of predicted and measured (a) dissipation (ε) and (b) velocity (u) for wind speed of 9.8 m s^{-1} on surfactant contaminated water surface. Solid line is the model predictions of (a) ε and (b) u for parameter values of $\tau = 0.069$ Nm^{-2}, $z_{ot} = 0.001$m and $\alpha = 6$, ▲is experimental data points.

(a)

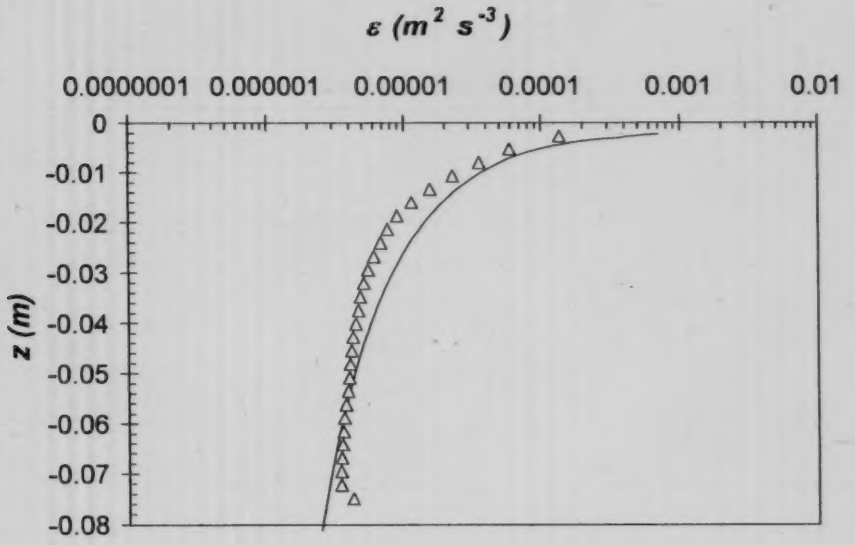

(b)

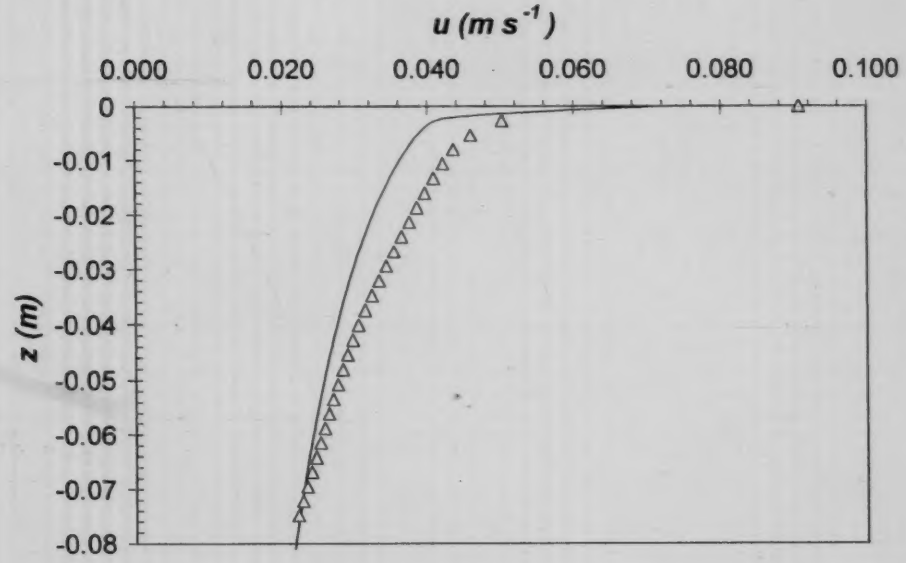

Figure A.21: Comparison of the profiles of predicted and measured (a) dissipation (ε) and (b) velocity (u) for wind speed of 3.9 m s^{-1} on clean water surface. Solid line is the model predictions (using Eq. 3.16) of (a) ε and (b) u for parameter values of $\tau = 0.0202$ Nm^{-2}, $z_{ot} = 0.0069$m and $\alpha = 20$, Δ is experimental data points.

(a)

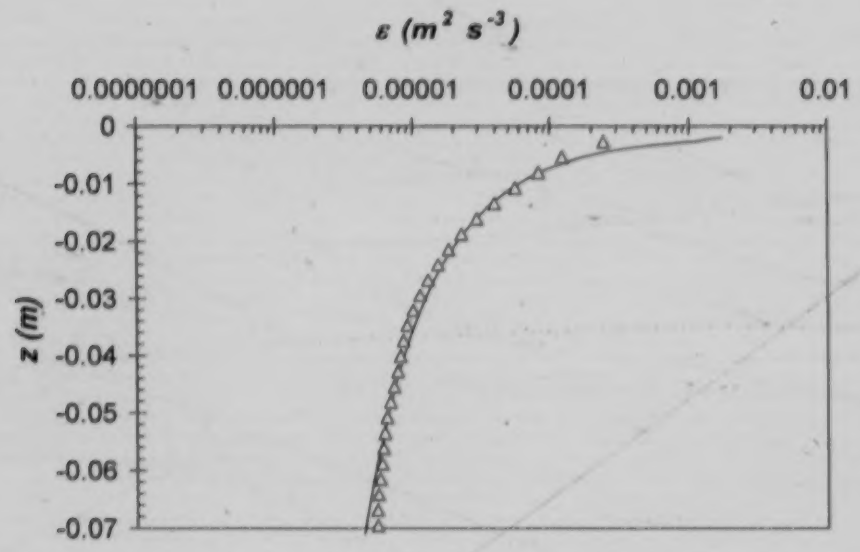

(b)

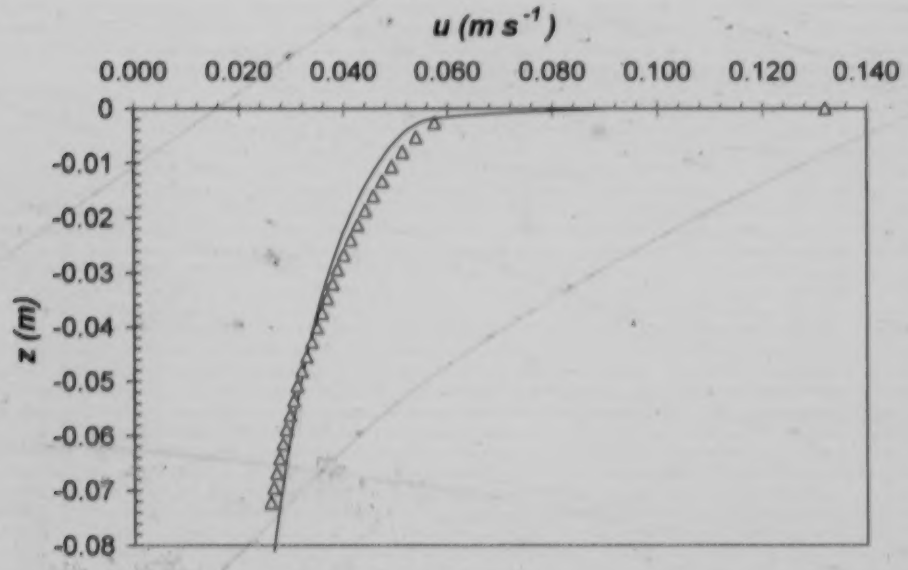

Figure A.22: Comparison of the profiles of predicted and measured (a) dissipation (ε) and (b) velocity (u) for wind speed of 4.9 m s^{-1} on clean water surface. Solid line is the model predictions (using Eq. 3.16) of (a) ε and (b) u for parameter values of $\tau = 0.028$ Nm^{-2}, z_{ot} = 0.0032m and $a = 24$, Δ is experimental data points.

(a)

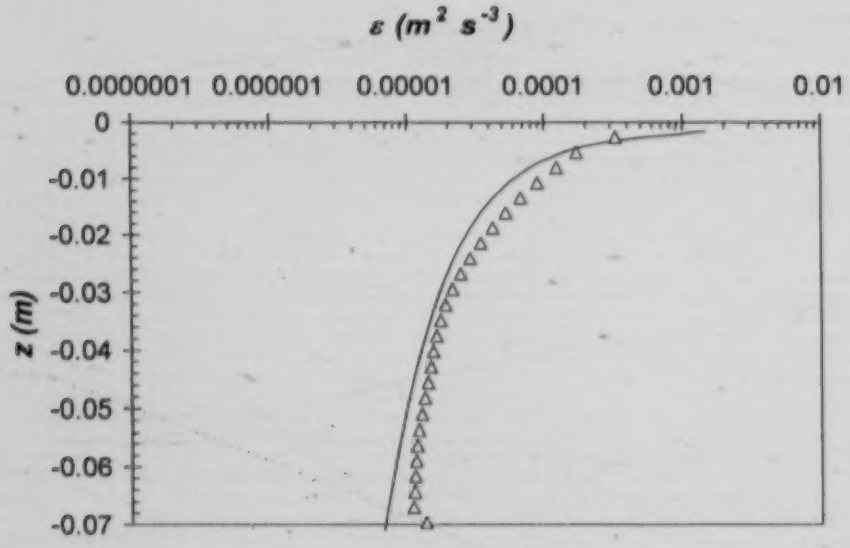

(b)

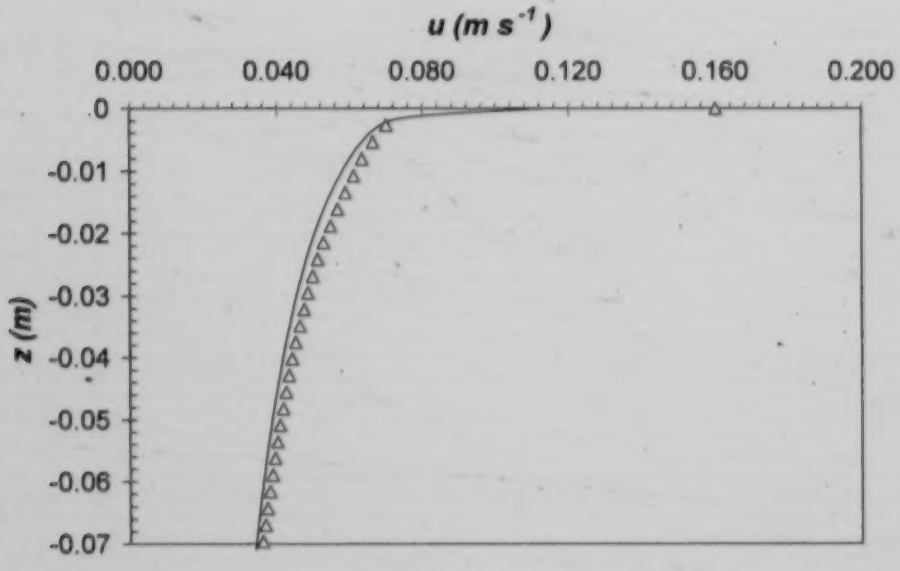

Figure A.23: Comparison of the profiles of predicted and measured (a) dissipation (ε) and (b) velocity (u) for wind speed of 6.2 m s^{-1} on clean water surface. Solid line is the model predictions (using Eq. 3.16) of (a) ε and (b) u for parameter values of $\tau = 0.039$ Nm^{-2}, z_{ot} = 0.0031m and $\alpha = 10$, Δ is experimental data points.

(a)

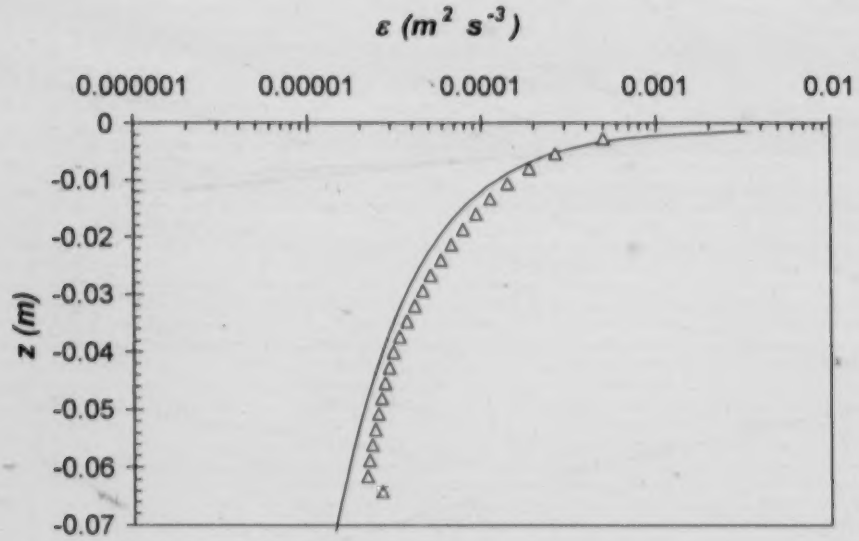

(b)

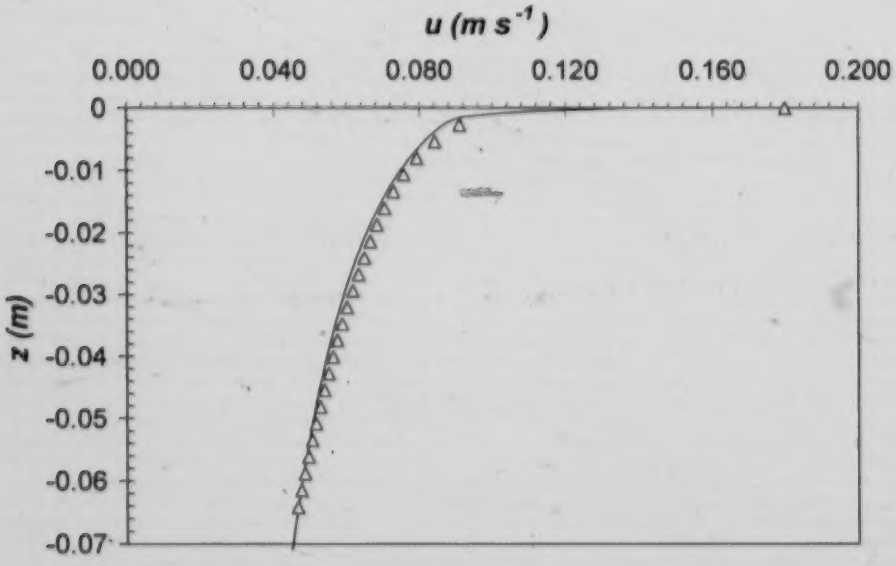

Figure A.24: Comparison of the profiles of predicted and measured (a) dissipation (ε) and (b) velocity (u) for wind speed of 8.0 m s^{-1} on clean water surface. Solid line is the model predictions of (using Eq. 3.16) (a) ε and (b) u for parameter values of $\tau = 0.065$ Nm^{-2}, z_{ot} = 0.004m and $\alpha = 10$, Δ is experimental data points.

(a)

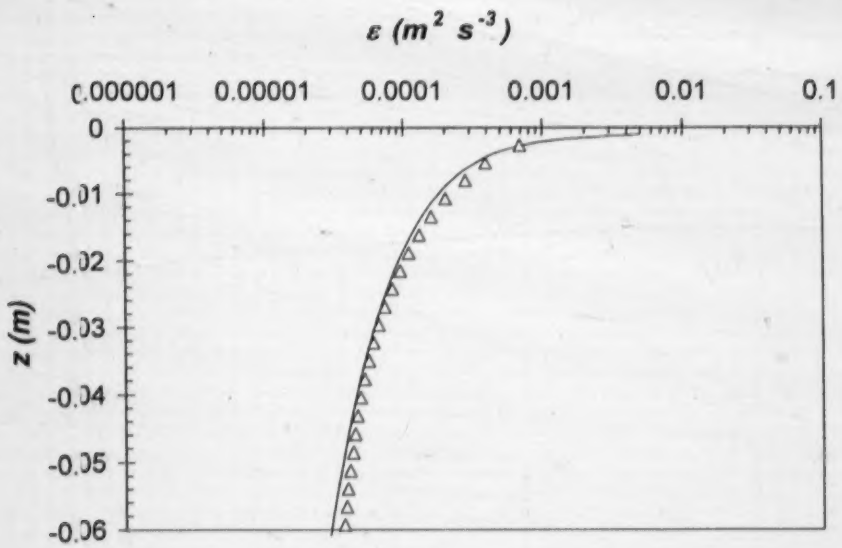

(b)

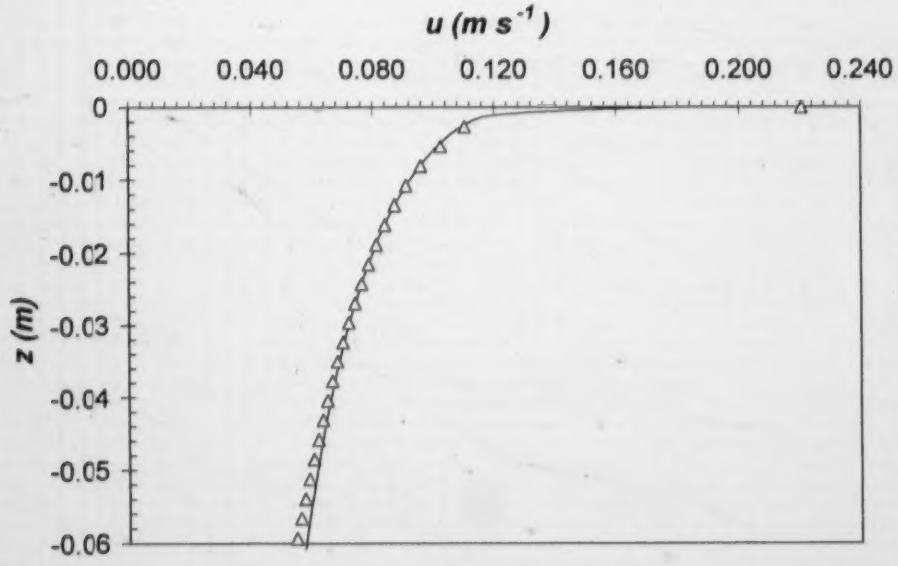

Figure A.25: Comparison of the profiles of predicted and measured (a) dissipation (ε) and (b) velocity (u) for wind speed of 9.5 m s^{-1} on clean water surface. Solid line is the model predictions of (using Eq. 3.16) (a) ε and (b) u for parameter values of $\tau = 0.094$ Nm^{-2}, z_{ot} = 0.0032m and $\alpha = 5$, Δ is experimental data points.

(a)

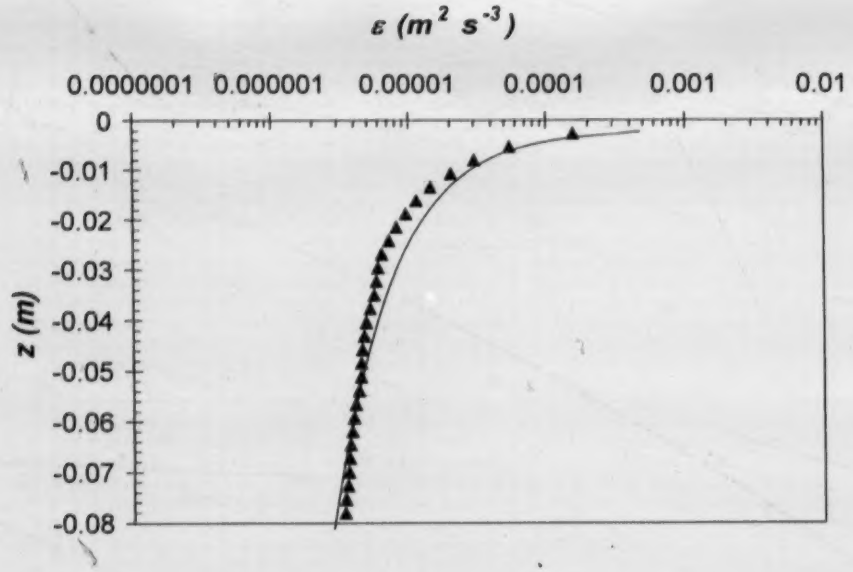

(b)

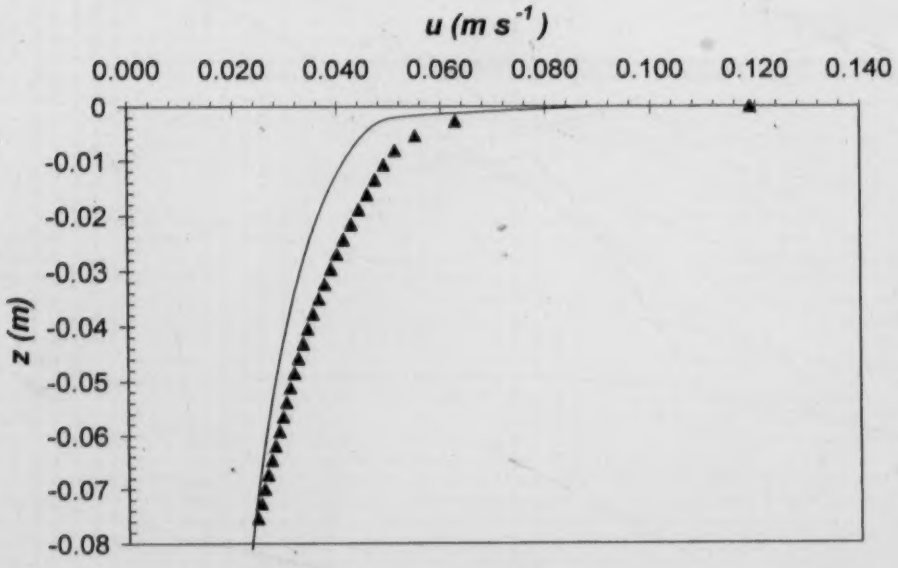

Figure A.26: Comparison of the profiles of predicted and measured (a) dissipation (ε) and (b) velocity (u) for wind speed of 3.9 m s^{-1} on surfactant contaminated water surface. Solid line is the model predictions (using Eq. 3.16) of (a) ε and (b) u for parameter values of $\tau = 0.023$ Nm^{-2}, $z_{ol} = 0.0049$m and $\alpha = 10$, ▲is experimental data points.

(a)

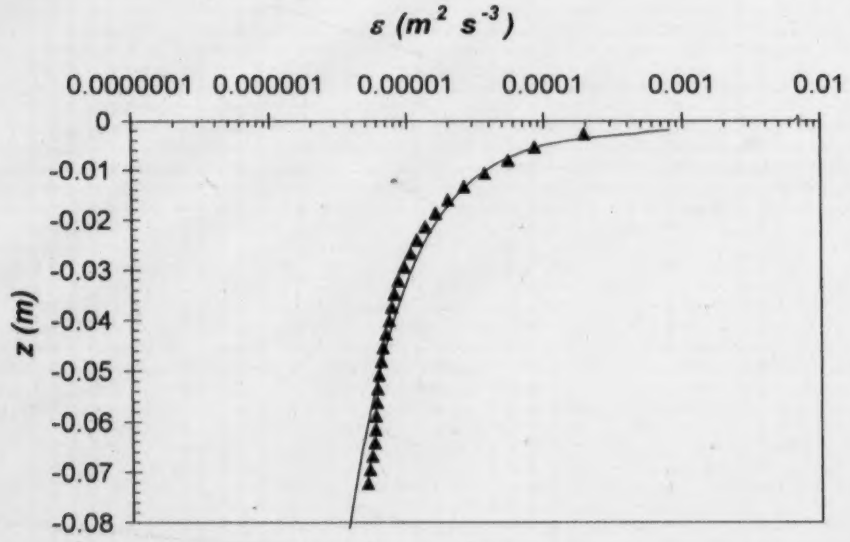

(b)

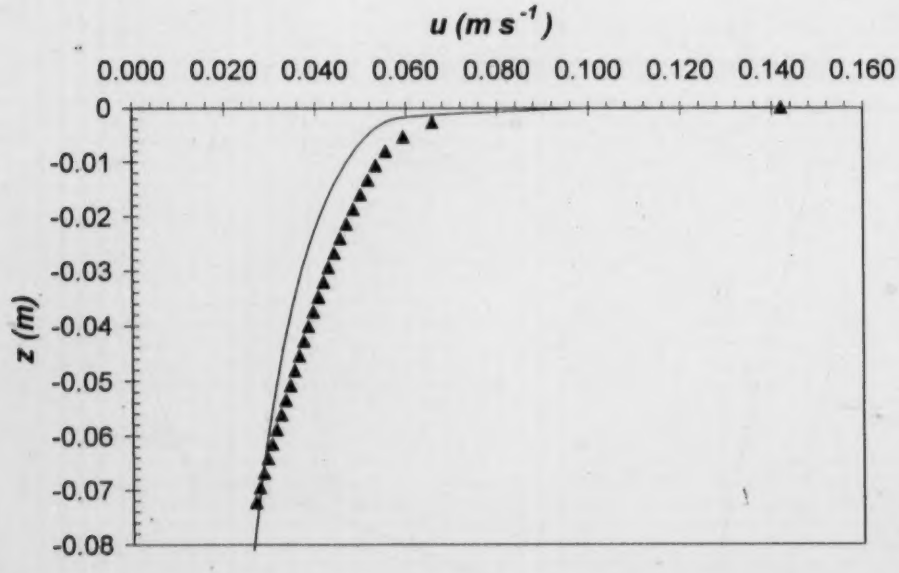

Figure A.27: Comparison of the profiles of predicted and measured (a) dissipation (ε) and (b) velocity (u) for wind speed of 4.9 m s^{-1} on surfactant contaminated water surface. Solid line is the model predictions (using Eq. 3.16) of (a) ε and (b) u for parameter values of $\tau = 0.028$ Nm^{-2}, $z_{ot} = 0.004$m and $\alpha = 10$, ▲is experimental data points.

(a)

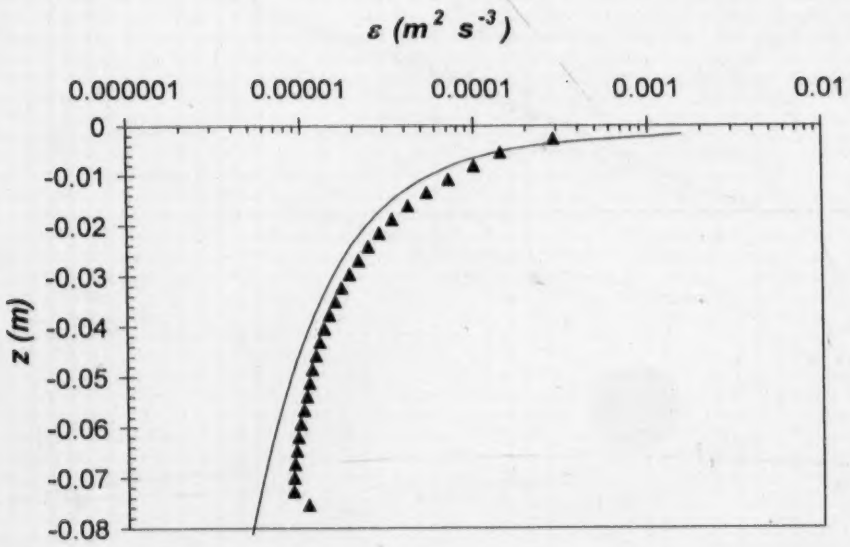

(b)

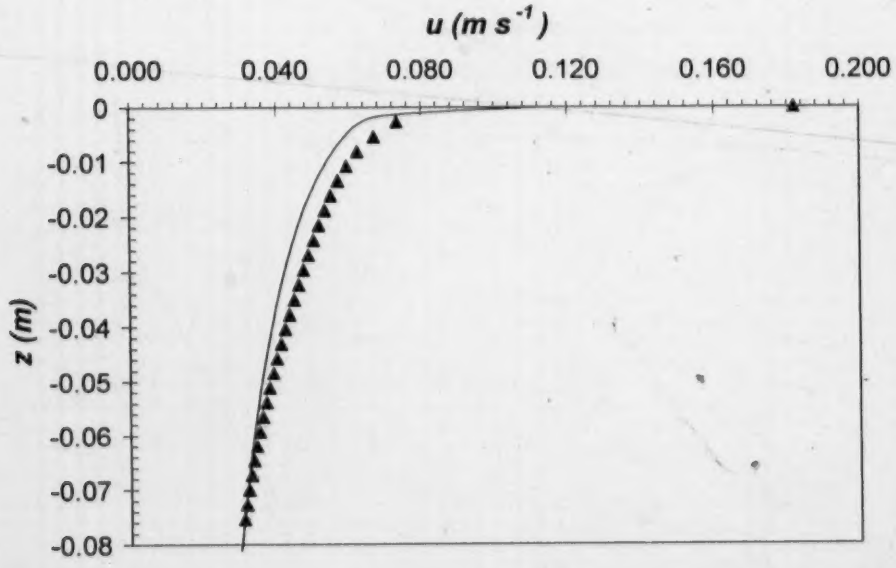

Figure A.28: Comparison of the profiles of predicted and measured (a) dissipation (ε) and (b) velocity (u) for wind speed of 6.2 m s^{-1} on surfactant contaminated water surface. Solid line is the model predictions (using Eq. 3.16) of (a) ε and (b) u for parameter values of $\tau = 0.035$ Nm^{-2}, $z_{ot} = 0.0031$m and $\alpha = 13$, ▲is experimental data points.

(a)

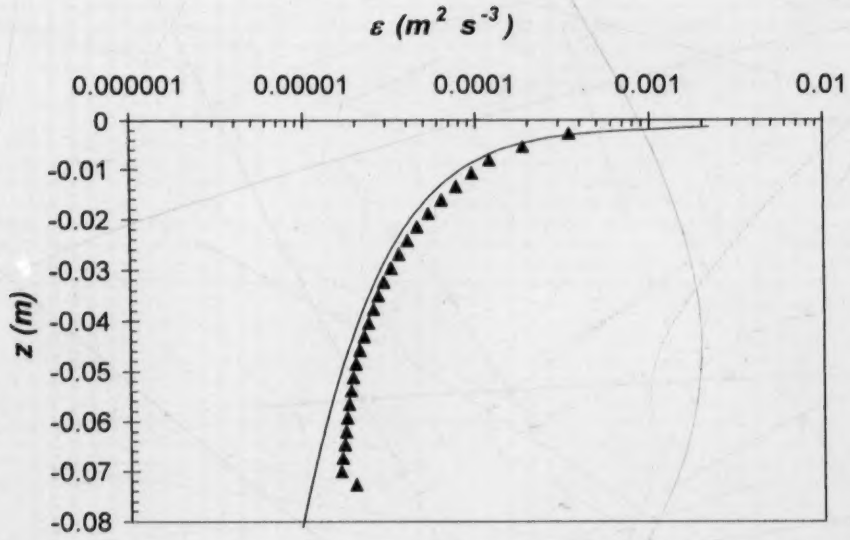

(b)

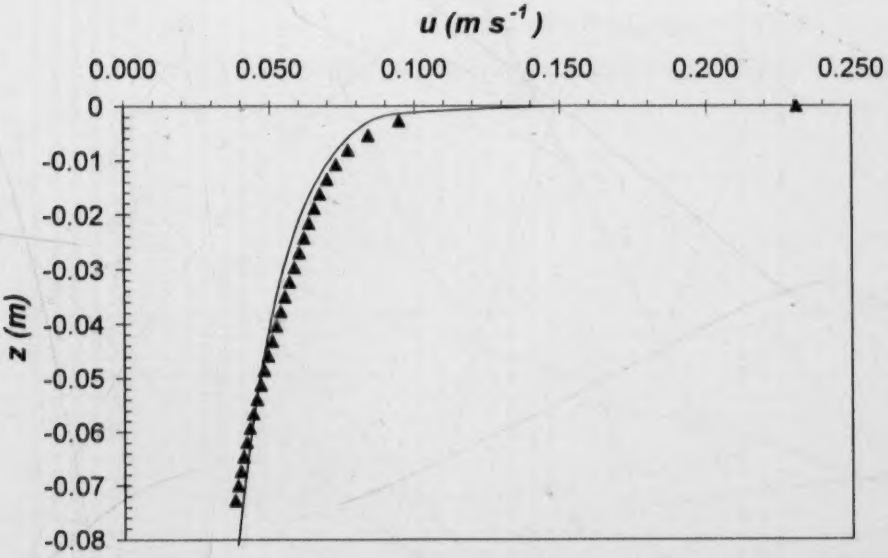

Figure A.29: Comparison of the profiles of predicted and measured (a) dissipation (ε) and (b) velocity (u) for wind speed of 8.2 m s^{-1} on surfactant contaminated water surface. Solid line is the model predictions (using Eq. 3.16) of (a) ε and (b) u for parameter values of $\tau = 0.055$ Nm^{-2}, $z_{ot} = 0.0026$m and $\alpha = 5$, ▲is experimental data points.

(a)

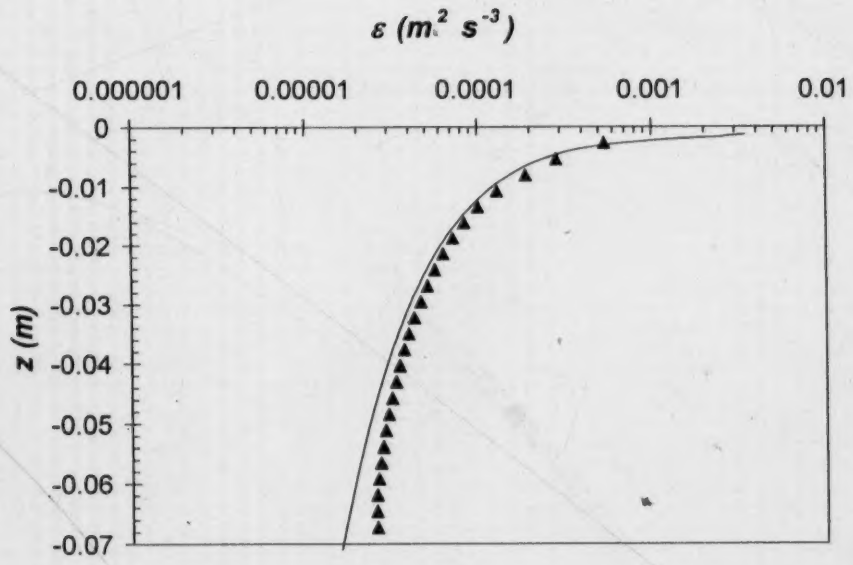

(b)

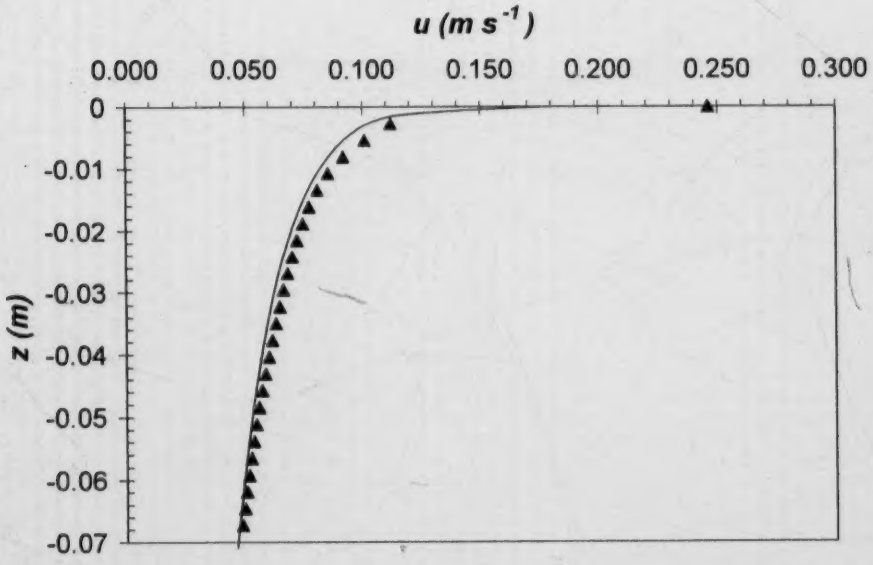

Figure A.30: Comparison of the profiles of predicted and measured (a) dissipation (ε) and (b) velocity (u) for wind speed of 9.8 m s^{-1} on surfactant contaminated water surface. Solid line is the model predictions (using Eq. 3.16) of (a) ε and (b) u for parameter values of $\tau = 0.069$ Nm^{-2}, $z_{ot} = 0.001$m and $\alpha = 6$, ▲is experimental data points.